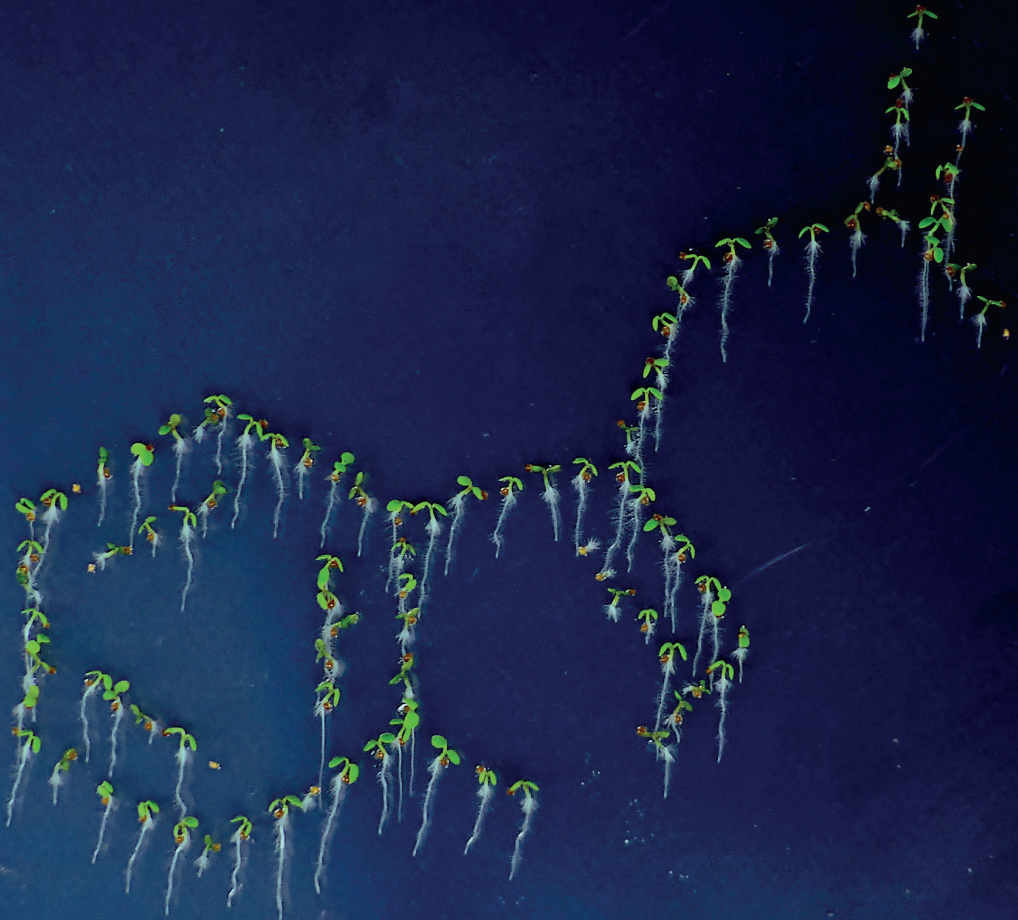# From bottom to top

## tweaking auxin homeostasis
## to deal with salt stress

Iko Tamar Koevoets

**Propositions**

1. Local auxin biosynthesis is more important than auxin transport for root development during stress.
   (this thesis)

2. Plant breeding aimed at stress tolerance does not deliver crops optimally producing under stress.
   (this thesis)

3. Roots hold more breeding potential than shoots.

4. Human selection creates more diversity than environmental selection.

5. Pursuing a PhD part-time is more efficient than full-time.

6. Appointing specialized staff members responsible for course development and teaching is necessary to ensure high quality of education.

Propositions belonging to the thesis, entitled

From bottom to top: tweaking auxin metabolism during salt stress

Iko Tamar Koevoets
Wageningen, 15 June 2021

# From bottom to top – tweaking auxin homeostasis to deal with salt stress

Iko Tamar Koevoets

# From bottom to top – tweaking auxin homeostasis to deal with salt stress

**Iko Tamar Koevoets**

**Thesis**
submitted in fulfilment of the requirements for the degree of doctor
at Wageningen University
by the authority of the Rector Magnificus,
Prof. Dr A.P.J. Mol,
in the presence of the
Thesis Committee appointed by the Academic Board
to be defended in public
on Tuesday 15 June, 2021
at 11 a.m. in the Aula.

# TABLE OF CONTENTS

**CHAPTER 1**

1

# General Introduction

**1**

**From bottom to top: how salt affects plant growth**

Over the past decades, plant breeders have focused on developing crops with high yields when growing under optimal conditions. With global climate change increasingly having a negative impact on agriculture, combined with an ever-growing food demand, we will now need to focus on developing crops with high yield under less optimal conditions.

Salinity is a major and increasing problem for agriculture. Due to irrigation salinized land is rapidly expanding and fresh water is getting scarcer (Ivushkin et al., 2019). Most crop species are salt sensitive and grow poorly on salinized soils (Yamaguchi and Blumwald, 2005; Munns et al., 2006; Roy et al., 2014; Munns and Gilliham, 2015). Salinity confronts the plant with a combination of osmotic stress and sodium toxicity, inducing specific mechanisms (as reviewed in Van Zelm et al., 2020). Osmotic stress is caused by the accumulation of sodium ions outside the plant, reducing water availability. To compensate for the increased osmotic potential in the soil, plants can accumulate osmolytes, soluble compounds such as proline and sorbitol (Trovato et al., 2019; Slama et al., 2015). Although effective, the production of these osmolytes redirects resources from growth and reproduction. In addition, plants close their stomata to prevent water loss, reducing the availability of $CO_2$ for photosynthesis (Chaves et al., 2009). As sodium ions enter the plant, differences in osmotic potential will reduce, but the plant has to cope with sodium toxicity. Due to chemical similarities between sodium and potassium ions, sodium ions can interfere with processes in which potassium plays an essential role, such as ion transport and photosynthesis (Benito et al., 2014; Wakeel et al., 2011).

In the end, plant fitness and survival are determined by reproduction. Most plants, including the model species *Arabidopsis thaliana*, show a delay in flowering in response to salt stress (Li et al., 2007). Flowering time in Arabidopsis is determined by two major pathways: the endogenous pathway, mainly regulated by plant age and the photoperiodic pathway, mainly regulated by daylength (as reviewed in Kinoshita & Richter, 2020). Salinity, like many other abiotic stresses, affects the photoperiodic pathway. The key players of the photoperiodic pathway are CONSTANS (CO), GIGANTEA (GI) and FLOWERING LOCUS T (FT). FT is known as the key flowering signal traveling from the leaf to the meristem, where it initiates the floral transition (Jaeger & Wigge, 2007). Induction of *FT* expression is regulated by CO (Adrian et al., 2010; Samach et al., 2000), which is in its turn regulated by GI, part of the circadian clock regulatory network (Sawa, Nusinow, Kay, & Imaizumi, 2007). High salinity degrades GI, preventing it from promoting *CO* transcription and subsequent *FT* activation, resulting in a delay in flowering time (Kim et al., 2013). Other studies have shown transcriptional and post-transcriptional regulation of *FT* and its homolog *BFT* by salt stress (Kim and Park, 2007; Kim et al., 2007; Ryu et al., 2011), but our understanding of regulation of flowering by salt stress remains limited.

**A bottom-up approach: the potential of roots in coping with salt stress**

The capacity to maintain a low $Na^+/K^+$ balance in the shoot has been shown to be closely linked to salt tolerance (Møller et al., 2009). Preventing $Na^+$ transport to the shoot is very important for most plant species, including Arabidopsis and several crop species. The root system plays an essential role in preventing $Na^+$ from entering the vascular system and reaching the shoot. Previous research in Arabidopsis accessions collected from diverse habitats has characterized four distinct root response types to salt stress (Julkowska et al., 2014). The differences between these root response strategies largely rely on lateral root formation and elongation. The development of a high number of shorter lateral roots correlated with a lower $Na^+/K^+$ balance in the shoot, indicating that a change in lateral root development can have implications for salt tolerance.

For a long time, crop selection has mainly focused on the shoot for two reasons: (1) the yield of most plants is dependent on aboveground plant organs and (2) belowground root development is hard to observe. Yet, many researchers have suggested that root systems are the optimal target for producing robust crops (Herder et al., 2010; Lynch, 2007). As roots have rarely been selected on, they provide opportunities to increase plant yield and robustness. The root system encounters certain stresses, such as water deficit, nutrient deficiencies and salinity first. As periods of drought are occurring more frequently due to climate change and the soil is getting depleted from nutrients, it is crucial to use the potential that roots hold. For many of these stresses, research has shown that plant root systems can functionally adapt to cope (as reviewed in Koevoets et al., 2016; **Chapter 2**). As new methods to observe the root system are being developed (as reviewed in Atkinson et al., 2019), knowledge on its development and plasticity is rapidly increasing These developments open up new possibilities to improve crop resistance and productivity.

**Auxin: the plant growth hormone**

Phytohormones play a key role in plant development, stress tolerance and defense against pathogens. Most major phytohormones have been recognized to play a role in salt stress signaling and tolerance, including abscisic acid (ABA), jasmonate, ethylene, cytokinins, brassinosteroids, gibberellin and auxin (as reviewed in Ryu and Cho, 2015; Yu et al., 2020). ABA is well known for its role in abiotic stress and especially in osmotic stresses such as drought and salinity (as reviewed in Vishwakarma et al., 2017). Upon exposure to salt stress, ABA accumulates in several tissues including stomata and roots (Waadt et al., 2014), triggering responses, including stomatal closure (Niu et al., 2018) and inhibition of root growth (Duan et al., 2013; Geng et al., 2013). ABA inhibits root development by inhibiting auxin metabolism and disturbing auxin distribution (Ding et al., 2015; Lu et al., 2019). Although an increasing number of studies shows involvement of auxin in responding to and coping with salt stress, its exact role needs further research.

Auxin was one of the first phytohormones discovered and is well described for its role in plant development (as reviewed in Weijers and Wagner, 2016; Vanneste and Friml, 2009). The temporal and spatial pattern of auxin guides many developmental processes including embryogenesis (Jenik and Barton, 2005), root gravitropism (Geisler et al., 2014), lateral root development (Lavenus et al., 2013; Wang and Jiao, 2018) and cell elongation (Masuda, 1990; Christian et al., 2006).

Several compounds have been recognized as auxins based on their effects on plant development. The currently described endogenous auxins are indole-3-butyric acid (IBA), indole-3-propionic acid (IPA), 4-Chloroindole-3-acetic acid (4-Cl-IAA), 2-phenylacetic acid (PAA) and indole-3-acetic acid (IAA) (Korasick et al., 2013; Simon and Petrášek, 2011). IAA is the most abundant endogenous form of auxin and is responsible for the majority of the described effects of auxin on the plant. The biosynthetic pathways of IAA have been under debate for a long time and are still partly unknown (Di et al., 2016; Zhao, 2010). The IPyA pathway is considered the main IAA biosynthesis pathway (Mashiguchi et al., 2011). Whether the other pathways contribute substantially to IAA biosynthesis has been questioned, but increasing evidence shows a role for some of these pathways under specific conditions such abiotic stress. For example, the Brassicaceae specific IAOx pathway has shown to contribute to IAA biosynthesis in heat stress (Zhao et al., 2002).

For years, the paradigm in auxin research has put polar auxin transport central. The accumulation and specific distribution of auxin influx and efflux carriers would redirect auxin to create auxin maxima and gradients responsible for plant development (as reviewed in Habets and Offringa, 2014; Swarup and Bhosale, 2019). Although undoubtingly polar auxin transport plays an important role in plant development, the role of local auxin biosynthesis, especially in stress conditions, is gaining attention (as reviewed in Lv et al., 2019). For example, in aluminum stress, the IPyA pathway is strongly upregulated in the root apex transition zone (Yang et al., 2014). This upregulation leads to accumulation of auxin and subsequent inhibition of root elongation. During salt stress, auxin transport is disturbed (Korver et al., 2018; Liu et al., 2015; **Chapter 6**), and local auxin biosynthesis might be essential for maintaining auxin maxima at sites of lateral root development.

**Tweaking auxin metabolism to survive salt stress – outline of this thesis**

The research presented in this thesis is aimed at unraveling how plants acclimate and adapt to cope with salt stress, with a large focus on belowground development. In Arabidopsis and in some crop species, favorable adaptations to the root system to cope with abiotic stress have been described. For example, deeper rooting in response to drought has been shown favorable for rice (Uga et al., 2013), as it enables reaching for water in deeper layers of the soil. In contrast, in case of phosphate deprivation, plants develop shallow root systems, as phosphate accumulates in the top layer (Pérez-Torres et al., 2008). **Chapter 2** is a further **introduction** to the main concepts in this thesis

regarding root developmental plasticity, by reviewing these functional root responses and their molecular regulation for some of the most common abiotic stresses.

For salinity the best strategy to adapt the root system has yet to be defined. Julkowska et al. (2014) studied natural variation in root system architecture in Arabidopsis accessions in response to salt stress. These accessions displayed four different strategies mainly differing in the balance between investment in lateral and main root growth. A first indication of a functional response was a lower sodium/potassium ratio in accessions developing many but short lateral roots. In **Chapter 3** we exploit natural variation in Arabidopsis to find new candidate genes regulating lateral root development during salt stress. Genome wide association studies (GWAS) yielded two candidate genes: *HIGH AFFINITY K+ TRANSPORTER 1 (HKT1)* and *CYTOCHROME P450 FAMILY 79 SUBFAMILY B2 (CYP79B2)*. Both influence lateral root development during salt stress.

CYP79B2 converts tryptophan to indole-3-acetaldoxime in the IAOx pathway which leads to production of camalexin, indole glucosinolates and auxin. As the IAOx pathway seems essential for maintaining lateral root development during salt stress, we further investigate this pathway in **Chapter 4**. The metabolic compound indole-3-acetonitrile (IAN) appears to be central in maintaining lateral root development during salt stress. We show two possible biosynthetic pathways of IAN: as a breakdown product of indole glucosinolates which we show to accumulate during salt stress, or through direct biosynthesis from IAOx by a novel candidate enzyme CYP71A19, further characterized in this chapter. As we could not directly prove a role for IAA, we suggest IAN might itself influence auxin signaling by binding the TIR1 receptor, as proposed in a previous study (Katz et al., 2015).

Although the root system is the first part of the plant to encounter salt stress, aboveground plant development and timing of flowering also largely determine yield. In **Chapter 5** we again use GWAS, this time to find candidate genes involved in the timing of flowering in response to salt stress. We show that early flowering in response to salt stress is rarely observed and almost all studied accessions are delayed in flowering. Again, auxin metabolism seems to play a major role, as natural variation in the promoter of *UDP-glycosyltransferase 74E2 (UGT74E2)*, an IBA conjugase, correlates with the extent of delay in bolting in salt stress.

In summary, this thesis illustrates that salt induced changes in both above and belowground development are guided by changes in auxin metabolism. **Chapter 6** integrates the current knowledge on both auxin transport and auxin metabolism during salt stress. We argue that both components should be studied together, and that mathematical modelling will be critical to understand how auxin patterns change and influence plant development during stress. **Chapter 7** continues the **discussion** by summarizing our results and providing future directions. Here, I also take one step back, looking at the upstream regulation of auxin metabolism under salt stress, and one step forward, discussing how altered root development might lead to salt tolerance.

## REFERENCES

**Atkinson, J.A., Pound, M.P., Bennett, M.J., and Wells, D.M.** (2019). Uncovering the hidden half of plants using new advances in root phenotyping. Curr. Opin. Biotechnol. **55**: 1–8.

**Benito, B., Haro, R., Amtmann, A., Cuin, T.A., and Dreyer, I.** (2014). The twins K+ and Na+ in plants. J. Plant Physiol. **171**: 723–731.

**Chaves, M.M., Flexas, J., and Pinheiro, C.** (2009). Photosynthesis under drought and salt stress: Regulation mechanisms from whole plant to cell. Ann. Bot. **103**: 551–560.

**Christian, M., Steffens, B., Schenck, D., Burmester, S., Böttger, M., and Lüthen, H.** (2006). How does auxin enhance cell elongation? Roles of auxin-binding proteins and potassium channels in growth control. Plant Biol. **8**: 346–352.

**Di, D.W., Zhang, C., Luo, P., An, C.W., and Guo, G.Q.** (2016). The biosynthesis of auxin: how many paths truly lead to IAA? Plant Growth Regul. **78**: 275–285.

**Ding, Z.J., Yan, J.Y., Li, C.X., Li, G.X., Wu, Y.R., and Zheng, S.J.** (2015). Transcription factor WRKY46 modulates the development of Arabidopsis lateral roots in osmotic/salt stress conditions via regulation of ABA signaling and auxin homeostasis. Plant J. **84**: 56–69.

**Duan, L., Dietrich, D., Ng, C.H., Chan, P.M.Y., Bhalerao, R., Bennett, M.J., and Dinneny, J.R.** (2013). Endodermal ABA signaling promotes lateral root quiescence during salt stress in Arabidopsis seedlings. Plant Cell **25**: 324–41.

**Geisler, M., Wang, B., and Zhu, J.** (2014). Auxin transport during root gravitropism: Transporters and techniques. Plant Biol. **16**: 50–57.

**Geng, Y., Wu, R., Wee, C.C.W., Xie, F., Wei, X., Chan, P.M.Y., Tham, C., Duan, L., and Dinneny, J.R.** (2013). A spatio-temporal understanding of growth regulation during the salt stress response in Arabidopsis. Plant Cell **25**: 2132–54.

**Habets, M.E.J. and Offringa, R.** (2014). PIN-driven polar auxin transport in plant developmental plasticity: A key target for environmental and endogenous signals. New Phytol. **203**: 362–377.

**Herder, G. Den, Van Isterdael, G., Beeckman, T., De Smet, I., Isterdael, G. Van, Beeckman, T., and Smet, I. De** (2010). The roots of a new green revolution. Trends Plant Sci. **15**: 600–607.

**Ivushkin, K., Bartholomeus, H., Bregt, A.K., Pulatov, A., Kempen, B., and de Sousa, L.** (2019). Global mapping of soil salinity change. Remote Sens. Environ. **231**: 111260.

**Jenik, P.D. and Barton, M.K.** (2005). Surge and destroy: The role of auxin in plant embryogenesis. Development **132**: 3577–3585.

**Julkowska, M.M., Hoefsloot, H.C.J., Mol, S., Feron, R., de Boer, G.-J., Haring, M. a, and Testerink, C.** (2014). Capturing Arabidopsis root architecture dynamics with ROOT-FIT reveals diversity in responses to salinity. Plant Physiol. **166**: 1387–1402.

**Katz, E., Nisani, S., Yadav, B.S., Woldemariam, M.G., Shai, B., Obolski, U., Ehrlich, M., Shani, E., Jander, G., and Chamovitz, D.A.** (2015). The glucosinolate breakdown product indole-3-carbinol acts as an auxin antagonist in roots of Arabidopsis thaliana. Plant J. **82**: 547–555.

1

**Kim, S.G., Kim, S.Y., and Park, C.M.** (2007). A membrane-associated NAC transcription factor regulates salt-responsive flowering via FLOWERING LOCUS T in Arabidopsis. Planta **226**: 647–654.

**Kim, S.G. and Park, C.M.** (2007). Membrane-mediated salt stress signaling in flowering time control. Plant Signal. Behav. **2**: 517–518.

**Kim, W.Y. et al.** (2013). Release of SOS2 kinase from sequestration with GIGANTEA determines salt tolerance in Arabidopsis. Nat. Commun. **4**: 1312–1357.

**Kinoshita, A. and Richter, R.** (2020). Genetic and molecular basis of floral induction in Arabidopsis thaliana. J. Exp. Bot. **71**: 2490–2504.

**Koevoets, I.T., Venema, J.H., Elzenga, J.T.M., and Testerink, C.** (2016). Roots Withstanding their Environment: Exploiting Root System Architecture Responses to Abiotic Stress to Improve Crop Tolerance. Front. Plant Sci. **07**: 1335.

**Korasick, D.A., Enders, T.A., and Strader, L.C.** (2013). Auxin biosynthesis and storage forms. J. Exp. Bot. **64**: 2541–2555.

**Korver, R.A., Koevoets, I.T., and Testerink, C.** (2018). Out of Shape During Stress: A Key Role for Auxin. Trends Plant Sci. **23**: 783–793.

**Lavenus, J., Goh, T., Roberts, I., Guyomarc'h, S., Lucas, M., De Smet, I., Fukaki, H., Beeckman, T., Bennett, M., and Laplaze, L.** (2013). Lateral root development in Arabidopsis: Fifty shades of auxin. Trends Plant Sci. **18**: 1360–1385.

**Li, K., Wang, Y., Han, C., Zhang, W., Jia, H., and Li, X.** (2007). GA signaling and CO/FT regulatory module mediate salt-induced late flowering in Arabidopsis thaliana. Plant Growth Regul. **53**: 195–206.

**Liu, W., Li, R.-J., Han, T.-T., Cai, W., Fu, Z.-W., and Lu, Y.-T.** (2015). Salt Stress Reduces Root Meristem Size by Nitric Oxide-Mediated Modulation of Auxin Accumulation and Signaling in Arabidopsis. Plant Physiol. **168**: 343–356.

**Lu, C., Chen, M.X., Liu, R., Zhang, L., Hou, X., Liu, S., Ding, X., Jiang, Y., Xu, J., Zhang, J., Zhao, X., and Liu, Y.G.** (2019). Abscisic acid regulates auxin distribution to mediate maize lateral root development under salt stress. Front. Plant Sci. **10**: 1–16.

**Lv, B., Yan, Z., Tian, H., Zhang, X., and Ding, Z.** (2019). Local Auxin Biosynthesis Mediates Plant Growth and Development. Trends Plant Sci. **24**: 6–9.

**Lynch, J.P.** (2007). Turner review no. 14 Roots Second green Revolut. Aust J Bot **55 SRC**-: 493–512.

**Mashiguchi, K. et al.** (2011). The main auxin biosynthesis pathway in Arabidopsis. Proc. Natl. Acad. Sci. **108**: 18512–18517.

**Masuda, Y.** (1990). A u x i n - I n d u c e d Cell Elongation and Cell Wall C h a n g e s. Bot. Mag. **103**: 345–370.

**Møller, I.S., Gilliham, M., Jha, D., Mayo, G.M., Roy, S.J., Coates, J.C., Haseloff, J., and Tester, M.** (2009). Shoot Na+ exclusion and increased salinity tolerance engineered by cell type-specific alteration of Na+ transport in Arabidopsis. Plant Cell **21**: 2163–2178.

**Munns, R. and Gilliham, M.** (2015). Salinity tolerance of crops - what is the cost ? New Phytol.: 668–273.

**Munns, R., James, R.R.A., Lauchli, A., and Láuchli, A.** (2006). Approaches to increasing the salt tolerance of wheat and other cereals. J. Exp. Bot. **57**: 1025–1043.

**Niu, M., Xie, J., Chen, C., Cao, H., Sun, J., Kong, Q., Shabala, S., Shabala, L., Huang, Y., and Bie, Z.** (2018). An early ABA-induced stomatal closure, Na + sequestration in leaf vein and K + retention in mesophyll confer salt tissue tolerance in Cucurbita species. J. Exp. Bot. **69**: 4945–4960.

**Pérez-Torres, C.A., López-Bucio, J., Herrera-Estrella, L., Cruz-Ramírez, A., Ibarra-Laclette, E., Dharmasiri, S., Estelle, M., and Herrera-Estrella, L.** (2008). Phosphate Availability Alters Lateral Root Development in Arabidopsis by Modulating Auxin Sensitivity via a Mechanism Involving the TIR1 Auxin Receptor. Plant Cell **20**: 3258–3272.

**Roy, S.J., Negrao, S., and Tester, M.** (2014). Salt resistant crop plants. Curr. Opin. Biotechnol. **26**: 115–124.

**Ryu, H. and Cho, Y.G.** (2015). Plant hormones in salt stress tolerance. J. Plant Biol. **58**: 147–155.

**Ryu, J.Y., Park, C., and Seo, P.J.** (2011). The Floral Repressor BROTHER OF FT AND TFL1 ( BFT ) Modulates Flowering Initiation under High Salinity in Arabidopsis.: 295–303.

**Simon, S. and Petrášek, J.** (2011). Why plants need more than one type of auxin. Plant Sci. **180**: 454–460.

**Slama, I., Abdelly, C., Bouchereau, A., Flowers, T., and Savouré, A.** (2015). Diversity, distribution and roles of osmoprotective compounds accumulated in halophytes under abiotic stress. Ann. Bot. **115**: 433–447.

**Swarup, R. and Bhosale, R.** (2019). Developmental Roles of AUX1/LAX Auxin Influx Carriers in Plants. Front. Plant Sci. **10**: 1–14.

**Trovato, M., Forlani, G., Signorelli, S., and Funck, D.** (2019). Proline Metabolism and Its Functions in Development and Stress Tolerance. In Osmoprotectant-Mediated Abiotic Stress Tolerance in Plants: Recent Advances and Future Perspectives, M.A. Hossain, V. Kumar, D.J. Burritt, M. Fujita, and P.S.A. Mäkelä, eds (Springer International Publishing: Cham), pp. 41–72.

**Uga, Y. et al.** (2013). Control of root system architecture by DEEPER ROOTING 1 increases rice yield under drought conditions. Nat. Genet. **45**: 1097–102.

**Vanneste, S. and Friml, J.** (2009). Auxin: A Trigger for Change in Plant Development. Cell **136**: 1005–1016.

**Vishwakarma, K., Upadhyay, N., Kumar, N., Yadav, G., Singh, J., Mishra, R.K., Kumar, V., Verma, R., Upadhyay, R.G., Pandey, M., and Sharma, S.** (2017). Abscisic acid signaling and abiotic stress tolerance in plants: A review on current knowledge and future prospects. Front. Plant Sci. **8**: 1–12.

**Waadt, R., Hitomi, K., Nishimura, N., Hitomi, C., Adams, S.R., Getzoff, E.D., and Schroeder, J.I.** (2014). FRET-based reporters for the direct visualization of abscisic acid concentration changes and distribution in Arabidopsis. Elife **2014**: 1–28.

**Wakeel, A., Farooq, M., Qadir, M., and Schubert, S.** (2011). Potassium substitution by sodium in plants. CRC. Crit. Rev. Plant Sci. **30**: 401–413.

**Wang, Y. and Jiao, Y.** (2018). Auxin and above-ground meristems. J. Exp. Bot. **69**: 147–154.

**Weijers, D. and Wagner, D.** (2016). Transcriptional Responses to the Auxin Hormone. Annu. Rev. Plant Biol. **67**: 539–574.

1

**Yamaguchi, T. and Blumwald, E.** (2005). Developing salt-tolerant crop plants: Challenges and opportunities. Trends Plant Sci. **10**: 615–620.

**Yang, Z.-B., Geng, X., He, C., Zhang, F., Wang, R., Horst, W.J., and Ding, Z.** (2014). TAA1-Regulated Local Auxin Biosynthesis in the Root-Apex Transition Zone Mediates the Aluminum-Induced Inhibition of Root Growth in *Arabidopsis*. Plant Cell **26**: 2889–2904.

**Yu, Z., Duan, X., Luo, L., Dai, S., Ding, Z., and Xia, G.** (2020). How Plant Hormones Mediate Salt Stress Responses. Trends Plant Sci. **25**: 1117–1130.

**Van Zelm, E., Zhang, Y., and Testerink, C.** (2020). Salt Tolerance Mechanisms of Plants. Annu. Rev. Plant Biol. **71**: 403–433.

**Zhao, Y.** (2010). Auxin Biosynthesis and Its Role in Plant Development. Annu. Rev. Plant Biol. **61**: 49–64.

**Zhao, Y., Hull, A.K., Gupta, N.R., Goss, K.A., Alonso, J., Ecker, J.R., Normanly, J., Chory, J., and Celenza, J.L.** (2002). Trp-dependent auxin biosynthesis in Arabidopsis: involvement of cytochrome P450s CYP79B2 and CYP79B3. Genes Dev. **16**: 3100–3112.

**CHAPTER 2**

# Roots withstanding their environment: exploiting root system architecture responses to abiotic stress to improve crop tolerance

Iko Koevoets[1] | Jan Henk Venema[2] | J. Theo M. Elzenga[2] | Christa Testerink[1]

[1]University of Amsterdam, Swammerdam Institute for Life Sciences, Plant Cell Biology. Postbus 94215, 1090 GE Amsterdam, the Netherlands
[2]University of Groningen, Genomics Research in Ecology & Evolution in Nature (GREEN) - Plant Physiology, Groningen Institute for Evolutionary Life Sciences (GELIFES), P.O. Box 11103, 9700 CC Groningen, The Netherlands

**ABSTRACT**

To face future challenges in crop production dictated by global climate changes, breeders and plant researchers collaborate to develop productive crops that are able to withstand a wide range of biotic and abiotic stresses. However, crop selection is often focused on shoot performance alone, as observation of root properties is more complex and asks for artificial and extensive phenotyping platforms. In addition, most root research focuses on development, while a direct link to the functionality of plasticity in root development for tolerance is often lacking.

In this paper we review the currently known root system architecture (RSA) responses in Arabidopsis and a number of crop species to a range of abiotic stresses, including nutrient limitation, drought, salinity, flooding and extreme temperatures. For each of these stresses, the key molecular and cellular mechanisms underlying the RSA response are highlighted. To explore the relevance for crop selection, we especially review and discuss studies linking root architectural responses to stress tolerance. This will provide a first step towards understanding the relevance of adaptive root development for a plant's response to its environment. We suggest that functional evidence on the role of root plasticity will support breeders in their efforts to include root properties in their current selection pipeline for abiotic stress tolerance, aimed to improve the robustness of crops.

## INTRODUCTION

*From optimal to suboptimal conditions – closing the yield gap*
The world population is growing rapidly and this is accompanied by an increased food demand. In past decades, this growing food demand has been addressed by plant breeding consistent with optimal conditions for plant growth. In agricultural practices, the use of fertilizers, irrigation, pesticides and other inputs can create these optimal conditions on the short-term. However, increasing evidence exists for the negative consequences of these practices on the long-term.

First of all, irrigation accounts for almost 70% of all freshwater usage in the world (FAO and ITPS, 2015). Freshwater scarcity is a big threat to the human population and the current water usage for agriculture is not sustainable (Rosegrant et al., 2009). Furthermore, irrigation causes salinization of soils (Smedema and Shiati, 2002) and increases leaching of fertilizer. This leaching, together with excess use of fertilizer and deep tilling leads to higher greenhouse gas emissions (Snyder et al., 2009).

These problems illustrate the unsustainability of creating the optimal conditions for which our crops are selected. In addition, climate change will further increase this challenge. Agriculture will have to deal with growing crops under suboptimal conditions, creating a gap between the yield potential and the currently reached yield – the so-called yield gap. An extensive research field tries to map the current yield gap (Van Ittersum et al., 2013; Licker et al., 2010; Lobell et al., 2009) with much focus on improving land management practices (Lobell et al., 2009; Mueller et al., 2012). In concert, plant breeding is shifting from creating "specialist" cultivars that require optimal conditions for their performance towards creating "robust" cultivars that can perform optimal in a broad range of suboptimal conditions, with the ultimate goal of closing the yield gap.

Crop yield is driven by the combination of climate, soil, management and genetics. Under optimal circumstances the soil provides plants with stability, water and nutrients. However, soils are heterogeneous environments, strongly influenced by outside factors. Nutrient deficiency, drought, salinity, flooding and temperature are major drivers of the current and future yield gap. Researchers and breeders work together to develop crops that are able to withstand these stresses (as reviewed in Mickelbart et al., 2015). However, most current selection is focused on the shoot, whereas most major drivers of the yield gap affect soil properties, directly influencing the root system. This paper will therefore focus on the potential of optimizing root systems for improving crop abiotic stress tolerance.

*Roots bridging the yield gap*

Breeding efforts to improve crop yield are in general focused on aboveground, shoot-related phenotypes, whereas the roots as 'hidden half' of the plant are still an under-utilized source of crop improvement (Herder et al., 2010; Wachsman et al., 2015). Trials aimed to select for new cultivars with improved crop yield are in general performed under optimal nutrient concentrations, which has often led to selection for smaller and less plastic roots (White et al., 2013). Moreover, modern cultivars develop in general faster and the earlier initiation of shoot sinks stimulates the investment of biomass into the shoots rather than into the roots. Modern wheat cultivars indeed have smaller root sizes and root:shoot ratios than older ones (Siddique et al., 1990; Waines and Ehdaie, 2007). Given the crucial role roots play in the establishment and performance of plants, researchers have started 'the second green revolution' to explore the possibility of yield improvements through optimization of root systems (Lynch, 2007).
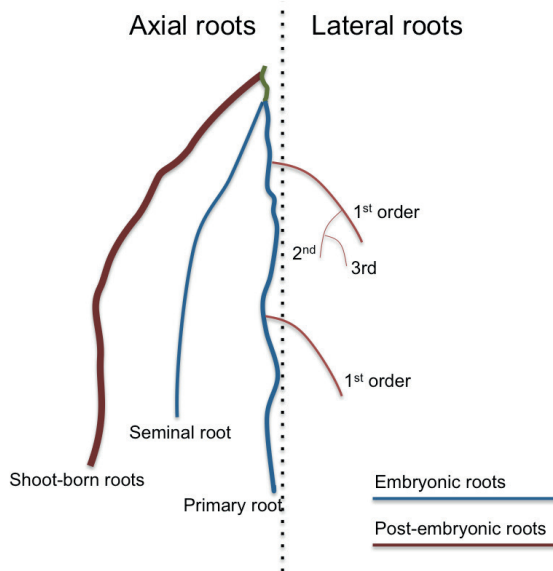


**Figure 1.** An overview of the different root types that together form the root system. A dicot root system consists only of one primary root and several orders of lateral roots. In addition, dicots can produce special stress-induced shoot-born roots called adventitious roots. A monocot root system produces additional axial roots, which can be separated in embryonic seminal roots and non-embryonic shoot-born roots. There are several types of shoot-borne roots, such as nodal and crown roots, often distinguished by the exact place they develop and their increasing thickness. In monocots, the primary and seminal roots are especially important during early seedling establishment but shoot-born roots soon take over and are responsible for most of the water and nutrient uptake. All axial root types can produce several orders of lateral roots.

Because water and nutrients are not evenly distributed in the soil, the spatial arrangement of the root system is crucial for optimal use of the available resources. This spatial arrangement of the root and its components is referred to as root system architecture

(RSA). Length, number, positioning and angle of root components (as described in Figure 1) together determine RSA (Figure 2). These traits determine the soil volume that is explored. In addition, the root surface area depends on root hair development and root diameter. The ability to adjust RSA is an important aspect of plant performance and its plasticity to a large variety of abiotic conditions (Smith and De Smet, 2012). Root development is guided by environmental information that is integrated into decisions regarding how fast and in which direction to grow, and where and when to develop new lateral roots (Malamy, 2005). The limits of root system plasticity are determined by intrinsic pathways governed by genetic components (Gifford et al., 2013; Jung and McCouch, 2013; Pigliucci, 2005; Smith and De Smet, 2012). Understanding the development and architecture of roots, as well its plasticity, holds thus great potential for stabilizing the productivity under suboptimal conditions in the root environment (de Dorlodot et al., 2007; Herder et al., 2010; Zhu et al., 2011). Although plants are capable of adjusting a wide range of developmental and molecular processes in the root to cope with abiotic stress, this review will mainly focus on the plasticity of RSA, their proposed adaptive values, and its use in the selection and breeding of more robust crops.

2
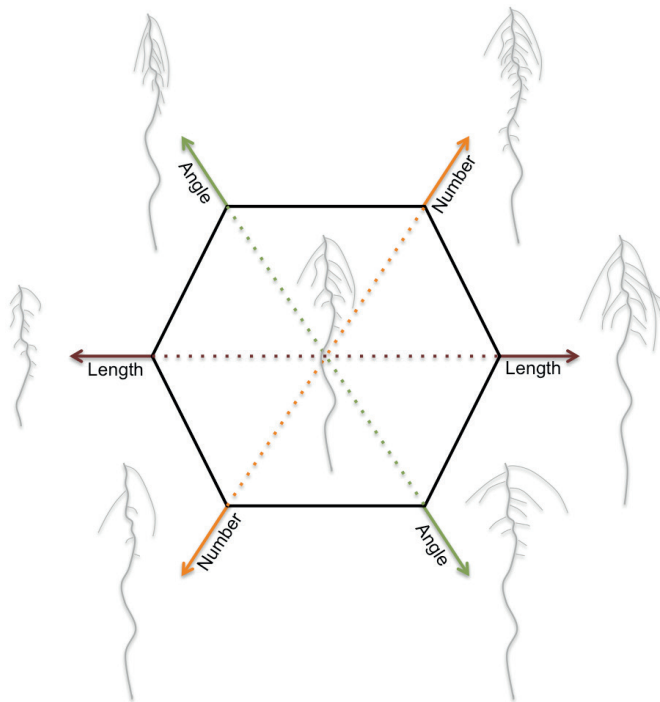


**Figure 2.** RSA is defined as the spatial configuration of root components and determines the soil volume that can be explored by the roots. Dicot roots consist of a main root and several orders of lateral roots. Monocot roots contain in addition seminal roots and shoot-borne roots. Each plant species has genetically defined limits to its RSA. Within these limits, the RSA is plastic and external (abiotic stress) factors modulate the length, number, positioning and angle of root components. The RSA plasticity varies strongly among and within plant species. This figure illustrates the modulations in RSA for a typical dicot root system.

**Nutrient limitation: adapting RSA for optimal foraging**

Plants use macronutrients as the basis of proteins and nucleic acids. Especially the availability of phosphorus (P) and nitrogen (N) determine plant performance. Other nutrients are used as co-factors for enzymes or to drive membrane transport. Complications in nutrient acquisition can arise because of nutrient shortage in the soil, but other factors such as pH, the balance of different nutrients and soil composition also play a role. For examples, high salinity can decrease the solubility and thus availability of phosphate (Grattan and Grieve, 1998; Hu and Schmidhalter, 2005).

Nutrient deficiencies are responsible for the major part of currently observed yield gaps worldwide. Mueller et al. (2012) estimated that for 73% of the areas with a yield gap bigger than 25%, solely improving nutrient balances in the soil could close this gap. This illustrates the impact of nutrient imbalances and deficiencies on plant productivity. If we also consider the high use of fertilizer in agriculture, improving plant capability of dealing with nutrient deficiencies and increasing the plants ability of nutrient acquisition is of major importance.

Nutrients are distributed heterogeneously and often have a strong vertical distribution pattern. Leaching on the one hand and plant cycling on the other hand influence the nutrient distribution pattern. Leaching is caused by vertical water flow and takes nutrients down to lower soil layers, were water flow decreases and nutrients accumulate. Plant cycling is based on nutrients taken up from and cycled back to the soil, which causes nutrients to deplete in the root zone and accumulate in the topsoil. Horizontal distribution of nutrients is mainly dependent on the plant distribution aboveground, leading to higher nutrient accumulation underneath canopies. Vertical distribution depends on the balance between leaching and plant cycling, which differs strongly between nutrients. Low mobile nutrients with a prominent role in plant growth, such as phosphate and potassium, undergo high plant cycling, leading to topsoil accumulation. In contrast, mobile nutrients, such as nitrate and chloride, are subject to leaching leading to accumulation in deeper soils (Jobbágy and Jackson, 2001, 2004). The challenge for plants is to cope with this heterogeneous and sometimes contrasting distribution of nutrients and other resources. In agriculture, plant cycling is often reduced, due to harvesting of plant material, increasing leaching and loss of nutrients. To cope with this heterogeneity, plants can adapt their RSA to specifically forage those parts of the soils where nutrient availability is high.

Recently, RSA changes upon a wide range of nutrient deficiencies have been mapped in Arabidopsis growing on agar plates (Gruber et al., 2013). Each deficiency led to a distinct response in RSA development, which is consistent with the fact that not all nutrients have the same accumulation pattern and thus ask for a different response. For example, the readily available forms of the two most limiting nutrients, nitrate ($NO_3^-$) and phosphate ($PO_4^{3-}$), have an almost opposite accumulation pattern in the soil (Jobbágy and Jackson, 2001). Whereas immobile phosphate accumulates in the topsoil, mobile nitrate quickly leaches to deeper soils. This challenges the plant to respond differently to a deficiency in these nutrients. Fortunately, the RSA responses to

these deficiencies have been mapped extensively in both Arabidopsis and crop species, offering us many insights in functional RSA development.

*Topsoil foraging for phosphate*
Phosphate is a building block of, for example, nucleic acids and membrane phospholipids. Because of the high phosphate demand of plants, limitation in phosphate has a strong effect on plant growth (as reviewed in López-Arredondo et al., 2014; Péret et al., 2011). Efficient uptake of phosphate is therefore essential. High plant cycling, in combination with low mobility, leads to accumulation of phosphate in the topsoil. To optimally forage the soil for phosphate, plants need to develop a shallow root system (as reviewed in Lynch and Brown, 2001). The RSA response to phosphate deficiency in Arabidopsis is well characterized (as reviewed by Péret et al., 2011). A strong shift from main root growth to lateral root growth is observed, which leads to a short root with a high number of long laterals (figure 3A; Gruber et al., 2013; Linkohr et al., 2002; López-Bucio et al., 2002; Williamson, 2001). In addition, a strong proliferation of root hairs is observed. These changes result in a shallow root system, optimal for topsoil foraging.

In maize a series of papers was published in which the value of certain root traits for phosphate acquisition was evaluated using a set of RILS distinctly different in these root traits. Shallow rooting maize varieties showed increased net phosphate acquisition, corrected for possible higher phosphate investments (Zhu et al., 2005b). A big screen of 242 accessions of maize on high and low phosphate availability confirmed the importance of root plasticity under low phosphate conditions (Bayuelo-Jiménez et al., 2011). Yield and biomass was increased for accessions with a higher number of nodal and lateral roots. In addition, dense root hair formation also correlated with higher biomass under low P conditions.

Shallow root system development is a result of strong investment in lateral root growth. Zhu and Lynch (2004) confirmed that in maize enhanced lateral root formation is beneficial for net phosphate acquisition. In comparison to the primary root and other components of the root system, lateral roots are cheap in terms of phosphate use. Similar results were found for enhanced seminal root growth, which is especially important for phosphate acquisition during early seedling development (Zhu et al., 2006). Several studies show that strigolactones are key regulators of both root and shoot responses to the level of available phosphate (Koltai, 2011; Matthys et al., 2016; Mayzlish-Gati et al., 2012; Ruyter-Spira et al., 2011). The effect of strigolactones on RSA depends on phosphate availability. Whereas strigolactones inhibit lateral root emergence and elongation and promote primary root elongation when phosphate is sufficient (Kapulnik et al., 2011a; Matthys et al., 2016), the opposite is observed when phosphate is depleted (Ruyter-Spira et al., 2011). Interestingly, a similar phosphate dependent effect of ABA on lateral root development has recently been observed (Kawa et al., 2016). The contrasting effect of strigolactones is a result of modulation of auxin distribution and sensitivity (Koltai et al., 2010; Mayzlish-Gati et al., 2012; Ruyter-Spira et al., 2011), both underlying the strong shift from primary to lateral root growth (López-Bucio et al., 2002; Miura et al., 2011; Nacry, 2005; Pérez-Torres et al., 2008a, 2008b). Addition of the synthetic auxin NAA doubled expression levels of genes involved in the cell cycle

**2**

specifically during phosphate starvation (Pérez-Torres et al., 2008b). Increased auxin sensitivity during phosphate starvation appears to be explained by increased expression of the auxin receptor TRANSPORT INHIBITOR RESPONSE1 (TIR1), leading to increased degradation of AUX/IAA and released repression on auxin response modules (Pérez-Torres et al., 2008a). Interestingly, strigolactones have been shown to be responsible for the increase of TIR1 expression during phosphate limitation (Mayzlish-Gati et al., 2012).

The inhibition of primary root growth in Arabidopsis (Col-0) in response to phosphate starvation has been shown to be strong and irreversible (Sánchez-Calderón et al., 2005). During phosphate starvation, primary root development changes drastically, shifting from indeterminate growth to determinate growth (Kawa et al., 2016; Sánchez-Calderón et al., 2005). Preceding this drastic shift, changes in the quiescence center are observed, suggesting an important role during phosphate starvation. Consistently, Svistoonoff et al. (2007) show that specifically exposing the root cap to low phosphate is sufficient to induce growth arrest in the primary root. Mutants lacking determinate growth in low phosphate conditions show reduced activation of the phosphate starvation rescue system (Sánchez-Calderón et al., 2006). These findings suggest an important role for the root cap in sensing environmental conditions.

During phosphate limitation, Arabidopsis develops a high number of long root hairs (Bates and Lynch, 1996). Compared to mutants lacking root hairs, wild type plants have a higher phosphate uptake resulting in more plant growth (Bates and Lynch, 2000). Gahoonia and Nielsen (1998) measured phosphate uptake of root hairs by providing the radioisotope $^{32}P$ to root hairs of rye plants in the soil. The root hairs contributed to a substantial amount of 63% of total phosphate uptake. Consistently, a mutant of barley lacking root hairs took up half the amount of phosphate compared to the wild type (Gahoonia et al., 2001). Under low phosphate conditions, cultivars of barley with long root hairs are able to sustain high yields, whereas cultivars with short root hairs produce substantially less yield (Gahoonia and Nielsen, 2004). Interestingly, no disadvantage of root hair development under high phosphate availability is found for either Arabidopsis and Barley (Bates and Lynch, 2000, 2001; Gahoonia and Nielsen, 2004). As for other root traits, strigolactones seem to play a major role in the regulation of the number and length of root hairs (Kapulnik et al., 2011a, 2011b; Koltai et al., 2010; Mayzlish-Gati et al., 2012).

Next to length and number of root components, the angle of the roots also determines whether a root system develops shallow or deep. Roots are able to sense gravity, allowing the main root to grow down into the soil, a response called gravitropism. Although lateral roots are also gravitropic, they typically show a gravitropic setpoint angle (Rosquete et al., 2013; Roychoudhry et al., 2013), resulting in non-vertical emergence from the main root (see also salinity and drought sections). Under low phosphate conditions, gravitropism could be expected to counteract development of a shallow root system ideal for topsoil foraging. In accordance, in common bean, development of a shallow root system depends on the ability to adjust the gravitropic offset angle. This ability indeed correlated with its ability to cope with low phosphate conditions (Bonser et al.,

1995). Subsequent investigation of RILs with contrasting root gravitropic offset angles showed a strong correlation with phosphate acquisition and plant growth (Liao et al., 2004).

*Deep rooting and selective root placement for nitrate*
In contrast to phosphate, nitrate is highly mobile in soils and is therefore prone to leaching. In environments where nitrate is limiting, deeper soil layers can often offer nitrogen supplies. Consistently, availability of phosphate and nitrate has contrasting effects on root system architecture. Low nitrate availability in general limits plant growth. However, low nitrate availability does not limit primary and lateral root elongation, enabling the root system to reach deeper layers of the soil (figure 3B; Gruber et al., 2013; Linkohr et al., 2002). This shift in investment results in an increase in root: shoot ratio. For maize, a monocot species, reaching greater rooting depth requires the development of a lower number of crown roots. Maize genotypes with lower crown root number showed 45% greater rooting depth, which was accompanied with higher N acquisition (Saengwilai et al., 2014). The biggest difference in N acquisition was found in deeper layers, emphasizing the importance of a deep root system for nitrogen acquisition.

Lateral root density is not affected by homogeneous nitrate limitation. Interestingly, in a heterogeneous environment, a strong increase in lateral root density in nitrate patches is observed in both Arabidopsis and maize (Linkohr et al., 2002; in 't Zandt et al., 2015). When plants are exposed to nitrate patches, lateral root elongation rates outside the patches were strongly decreased, indicating a shift of investment of resources. Plants are thus able to selectively place their roots to efficiently forage the soil. The mechanism of utilization of heterogeneously distributed nutrients by selective placement of lateral roots in or near nutrient enriched patches is best studied for nitrogen. However, selective root placement for a wide range of nutrients was already illustrated in 1975. A limited part of the root system of barley was exposed to high concentrations of phosphate, nitrate, ammonium and potassium (Drew, 1975). For all of these nutrients a strong proliferation of lateral roots in the zone of high availability was observed. Growth of lateral roots in other zones was strongly limited. This emphasizes the importance of investigating this response for other nutrients.

The nitrate transporter NRT1.1 plays an important role in perceiving nitrate levels in the soil. The *nrt1.1* mutant displays no increase in lateral root proliferation in nitrate rich patches (Remans et al., 2006a), while the RSA response to homogeneous nitrate limitation is not affected in this mutant, indicating that this is not an effect of reduced nitrate uptake. Interestingly, NRT1.1 has the ability to transport auxin and this transport is inhibited by nitrate (Krouk et al., 2010). Mounier et al. (2014) showed that in nitrate patches, nitrate inhibits auxin transport by NRT1.1 out of lateral root tips and primordia, leading to auxin accumulation and stimulation of lateral root growth. Outside these patches, nitrate levels are low and NRT1.1 prevents accumulation and thus lateral root growth.

NRT1.1 has been shown to affect expression of several downstream genes involved in nitrate starvation responses, including NRT2.1 (Muñoz et al., 2004). NRT2.1 is

2

a major component of high-affinity nitrate uptake in the root (Wirth et al., 2007). NRT1.1 and NRT2.1 seem to be responsible for repression of lateral root growth outside nitrate patches, based on their mutant phenotypes (Krouk et al., 2010; Little et al., 2005; Remans et al., 2006b). Nitrate starvation can trigger ethylene production, a phytohormone that influences root growth (Tian et al., 2009). NRT2.1, also induced by nitrate starvation, seems to stimulate ethylene production (Zheng et al., 2013). Conversely, ethylene inhibits NRT1.1 and NRT2.1 expression, possibly providing a negative feedback loop important for fine tuning responses (Leblanc et al., 2008; Tian et al., 2009).
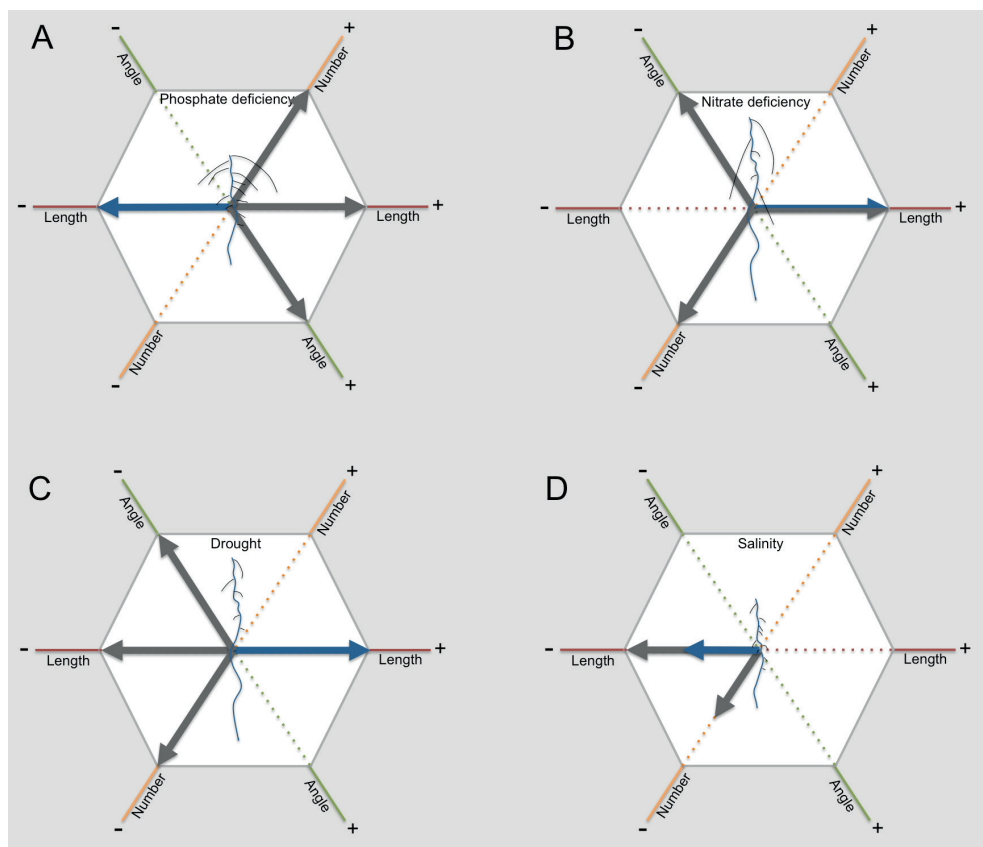


**Figure 3.** The RSA responds to abiotic stress in different ways. This figure illustrates for dicots how length, angle and number of primary (blue) and lateral roots (grey) change in response to phosphate deficiency (A), nitrate deficiency (B), drought (C) and salinity (D). The arrows indicate an either positive (to the right) or negative effect (to the left).

**Drought: Searching for water supplies**

Besides nutrient limitation, water limitation is the biggest driver of the yield gap. Mueller et al. (2012) have shown that in 16% of the areas with a current yield gap bigger then 25%, improving irrigation can solely close the gap. In addition, for all investigated areas improving irrigation would decrease the gap. This illustrates the importance of water availability for plants. Plants need water for transport, structure and photosynthesis among other processes. Most crops have high water requirements and are poorly drought resistant. However, irrigation is already responsible for 70% of the total use of available freshwater (FAO and ITPS, 2015). The present focus of plant breeders therefore is on improving water use efficiency of crops.

When water availability is limited, the soil osmotic potential decreases and plants are confronted with osmotic stress. Plants cannot take up water and sometimes even loose water to the soil. The high surrounding osmotic potential leads to loss of turgor, starting in the root. The combination of rapid sensing and signaling, followed by adjustments on both cellular and organ level, can enable the plant to limit water loss and survive drought stress (as reviewed in Robbins and Dinneny, 2015). Drought stress leads to distinct changes in RSA, both on whole-root system and sub-organ level.

*Whole-root level: deeper rooting for water*
Water is generally stored in deeper soil layers, because the topsoil dries more quickly. Plants that develop deeper root systems will have access to water stored in these deeper layers. Among other traits, deeper rooting has been shown to be beneficial for plant production and survival under water limiting conditions (as reviewed in Comas et al., 2013). For example, the generally deeper rooting mutant *extremely drought tolerant1 (edt1)* in Arabidopsis shows high drought tolerance (Yu et al., 2008). This is explained by the ectopic overexpression of the HD-ZIP transcription factor *HDG11,* which directly promotes the transcription of genes encoding cell wall loosening proteins. These proteins promote cell elongation in the root, leading to an extended root system (Xu et al., 2014). Interestingly, expression of *HDG11* in other species such as rice, poplar and cotton, also confers drought tolerance (Yu et al., 2013, 2016).

Reaching deeper soils requires a shift from investment in lateral roots to investment in axile roots (figure 3C). Arabidopsis shows a strong inhibition of lateral root emergence and elongation when grown on agar medium containing an osmoticum, such as sorbitol or mannitol, mimicking osmotic stress (Deak and Malamy, 2005; Xiong et al., 2006). Importantly, Xiong et al. (2006) showed a possible link between inhibition of lateral root growth on agar and drought tolerance in soil. Mutants performing well under drought conditions in soil, showed high sensitivity to ABA leading to strong inhibition of lateral root length on agar media. In comparison, less tolerant mutants showed no inhibition of lateral root length. ABSCISIC ACID INSENSITIVE4 (ABI4), enhanced by ABA during drought stress, can inhibit PIN1 expression, leading to decreased polar auxin transport and decreased lateral root formation (Rowe et al., 2016; Shkolnik-Inbar and Bar-Zvi, 2010). This mode of action of ABA provides a possible mechanistic explanation for the effect of ABA on lateral root formation.

Polar auxin transport by influx and efflux carriers determines auxin distribution in the root, which is not only important for LR formation, but also for bending of plant organs by differentially affecting cell elongation. This bending is essential for gravitropism of the main root. Positive gravitropism, growing in the direction of gravity, orientates the root downward and enables penetration of the soil. However, other root components, such as lateral, seminal and crown roots can display very different growth angles, partly suppressing gravitropism. The angle of these roots strongly determines whether RSA develops shallow or deep. In lateral roots, PINs determine auxin distribution and thus the gravitropic setpoint angle (GSA) (Rosquete et al., 2013). The magnitude of the difference in auxin concentration between the upper and lower side of the lateral root determine how strong a lateral root will bend (Roychoudhry et al., 2013). As previously described, auxin transport is inhibited during drought stress due to the inhibition of PIN1 expression (Liu et al., 2015), which might facilitate increased downward bending of the roots.

In several crop species increased downward bending of the roots is correlated with drought tolerance. In rice, a strong correlation between the angle of roots and drought tolerance is observed (Kato et al., 2006). High expression of the DEEPER ROOTING1 (DRO1) gene in rice, responsible for increased downward bending of the roots by altering the auxin distribution, results in maintained high yield under drought stress (Uga et al., 2013). This example indicates that adapting RSA, in this case both using genetic and transgenic approaches, can result in increased drought tolerance. Similar to rice, the angle of seminal roots in wheat cultivars also correlates with drought tolerance (Manschadi et al., 2008). Drought tolerant wheat cultivars develop seminal roots with a narrow angle, growing deeper into the soil.

*Sub-organ level: Hydrotropism & Hydropatterning*
Although a strong vertical distribution pattern of water exists, soil heterogeneity in water content exists and sensing of available water is crucial for optimal water uptake. It has been shown that plants are able to partially repress gravitropism and grow towards water, the so-called hydrotropism response (as reviewed in Cassab et al., 2013; Eapen et al., 2005; Takahashi et al., 2009). To investigate hydrotropism in Arabidopsis, different growth systems have been used, in which either salt solutions or agar with sorbitol created a gradient in osmotic potential and thus a gradient in water availability. Arabidopsis was able to redirect growth of its main root away from a low osmotic potential and thus low water availability (Kaneyasu et al., 2007; Moriwaki et al., 2013; Takahashi et al., 2002). This moisture-driven hydrotropic response has also been observed in other species including maize (Takahashi and Scott, 1991), cucumber (Mizuno et al., 2002) and pea (Takahashi and Suge, 1991; Takahashi et al., 1996).

As described previously, the distribution of auxin, driven by polar auxin transport, has a central role in regulating bending of plant organs and response to gravity. Interestingly, hydrotropism seems to be independent from polar auxin transport, as the repression of influx and efflux carriers of auxin do not inhibit the response (Kaneyasu et al., 2007). Recently, auxin distribution during hydrotropism was measured with the DII-VENUS SENSOR (Shkolnik et al., 2016). Indeed, during the first 2 hours of hydrotropic

response, no change in auxin distribution was observed. In the presence of NPA, an inhibitor of auxin transport, hydrotropic bending was not inhibited. The involvement of auxin through changes in auxin sensitivity or biosynthesis remains ellusive, due to contrasting results showing either positive, negative or no effects of inhibition of auxin responses or sensitivity (Kaneyasu et al., 2007; Shkolnik et al., 2016; Takahashi et al., 2002).

It has been shown that Arabidopsis roots can distinguish a wet from a dry surface and selectively favor development of roots in these wet places over development in dry places (Bao et al., 2014). These wet surfaces determine where new lateral root founder cells are formed. Deak and Malamy (2005) have shown that under dry conditions lateral root primordia develop at similar rates as under control conditions. These primordia can subsequently be rapidly induced in zones with high water availability. The combination of formation and emergence of primordia leads to specific root proliferation at sites of high wateravailability, so-called hydropatterning. This process seems to be independent of the major drought stress hormone, ABA (Bao et al., 2014). Further research on this new topic is required to provide more knowledge on how plant roots sense moisture and adjust RSA accordingly.

**Salinity**

Salinity is a major and increasing problem for agriculture (Rengasamy, 2006). Most crop species are salt sensitive and grow poorly on salinized soils (Munns and Tester, 2008; Munns et al., 2006; Sairam and Tyagi, 2004). In 1992, the extent of salinity-affected soils was estimated at 410 billion ha. Although an adequate mapping of the current extent of salinized soils is lacking, over 100 countries are confronted with soil salinization. On a yearly basis between 0.3-1.5 million ha of arable land are lost to salinization and another 20-40 million ha are strongly affected by salinity (FAO and ITPS, 2015). Although some of these are naturally occurring saline soils, current observed salinization is often the result of irrigation practices. Irrigation in arid zones, accounting for approximately 40 percent of irrigation worldwide, mobilizes salts stored in the deeper soil layers (Smedema and Shiati, 2002). In addition, due to freshwater scarcity, an increased use of brackish irrigation increases salt levels even further. The increasing losses of arable land due to salinization ask for the development of salt tolerant crops.

Similar to drought, salinity can cause problems due to the high osmotic potential in the soil, leading to osmotic stress. In addition, salinity affects plant growth due to the toxicity of high sodium levels. $Na^+$ toxicity especially causes problems in the shoot by inhibiting photosynthesis among other processes (Munns, 2002). $Na^+$ is chemically similar to $K^+$ and can interfere with processes in which $K^+$ plays an essential role (Benito et al., 2014). The capacity to maintain a low $Na^+/K^+$ balance in the shoot has been shown to be closely linked to salt tolerance (Møller et al., 2009). Preventing $Na^+$ transport to the shoot is thus very important. The root system is responsible for water uptake, accompanied by dissolved ions including sodium, and thus plays an essential role in preventing $Na^+$ from entering the vascular system and reaching the shoot.

*Remodelling of the root system during salt stress*

Salt has a distinct effect on root growth (as reviewed in Galvan-Ampudia and Testerink, 2011). Although low salt concentrations up to 50 mM can promote plant growth in Arabidopsis (Julkowska et al., 2014; Zhao et al., 2011; Zolla et al., 2010), higher salt concentrations have severe negative effects. Both primary and lateral root growth is inhibited during salt stress (figure 3D; Julkowska et al., 2014). In addition, lateral root number specifically decreases in the root zone developed after exposure to salt stress (figure 3D; Julkowska et al., 2014). Most studies show no effect of salt stress on lateral root density, indicating that the decrease in number of lateral roots is related to the inhibition of primary root growth (Julkowska et al., 2014).

Within seconds after exposure to salt stress, plant signalling is activated. This early signalling leads to adjustments in plant growth (as reviewed in Julkowska and Testerink, 2015), starting with a quiescence of growth in all plant organs. The quiescence phase is caused by a temporary inhibition of mitotic activity, leading to lower cell division rates (West et al., 2004). After the quiescence phase, growth recovers again. However, growth rates only recover to a certain extent, because the inhibition of the cell cycle during the quiescence phase results in fewer cells in the meristem (West et al., 2004). In addition, mature cell length is smaller in salt stressed roots.

Quiescence is induced by abscisic acid (ABA), which is rapidly up-regulated under salt stress due to the decrease in osmotic potential (Duan et al., 2013; Geng et al., 2013; Jia et al., 2002). ABA in general inhibits both gibberellin (GA) and brassinosteroid (BR) signalling (Achard et al., 2006; Gallego-Bartolome et al., 2012) and stress-induced reduction of growth has been shown to benefit the plant (Achard et al., 2006). It is thus proposed that the quiescence phase is essential to induce changes to cope with salt stress. The quiescence phase is followed by a partial growth recovery, that is mainly guided by an increase in GA and BR levels (Geng et al., 2013).

The length of the quiescence phase differs strongly between root components. Whereas quiescence in the main root takes approximately 8 hours, this phase can take up to two days in lateral roots (Duan et al., 2013; Geng et al., 2013). In a similar way, the recovery extent of different organs differs. Although overall an inhibition of root growth is observed, there is a distinct difference between the effects of salt on primary in comparison to lateral root growth. Julkowska et al. (2014) have shown that in Col-0 the relative growth rate of the primary root was more strongly affected than the growth rate of the lateral roots. This indicates that the RSA is remodelled during salt stress. The adaptive value of this remodelling with respect to salinity tolerance is still unclear and requires further research.

In a screen of 32 Arabidopsis accessions, a first indication for a relation between remodelling of RSA during salt stress and salt tolerance was found (Julkowska et al., 2014). The screen revealed four distinct growth strategies during salt stress, depending on the relative inhibition of the number of lateral roots, main root and lateral root growth rates. One of these strategies was correlated with a much lower $Na^+/K^+$ level in the shoot, indicating less sodium uptake and thus a higher tolerance. This strategy is

characterized by a strong inhibition of lateral root growth rates, while main root growth rates and number of lateral roots are much less affected (figure 3D).

Besides remodelling of the root system during salt stress, plants also show reduced gravitropism under saline conditions (Sun et al., 2007). Galvan-Ampudia et al. (2013) showed that plants can specifically redirect growth away from higher salt concentrations, a response called halotropism. This response was observed in Arabidopsis, tomato and sorghum seedlings, both in agar media and in soil. Similar to gravitropism, auxin redistribution is central in regulating halotropism. Endocytosis of PIN2, an auxin efflux carrier, at the side of high salt concentrations, redistributes auxin in the root leading to bending away from salt (Galvan-Ampudia et al., 2013). The redistribution of auxin is supported by the auxin induced expression of AUX1, an auxin influx carrier (van den Berg et al., 2016). Both modelling and experimental data has shown that these processes, together with a transient PIN1 increase, are responsible for the root bending away from salt (van den Berg et al., 2016).

Part of the salinity response is also triggered by osmotic stress and shows overlap with drought responses. However, the changes in RSA show distinct differences. For example, main root growth is strongly promoted during drought, whereas it is inhibited during salt stress. It is not well known whether the above described quiescence phase is also displayed during drought stress. Because the osmotic component of salinity is believed to underlie this response, it is worth investigating. For halotropism and hydrotropism, although similar responses, the underlying mechanisms seem to differ. In contrast to halotropism, hydrotropism has shown to be independent of auxin transport (Kaneyasu et al., 2007). Halotropism is dependent on auxin distribution and occurs only in response to $Na^+$ ions, indicating it is a specific response to high salinity (Galvan-Ampudia et al., 2013; Pierik and Testerink, 2014). For drought stress, the function of changes in RSA has been studied extensively, whereas salinity research has been more focused on the underlying mechanistic principles. In future research, studying the overlaps and differences between these stresses can benefit knowledge in both areas.

Most crop species are highly sensitive to salinity. Tomato serves as a model crop that is widely used to study how salt tolerance can be enhanced in crop species. For a wide range of vegetables, including tomato, grafting is a very effective way to increase crop resistance to biotic and abiotic stresses, without affecting above ground characteristics (see also challenge 3 in section on crop selection). For several salt sensitive commercial tomato cultivars, grafting on root stocks of more tolerant cultivars has positive effects on productivity when exposed to high salinity (Estañ et al., 2005; Martinez-Rodriguez et al., 2008). The $Na^+/K^+$ levels in the shoot (scions) indicated that the other tolerant rootstocks prevented sodium reaching the shoot, illustrating the importance of the root system for salt tolerance. Unfortunately, only little is known about RSA development of crops during salt stress. In rice, rye and maize inhibition of root length has been observed under high salinity (Ogawa et al., 2006; Rahman et al., 2001; Rodriguez et al., 1997). Similar to Arabidopsis, maize shows a quiescence phase in response to exposure to high salinity, followed by recovery (Rodriguez et al., 1997). In rye, the reduction in root growth is related to a reduction in cell division and an increase in cell death (Ogawa

et al., 2006). Further research on remodelling of the root system of crop species will be necessary to use our current knowledge in Arabidopsis to improve crop tolerance to salinity.

## Flooding: anaerobic stress

Already 10% of cultivated land surface is so poorly drained that waterlogging, leading to anoxic conditions in the root zone, causes crop yield losses. Twenty percent of agricultural land in Eastern Europe and the Russian Federation and 16% in the USA are too wet for optimal plant functioning (Setter and Waters, 2003). As climate change is expected to lead to more frequent heavy precipitation during the plant growth season in some areas, these problems will increase. Flooding and hypoxia impose an immediate and dramatic limitation for root function. Limiting the oxygen supply to root cells causes an almost instantaneous arrest of root growth (as reviewed in Gibbs et al., 1998). Switching from aerobic respiration to the glycolytic generation of ATP leads to a severe reduction in energy available for maintenance, growth and ion uptake. Of these three different functions, growth takes 20 to 45% of ATP generated through respiration (Poorter et al., 1991; Scheurwater et al., 1998, 1999; Veen, 1981; van der Werf et al., 1988). Balancing the demand for energy with the reduced production through glycolysis could therefore also cause limiting root growth. Arrest of root growth could, however, also caused by accumulation of products of anaerobic metabolism. A lethal drop in pH of the cytoplasm can occur when protons accumulate in the cytoplasm and the vacuole (Gerendás and Ratcliffe, 2002). In *Phragmites australis* addition of low molecular weight monocarboxylic acids, such as acetic acid, propionic acid, butyric acid and caproic acid, and sulphide, at concentration levels that have been measured *in situ*, arrested root elongation (Armstrong and Armstrong, 2001). As the rate of root elongation is one of the most important parameters determining nutrient uptake rate (Dunbabin, 2006; Silberbush and Barber, 1983), flooding-induced inhibition of root growth ultimately would lead to nutrient limitation and negatively impact the survival of the whole plant.

One of the best-studied adaptations of plants to flooding conditions is the formation of aerenchymatic tissue in the root, which provides an alternative pathway for the supply of oxygen to the root tissue (Gibberd et al., 2001; Jackson and Armstrong, 1999; Rubinigg et al., 2002). This requires that new, well-adapted, adventitious roots are being formed (Visser et al., 1996). In these roots, axial oxygen loss can be kept to a minimum so that the root tip becomes a well-oxygenated micro-climate (Jackson and Armstrong, 1999). Most of the disadvantages for root metabolism imposed by the flooding-induced hypoxic conditions are thereby ameliorated. In monocot plants the formation of new nodal roots, replacing the old seminal roots and often containing aerenchyma, can be stimulated, leading to superficial rooting patterns (Rich and Watt, 2013). If plants are not capable of increasing their oxygen supply through aerenchymous conducts in the root or by placing new roots close to the soil surface where the oxygen level might be higher, survival of flooding is unlikely.

**Temperature**

Temperature is a key abiotic factor involved in seed germination and subsequent root system development during early seedling establishment. The temperature of the soil fluctuates by sinusoidal oscillations on a diurnal scale. However, depending on soil depth, changes in soil temperature are delayed and much lower in amplitude than variations in the atmospheric temperature (Walter et al., 2009). The root-zone temperature thus fluctuates daily, seasonally, and with soil depth (Füllner et al., 2012). Depending on the season and the time of the day, the temperature of the root environment can be significantly different than the atmospheric temperature experienced by the shoots. The root-zone temperature directly affects root development, uptake and upward transport of water and nutrients (Aroca et al., 2001), phytohormone production (Ali et al., 1996; Veselova et al., 2005), which in turn affect water status (Bloom et al., 2004), stomatal conductance (Dodd et al., 2000), photosynthesis (Hurewitz and Janes, 1983), biomass partitioning (Delucia et al., 1992; Engels, 1994), leaf (Poiré et al., 2010) and shoot growth (Sakamoto and Suzuki, 2015; Venema et al., 2008). Plant species clearly differ in their optimal temperature range for root development; e.g. oat 4-7°C (Nielsen et al., 1960), wheat 14-18°C (Porter and Gawith, 1999), pea 15-20°C (Gladish and Rost, 1993), tomato 22-25°C (Gosselin and Trudel, 1984), sunflower 25-30°C (Seiler, 1998), and cotton 32-35°C (Mcmichael et al., 1993). Root:shoot ratios usually increase under unfavourable root-zone temperatures as long as temperature limits for root development are not reached (Engels, 1994; Füllner et al., 2012; Venema et al., 2008). This adaptation in root:shoot ratio may overcome restrictions in water and nutrient uptake due to increased water viscosity and/or decreased root hydraulic conductance (Aroca et al., 2012; Equiza et al., 2001). Global climate change is likely to exacerbate plant abiotic stress in coming decades by increasing fluctuations in soil temperature and (related) water availability (Lynch and Brown, 2012). Breeding crops with a broader temperature root-zone optimum is therefore of significant importance to improve future plant performance. Improved knowledge of the key regulators for RSA optimization would support these breeding efforts.

*Temperature effects on RSA*
The exposure of both mono- and dicot plant roots to temperatures below or above their optimum temperature generally decreases (i) primary root length, (ii) lateral root density (numbers of lateral roots per unit primary root length) and (iii) the angle under which lateral roots emerge from the primary root, whereas the average lateral root length is unaffected (Mcmichael et al., 1993; Nagel et al., 2009; Seiler, 1998). In addition, roots suffering from supraoptimal temperature stress start to initiate 2nd and 3rd order laterals (Pardales et al., 1999) and are characterized by an increased average root diameter (Qin et al., 2007). In general, the modulating effect of sub- and supraoptimal root-zone temperatures (RZT) on RSA development reduces the volume that roots may access for the uptake of water and nutrients. However, root temperature was kept spatially uniform in all these studies. Remarkably, monocot barley plants exposed to a vertical RZT gradient of 20-10°C showed increased shoot and root dry masses of 144 and 297%, respectively, and a 161% increase in root:shoot ratio compared with plants grown at a uniform RZT of 20°C (Füllner et al., 2012). Barley exposed to the

vertical RZT revealed also accelerated tiller formation. The higher root biomass of plants grown at the vertical RZT gradient was not the result of longer roots but was associated with a higher proportion of thicker roots. Additionally, root systems developed under a vertical RZT gradient were much stronger concentrated in the upper 10 cm of the soil substrate gradient and their N and C concentrations were significantly lower than under uniform RZT conditions. These data clearly demonstrate that knowledge gained from experiments with uniform root-zone temperatures cannot simply be extrapolated to the field where roots experience vertical temperature gradients.

The temperature dependence of RSA development shows strong inter- (Lee et al., 2009; Mcmichael et al., 1993) and intraspecific variation (Hund et al., 2007, 2008; Seiler, 1998). The temperature plasticity of the RSA is most extensively studied in maize. In this monocot species, the total lateral root length correlated significantly with improved photosynthesis-related traits and dry matter accumulation at suboptimal growth temperature (Hund et al., 2007). A high density of long lateral roots was therefore regarded as a promising trait to improve early seedling vigour at suboptimal soil temperatures (Hund et al., 2008). Nevertheless, breeding has to focus on optimizing RSA over a broad range of root-zone temperatures as roots also experience temperatures in the optimal- or even supraoptimal range during the entire growth season. At high (root-zone) temperatures the development of long axile roots is of greater importance than lateral roots to facilitate appropriate water uptake from the lower soil layers in times of drought stress (Hund et al. 2008). A schematic overview of general observed effects of non-optimal temperatures on RSA and its adaptations to broaden the root-zone temperature range for optimal plant performance are presented in figure 2.

To optimize RSA over a broader temperature range, Hund et al. (2012) provided the prove-of-concept that hybrids of southern dent and northern flint maize inbred lines, which contrast in temperature dependence of axile and lateral root elongation rates, showed improved rooting potential across the sum of all temperatures. Application of this heterosis effect can lead to hybrids that can perform well in a broader range of temperature conditions, thereby improving the robustness of whole-plant performance.

### Temperature modulation of root elongation
The primary stunting effect of sub- and supraoptimal temperatures on RSA is caused by inhibition of root elongation (Gladish and Rost, 1993; Nagel et al., 2009; Pahlavanian and Silk, 1988; Pardales et al., 1992; Pritchard et al., 1990). In Arabidopsis accessions, the relative decrease in root elongation rates after transfer from 21 to 10°C were not significantly correlated with the average temperature during the growing season of the specific ecotype, suggesting that primary root growth at 10°C is not a key factor in adaptation to colder habitats (Lee et al., 2009). Within tomato, however, the relative inhibition of root elongation and root growth rates at low temperatures were indicative for the difference in chilling tolerance between domestic cultivars and high-altitude accessions of the wild tomato *S. habrochaites* (Venema et al., 2008; Zamir and Gadish, 1987). Dynamic changes in temperature severely affect the elongation rate of root cells rather than the length of the elongation zone (Nagel et al., 2009). In the short-term (hours), inhibition in root cell elongation by low temperature is related to a decrease in

the *in vivo* extensibility of the cell wall (Pritchard et al., 1990). Gravitropism experiments with Arabidopsis roots demonstrated that acute cold stress (4°C) selectively inhibits the basipetal auxin transport due to blocking the intracellular trafficking of a subset of proteins that include auxin efflux carriers (*PIN2* and *PIN3*). As a consequence, auxin accumulates to a level at which root cell elongation is inhibited (Shibasaki et al., 2009). When plant roots have enough time to acclimate to a constant low root-zone temperature (weeks), cell elongation rates increase again and the length of the elongation zone expands (Pahlavanian and Silk, 1988). This may explain the strong linear relationship between temperature and elongation rates of both primary and later roots directly after germination and its disappearance later on during seedling establishment (Aguirrezabal and Tardieu, 1996).
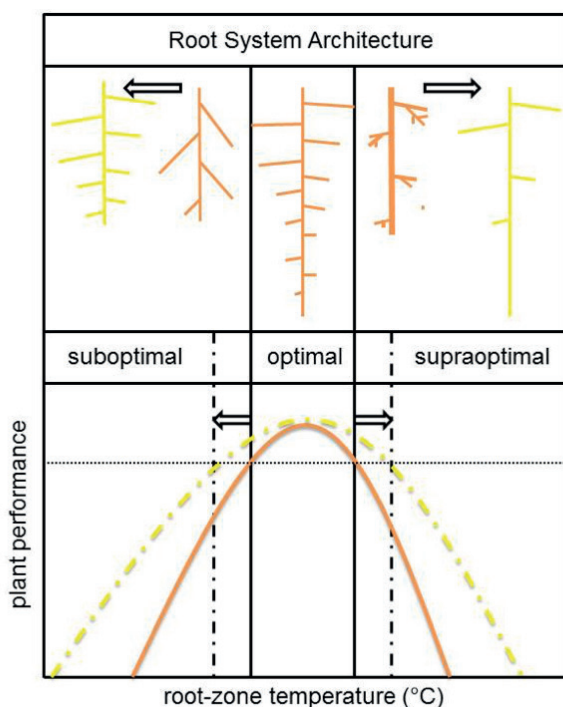


**Figure 4.** Schematic overview of the effect of root-zone temperature on plant performance and underlying general changes in RSA (brown). To broaden the temperature range for optimal plant performance (yellow), plants should invest in lateral root formation (suboptimal temperature range) and/or axile root length (supraoptimal temperature range). The adaptive value of these RSA changes are, respectively, an increased root surface area to improve resource uptake capacity and drought adaptation by penetration to lower soil layers.

Variation in root elongation rates among Arabidopsis accessions correlated at optimal temperature with the production rate of cells within the root meristem (Beemster et al, 2002). Cell production, in turn, was determined by variation in cell cycle duration and, to a lesser extent, by differences in the number of dividing cells. Cell production

rates strongly correlated with the activity of the cyclin-dependent kinase (CDKA). Low temperature decreased the division potential of the root meristem in Arabidopsis by reducing both the meristem size and cell number (Zhu et al., 2015). The repression of the division potential of root meristematic cells at a suboptimal temperature of 16°C could be ascribed to a reduced accumulation of auxin in the root apex. Long-term (7 days) exposure to 16°C inhibited the expression of *PIN1/3/7* and auxin biosynthesis-related genes suggesting that auxin transport and biosynthesis both contribute to the low-temperature mediated reduction of auxin accumulation in roots tips. Root length and meristem cell number of ARABIDOPSIS RESPONSE REGULATOR 1 (*arr1-3*) and 12 (*arr12-1*) cytokinin signalling mutants were much less susceptible to low temperature than wild-type roots. This difference was related to higher *PIN1/3* expression in the mutants, which in turn resulted in a less pronounced reduction in auxin accumulation. These data, together with the results obtained with the cytokinin signalling mutant *ahp1-1 ahp2-1 ahp3*, strongly suggest the involvement of cytokinin signalling in the modulation of RSA development at low temperature (Zhu et al., 2015).

High RZT (40°C) reduced the elongation and cell production rate of Sorghum seminal roots with 14 and 26%, respectively, for every 2 days of exposure (Pardales et al., 1992). In contrast to low temperatures, the underlying inhibitory effects of high temperatures and heat stress on root elongation are poorly studied. The limited information that is available in the literature excludes the involvement of altered IAA transport or levels (Gladish et al., 2000), but supports the involvement of increased ethylene levels (Qin et al., 2007). Inhibitors of ethylene biosynthesis partly alleviated the effect of high RZT on root elongation, stomatal conductance and shoot water status, however, they failed in ameliorating the negative effects on photosynthesis and biomass accumulation. This points to a non-stomatal limitation of photosynthesis mediated by high temperature-induced changes in nutrient uptake (Qin et al., 2007).

## Crop selection on RSA: the challenges

This review presents a number of examples in which plasticity of RSA traits considerably impact a plants' capability to cope with one or more abiotic stresses. These examples emphasize the great potential that selection on RSA traits holds for crop improvement. However, the aboveground focus of crop selection is not without reason. In this concluding section we will discuss three major challenges breeders face when applying selection for RSA in their crop improvement programs and possible ways to tackle these.

### Challenge 1: High throughput belowground screening
The most prominent challenge for crop selection on RSA is uncovering the hidden world of plant roots. Whether crops are grown in fields or in greenhouses, roots are usually grown in a substrate, which prevents easily screening their properties. The growth substrate also greatly affects how roots develop. The currently most common method to investigate RSA, growth on agar medium, is very artificial. Most often roots grow in light, with an excess of sucrose, in 2D and the humidity inside the petri dish is almost saturated. Effort is taken to improve this system, for example by shielding

the roots from light (Silva-Navas et al., 2015). Although agar media provide an easy, adequate and cheap method that can be used for research on Arabidopsis in the lab, its use in crop selection is not straightforward.

In the last decade a wide range of new and improved methods to research roots in a more natural environment have been developed (as reviewed in Downie et al., 2014; Judd et al., 2015; Kuijken et al., 2015; Zhu et al., 2011)). Most systems are based on either a transparent growth medium or a medium from which the roots can easily be removed without damage. Agar and other gel-like mediums are suited for imaging during growth, although the resistance of the medium influences root growth and the humidity in these substances is very high. A good alternative is hydroponics, in which the root is growing inside a nutrient solution (Chen et al., 2011; Le Marié et al., 2014; Mathieu et al., 2015; Tocquin et al., 2003). Hydroponics is also used in greenhouse culture, making it highly relevant for crop selection. This system also eases harvesting roots for different purposes and measuring exudates of roots. However, roots develop very differently, because resistance is lacking and humidity and nutrients are dispersed homogeneously. In addition, a good supply of oxygen is essential to prevent oxidative stress. A third alternative which is also very promising for automated imaging is aeroponics (Ritter et al., 2001; Zobel et al., 1976). In this system roots are grown in water-saturated air created by for example spraying with water and nutrients. This system lacks any material to grow in, which eases imaging. However, without much resistance, roots grow very vast and can have problems extending their root system to the sides against gravity. Last, root systems can be grown inside soil, which is of course most realistic for field crops and many greenhouse crops. However, non-destructive imaging inside soil asks for imaging methods that reach further than a simple camera. Several groups have recently reported the use of X-ray and MRI scans to image roots inside the soil (Mairhofer et al., 2013; Metzner et al., 2015; Mooney et al., 2012; Wang et al., 2015). Although these methods are more expensive, they offer great opportunities for automated imaging. An alternative method is GLO-Roots, based on luminescence genes expressed inside roots (Rellán-Álvarez et al., 2015). This system visualizes the root system through a thin layer of soil. For labs, this is more feasible and also offers the opportunities to image the expression of certain genes in the root system. For root breeding, this is less interesting, because the plants are genetically modified and grown in 2D systems.

As more methods come available to study the root system and also methods are developed suitable for high-throughput screening of root system, the need for good root image analysis software is growing. A wide range of root image analysis software exists (as reviewed in Kuijken et al., 2015; Lobet et al., 2013; Spalding and Miller, 2013). These tools range from automated to non-automated. For a limited amount of data, non-automated software prevents mistakes and gives the user a lot of freedom. However, the analysis is very time consuming and is therefore not suited for large datasets. Automated software can analyse a large dataset rapidly, but especially in complex root systems the analysis is limited to global data such as rooting depth and width. In semi-automated software, such as SmartRoot (Lobet et al., 2011) and EZ-rhizo (Armengaud et al., 2009), the level of user interactions is greater to ensure a lesser degree of analysis errors. Again, this will be more time consuming for larger root systems. In addition, when

observing very large root systems, it is even hard to separate roots by eye. Therefore, the development of new methods of root image analysis has high priority for the field.

Above described methods are all suited for 2D images of root systems. When simplifying root growth to a 2D system, spatial orientation of roots gets lost. Therefore, new methods such as growing roots in gel cylinders (Iyer-Pascuzzi et al., 2010) and using X-ray to image through soil will offer new opportunities to grow and image roots in 3D (as reviewed in Piñeros et al., 2016). Although only limited options for reconstructing and analysing 3D images are currently available, it might eventually be easier to analyse 3D than 2D images, because overlapping and clumping together of roots will be much less common. Developing a good automated imaging analysis set-up of root systems can offer great advancements in crop selection and would be an entirely feasible investment for breeding companies.

*Challenge 2: Dealing with the complexity of interacting stresses*
Although the complexity of the combination of different biotic and abiotic stresses is not restricted to the root system, it does make selecting on RSA more challenging. The described RSA responses are mostly known for single stresses and some of the responses are very contrasting. A good example for this is that in drought-tolerant cultivars with a deep-rooting water-conserving phenotype, less root mass is available to forage for phosphorous at shallow depths (Lynch and Wojciechowski, 2015). Certain stresses tend to occur together often and therefore it might be useful to further investigate the specific RSA response to these conditions. A good example is salt stress and phosphate starvation, as phosphate ions tend to precipitate in saline soils and become unavailable to plants (Grattan and Grieve, 1998; Naidu and Rengasamy, 1993). Both stresses have contrasting effects on several RSA traits and the inhibiting effect of salt on lateral root development might even further limit phosphate uptake. Crucial in crop breeding aimed to optimize RSA is the availability of variation and plasticity in RSA, as observed among Arabidopsis accessions (Mouchel et al., 2004; Ristova et al., 2013; Rosas et al., 2013), related tomato species (Ron et al. 2013) and wheat varieties (Pound et al. 2013). Recently, Kawa et al. (2016) studied the natural variation in the response of 330 Arabidopsis accessions to the combination of salinity and phosphate starvation. In general, responses to salt stress were favoured and especially lateral root growth was strongly inhibited. However, not all accessions showed the same response and this natural variation was associated with 13 genetic candidate loci for integrating the plants' response to combined stress (Kawa et al., 2016). For many crops, however, the natural variation in RSA is currently still underexploited. Moreover, we need to advance our understanding of the adaptive value of genetically determined differences in RSA on the level of crop performance, marketable yield and fruit quality in targeted root environments and growth conditions.

Because the complexity of experiments and screenings increases with every additional variable, modelling can provide very useful tools to support research and breeding. A wide range of plant models on different scales is available to the community. These models should now be integrated with a multiscale modelling approach (Band et al., 2012; Rellán-Álvarez et al., 2016) in which developmental processes, RSA, outside environmental factors and plant performance are connected. Current models, however,

are often not easy to integrate. When developing a model, the general challenge is to make it comprehensive, widely applicable and simple. For models describing RSA, most are falling short in one of these requirements. Some are only applicable for a certain species or stage of life, which limits the use for crop systems. As soon as models tend be more widely applicable or incorporate more conditions, they tend to become more complex and the number of parameters increases. This decreases the ease of interpretation and especially the ease of integration into a larger model (including soil and plant performance models). The last few years, a range of more simple models has been published. These models are often based on a few simple rules. For example, ArchiSimple bases root system development on the fact that the growth rate of a root depends on the thickness of the root (Pagès and Picon-Cochard, 2014; Pagés et al., 2014). By using a simple and widely applicable model, it will be possible to implement models of soil behaviour and of plant productivity. Some of the root models have already been integrated with models for changes in the soil (as reviewed in Dunbabin et al., 2013; Pedersen et al., 2010; Van der Putten et al., 2013) and show to be very promising in predicting the responses of the root system. One example is the ROOTMAP model, which integrates soil-water-nutrient dynamics with root growth responses in a three dimensional system (Dunbabin et al., 2002). Simulations are based on a simple external supply/internal demand principle. The model has shown its use in simulating the efficiency of different RSA types in both heterogeneous phosphate and nitrate supplies (Chen et al., 2008; Dunbabin, 2004). A good example of how such a model can provide valuable information is given by Chen et al. (2008), who show how the model can guide the efficient placement of phosphorus fertiliser. In a similar way, this kind of model could guide in selecting a preferred RSA and potentially even predicting possibly involved processes.

A model that integrates soil behaviour, root system architecture and plant performance will offer a lot of information to breeders. To confirm whether a root system is advantageous under certain stresses as predicted by the model, RILS with contrasting root systems could be exploited (as illustrated in Liao et al., 2004; Zhu and Lynch, 2004; Zhu et al., 2005a). If indeed the predicted root system is advantageous, breeders could screen for this type of root system in a high throughput phenotyping system as described in the previous section. This screen can then be used for determining genes that are involved with this trait and can be used as targets for further selection. The model could also predict whether changing certain root system characteristics would negatively influence productivity. Of course, developing such a model is a major challenge still, but investments in developing a good model will be able to speed up crop selection and could model complex combinations of stresses.

*Challenge 3: Improving RSA without compromising yields*
Crop selection on aboveground traits has lead to high-yielding cultivars and crop selection for a certain RSA may come with costs. The root:shoot ratio is known to increase during almost every abiotic stress that has been discussed in this review. On the other hand, selection on RSA does not equal selection for a bigger root system. Our examples show shifts between different root organs, rather than shifts in biomass partitioning between the shoot and the root. In this way, deeper rooting in rice, caused

by expression of *HDG11*, confers drought tolerance without any yield penalty (Yu et al., 2013, 2016). However, unwanted side effects of selection are not uncommon. An excellent tool to address this problem is to make use of grafting.

Grafting is the process in which the root system (rootstock) of one plant is connected to the shoot (scion) of another (as reviewed in Warschefsky et al., 2016). This process naturally occurs in some tree species (Mudge et al., 2009) and this phenomenon may have triggered the development of grafting in Asia where it is now used in agriculture for over 2000 years to improve plant production (Kubota et al., 2008). In woody perennial crops (Albacete et al., 2015; Warschefsky et al., 2016) as well as in annual vegetable crops (Albacete et al., 2015; Schwarz et al., 2010), the selection and breeding of suitable rootstocks offers a powerful tool to sustain and expand the cultivation under suboptimal growth conditions (Gregory et al., 2013). Grafting has the advantage that not every cultivar needs RSA optimization separately, allowing improvement of rooting and (a)biotic stress tolerance of already existing elite cultivars. As such, grafting is considered as a surgical and fast alternative to breeding. Designing rootstocks for specific environments is becoming a feasible target to face future cultivation problems all around the world associated with global climate change (drought, salinization, occurrence of temperature extremes) (Gregory et al., 2013). Important in this respect is to gain more knowledge of (i) the natural variation in RSA that exists within crops, and (ii) by what communication mechanisms the root(stock) modulates the shoot (scion) phenotype and performance, and visa versa (Warschefsky et al., 2016). In this way, grafting can rapidly advance our understanding of the adaptive value of differences in RSA on the level of shoot performance, marketable yield and fruit quality under targeted growth conditions is grafting.

**The value of model species**

A key aspect for engineering better performing crops via RSA optimization is improved understanding of the regulatory processes and underlying genetic components that regulate root growth. Root growth regulation, and its response to changing environmental conditions, is a highly complicated process that is controlled at many different levels by complex actions of gene networks in both time and space. Advances in this area are merely derived from work in Arabidopsis (as reviewed in Slovak et al., 2016; Wachsman et al., 2015). It is expected that due to the increasing number of highly efficient root phenotyping platforms, the use of GWAS for root traits, the increasing available functional genomics resources for roots, and the development of smart root model systems, much progress in our understanding of control mechanisms involved in root development will be achieved over the next 5-10 years.

Although Arabidopsis is often studied in artificial conditions, it is these conditions that make it possible to investigate the partly discussed mechanistic and cellular base behind the observed RSA responses. For crop species only limited information on these processes is available. Interestingly, most plasticity in RSA responses overlaps between our model species and crops, even independent of differences between monocots and

dicots. Sparsely investigated functionality of RSA in Arabidopsis supports the results found in crops and conversely sparsely investigated molecular insights in crops confirmed results already established in Arabidopsis. Of course, not all mechanisms, responses and genes can be transferred from Arabidopsis to crops, but taken together the reviewed research, Arabidopsis proves to provide very valuable information for the development of crops able to withstand a wide range of abiotic stresses. This review stresses the importance of incorporating RSA into current crop selection, but we should not forget the wonderful tools we already have. Incorporating RSA into current crop selection also means incorporating Arabidopsis research into the current breeding pipeline, possibly even more then for aboveground traits.

## ACKNOWLEDGEMENTS

2

## LITERATURE

Achard, P., Cheng, H., De Grauwe, L., Decat, J., Schoutteten, H., Moritz, T., et al. (2006). Integration of plant responses to environmentally activated phytohormonal signals. *Science* 311, 91–94. doi:10.1126/science.1118642.

Aguirrezabal, L. A. N., and Tardieu, F. (1996). An architectural analysis of the elongation of field-grown sunflower root systems. Elements for modelling the effects of temperature and intercepted radiation. *J. Exp. Bot.* 47, 411–420. doi:10.1093/jxb/47.3.411.

Albacete, A., Martínez-Andújar, C., Martínez-Pérez, A., Thompson, A. J., Dodd, I. C., and Pérez-Alfocea, F. (2015). Unravelling rootstock×scion interactions to improve food security. *J. Exp. Bot.* 66, 2211–2226. doi:10.1093/jxb/erv027.

Ali, I., Kafkafi, U., Yamaguchi, I., Sugimoto, Y., and Inanaga, S. (1996). Effects of low root temperature on sap flow rate, soluble carbohydrates, nitrate contents and on cytokinin and gibberellin levels in root xylem exudate of sand-grown tomato. *J. Plant Nutr.* 19.

Armengaud, P., Zambaux, K., Hills, A., Sulpice, R., Pattison, R. J., Blatt, M. R., et al. (2009). EZ-Rhizo: Integrated software for the fast and accurate measurement of root system architecture. *Plant J.* 57, 945–956. doi:10.1111/j.1365-313X.2008.03739.x.

Armstrong, J., and Armstrong, W. (2001). An overview of the effects of phytotoxins on Pragmites australis in relation to die-back. in *Aquatic Botany*, 251–268. doi:10.1016/S0304-3770(01)00142-5.

Aroca, R., Porcel, R., and Ruiz-Lozano, J. M. (2012). Regulation of root water uptake under abiotic stress conditions. *J. Exp. Bot.* 63, 43–57. doi:10.1093/jxb/err266.

Aroca, R., Tognoni, F., Irigoyen, J. J., Sánchez-Díaz, M., and Pardossi, A. (2001). Different root low temperature response of two maize genotypes differing in chilling sensitivity. *Plant Physiol. Biochem.* 39, 1067–1073. doi:10.1016/S0981-9428(01)01335-3.

Band, L. R., Fozard, J. A., Godin, C., Jensen, O. E., Pridmore, T., Bennett, M. J., et al. (2012). Multiscale systems analysis of root growth and development: modeling beyond the network and cellular scales. *Plant Cell* 24, 3892–906. doi:10.1105/tpc.112.101550.

Bao, Y., Aggarwal, P., Robbins, N. E., Sturrock, C. J., Thompson, M. C., Tan, H. Q., et al. (2014). Plant roots use a patterning mechanism to position lateral root branches toward available water. *Proc. Natl. Acad. Sci. U. S. A.* 111, 9319–24. doi:10.1073/pnas.1400966111.

Bates, T. R., and Lynch, J. P. (1996). Stimulation of root hair elongation in Arabidopsis thaliana by low phosphorus availability. *Plant. Cell Environ.* 19, 529–538. doi:10.1111/j.1365-3040.1996.tb00386.x.

Bates, T. R., and Lynch, J. P. (2000). The efficiency of Arabidopsis thaliana (Brassicaceae) root hairs in phosphorus acquisition. *Am. J. Bot.* 87, 964–970. doi:10.2307/2656995.

Bates, T. R., and Lynch, J. P. (2001). Root hairs confer a competitive advantage under low phosphorus availability. *Plant Soil* 236, 243–250. doi:10.1023/A:1012791706800.

Bayuelo-Jiménez, J. S., Gallardo-Valdéz, M., Perez-Decelis, V. A., Magdaleno-Armas, L., Ochoa, I., and Lynch, J. P. (2011). Genotypic variation for root traits of maize (Zea mays L.) from the Purhepecha Plateau under contrasting phosphorus availability. *F. Crop. Res.* 121, 350–362. doi:10.1016/j.fcr.2011.01.001.

Benito, B., Haro, R., Amtmann, A., Cuin, T. A., and Dreyer, I. (2014). The twins K+ and Na+ in plants. *J. Plant Physiol.* 171, 723–731. doi:10.1016/j.jplph.2013.10.014.

van den Berg, T., Korver, R. A., Testerink, C. S., and ten Tusscher, K. H. W. J. (2016). Modeling halotropism: A key role for root tip architecture and reflux loop remodeling in redistributing auxin. *Development*, dev.135111. doi:10.1242/dev.135111.

Bloom, A. J., Zwieniecki, M. A., Passioura, J. B., Randall, L. B., Holbrook, N. M., and St. Clair, D. A. (2004). Water relations under root chilling in a sensitive and tolerant tomato species. *Plant, Cell Environ.* 27, 971–979. doi:10.1111/j.1365-3040.2004.01200.x.

Bonser, a M., Lynch, J., and Snapp, S. (1995). Effect of Phosphorus Availability on Basal Root-Growth Angle in Bean. *Plant Physiol.* 108, 112. Available at: <Go to ISI>:// A1995RE28900598.

Cassab, G. I., Eapen, D., and Campos, M. E. (2013). Root hydrotropism: An update. *Am. J. Bot.* 100, 14–24. doi:10.3732/ajb.1200306.

Chen, W., Dunbabin, V., Bell, R., Brennan, R., and Bowden, B. (2008). Simulating and understanding root growth using ROOTMAP to guide phosphorus fertiliser placement in wide row lupin cropping systems. in *"Lupins for Health and Wealth' Proaceedings of the 12th International Lupin conference* (Canterbury, New Zealand).

Chen, Y. L., Dunbabin, V. M., Diggle, A. J., Siddique, K. H. M., and Rengel, Z. (2011). Development of a novel semi-hydroponic phenotyping system for studying root architecture. *Funct. Plant Biol.* 38, 355–363. doi:10.1071/FP10241.

Comas, L. H., Becker, S. R., Cruz, V. M. V, Byrne, P. F., and Dierig, D. a (2013). Root traits contributing to plant productivity under drought. *Front. Plant Sci.* 4, 442. doi:10.3389/ fpls.2013.00442.

Deak, K. I., and Malamy, J. (2005). Osmotic regulation of root system architecture. *Plant J.* 43, 17–28. doi:10.1111/j.1365-313X.2005.02425.x.

Delucia, E. H., Heckathorn, S. A., and Day, T. A. (1992). Effects of Soil-Temperature on Growth, Biomass Allocation and Resource Acquisition of Andropogon-Gerardii Vitman. *New Phytol.* 120, 543–549. doi:DOI 10.1111/j.1469-8137.1992.tb01804.x.

Dodd, I. C., He, J., Turnbull, C. G., Lee, S. K., and Critchley, C. (2000). The influence of supra-optimal root-zone temperatures on growth and stomatal conductance in Capsicum annuum L. *J. Exp. Bot.* 51, 239–48. doi:10.1093/jexbot/51.343.239.

de Dorlodot, S., Forster, B., Pagès, L., Price, A., Tuberosa, R., and Draye, X. (2007). Root system architecture: opportunities and constraints for genetic improvement of crops. *Trends Plant Sci.* 12, 474–481. doi:10.1016/j.tplants.2007.08.012.

Downie, H. F. F., Adu, M. O. O., Schmidt, S., Otten, W., Dupuy, L. X. X., White, P. J. J., et al. (2014). Challenges and opportunities for quantifying roots and rhizosphere interactions through imaging and image analysis. *Plant. Cell Environ.*, n/a–n/a. doi:10.1111/ pce.12448.

Drew, M. C. (1975). Comparison of the Effects of a Localised Supply of Phosphate, Nitrate, Ammonium and Potassium on the Growth of the Seminal Root System, and the Shoot, in Barley. *New Phytol.* 75, 479–490. doi:10.1111/j.1469-8137.1975.tb01409.x.

Duan, L., Dietrich, D., Ng, C. H., Chan, P. M. Y., Bhalerao, R., Bennett, M. J., et al. (2013). Endodermal ABA signaling promotes lateral root quiescence during salt stress in Arabidopsis seedlings. *Plant Cell* 25, 324–41. doi:10.1105/tpc.112.107227.

Dunbabin, V. (2004). Simulating form and function of root systems : efficiency of nitrate uptake is dependent on root system architecture and. 204–211.

2

Dunbabin, V. (2006). "Using the ROOTMAP model of crop root growth to investigate root-soil interactions," in *Ground-breaking stuff". Proceedings of the 13th Australian Agronomy Conference, 10-14 September 2006, Perth, Western Australia.*, eds. N. C. Turner, T. Acuna, and R. C. Johnson (Australian Society of Agronomy), 10–14.

Dunbabin, V., Diggle, A. J., and Rengel, Z. (2002). Modeling the interactions between water and nutrient uptake and root growth. *Plant Soil*, 29–38. doi:10.1023/A.

Dunbabin, V. M., Postma, J. A., Schnepf, A., Pagès, L., Javaux, M., Wu, L., et al. (2013). Modelling root-soil interactions using three-dimensional models of root growth, architecture and function. *Plant Soil* 372, 93–124. doi:10.1007/s11104-013-1769-y.

Eapen, D., Barroso, M. L., Ponce, G., Campos, M. E., and Cassab, G. I. (2005). Hydrotropism: Root growth responses to water. *Trends Plant Sci.* 10, 44–50. doi:10.1016/j.tplants.2004.11.004.

Engels, C. (1994). Effect of root and shoot meristem temperature on shoot to root dry matter partitioning and the internal concentrations of nitrogen and carbohydrates in maize and wheat. *Ann. Bot.* 73, 211–219. doi:10.1006/anbo.1994.1025.

Equiza, M. a, Miravea, J. P., and Tognetti, J. a (2001). Morphological, Anatomical and Physiological Responses Related to Differential Shoot vs.\nRoot Growth Inhibition at Low Temperature in Spring and Winter Wheat. *Ann. Bot.* 87, 67–76. doi:10.1006/anbo.2000.1301.

Estañ, M. T., Martinez-Rodriguez, M. M., Perez-Alfocea, F., Flowers, T. J., and Bolarin, M. C. (2005). Grafting raises the salt tolerance of tomato through limiting the transport of sodium and chloride to the shoot. *J. Exp. Bot.* 56, 703–712. doi:10.1093/jxb/eri027.

FAO and ITPS (2015). Status of the World's Soil Resources (SWSR) – Main Report. Rome, Italy: Food and Agriculture Organization of the United Nations doi:ISBN 978-92-5-109004-6.

Füllner, K., Temperton, V. M., Rascher, U., Jahnke, S., Rist, R., Schurr, U., et al. (2012). Vertical gradient in soil temperature stimulates development and increases biomass accumulation in barley. *Plant, Cell Environ.* 35, 884–892. doi:10.1111/j.1365-3040.2011.02460.x.

Gahoonia, T. S., and Nielsen, N. E. (1998). Direct evidence on participation of root hairs in phosphorus (32P) uptake from soil. *Plant Soil* 198, 147–152. doi:10.1023/A:1004346412006.

Gahoonia, T. S., and Nielsen, N. E. (2004). Barley genotypes with long root hairs sustain high grain yields in low-P field. *Plant Soil* 262, 55–62. doi:10.1023/B:PLSO.0000037020.58002.ac.

Gahoonia, T. S., Nielsen, N. E., Joshi, P. A., and Jahoor, A. (2001). A root hairless barley mutant for elucidating genetic of root hairs and phosphorus uptake. *Plant Soil* 235, 211–219. doi:10.1023/A:1011993322286.

Gallego-Bartolome, J., Minguet, E. G., Grau-Enguix, F., Abbas, M., Locascio, a., Thomas, S. G., et al. (2012). Molecular mechanism for the interaction between gibberellin and brassinosteroid signaling pathways in Arabidopsis. *Proc. Natl. Acad. Sci.* 109, 13446–13451. doi:10.1073/pnas.1119992109.

Galvan-Ampudia, C. S., Julkowska, M. M., Darwish, E., Gandullo, J., Korver, R. A., Brunoud, G., et al. (2013). Halotropism is a response of plant roots to avoid a saline environment. *Curr. Biol.* 23, 2044–2050. doi:10.1016/j.cub.2013.08.042.

Galvan-Ampudia, C. S., and Testerink, C. (2011). Salt stress signals shape the plant root. *Curr. Opin. Plant Biol.* 14, 296–302. doi:10.1016/j.pbi.2011.03.019.

Geng, Y., Wu, R., Wee, C. W., Xie, F., Wei, X., Chan, P. M. Y., et al. (2013). A spatio-temporal understanding of growth regulation during the salt stress response in Arabidopsis. *Plant Cell* 25, 2132–54. doi:10.1105/tpc.113.112896.

Gerendás, J., and Ratcliffe, R. (2002). "Root pH regulation," in *Plant Roots: The Hidden Half, Ed*, eds. Y. Waisel, A. Eshel, and U. Kafkafi (Marcel Dekker, New York), 23–1 – 23–18. doi:doi:10.1201/9780203909423.ch33.

Gibberd, M. R., Gray, J. D., Cocks, P. S., and Colmer, T. D. (2001). Waterlogging Tolerance Among a Diverse Range of Trifolium Accessions is Related to Root Porosity, Lateral Root Formation and `Aerotropic Rooting'. *Ann. Bot.* 88, 579–589. doi:10.1006/anbo.2001.1506.

Gibbs, J., Turner, D. W., Armstrong, W., Sivasithamparam, K., and Greenway, H. (1998). Response to oxygen deficiency in primary maize roots. II. Development of oxygen deficiency in the stele has limited short-term impact on radial hydraulic conductivity. *Aust. J. Plant Physiol.* 25, 759. doi:10.1071/PP98087.

Gifford, M. L., Banta, J. A., Katari, M. S., Hulsmans, J., Chen, L., Ristova, D., et al. (2013). Plasticity Regulators Modulate Specific Root Traits in Discrete Nitrogen Environments. *PLoS Genet.* 9. doi:10.1371/journal.pgen.1003760.

Gladish, D. K., and Rost, T. L. (1993). The effects of temperature on primary root growth dynamics and lateral root distribution in garden pea (Pisum sativum L., cv. "Alaska"). *Environ. Exp. Bot.* 33, 243–258. doi:10.1016/0098-8472(93)90070-V.

Gladish, D. K., Sutter, E. G., and Rost, T. L. (2000). The Role of Free Indole-3-acetic Acid ( IAA ) Levels , IAA Transport , and Sucrose Transport in the High Temperature Inhibition of Primary Root Development in Pea ( Pisum sativum L . cv . Alaska ). *J. Plant Growth Regul* 19, 347–358. doi:10.1007/s003440000017.

Gosselin, A., and Trudel, M. J. (1984). Interactions between root-zone temperature and light levels on growth, development and photosynthesis of Lycopersicon esculentum Mill. cultivar "Vendor." *Sci. Hortic. (Amsterdam).* 23, 313–321. doi:10.1016/0304-4238(84)90027-X.

Grattan, S. R., and Grieve, C. M. (1998). Salinity-mineral nutrient relations in horticultural crops. *Sci. Hortic. (Amsterdam).* 78, 127–157. doi:10.1016/S0304-4238(98)00192-7.

Gregory, P. J., Atkinson, C. J., Bengough, A. G., Else, M. A., Fernández-Fernández, F., Harrison, R. J., et al. (2013). Contributions of roots and rootstocks to sustainable, intensified crop production. *J. Exp. Bot.* 64, 1209–1222. doi:10.1093/jxb/ers385.

Gruber, B. D., Giehl, R. F. H., Friedel, S., and von Wirén, N. (2013). Plasticity of the Arabidopsis root system under nutrient deficiencies. *Plant Physiol.* 163, 161–79. doi:10.1104/pp.113.218453.

Herder, G. Den, Van Isterdael, G., Beeckman, T., and De Smet, I. (2010). The roots of a new green revolution. *Trends Plant Sci.* 15, 600–607. doi:10.1016/j.tplants.2010.08.009.

Hu, Y., and Schmidhalter, U. (2005). Drought and salinity: A comparison of their effects on mineral nutrition of plants. *J. Plant Nutr. Soil Sci.* 168, 541–549. doi:10.1002/jpln.200420516.

**2**

Hund, A., Fracheboud, Y., Soldati, A., and Stamp, P. (2008). Cold tolerance of maize seedlings as determined by root morphology and photosynthetic traits. *Eur. J. Agron.* 28, 178–185. doi:10.1016/j.eja.2007.07.003.

Hund, A., Reimer, R., Stamp, P., and Walter, A. (2012). Can we improve heterosis for root growth of maize by selecting parental inbred lines with different temperature behaviour? *Philos. Trans. R. Soc. Lond. B. Biol. Sci.* 367, 1580–8. doi:10.1098/rstb.2011.0242.

Hund, A., Richner, W., Soldati, A., Fracheboud, Y., and Stamp, P. (2007). Root morphology and photosynthetic performance of maize inbred lines at low temperature. *Eur. J. Agron.* 27, 52–61. doi:10.1016/j.eja.2007.01.003.

Hurewitz, J., and Janes, H. W. (1983). Effect of Altering the Root-Zone Temperature, Carbon Exchange Rate, and Leaf Starch Accumulation in the Tomato. *Plant Physiol.* 73, 46–50. doi:10.1104/pp.73.1.46.

Van Ittersum, M. K., Cassman, K. G., Grassini, P., Wolf, J., Tittonell, P., and Hochman, Z. (2013). Yield gap analysis with local to global relevance-A review. *F. Crop. Res.* 143, 4–17. doi:10.1016/j.fcr.2012.09.009.

Iyer-Pascuzzi, A. S., Symonova, O., Mileyko, Y., Hao, Y., Belcher, H., Harer, J., et al. (2010). Imaging and analysis platform for automatic phenotyping and trait ranking of plant root systems. *Plant Physiol.* 152, 1148–1157. doi:10.1104/pp.109.150748.

Jackson, M. B., and Armstrong, W. (1999). Formation of Aerenchyma and the Processes of Plant Ventilation in Relation to Soil Flooding and Submergence. *Plant Biol.* 1, 274–287. doi:10.1111/j.1438-8677.1999.tb00253.x.

Jia, W., Wang, Y., Zhang, S., and Zhang, J. (2002). Salt-stress-induced ABA accumulation is more sensitively triggered in roots than in shoots. *J. Exp. Bot.* 53, 2201–2206. doi:10.1093/jxb/erf079.

Jobbágy, E. G., and Jackson, R. B. (2001). The distribution of soil nutrients with depth: Global patterns and the imprint of plants. *Biogeochemistry* 53, 51–77. doi:10.1023/A:1010760720215.

Jobbágy, E. G., and Jackson, R. B. (2004). The uplift of soil nutrients by plants: Biogeochemical consequences across scales. *Ecology* 85, 2380–2389. doi:10.1890/03-0245.

Judd, L., Jackson, B., and Fonteno, W. (2015). Advancements in Root Growth Measurement Technologies and Observation Capabilities for Container-Grown Plants. *Plants* 4, 369–392. doi:10.3390/plants4030369.

Julkowska, M. M., Hoefsloot, H. C. J., Mol, S., Feron, R., de Boer, G.-J., Haring, M. a, et al. (2014). Capturing Arabidopsis root architecture dynamics with ROOT-FIT reveals diversity in responses to salinity. *Plant Physiol.* 166, 1387–1402. doi:10.1104/pp.114.248963.

Julkowska, M. M., and Testerink, C. (2015). Tuning plant signaling and growth to survive salt. *Trends Plant Sci.* 20, 586–594. doi:10.1016/j.tplants.2015.06.008.

Jung, J. K., and McCouch, S. (2013). Getting to the roots of it: Genetic and hormonal control of root architecture. *Front Plant Sci* 4, 186. doi:10.3389/fpls.2013.00186.

Kaneyasu, T., Kobayashi, A., Nakayama, M., Fujii, N., Takahashi, H., and Miyazawa, Y. (2007). Auxin response, but not its polar transport, plays a role in hydrotropism of Arabidopsis roots. *J. Exp. Bot.* 58, 1143–1150. doi:10.1093/jxb/erl274.

Kapulnik, Y., Delaux, P. M., Resnick, N., Mayzlish-Gati, E., Wininger, S., Bhattacharya, C., et al. (2011a). Strigolactones affect lateral root formation and root-hair elongation in Arabidopsis. *Planta* 233, 209–216. doi:10.1007/s00425-010-1310-y.

Kapulnik, Y., Resnick, N., Mayzlish-Gati, E., Kaplan, Y., Wininger, S., Hershenhorn, J., et al. (2011b). Strigolactones interact with ethylene and auxin in regulating root-hair elongation in Arabidopsis. *J. Exp. Bot.* 62, 2915–2924. doi:10.1093/jxb/erq464.

Kato, Y., Abe, J., Kamoshita, A., and Yamagishi, J. (2006). Genotypic variation in root growth angle in rice (Oryza sativa L.) and its association with deep root development in upland fields with different water regimes. *Plant Soil* 287, 117–129. doi:10.1007/s11104-006-9008-4.

Kawa, D., Julkowska, M., Montero Sommerfeld, H., Horst, A. ter, Haring, M. A., and Testerink, C. (2016). Phosphate-dependent root system architecture responses to salt stress. *Plant Physiol.*, pp.00712.2016. doi:10.1104/pp.16.00712.

Koltai, H. (2011). Strigolactones are regulators of root development. *New Phytol.* 190, 545–549. doi:10.1111/j.1469-8137.2011.03678.x.

Koltai, H., Dor, E., Hershenhorn, J., Joel, D. M., Weininger, S., Lekalla, S., et al. (2010). Strigolactones' effect on root growth and root-hair elongation may be mediated by auxin-efflux carriers. *J. Plant Growth Regul.* 29, 129–136. doi:10.1007/s00344-009-9122-7.

Krouk, G., Lacombe, B., Bielach, A., Perrine-Walker, F., Malinska, K., Mounier, E., et al. (2010). Nitrate-regulated auxin transport by NRT1.1 defines a mechanism for nutrient sensing in plants. *Dev. Cell* 18, 927–937. doi:10.1016/j.devcel.2010.05.008.

Kubota, C., McClure, M. a., Kokalis-Burelle, N., Bausher, M. G., and Rosskopf, E. N. (2008). Vegetable grafting: History, use, and current technology status in North America. *Hortscience* 43, 1664–1669. Available at: <Go to ISI>://WOS:000259483900008.

Kuijken, R. C. P., Van Eeuwijk, F. A., Marcelis, L. F. M., and Bouwmeester, H. J. (2015). Root phenotyping: From component trait in the lab to breeding. *J. Exp. Bot.* 66, 5389–5401. doi:10.1093/jxb/erv239.

Leblanc, A., Renault, H., Lecourt, J., Etienne, P., Deleu, C., and Le Deunff, E. (2008). Elongation changes of exploratory and root hair systems induced by aminocyclopropane carboxylic acid and aminoethoxyvinylglycine affect nitrate uptake and BnNrt2.1 and BnNrt1.1 transporter gene expression in oilseed rape. *Plant Physiol.* 146, 1928–1940. doi:10.1104/pp.107.109363.

Lee, Y. P., Fleming, A. J., K??rner, C., and Meins, F. (2009). Differential expression of the CBF pathway and cell cycle-related genes in Arabidopsis accessions in response to chronic low-temperature exposure. *Plant Biol.* 11, 273–283. doi:10.1111/j.1438-8677.2008.00122.x.

Liao, H., Yan, X., Rubio, G., Beebe, S. E., Blair, M. W., and Lynch, J. P. (2004). Genetic mapping of basal root gravitropism and phosphorus acquisition efficiency in common bean. *Funct. Plant Biol.* 31, 959–970. doi:10.1071/FP03255.

Licker, R., Johnston, M., Foley, J. A., Barford, C., Kucharik, C. J., Monfreda, C., et al. (2010). Mind the gap: How do climate and agricultural management explain the "yield gap" of croplands around the world? *Glob. Ecol. Biogeogr.* 19, 769–782. doi:10.1111/j.1466-8238.2010.00563.x.

Linkohr, B. I., Williamson, L. C., Fitter, A. H., and Leyser, H. M. O. (2002). Nitrate and phosphate availability and distribution have different effects on root system architecture of Arabidopsis. *Plant J.* 29, 751–760. doi:10.1046/j.1365-313X.2002.01251.x.

**2**

Little, D. Y., Rao, H., Oliva, S., Daniel-Vedele, F., Krapp, A., and Malamy, J. E. (2005). The putative high-affinity nitrate transporter NRT2.1 represses lateral root initiation in response to nutritional cues. *Proc. Natl. Acad. Sci. U. S. A.* 102, 13693–13698. doi:10.1073/pnas.0504219102.

Liu, W., Li, R.-J., Han, T.-T., Cai, W., Fu, Z.-W., and Lu, Y.-T. (2015). Salt stress reduces root meristem size by nitric oxide-mediated modulation of auxin accumulation and signaling in Arabidopsis. *Plant Physiol.* 168, pp.00030.2015. doi:10.1104/pp.15.00030.

Lobell, D. B., Cassman, K. G., and Field, C. B. (2009). Crop Yield Gaps: Their Importance, Magnitudes, and Causes. *Annu. Rev. Environ. Resour.* 34, 179–204. doi:10.1146/annurev.environ.041008.093740.

Lobet, G., Draye, X., and Perilleux, C. (2013). An online database for plant image analysis software tools. *Plant Methods* 9, 38. doi:10.1186/1746-4811-9-38.

Lobet, G., Pagès, L., and Draye, X. (2011). A Novel Image Analysis Toolbox Enabling Quantitative Analysis of Root System Architecture. *Plant Physiol.* 157, 29–39. doi:10.1104/pp.111.179895.

López-Arredondo, D. L., Leyva-González, M. A., González-Morales, S. I., López-Bucio, J., and Herrera-Estrella, L. (2014). Phosphate Nutrition: Improving Low-Phosphate Tolerance in Crops. *Annu. Rev. Plant Biol.* 65, 95–123. doi:10.1146/annurev-arplant-050213-035949.

López-Bucio, J., Hernández-Abreu, E., Sánchez-Calderón, L., Nieto-Jacobo, M. F., Simpson, J., and Herrera-Estrella, L. (2002). Phosphate Availability Alters Architecture and Causes Changes in Hormone Sensitivity in the Arabidopsis Root System. *Plant Physiol.* 129, 244–256. doi:10.1104/pp.010934.

Lynch, J. P. (2007). Turner review no. 14. Roots of the second green revolution. *Aust. J. Bot.* 55, 493–512. doi:10.1071/BT06118.

Lynch, J. P., and Brown, K. M. (2001). Topsoil foraging - An architectural adaptation of plants to low phosphorus availability. *Plant Soil* 237, 225–237. doi:10.1023/A:1013324727040.

Lynch, J. P., and Brown, K. M. (2012). New roots for agriculture: exploiting the root phenome. *Philos. Trans. R. Soc. Lond. B. Biol. Sci.* 367, 1598–604. doi:10.1098/rstb.2011.0243.

Lynch, J. P., and Wojciechowski, T. (2015). Opportunities and challenges in the subsoil: Pathways to deeper rooted crops. *J. Exp. Bot.* 66, 2199–2210. doi:10.1093/jxb/eru508.

Mairhofer, S., Zappala, S., Tracy, S., Sturrock, C., Bennett, M. J., Mooney, S. J., et al. (2013). Recovering complete plant root system architectures from soil via X-ray μ-Computed Tomography. *Plant Methods* 9, 1. doi:10.1186/1746-4811-9-8.

Malamy, J. E. (2005). Intrinsic and environmental response pathways that regulate root system architecture. *Plant, Cell Environ.* 28, 67–77. doi:10.1111/j.1365-3040.2005.01306.x.

Manschadi, A. M., Hammer, G. L., Christopher, J. T., and DeVoil, P. (2008). Genotypic variation in seedling root architectural traits and implications for drought adaptation in wheat (Triticum aestivum L.). *Plant Soil* 303, 115–129. doi:10.1007/s11104-007-9492-1.

Le Marié, C., Kirchgessner, N., Marschall, D., Walter, A., and Hund, A. (2014). *Rhizoslides: paper-based growth system for non-destructive, high throughput phenotyping of root development by means of image analysis.* doi:10.1186/1746-4811-10-13.

Martinez-Rodriguez, M. M., Estañ, M. T., Moyano, E., Garcia-Abellan, J. O., Flores, F. B., Campos, J. F., et al. (2008). The effectiveness of grafting to improve salt tolerance in tomato when an "excluder" genotype is used as scion. *Environ. Exp. Bot.* 63, 392–401. doi:10.1016/j.envexpbot.2007.12.007.

Mathieu, L., Lobet, G., Tocquin, P., and Périlleux, C. (2015). "Rhizoponics": a novel hydroponic rhizotron for root system analyses on mature Arabidopsis thaliana plants. *Plant Methods* 11, 3. doi:10.1186/s13007-015-0046-x.

Matthys, C., Walton, A., Struk, S., Stes, E., Boyer, F.-D., Gevaert, K., et al. (2016). The Whats, the Wheres and the Hows of strigolactone action in the roots. *Planta*, 1327–1337. doi:10.1007/s00425-016-2483-9.

Mayzlish-Gati, E., De-Cuyper, C., Goormachtig, S., Beeckman, T., Vuylsteke, M., Brewer, P. B., et al. (2012). Strigolactones Are Involved in Root Response to Low Phosphate Conditions in Arabidopsis. *Plant Physiol.* 160, 1329–1341. doi:10.1104/pp.112.202358.

Mcmichael, B. L., Quisenberry, E., Systems, C., Stress, P., and Conservation, W. (1993). the Impact of the Soil Environment on the Growth of Root Systems. *Environ. Exp. Bot.* 33, 53–61.

Metzner, R., Eggert, A., van Dusschoten, D., Pflugfelder, D., Gerth, S., Schurr, U., et al. (2015). Direct comparison of MRI and X-ray CT technologies for 3D imaging of root systems in soil: potential and challenges for root trait quantification. *Plant Methods* 11, 1–11. doi:10.1186/s13007-015-0060-z.

Mickelbart, M. V., Hasegawa, P. M., and Bailey-Serres, J. (2015). Genetic mechanisms of abiotic stress tolerance that translate to crop yield stability. *Nat. Rev. Genet.* 16, 237–251. doi:10.1038/nrg3901.

Miura, K., Lee, J., Gong, Q., Ma, S., Jin, J. B., Yoo, C. Y., et al. (2011). SIZ1 Regulation of Phosphate Starvation-Induced Root Architecture Remodeling Involves the Control of Auxin Accumulation. *Plant Physiol.* 155, 1000–1012. doi:10.1104/pp.110.165191.

Mizuno, H., Kobayashi, A., Fujii, N., Yamashita, M., and Takahashi, H. (2002). Hydrotropic response and expression pattern of auxin-inducible gene, CS-IAA1, in the primary roots of clinorotated cucumber seedlings. *Plant Cell Physiol.* 43, 793–801. doi:Doi 10.1093/Pcp/Pcf093.

Møller, I. S., Gilliham, M., Jha, D., Mayo, G. M., Roy, S. J., Coates, J. C., et al. (2009). Shoot Na+ exclusion and increased salinity tolerance engineered by cell type-specific alteration of Na+ transport in Arabidopsis. *Plant Cell* 21, 2163–2178. doi:10.1105/tpc.108.064568.

Mooney, S. J., Pridmore, T. P., Helliwell, J., and Bennett, M. J. (2012). Developing X-ray computed tomography to non-invasively image 3-D root systems architecture in soil. *Plant Soil* 352, 1–22. doi:10.1007/s11104-011-1039-9.

Moriwaki, T., Miyazawa, Y., Kobayashi, A., and Takahashi, H. (2013). Molecular mechanisms of hydrotropism in seedling roots of Arabidopsis Thaliana (Brassicaceae). *Am. J. Bot.* 100, 25–34. doi:10.3732/ajb.1200419.

Mouchel, C. F., Briggs, G. C., and Hardtke, C. S. (2004). Natural genetic variation in Arabidopsis identifies BREVIS RADIX, a novel regulator of cell proliferation and elongation in the root. *Genes Dev.* 18, 700–714. doi:10.1101/gad.1187704.

**2**

Mounier, E., Pervent, M., Ljung, K., Gojon, A., and Nacry, P. (2014). Auxin-mediated nitrate signalling by NRT1.1 participates in the adaptive response of Arabidopsis root architecture to the spatial heterogeneity of nitrate availability. *Plant, Cell Environ.* 37, 162–174. doi:10.1111/pce.12143.

Mudge, K., Janick, J., Scofield, S., and Goldschmidt, E. (2009). A history of grafting. *Hortic. Rev. (Am. Soc. Hortic. Sci).* 35. Available at: http://onlinelibrary.wiley.com/ doi/10.1002/9780470593776.ch9/summary\npapers3://publication/uuid/DA5A7C5B-D8A3-45AB-9942-0338811197CF.

Mueller, N. D., Gerber, J. S., Johnston, M., Ray, D. K., Ramankutty, N., and Foley, J. a. (2012). Closing yield gaps through nutrient and water management. *Nature* 490, 254–257. doi:10.1038/nature11420.

Munns, R. (2002). Comparative physiology of salt and water stress. *Plant Cell Environ.* 25, 239–250. doi:10.1046/j.0016-8025.2001.00808.x.

Munns, R., James, R. A., and Láuchli, A. (2006). Approaches to increasing the salt tolerance of wheat and other cereals. *J. Exp. Bot.* 57, 1025–1043. doi:10.1093/jxb/erj100.

Munns, R., and Tester, M. (2008). Mechanisms of salinity tolerance. *Annu. Rev. Plant Biol.* 59, 651–81. doi:10.1146/annurev.arplant.59.032607.092911.

Muños, S., Cazettes, C., Fizames, C., Gaymard, F., Tillard, P., Lepetit, M., et al. (2004). Transcript profiling in the chl1-5 mutant of Arabidopsis reveals a role of the nitrate transporter NRT1. 1 in the regulation of another nitrate transporter, NRT2. 1. *Plant Cell …* 16, 2433–2447. doi:10.1105/tpc.104.024380.tration.

Nacry, P. (2005). A Role for Auxin Redistribution in the Responses of the Root System Architecture to Phosphate Starvation in Arabidopsis. *Plant Physiol.* 138, 2061–2074. doi:10.1104/pp.105.060061.

Nagel, K., Kastenholz, B., Jahnke, S., van Dusschoten, D., Aach, T., Muhlich, M., et al. (2009). Temperature responses of roots: impact on growth, root system archetecture and implications for phenotyping. *Funct. Plant Biol.* 36, 947–959.

Naidu, R., and Rengasamy, P. (1993). Ion Interactions and Constraints to Plant Nutrition in Australian Sodic Soils. *Aust. J. Soil Res.* 31, 801–819. doi:Doi 10.1071/Sr9930801.

Nielsen, K. F., Halstead, R. L., MacLean, A. J., Holmes, R. M., and Bourget, S. J. (1960). the Influence of Soil Temperature on the Growth and Mineral Composition of Oats. *Can. J. Soil Sci.* 40, 255–263. doi:10.4141/cjss60-032.

Ogawa, A., Kitamichi, K., Toyofuku, K., and Kawashima, C. (2006). Quantitative analysis of cell division and cell death in seminal root of rye under salt stress. *Plant Prod. Sci.* 9, 56–64. doi:10.1626/pps.9.56.

Pagés, L., Bécel, C., Boukcim, H., Moreau, D., Nguyen, C., and Voisin, A. S. (2014). Calibration and evaluation of ArchiSimple, a simple model of root system architecture. *Ecol. Modell.* 290, 76–84. doi:10.1016/j.ecolmodel.2013.11.014.

Pagès, L., and Picon-Cochard, C. (2014). Modelling the root system architecture of Poaceae. Can we simulate integrated traits from morphological parameters of growth and branching? *New Phytol.* 204, 149–158. doi:10.1111/nph.12904.

Pahlavanian, A. L. I. M., and Silk, W. K. (1988). Effect of Temperature on Spatial and Temporal Aspects of Growth in the Primary Maize Root '. 529–532.

Pardales, J. R. J., Banoc, D. M., Yamauchi, A., Iijima, M., and Kono, Y. (1999). Root System Development of Cassava and Sweetpotato during Early Growth Stage as Affected by High Root Zone Temperature. *Plant Prod. Sci.* 2, 247–251. doi:10.1626/pps.2.247.

Pardales, J. R., Kono, Y., and Yamauchi, A. (1992). Epidermal cell elongation in sorghum seminal roots exposed to high root-zone temperature. *Plant Sci.* 81, 143–146. doi:10.1016/0168-9452(92)90035-K.

Pedersen, A., Zhang, K., Thorup-Kristensen, K., and Jensen, L. S. (2010). Modelling diverse root density dynamics and deep nitrogen uptake-a simple approach. *Plant Soil* 326, 493–510. doi:10.1007/s11104-009-0028-8.

Péret, B., Clément, M., Nussaume, L., and Desnos, T. (2011). Root developmental adaptation to phosphate starvation: Better safe than sorry. *Trends Plant Sci.* 16, 442–450. doi:10.1016/j.tplants.2011.05.006.

Pérez-Torres, C. A., López-Bucio, J., Cruz-Ramírez, A., Ibarra-Laclette, E., Dharmasiri, S., Estelle, M., et al. (2008a). Phosphate Availability Alters Lateral Root Development in Arabidopsis by Modulating Auxin Sensitivity via a Mechanism Involving the TIR1 Auxin Receptor. *Plant Cell* 20, 3258–3272. doi:10.1105/tpc.108.058719.

Pérez-Torres, C. A., López-Bucio, J., and Herrera-Estrella, L. (2008b). Phosphate Availability Alters Lateral Root Development in Arabidopsis by Modulating Auxin Sensitivity via a Mechanism Involving the TIR1 Auxin Receptor. *Plant Cell* 20, 3258–3272. doi:10.1105/tpc.108.058719.

Pierik, R., and Testerink, C. (2014). The art of being flexible: how to escape from shade, salt, and drought. *Plant Physiol.* 166, 5–22. doi:10.1104/pp.114.239160.

Pigliucci, M. (2005). Evolution of phenotypic plasticity: Where are we going now? *Trends Ecol. Evol.* 20, 481–486. doi:10.1016/j.tree.2005.06.001.

Piñeros, M. A., Larson, B. G., Shaff, J. E., Schneider, D. J., Falcão, A. X., Yuan, L., et al. (2016). Evolving technologies for growing, imaging and analyzing 3D root system architecture of crop plants. *J. Integr. Plant Biol.* 58, 230–241. doi:10.1111/jipb.12456.

Poiré, R., Wiese-Klinkenberg, A., Parent, B., Mielewczik, M., Schurr, U., Tardieu, F., et al. (2010). Diel time-courses of leaf growth in monocot and dicot species: Endogenous rhythms and temperature effects. *J. Exp. Bot.* 61, 1751–1759. doi:10.1093/jxb/erq049.

Poorter, H., van der Werf, A., Atkin, O. K., and Lambers, H. (1991). Respiratory energy requirements of roots vary with the potential growth rate of a plant species. *Physiol. Plant.* 83, 469–475. doi:10.1034/j.1399-3054.1991.830321.x.

Porter, J. R., and Gawith, M. (1999). Temperatures and the growth and development of wheat: A review. *Eur. J. Agron.* 10, 23–36. doi:10.1016/S1161-0301(98)00047-1.

Pritchard, J., Barlow, P. W., Adam, J. S., and Tomos, A. D. (1990). Biophysics of the inhibition of the growth of maize roots by lowered temperature. *Plant Physiol.* 93, 222–230. doi:10.1104/pp.93.1.222.

Van der Putten, W. H., Bardgett, R. D., Bever, J. D., Bezemer, T. M., Casper, B. B., Fukami, T., et al. (2013). Plant-soil feedbacks: The past, the present and future challenges. *J. Ecol.* 101, 265–276. doi:10.1111/1365-2745.12054.

Qin, L., He, J., Lee, S. K., and Dodd, I. C. (2007). An assessment of the role of ethylene in mediating lettuce (Lactuca sativa) root growth at high temperatures. *J. Exp. Bot.* 58, 3017–3024. doi:10.1093/jxb/erm156.

**2**

Rahman, M. S., Matsumuro, T., Miyake, H., and Takeoka, Y. (2001). Effects of salinity stress on the seminal root tip ultrastructures of rice seedlings (Oryza sativa L.). *Plant Prod. Sci.* 4, 103–111. doi:10.1626/pps.4.103.

Rellán-Álvarez, R., Lobet, G., and Dinneny, J. R. (2016). Environmental control of root system biology. *Annu. Rev. Plant Biol.* 67, 1–26. doi:10.1146/)).

Rellán-Álvarez, R., Lobet, G., Lindner, H., Pradier, P. L., Sebastian, J., Yee, M. C., et al. (2015). GLO-Roots: An imaging platform enabling multidimensional characterization of soil-grown root systems. *Elife* 4, e07597. doi:10.7554/eLife.07597.

Remans, T., Nacry, P., Pervent, M., Filleur, S., Diatloff, E., Mounier, E., et al. (2006a). The Arabidopsis NRT1.1 transporter participates in the signaling pathway triggering root colonization of nitrate-rich patches. *Proc. Natl. Acad. Sci. U. S. A.* 103, 19206–11. doi:10.1073/pnas.0605275103.

Remans, T., Nacry, P., Pervent, M., Girin, T., Tillard, P., Lepetit, M., et al. (2006b). A central role for the nitrate transporter NRT2.1 in the integrated morphological and physiological responses of the root system to nitrogen limitation in Arabidopsis. *Plant Physiol.* 140, 909–921. doi:10.1104/pp.105.075721.

Rengasamy, P. (2006). World salinization with emphasis on Australia. *J. Exp. Bot.* 57, 1017–1023. doi:10.1093/jxb/erj108.

Rich, S. M., and Watt, M. (2013). Soil conditions and cereal root system architecture: Review and considerations for linking Darwin and Weaver. *J. Exp. Bot.* 64, 1193–1208. doi:10.1093/jxb/ert043.

Ristova, D., Rosas, U., Krouk, G., Ruffel, S., Birnbaum, K. D., and Coruzzi, G. M. (2013). RootScape: a landmark-based system for rapid screening of root architecture in Arabidopsis. *Plant Physiol.* 161, 1086–96. doi:10.1104/pp.112.210872.

Ritter, E., Angulo, B., Riga, P., Herrán, C., Relloso, J., and San Jose, M. (2001). Comparison of hydroponic and aeroponic cultivation systems for the production of potato minitubers. *Potato Res.* 44, 127–135. doi:10.1007/BF02410099.

Robbins, N. E., and Dinneny, J. R. (2015). The divining root: Moisture-driven responses of roots at the micro- and macro-scale. *J. Exp. Bot.* 66, 2145–2154. doi:10.1093/jxb/eru496.

Rodriguez, H. G., Roberts, J. K. M., Jordan, W. R., and Drew, M. C. (1997). Growth, water relations, and accumulation of organic and inorganic solutes in roots of maize seedlings during salt stress. *Plant Physiol.* 113, 881–893. doi:10.1104/pp.113.3.881.

Rosas, U., Cibrian-Jaramillo, A., Ristova, D., Banta, J. a, Gifford, M. L., Fan, A. H., et al. (2013). Integration of responses within and across Arabidopsis natural accessions uncovers loci controlling root systems architecture. *Proc. Natl. Acad. Sci. U. S. A.* 110, 15133–8. doi:10.1073/pnas.1305883110.

Rosegrant, M. W., Ringler, C., and Zhu, T. (2009). Water for Agriculture: Maintaining Food Security under Growing Scarcity. *Annu. Rev. Environ. Resour.* 34, 205–222. doi:10.1146/annurev.environ.030308.090351.

Rosquete, M. R., Von Wangenheim, D., Marhav??, P., Barbez, E., Stelzer, E. H. K., Benkov??, E., et al. (2013). An auxin transport mechanism restricts positive orthogravitropism in lateral roots. *Curr. Biol.* 23, 817–822. doi:10.1016/j.cub.2013.03.064.

Rowe, J. H., Topping, J. F., Liu, J., and Lindsey, K. (2016). Abscisic acid regulates root growth under osmotic stress conditions via an interacting hormonal network with cytokinin, ethylene and auxin. *New Phytol.*, n/a–n/a. doi:10.1111/nph.13882.

Roychoudhry, S., Del Bianco, M., Kieffer, M., and Kepinski, S. (2013). Auxin controls gravitropic setpoint angle in higher plant lateral branches. *Curr. Biol.* 23, 1497–1504. doi:10.1016/j.cub.2013.06.034.

Rubinigg, M., Stulen, I., Theo, M. E. J., and Colmer, T. D. (2002). Spatial patterns of radial oxygen loss and nitrate net flux along adventitious roots of rice raised in aerated or stagnant solution. *Funct. Plant Biol.* 29, 1475–1481. doi:10.1071/FP02081.

Ruyter-Spira, C., Kohlen, W., Charnikhova, T., van Zeijl, A., van Bezouwen, L., de Ruijter, N., et al. (2011). Physiological effects of the synthetic strigolactone analog GR24 on root system architecture in Arabidopsis: another belowground role for strigolactones? *Plant …* 155, 721–34. doi:10.1104/pp.110.166645.

Saengwilai, P., Tian, X., and Lynch, J. P. (2014). Low Crown Root Number Enhances Nitrogen Acquisition from Low-Nitrogen Soils in Maize. *Plant Physiol.* 166, 581–589. doi:10.1104/pp.113.232603.

Sairam, R. K., and Tyagi, A. (2004). Physiology and molecular biology of salinity stress tolerance in plants. *Curr. Sci.* 86, 407–421. doi:10.1016/j.tplants.2005.10.002.

Sakamoto, M., and Suzuki, T. (2015). Effect of Root-Zone Temperature on Growth and Quality of Hydroponically Grown Red Leaf Lettuce ( Lactuca sativa L . cv . Red Wave ). 2350–2360.

Sánchez-Calderón, L., López-Bucio, J., Chacón-López, A., Cruz-Ramírez, A., Nieto-Jacobo, F., Dubrovsky, J. G., et al. (2005). Phosphate starvation induces a determinate developmental program in the roots of Arabidopsis thaliana. *Plant Cell Physiol.* 46, 174–184. doi:10.1093/pcp/pci011.

Sánchez-Calderón, L., López-Bucio, J., Chacón-López, A., Gutiérrez-Ortega, A., Hernández-Abreu, E., and Herrera-Estrella, L. (2006). Characterization of low phosphorus insensitive mutants reveals a crosstalk between low phosphorus-induced determinate root development and the activation of genes involved in the adaptation of Arabidopsis to phosphorus deficiency. *Plant Physiol.* 140, 879–889. doi:10.1104/pp.105.073825.

Scheurwater, I., Clarkson, D. T., Purves, J. V., Van Rijt, G., Saker, L. R., Welschen, R., et al. (1999). Relatively large nitrate efflux can account for the high specific respiratory costs for nitrate transport in slow-growing grass species. *Plant Soil* 215, 123–134. doi:10.1023/A:1004559628401.

Scheurwater, I., Cornelissen, C., Dictus, F., Welschen, R., and Lambers, H. (1998). Why do fast- and slow-growing grass species differ so little in their rate of root respiration, considering the large differences in rate of growth and ion uptake? *Plant, Cell Environ.* 21, 995–1005. doi:10.1046/j.1365-3040.1998.00341.x.

Schwarz, D., Rouphael, Y., Colla, G., and Venema, J. H. (2010). Grafting as a tool to improve tolerance of vegetables to abiotic stresses: Thermal stress, water stress and organic pollutants. *Sci. Hortic. (Amsterdam).* 127, 162–171. doi:10.1016/j.scienta.2010.09.016.

Seiler, G. J. (1998). Influence of temperature on primary and lateral root growth of sunflower seedlings. *Environ. Exp. Bot.* 40, 135–146. doi:10.1016/S0098-8472(98)00027-6.

**2**

Setter, T. L., and Waters, I. (2003). Review of prospects for germplasm improvement for waterlogging tolerance in wheat, barley and oats. *Plant Soil* 253, 1–34. doi:10.1023/A:1024573305997.

Shibasaki, K., Uemura, M., Tsurumi, S., and Rahman, A. (2009). Auxin response in Arabidopsis under cold stress: underlying molecular mechanisms. *Plant Cell* 21, 3823–38. doi:10.1105/tpc.109.069906.

Shkolnik-Inbar, D., and Bar-Zvi, D. (2010). ABI4 mediates abscisic acid and cytokinin inhibition of lateral root formation by reducing polar auxin transport in Arabidopsis. *Plant Cell* 22, 3560–73. doi:10.1105/tpc.110.074641.

Shkolnik, D., Krieger, G., Nuriel, R., and Fromm, H. (2016). Hydrotropism: root bending does not require auxin redistribution. *Mol. Plant*, 757–759. doi:10.1016/j.molp.2016.02.001.

Siddique, K. H. M., Belford, R. K., and Tennant, D. (1990). Root:shoot ratios of old and modern, tall and semi-dwarf wheats in a mediterranean environment. *Plant Soil* 121, 89–98. doi:10.1007/BF00013101.

Silberbush, M., and Barber, S. (1983). Sensitivity of simulated phosphorus uptake to parameters used by a mechanistic-mathematical model. *Plant Soil* 74, 93–100.

Silva-Navas, J., Moreno-Risueno, M. A., Manzano, C., Pallero-Baena, M., Navarro-Neila, S., T??llez-Robledo, B., et al. (2015). D-Root: A system for cultivating plants with the roots in darkness or under different light conditions. *Plant J.* 84, 244–255. doi:10.1111/tpj.12998.

Slovak, R., Ogura, T., Satbhai, S. B., Ristova, D., and Busch, W. (2016). Genetic control of root growth: From genes to networks. *Ann. Bot.* 117, 9–24. doi:10.1093/aob/mcv160.

Smedema, L. K., and Shiati, K. (2002). Irrigation and salinity: A perspective review of the salinity hazards of irrigation development in the arid zone. *Irrig. Drain. Syst.* 16, 161–174. doi:10.1023/A:1016008417327.

Smith, S., and De Smet, I. (2012). Root system architecture: insights from Arabidopsis and cereal crops. *Philos. Trans. R. Soc. B Biol. Sci.* 367, 1441–1452. doi:10.1098/rstb.2011.0234.

Snyder, C. S., Bruulsema, T. W., Jensen, T. L., and Fixen, P. E. (2009). Review of greenhouse gas emissions from crop production systems and fertilizer management effects. *Agric. Ecosyst. Environ.* 133, 247–266. doi:10.1016/j.agee.2009.04.021.

Spalding, E. P., and Miller, N. D. (2013). Image analysis is driving a renaissance in growth measurement. *Curr. Opin. Plant Biol.* 16, 100–104. doi:10.1016/j.pbi.2013.01.001.

Sun, F., Zhang, W., Hu, H., Li, B., Wang, Y., Zhao, Y., et al. (2007). Salt Modulates Gravity Signaling Pathway to Regulate Growth Direction of Primary Roots in Arabidopsis. *Plant Physiol.* 146, 178–188. doi:10.1104/pp.107.109413.

Svistoonoff, S., Creff, A., Reymond, M., Sigoillot-Claude, C., Ricaud, L., Blanchet, A., et al. (2007). Root tip contact with low-phosphate media reprograms plant root architecture. *Nat. Genet.* 39, 792–796. doi:10.1038/ng2041.

Takahashi, H., Miyazawa, Y., and Fujii, N. (2009). Hormonal interactions during root tropic growth: Hydrotropism versus gravitropism. *Plant Mol. Biol.* 69, 489–502. doi:10.1007/s11103-008-9438-x.

Takahashi, H., and Scott, T. K. (1991). Hydrotropism and its interactions with gravitropism in maize roots. *Plant Physiol.* 96, 558–564.

Takahashi, H., and Suge, H. (1991). Root hydrotropism of an agravitropic pea mutant, ageotropum. *Physiol. Plant.* 82, 24–31.

Takahashi, H., Takano, M., Fujii, N., Yamashita, M., and Suge, H. (1996). Induction of hydrotropism in clinorotated seedling roots of Alaska pea, Pisum sativum L. *J. Plant Res.* 109, 335–337. doi:Doi 10.1007/Bf02344481.

Takahashi, N., Goto, N., Okada, K., and Takahashi, H. (2002). Hydrotropism in abscisic acid, wavy, and gravitropic mutants of Arabidopsis thaliana. *Planta* 216, 203–211. doi:10.1007/s00425-002-0840-3.

Tian, Q. Y., Sun, P., and Zhang, W. H. (2009). Ethylene is involved in nitrate-dependent root growth and branching in Arabidopsis thaliana. *New Phytol.* 184, 918–931. doi:10.1111/j.1469-8137.2009.03004.x.

Tocquin, P., Corbesier, L., Havelange, A., Pieltain, A., Kurtem, E., Bernier, G., et al. (2003). A novel high efficiency, low maintenance, hydroponic system for synchronous growth and flowering of Arabidopsis thaliana. *BMC Plant Biol.* 3, 2. doi:10.1186/1471-2229-3-2.

Uga, Y., Sugimoto, K., Ogawa, S., Rane, J., Ishitani, M., Hara, N., et al. (2013). Control of root system architecture by DEEPER ROOTING 1 increases rice yield under drought conditions. *Nat. Genet.* 45, 1097–102. doi:10.1038/ng.2725.

Veen, B. (1981). Relation between root respiration and root activity. *Plant Soil* 63, 73–76.

Venema, J. H., Dijk, B. E., Bax, J. M., van Hasselt, P. R., and Elzenga, J. T. M. (2008). Grafting tomato (Solanum lycopersicum) onto the rootstock of a high-altitude accession of Solanum habrochaites improves suboptimal-temperature tolerance. *Environ. Exp. Bot.* 63, 359–367. doi:10.1016/j.envexpbot.2007.12.015.

Veselova, S. V., Farhutdinov, R. G., Veselov, S. Y., Kudoyarova, G. R., Veselov, D. S., and Hartung, W. (2005). The effect of root cooling on hormone content, leaf conductance and root hydraulic conductivity of durum wheat seedlings (Triticum durum L.). *J. Plant Physiol.* 162, 21–26. doi:10.1016/j.jplph.2004.06.001.

Visser, E. J. W., Bogemann, G. M., Blom, C. W. P. M., and Voesenek, L. a C. J. (1996). Ethylene accumulation in waterlogged Rumex plants promotes formation of adventitious roots. *J. Exp. Bot.* 47, 403–410. Available at: http://jxb.oxfordjournals.org/content/47/3/403.abstract.

Wachsman, G., Sparks, E. E., and Benfey, P. N. (2015). Genes and networks regulating root anatomy and architecture. *New Phytol.* 208, 26–38. doi:10.1111/nph.13469.

Waines, J. G., and Ehdaie, B. (2007). Domestication and crop physiology: Roots of green-revolution wheat. *Ann. Bot.* 100, 991–998. doi:10.1093/aob/mcm180.

Walter, A., Silk, W. K., and Schurr, U. (2009). Environmental effects on spatial and temporal patterns of leaf and root growth. *Annu. Rev. Plant Biol.* 60, 279–304. doi:10.1146/annurev.arplant.59.032607.092819.

Wang, Q., Komarov, S., Mathews, A., and Li, K. (2015). Combined 3D PET and Optical Projection Tomography Techniques for Plant Root Phenotyping. *arXiv Prepr. arXiv …*, 5. Available at: arXiv:1501.02427\nhttp://arxiv.org/abs/1501.0242\nhttp://arxiv.org/abs/1501.00242.

Warschefsky, E. J., Klein, L. L., Frank, M. H., Chitwood, D. H., Londo, J. P., von Wettberg, E. J. B., et al. (2016). Rootstocks: Diversity, Domestication, and Impacts on Shoot Phenotypes. *Trends Plant Sci.* 21, 418–437. doi:10.1016/j.tplants.2015.11.008.

**2**

van der Werf, A., Kooijman, A., Welschen, R., and Lambers, H. (1988). Respiratory energy costs for the maintenance of biomass, for growth and for ion uptake in roots of Carex diandra and Carex acutiformis. *Physiol. Plant.* 72, 483–491. doi:10.1111/j.1399-3054.1988. tb09155.x.

West, G., Inze, D., Inzé, D., Beemster, G., and Inze, D. (2004). Cell cycle modulation in the response of the primary root of Arabidopsis to salt stress. *Plant Physiol.* 135, 1050–1058. doi:10.1104/pp.104.040022.termining.

White, P. J., George, T. S., Gregory, P. J., Bengough, A. G., Hallett, P. D., and McKenzie, B. M. (2013). Matching roots to their environment. *Ann. Bot.* 112, 207–222. doi:10.1093/ aob/mct123.

Williamson, L. C. (2001). Phosphate Availability Regulates Root System Architecture in Arabidopsis. *Plant Physiol.* 126, 875–882. doi:10.1104/pp.126.2.875.

Wirth, J., Chopin, F., Santoni, V., Viennois, G., Tillard, P., Krapp, A., et al. (2007). Regulation of root nitrate uptake at the NRT2.1 protein level in Arabidopsis thaliana. *J. Biol. Chem.* 282, 23541–23552. doi:10.1074/jbc.M700901200.

Xiong, L., Wang, R.-G., Mao, G., and Koczan, J. M. (2006). Identification of drought tolerance determinants by genetic analysis of root response to drought stress and abscisic Acid. *Plant Physiol.* 142, 1065–74. doi:10.1104/pp.106.084632.

Xu, P., Cai, X. T., Wang, Y., Xing, L., Chen, Q., and Xiang, C. Bin (2014). HDG11 upregulates cell-wall-loosening protein genes to promote root elongation in Arabidopsis. *J. Exp. Bot.* 65, 4285–4295. doi:10.1093/jxb/eru202.

Yu, H., Chen, X., Hong, Y.-Y., Wang, Y., Xu, P., Ke, S.-D., et al. (2008). Activated expression of an Arabidopsis HD-START protein confers drought tolerance with improved root system and reduced stomatal density. *Plant Cell* 20, 1134–1151. doi:10.1105/tpc.108.058263.

Yu, L., Chen, X., Wang, Z., Wang, S., Wang, Y., Zhu, Q., et al. (2013). Arabidopsis enhanced drought tolerance1/HOMEODOMAIN GLABROUS11 confers drought tolerance in transgenic rice without yield penalty. *Plant Physiol.* 162, 1378–91. doi:10.1104/ pp.113.217596.

Yu, L. H., Wu, S. J., Peng, Y. S., Liu, R. N., Chen, X., Zhao, P., et al. (2016). Arabidopsis EDT1/ HDG11 improves drought and salt tolerance in cotton and poplar and increases cotton yield in the field. *Plant Biotechnol. J.* 14, 72–84. doi:10.1111/pbi.12358.

Zamir, D., and Gadish, I. (1987). Pollen selection for low temperature adaptation in tomato. *Theor. Appl. Genet.* 74, 545–548. doi:10.1007/BF00288849.

in 't Zandt, D., Le Marié, C., Kirchgessner, N., Visser, E. J. W., and Hund, A. (2015). High-resolution quantification of root dynamics in split-nutrient rhizoslides reveals rapid and strong proliferation of maize roots in response to local high nitrogen. *J. Exp. Bot.* 66, 5507–5517. doi:10.1093/jxb/erv307.

Zhao, Y., Wang, T., Zhang, W., and Li, X. (2011). SOS3 mediates lateral root development under low salt stress through regulation of auxin redistribution and maxima in Arabidopsis. *New Phytol.* 189, 1122–1134. doi:10.1111/j.1469-8137.2010.03545.x.

Zheng, D., Han, X., An, Y., Guo, H., Xia, X., and Yin, W. (2013). The nitrate transporter NRT2.1 functions in the ethylene response to nitrate deficiency in Arabidopsis. *Plant, Cell Environ.* 36, 1328–1337. doi:10.1111/pce.12062.

Zhu, J., Ingram, P. A., Benfey, P. N., and Elich, T. (2011). From lab to field, new approaches to phenotyping root system architecture. *Curr. Opin. Plant Biol.* 14, 310–317. doi:10.1016/j.pbi.2011.03.020.

Zhu, J., Kaeppler, S. M., and Lynch, J. P. (2005a). Mapping of QTLs for lateral root branching and length in maize (Zea mays L.) under differential phosphorus supply. *Theor. Appl. Genet.* 111, 688–695. doi:10.1007/s00122-005-2051-3.

Zhu, J., Kaeppler, S. M., and Lynch, J. P. (2005b). Topsoil foraging and phosphorus acquisition efficiency in maize (Zea mays). *Funct. Plant Biol.* 32, 749–762. doi:10.1071/FP05005.

Zhu, J., and Lynch, J. P. (2004). The contribution of lateral rooting to phosphorus acquisition efficiency in maize (Zea mays) seedlings. *Funct. Plant Biol.* 31, 949–958. doi:10.1071/FP04046.

Zhu, J., Mickelson, S. M., Kaeppler, S. M., and Lynch, J. P. (2006). Detection of quantitative trait loci for seminal root traits in maize (Zea mays L.) seedlings grown under differential phosphorus levels. *Theor. Appl. Genet.* 113, 1–10. doi:10.1007/s00122-006-0260-z.

Zhu, J., Zhang, K. X., Wang, W. S., Gong, W., Liu, W. C., Chen, H. G., et al. (2015). Low temperature inhibits root growth by reducing auxin accumulation via ARR1/12. *Plant Cell Physiol.* 56, 727–736. doi:10.1093/pcp/pcu217.

Zobel, R. W., Del Tredici, P., and Torrey, J. G. (1976). Method for growing plants aeroponically. *Plant Physiol.* 57, 344–6. doi:10.1104/pp.57.3.344.

Zolla, G., Heimer, Y. M., and Barak, S. (2010). Mild salinity stimulates a stress-induced morphogenic response in Arabidopsis thaliana roots. *J. Exp. Bot.* 61, 211–224. doi:10.1093/jxb/erp290.

2

**CHAPTER 3**

# Genetic Components of Root Architecture Remodeling in Response to Salt Stress

Magdalena M. Julkowska[1,2], Iko T. Koevoets[2,5], Selena Mol[1,2], Huub Hoefsloot[3], Daan Mangé[2], Richard Feron[6], Mark A. Tester[7], Joost J.B. Keurentjes[4,8], Arthur Korte[9], Michel A. Haring[1], Gert-Jan de Boer[6], Christa Testerink[2,5]

University of Amsterdam, [1]Plant Physiology, [2]Plant Cell Biology, [3]Biosystems Data Analysis, [4]Applied Quantitative Genetics, Swammerdam Institute for Life Sciences, 1090GE Amsterdam, the Netherlands
[5]Laboratory of Plant Physiology, Wageningen University & Research, 6708PB Wageningen, the Netherlands
[6]Enza Zaden Research and Development B.V., 1602DB Enkhuizen, the Netherlands
[7]Department of Biological and Environmental Sciences and Engineering, King Abdullah University of Science and Technology, 23955-6900 Thuwal-Jeddah, Kingdom of Saudi Arabia
[8]Laboratory of Genetics, 6708PB Wageningen University & Research, Wageningen, the Netherlands
[9]Center for Computational and Theoretical Biology, Wuerzburg Universitat, 97074 Wuerzburg, Germany

**ABSTRACT**

Salinity of the soil is highly detrimental to plant growth. Plants respond by a redistribution of root mass between main and lateral roots, yet the genetic machinery underlying this process is still largely unknown. Here, we describe the natural variation among 347 *Arabidopsis thaliana* accessions in root system architecture (RSA) and identify the traits with highest natural variation in their response to salt. Salt-induced changes in RSA were associated with 100 genetic loci using genome-wide association studies (GWAS). Two candidate loci associated with lateral root development were validated and further investigated. High *HKT1* expression in the root repressed lateral root development. By contrast, changes in *CYP79B2* expression in salt stress positively correlated with lateral root development in accessions, and *cyp79b2cyp79b3* double mutants developed fewer and shorter lateral roots under salt stress, but not in control conditions. The collected data and Multi-Variate analysis of multiple RSA traits, available through the Salt_NV_Root App, capture root responses to salinity. Together, our results provide a better understanding of effective RSA remodeling responses, and the genetic components involved, for plant performance in stress conditions.

## INTRODUCTION

Salt stress is a major threat in modern agriculture, affecting 20% of the cultivated area worldwide and half of the irrigated farmlands (OECD, 2012). Plants can adopt multiple strategies to increase their salinity tolerance, such as reduced growth rate, compartmentalization of ions or synthesis of compatible solutes (Munns and Tester, 2008; Munns and Gilliham, 2015). One of the most robust phenotypes used for screening salinity tolerance is accumulation of sodium in shoot tissue. Exclusion of sodium from the shoot is correlated with maintenance of high rates of photosynthesis, growth, and yield (Munns and Tester, 2008). Allelic variation affecting transcription of *HKT1* and *CIPK13* was previously established to play a major role in sodium exclusion and therefore salinity tolerance (Rus et al., 2006; Munns et al., 2012; Roy et al., 2012). Another trait broadly used for identification of salt stress-related mechanisms is elongation of the main root (Wu et al., 1996; Ding and Zhu, 1997; Liu and Zhu, 1997). While main root elongation is instrumental for seedling establishment, the distribution of the root mass between main and lateral roots is also affected by salt, yet the genetic machinery underlying this process as well as its significance in salt stress tolerance are only now starting to be unraveled (Duan et al., 2013; Geng et al., 2013; Julkowska et al., 2014; Julkowska and Testerink, 2015; Kobayashi et al., 2016; Kawa et al., 2016).

The root is the first plant organ exposed to salinity stress and plays an important role in salt sensing (Galvan-Ampudia et al., 2013; Robbins et al., 2014) as well as signal transduction to the shoot tissue (Choi et al., 2014; Jiang et al., 2013). Salt stress reduces the cell cycle activity at the root meristems, resulting in growth reduction (West et al., 2004). Quiescence of lateral roots is initiated by endodermal ABA signaling, which interestingly is also involved in recovery of lateral root growth (Duan et al., 2013). In the long term, salt stress reduces main root growth more severely than lateral root elongation in the *Arabidopsis thaliana* accession Col-0 (Julkowska et al., 2014), causing remodeling of Root System Architecture (RSA) compared to control conditions. Interestingly, other Arabidopsis accessions show different RSA remodeling response to salt stress, indicating natural variation that can be exploited for candidate gene identification by means of Genome Wide Association Studies (GWAS). Since the root system is important for efficient water uptake and ion exclusion (Faiyue et al., 2010; Ristova and Busch, 2014), changes in RSA are likely to contribute to plant performance under salt stress conditions (Julkowska and Testerink, 2015).

In this study we explore natural variation in RSA development under control and salt stress conditions by screening 347 Arabidopsis accessions of the HapMap population (Horton et al., 2012; Li et al., 2010). Our results indicate increased phenotypic variation in main and lateral root length in salt stress conditions compared to control conditions. By performing GWAS, we identified several candidate genetic loci to be associated with the remodeling of root architecture in response to salt. Further analysis of *HKT1* and *CYP79B2/B3* candidate genes supports a role for them in modulation of lateral root development under salt stress conditions, increasing our understanding of root responses in contributing to plant performance under stress. To optimally exploit our complex RSA phenotyping dataset beyond the analysis described in this scientific publication,

we also make our data available through the Salt_NV_Root App (http://genseq-h0. science.uva.nl/shiny/App/Salt_NV_Root/). This tool will facilitate other researchers in exploring our dataset and finding new leads for further research on RSA remodeling.


## RESULTS

*Salt-induced remodeling of RSA relies on altered lateral root development*
To examine natural variation in root architecture under salt stress conditions, 347 Arabidopsis accessions of the HapMap population (Weigel and Mott, 2009; Supplemental Dataset 1) were grown on agar plates under control and two salt stress conditions (75 and 125 mM NaCl). Using EZ-Rhizo software, 17 RSA traits (Figure 1A, Supplemental Dataset 2) were extracted from the images of 8-day-old plants grown under control condition and 12-day-old plants for both salt stress conditions. Col-0 was used as the reference accession across individual experimental batches, validating the reproducibility of the experiment (Supplemental Figure 1). Using ANOVA, we identified significant effects of medium and genotype on all RSA traits except for lateral root patterning (lateral root density per branched zone) (Supplemental Dataset 2). Additionally, using two-way ANOVA we identified significant interactions between medium and genotype in root angle traits (main root vector angle and straightness) and distribution of mass between main and lateral root (for example lateral root density per main root length) (Supplemental Dataset 2).

Substantial natural variation was observed for all recorded RSA traits, and accessions identified as outliers differed among traits and conditions (Figure 1B, Supplemental Figure 2). The variance within the population differed between individual traits: straightness showing the smallest, and main root vector angle the largest, variance (Figure 1C). Salt stress increased the observed variance in traits related to main and lateral root length, but not in lateral root density, indicating that observed natural variation in response to salt stress is mainly due to differences between accessions in maintenance of main and lateral root growth rather than root patterning.
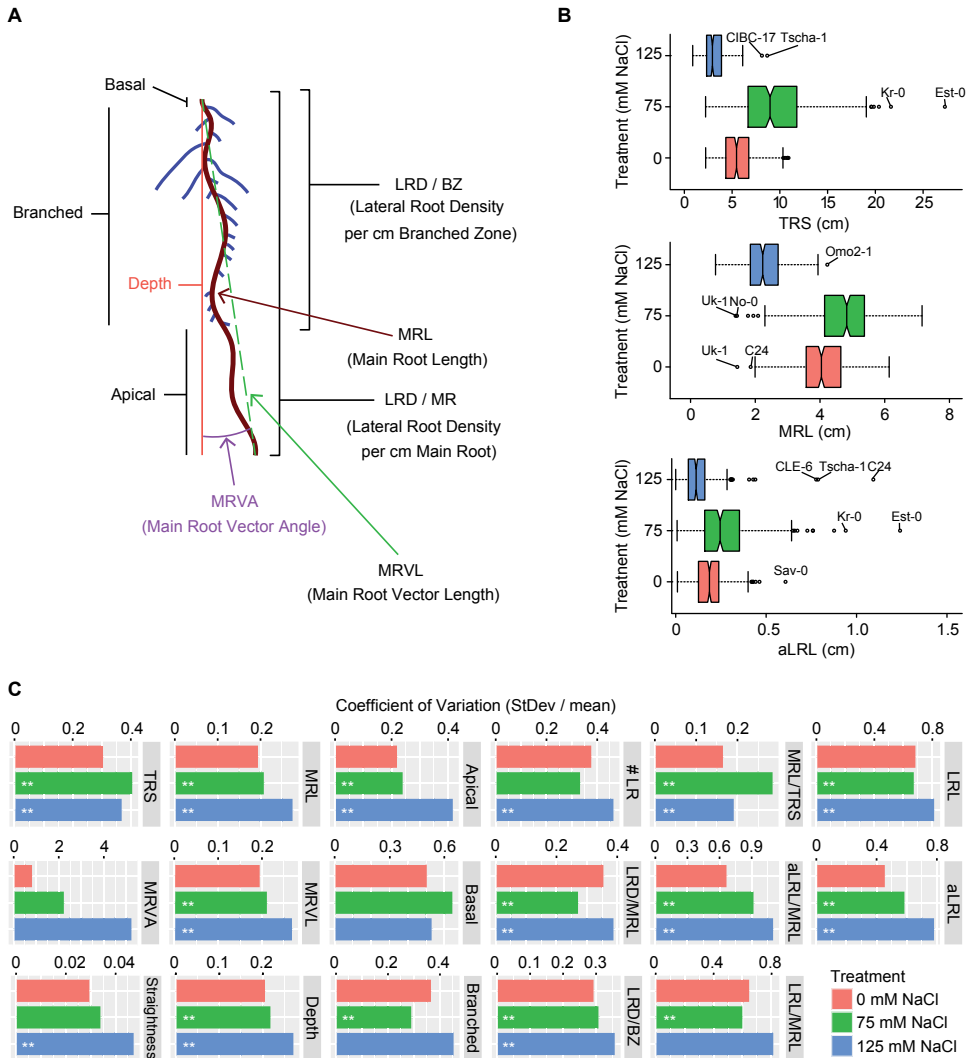
**Figure 1. Natural variation observed in RSA plasticity in response to salt stress.** The effect of salt stress on RSA was examined for 347 Arabidopsis accessions (Supplemental Dataset 1) on 8- and 12-day-old seedlingsgrown in control and salt stress conditions respectively. (**A**) Overview of RSA parameters obtained from EZ-rhizo quantification. Additionally, lateral root length (LRL), average lateral root length (aLRL) as well as the ratios between main root (MRL), average lateral root length (aLRL) and total root size (TRS) were calculated. All RSA traits are listed in Supplemental Dataset 2. (**B**) Natural variation in total root size (TRS), main root length (MRL) and average lateral root length (aLRL) is presented with notched box-plots. The accessions representing outliers in individual traits are indicated. Boxplots of all RSA traits are presented in Supplemental Figure 2. (**C**) Coefficient of variation observed in all 17 RSA traits per salt stress condition for 347 Arabidopsis accessions studied. The significant differences in variation between control and salt stress are indicated with * for p-value < 0.05 and ** for p-value < 0.01, as calculated using f-tests.

Individual components of RSA were strongly correlated under control conditions (Figure 2A-B, Supplemental Dataset 3). Several of these correlations, including the number of lateral roots with main root length, were significant across all conditions, indicating again that salt does not alter lateral root patterning or that the natural variation therein is limited (Supplemental Dataset 3). However, a significant correlation between the length of the apical zone and lateral root length was observed only under control conditions (Figure 2A), indicating that salt stress increased the variation in the distance from the root tip to the point at which lateral roots start to emerge and elongate, which might be related to different rates of lateral root emergence upon salt stress. The correlation between lateral root length and lateral root number was maintained in seedlings grown under salt stress conditions (Figure 2B), although a decrease in correlation strength was observed. Thus, lateral root emergence had a significant contribution to lateral root size in all conditions despite the increased variability in lateral root length (Figure 1C). The 17 RSA traits, together with the length of the individual zones relative to the main root length, were used for Principal Component Analysis, reducing the data dimensionality to three Principal Components (PC1–3) (Figure 2C, Supplemental Figure 3, Supplemental Dataset 4). Traits corresponding to lateral root development, such as number of lateral roots per main root, lateral root length, and size of the branched zone significantly contributed to PC1, explaining 41% of the variance. PC2, explaining 18.8% of the variance, corresponded to the main root-related traits, such as main root path length, vector length, and depth. The traits related to lateral root elongation, such as average lateral root length, significantly contributed to PC3, explaining 11.2% of the observed variance. Thus, the majority of the natural variation in RSA is harbored in the distribution of the root mass between main and lateral roots (PC1), maintenance of main root growth (PC2) and lateral root emergence and elongation (PC3). Summarizing the RSA results in three PCs allowed identification of the RSA traits exhibiting most natural variation and reveals phenotypic plasticity in response to salt stress, as the differences between the accessions grown under different conditions are evident even when the dimensionality of the RSA is reduced to three PCs (Supplemental Figure 3).
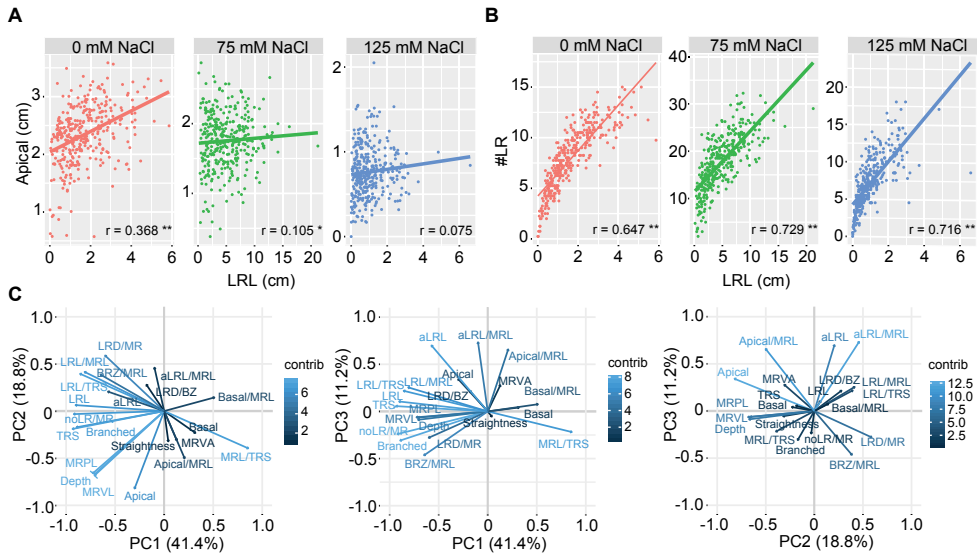
**Figure 2. Salt affects the relationship between RSA components, with lateral root development explaining the majority of the observed variation. (A)** The correlation between apical zone size and total lateral root length (LRL) and **(B)** lateral root number (#LR) and total lateral root length (LRL) for plants grown under 0, 75 and 125 mM NaCl are presented with red, green and blue dots respectively. The lines in corresponding color represent the linear model fitting the correlation per condition. The Pearson correlation coefficients [*] are presented in the lower right corner of each correlation graph, with ** indicating p-value < 0.01 and * p-value < 0.05. **(C)** Principal Component Analysis revealed three PCs explaining 71.4% of variation. The contribution plots show how each RSA trait contributes to each PC, ranging from low contribution (dark-blue) to high contribution (light-blue). The contribution of individual traits to each PC is listed in Supplemental Dataset 4.

## GWAS reveals *HKT1* and *CYP79B2* as candidate genes explaining natural variation in the response of lateral roots to salt

Natural variation in 17 RSA traits and three PCs (Supplemental Dataset 5) was used as an input for genome-wide association study (GWAS) using the scan_GLS algorithm (Kruijer et al., 2015). After applying correction for population structure (Kang et al., 2008) and exclusion of traits with low narrow heritability ($h^2$ < 0.2, Supplemental Dataset 6) GWAS identified 150, 132 and 254 significantly [–log10(p-value) above 5.6] associated SNPs for RSA traits in 0, 75, and 125 mM NaCl respectively (Supplemental Dataset 7). Most SNPs were associated with the average lateral root length per main root length. The largest variation observed in the relative distribution of root mass from main root length to lateral root length corresponds with the high number of associations found for PC3 and average lateral root length measured under salt stress conditions. Identified associations were examined in detail considering their association with multiple traits, using both individual replicates and average value per accession. As the majority of the associations was mapped using the SNP set with Minor Allele Frequency above 0.01, we selected for the associations mapped with MAF of at least 0.01 or with the –log10(p-value) score above strict Bonferroni threshold, based on the collection of SNPs including the rare alleles, corresponding to the score of 6.6. We further explored the associations identified with multiple RSA traits and different conditions (Supplemental Figure 4,

Supplemental Datasets 8–10). Our selection yielded 100 candidate loci for RSA traits under salt stress conditions, and we subsequently compared their transcriptional changes in tissue-specific expression in response to salt (Dinneny et al. 2008), revealing 10 genes directly underlying the associated SNPs and 60 genes within the 10-kb window of the mapped SNPs to be significantly altered in the cell type-specific expression dataset in response to salt (Supplemental Dataset 11). The candidate genes that were either directly underlying the associated SNP, or located within the linkage disequilibrium of the identified SNP, were found to be significantly enriched in the genes with tissue specific alterations in response to salt stress as tested per hyper-geometric test. Since natural variation in salt stress response was mostly found in traits related to the relative distribution of root mass between lateral and main roots, we selected six loci associated with average lateral root length, average lateral root length per main root length and PC3 in salt stress (Figure 3A, Supplemental Dataset 12) for further analysis.

To fine-map the selected loci, the RSA phenotypes were associated with the SNPs based on the whole-genome sequencing data of the accessions (Alonso-Blanco et al., 2016), to identify additional SNPs and increase the mapping resolution. We identified between 2 and 26 additional SNPs for loci 1, 2, 5, and 6 (Supplemental Dataset 13). For the chosen loci, the regions surrounding the identified SNPs were further examined for sequence variation (Figure 3B-C, Supplemental Figures 5-8A). Genes located in the 10-kb window of the associated SNPs were examined for natural variation in their expression in root and shoot tissue under control and salt stress conditions using 48 accessions, chosen based on the SNP diversity of the candidate loci and the pronounced differences between their RSA under all conditions studied (Supplemental Figures 5-8B-C, Supplemental Figure 9a, Supplemental Figure 10, Supplemental Dataset 14). For four loci (1,2,3, and 6), we were not able to validate candidate genes due to lack of available mutant lines and/or limited phenotypic changes in response to salt in Col-0 background (Supplemental Figure 7e). Nevertheless, the natural variation in the expression observed among 48 accessions identified candidate background lines for future studies on these loci and can be accessed in the supplemental data (Supplemental Dataset 14).

The genomic region surrounding the 4th locus, associated with average lateral root length and the ratio of average lateral root length and main root length at 75 mM NaCl (Figure 3A-B, Supplemental Dataset 12), was found to contain only one gene, At4g10310, also known as *Arabidopsis HIGH AFFINITY K$^+$ TRANSPORTER 1* (*AtHKT1*). This gene was previously identified for its role in salinity tolerance (Rus et al., 2001; Munns et al., 2012), although no role in the regulation of root system architecture was noted. The genomic region around the associated SNP contained a high number of SNPs and a number of insertions / deletions in the promoter and intron regions of HKT1 (Figure 3B).
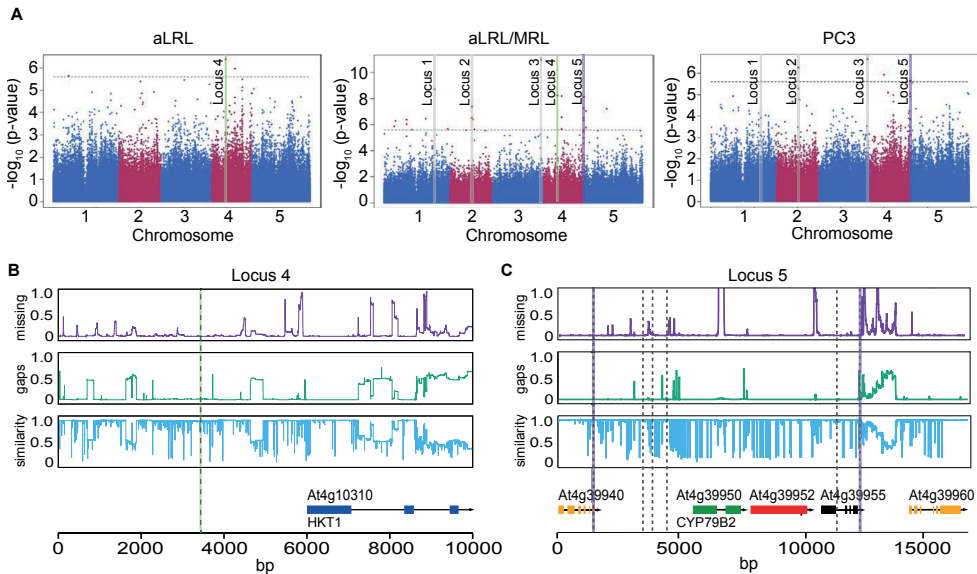
**Figure 3. GWAS identifies loci with high and low allele diversity.** GWAS was performed on **(A)** average Lateral Root Length (aLRL), ratio of average Lateral and Main Root Length (aLRL/MRL) and Principle Component 3 (PC3) at low salt stress conditions (75 mM NaCl) and significant associations above LOD 5.6 with MAF > 0.01 were identified. The dotted line represents the threshold of a LOD of 5.6. The 6 chosen loci (Supplemental Dataset 12) are marked. The validated loci containing *HKT1* (locus 4) is marked with green and *CYP79B2* (locus 5) with purple. Genetic variation in locus 4 **(B)** and 5 **(C)** was studied in 147 HapMap population accessions. The purple graphs represent the portion of missing data, while the green graphs represent deletions present in accessions other than Col-0. The blue graphs represent the sequence similarity compared to Col-0. The Open Reading Frames are aligned in the lowest panel. The location of the associated SNPs from 250k SNP set is represented with highlighted dashed-lines, while the SNPs mapped using the 4M SNP set are represented with gray dashed-lines.

Locus 5 contains six SNPs, spanning from the coding region of At4g39940 up to the coding region of At4g39955 (Figure 3C, Supplemental Datasets 12-13). The SNPs were associated with variation in average lateral root length in 125 mM of NaCl, average lateral root length per main root length in both salt stress conditions, and PC3 in 75 mM of NaCl. Interestingly, the expression of At4g39950, also known as *CYTOCHROME P450 FAMILY 79 SUBFAMILY B2* (*CYP79B2*), was reported to exhibit zone-specific expression changes in response to salt (Dinneny et al., 2008) (Supplemental Dataset 11). CYP79B2 is known to convert tryptophan (Trp) to indole-3-acetaldoxime (IAOx) in the biosynthesis pathway of camalexin, indole glucosinolates and auxin (Hull et al., 2000; Mikkelsen et al., 2000; Zhao et al., 2002; Glawischnig et al., 2004; Sugawara et al. 2009) and its expression was reported at the sites of lateral root development and in the quiescent center, but no role for CYP79B2 in root development has been reported (Ljung et al., 2005). The promoter region of *CYP79B2* showed extensive sequence divergence among the accessions and three SNPs were mapped to the promoter of this gene (Figure 3C), but the region was too diverse to conduct haplotype analysis. No non-synonymous SNPs were identified in the protein coding sequence of *CYP79B2*.

*High HKT1 expression reduces lateral root development in saline conditions*
Extensive natural variation in *HKT1* expression in the set of 48 accessions was observed in the root tissue of seedlings exposed to salt stress (Figure 4A, Supplemental Figure 9A), with Gr-5, Hs-0, N4, Ga-2 and Jl-3 showing the highest and LDV-58, CUR-3 and Tsu-0 the lowest expression. Although only few accessions exhibited high *HKT1* expression, all of these tended to develop shorter lateral roots under salt stress conditions (Figure 4B). By contrast, T-DNA insertion lines with reduced *HKT1* expression in the Col-0 background did not exhibit any differences in RSA development compared to wild type Col-0 (Supplemental Figure 12), consistent with the natural variation expression data. Since ubiquitous overexpression of *HKT1* was previously observed to have a detrimental effect on plant development (Moller et al., 2009), we studied the phenotypes of two available lines with enhanced *HKT1* expression at the native expression site, the root pericycle (Mäser et al., 2002; Moller et al., 2009): E2586 UAS-HKT1 in Col-0 background and J2731 UAS-HKT1 in C24 background, (Moller *et al.*, 2009). No significant differences between the background lines and lines with enhanced *HKT1* expression were observed under our *control* conditions. Interestingly though, under salt stress conditions lines with enhanced HKT1 expression developed fewer and shorter lateral roots in both Col-0 and C24 backgrounds (Figure 4C-D), while the high *HKT1* expression caused severe reduction in main root length only in Col-0 background (E2586 UAS-HKT1) (Figure 4C-D). Thus, while low expression levels of *HKT1*, either in Arabidopsis accessions or T-DNA lines, seem to have no obvious effects on root morphology, enhanced expression can cause severe alterations in root architecture under salt stress, possibly due to toxic effects of high $Na^+$ concentrations or changes in osmotic potential of root cells.

*Salt-induced changes in CYP79B2 expression correlate with maintenance of lateral root development*
We further investigated the natural variation in transcriptional changes of *CYP79B2*, and other genes at the same locus, in response to salt stress. *CYP79B2* expression significantly increased upon salt stress in both root and shoot tissue in most of the 48 accessions studied, but much variation was observed (Figure 5A, Supplemental Dataset 14). A three-way ANOVA showed that the response was the same in both tissues as no interaction effect was found, although expression in the root was significantly higher. While At4g39960 also showed significant induction of expression in salt stress in both root and shoot, the effect was more pronounced in the shoot. At4g39940 showed reduced expression in the root and induced expression in the shoot and At4g39955 showed no change upon salt stress (Supplemental Figure 10, Supplemental Dataset 14). For At4g39952 only very recently transcripts were found, and it likely has very low expression (Liu et al., 2016). We have thus decided to focus on *CYP79B2* for further analysis. The effect of salt on *CYP79B2* expression in the root showed much variation between accessions. The log2 fold change in gene expression in the root upon salt stress ranged from -2.2 in MNF-Pot-4 to 7.2 in Brö1-6 (Supplemental Dataset 14).
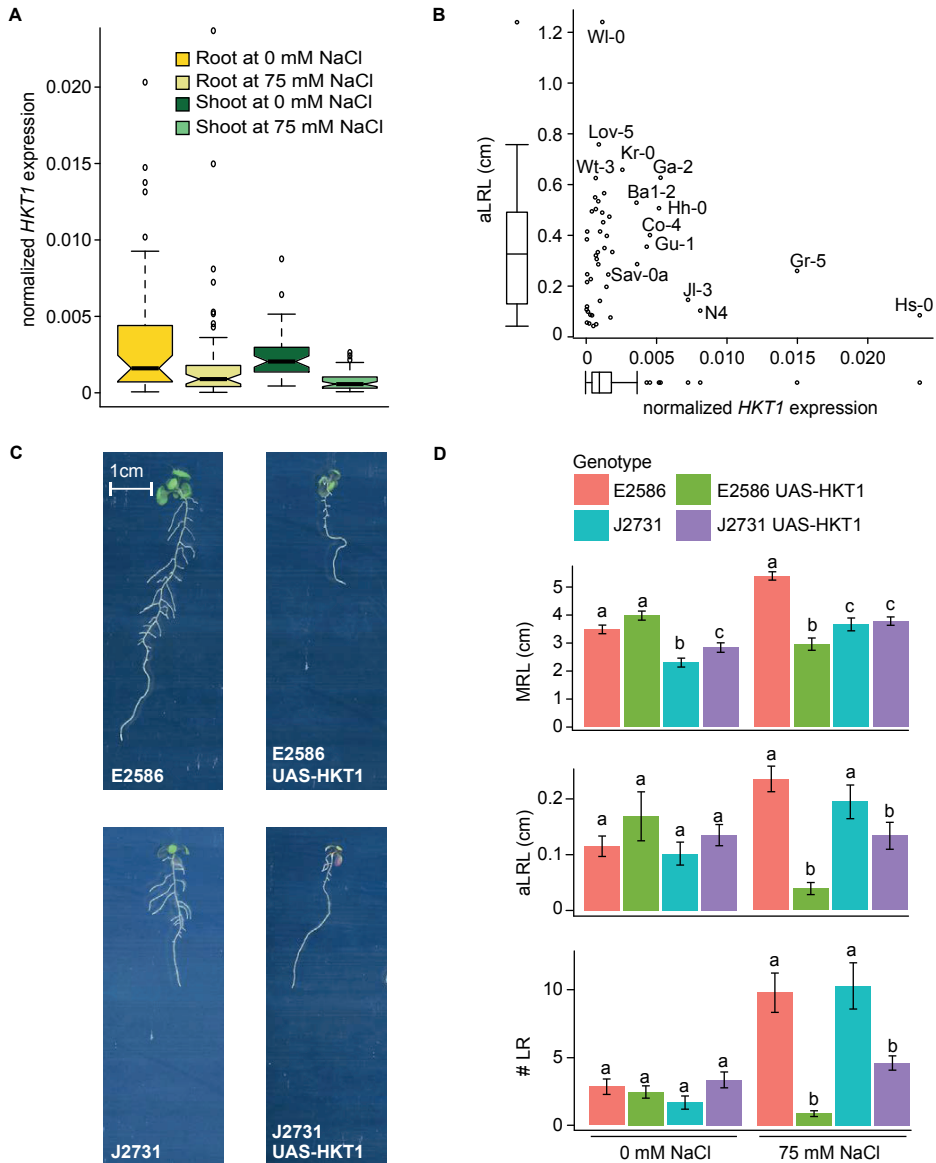
**Figure 4. High *HKT1* expression reduces LR development in salt stress conditions. (A)** Natural variation in the *HKT1* expression was studied in root and shoot tissue in 5-day-old seedlings treated with mock (C) or 75mM NaCl (S) conditions for 24 hours. The boxplots represent the median and extent of natural variation as observed for population of 48 accessions (Supplemental figure 11A, Supplemental Dataset 14). **(B)** A trend between *HKT1* expression and average lateral root length (aLRL) was observed, with accessions with high *HKT1* expression developing short lateral roots. **(C)** Pictures of representative 12-day-old seedlings of UAS-HKT1 lines grown at 75 mM NaCl. **(D)** UAS-HKT1 lines, with enhanced *HKT1* expression in the root pericycle in Col-0 (E2586) and C24 (J2731) backgrounds, were examined for salt induced changes in RSA. 4-day-old seedlings were transferred to 0 and 75 mM NaCl and the RSA of 8- and 12-day-old seedlings, respectively, was quantified. The bar-plots represent the average trait value (n=16) and error bars represent SE. Different letters indicate significant differences (p<0.05) between the genotypes per condition calculated using one-way ANOVA followed by Tukey's post-hoc test.
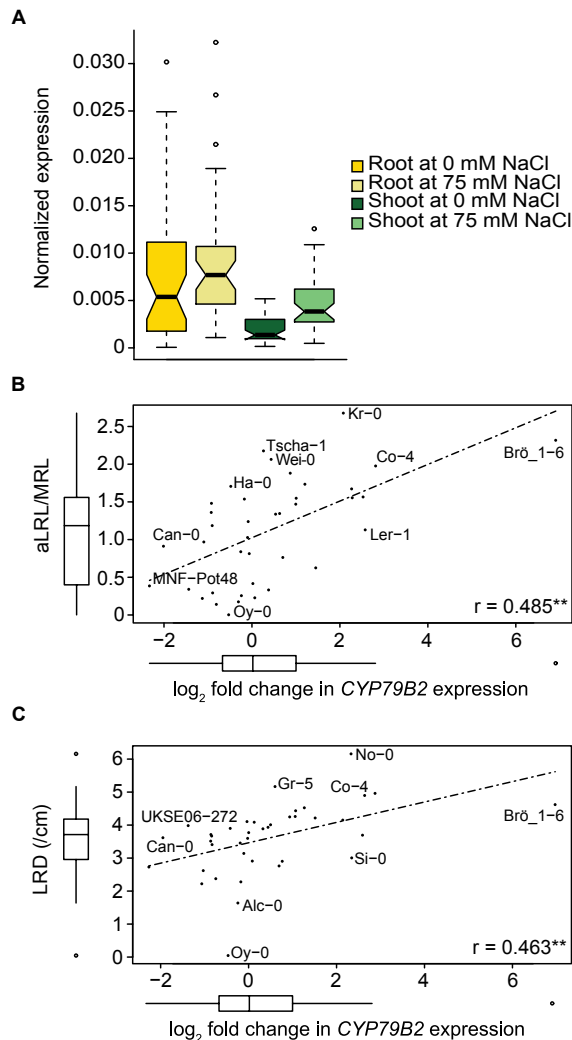
**Figure 5. Change in *CYP79B2* expression in response to salt stress correlates with lateral root development during salt stress.** Natural variation in genes in locus 5 was studied in root and shoot tissue in 5-day-old seedlings treated with mock or 75 mM NaCl for 24 hours. The boxplot **(A)** represents the median and extent of natural variation in *CYP79B2* expression as observed for population of 48 accessions. Boxplots for the other gens in the same locus can be found in Supplemental Dataset 14. The relative $\log_2$ fold change in expression of *CYP79B2* between control and salt stress positively correlated with several root architecture traits in the accessions, including **(B)** average lateral root length per main root length (aLRL/MRL) at 75 mM NaCl and **(C)** the lateral root density (LRD) at 75 mM NaCl. The Pearson correlation coefficients (r) are presented in the lower right corner of each correlation graph, with ** indicating p-value < 0.01 and * p-value < 0.05.

To investigate whether the change in *CYP79B2* expression upon salt stress would correspond with lateral root development, we examined the correlations between the log2 fold change in expression of *CYP79B2* and associated RSA traits. The average lateral root length at 75 mM of NaCl significantly correlated with the log2 fold change in *CYP79B2* expression upon salt stress (Figure 5B). In addition, the log2 fold change showed a significant positive correlation with the lateral root density in salt stress conditions (Figure 5C).
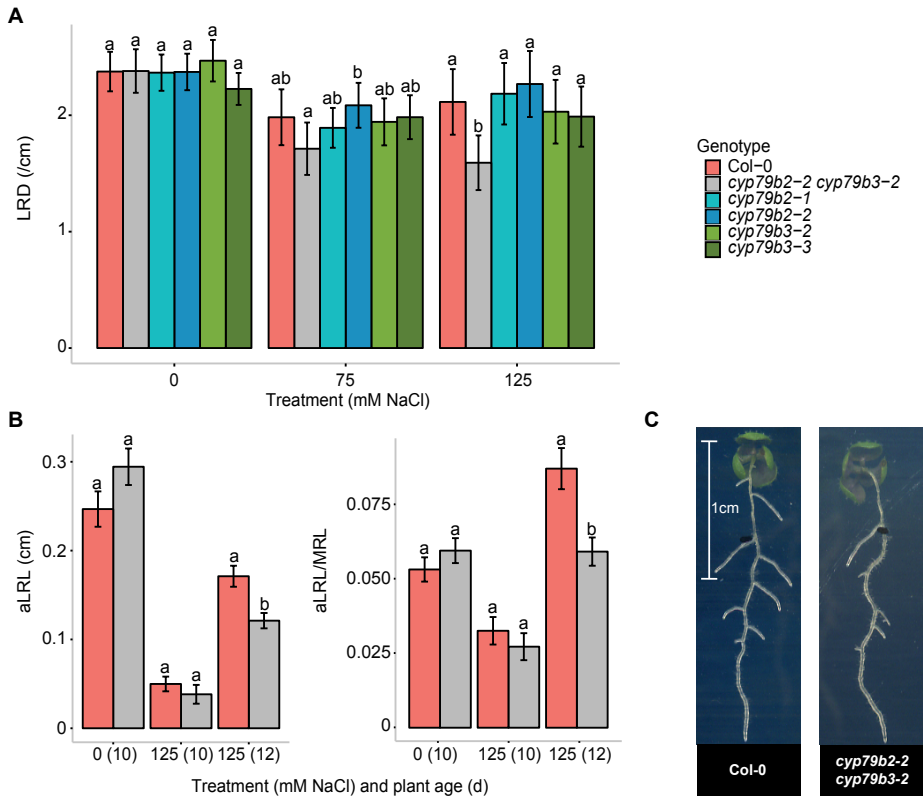


**Figure 6. Loss-of-function of both CYP79B2 and CYP79B3 results in reduced lateral root development during salt stress. (A)** 4-day-old seedlings of Col-0, *cyp79b2*, *cyp79b3* and *cyp79b2-2cyp79b3-2* lines were transferred to 0, 75 and 125 mM NaCl and RSA of 10-day-old seedlings was quantified. The bar-plots represent the average lateral root density (LRD) of three experiments with each 20 replicates; error bars represent pooled SE. A mixed linear model was used to determine significant differences and a significant interaction between treatment and genotype was found. Letters indicate significant differences (p < 0.05) following a manual-contrasts post-hoc comparison within treatment. **(B)** Average lateral root length per main root (aLRL/MRL) and average lateral root length (aLRL) for Col-0 and *cyp79b2-2cyp79b3-2* in 0 mM (10-day-old seedlings )and 12 mM (10- and 12-day-old seedlings) NaCl. Other lateral root traits are presented in Supplemental figure 11. Bar-plots represent the average trait value as observed in 20 replicates and error bars represent SE. All traits were analyzed using two-way ANOVA and significant interactions were found for shown traits. Letters represent significant differences (p < 0.05) following a manual-contrasts post-hoc comparison within treatment. **(C)** Pictures of representative 12-day-old seedlings of Col-0 and the *cyp79b2-2cyp79b3-2* mutant at 125 mM NaCl.

As the function of *CYP79B2* is known to partially overlap with that of *CYP79B3* (Hull et al., 2000; Zhao et al., 2002; Glawischnig et al., 2004), we investigated the root system architecture of T-DNA insertion lines (Supplemental Figure 11A) for both genes and the *cyp79b2-2cyp79b3-2* double mutant at different salt concentrations. The *cyp79b2-1* and *cyp79b2-2* lines as well as the double mutant *cyp79b2-2cyp79b3-2* showed a slightly, but significantly, longer main root independent of the conditions (Supplemental Figure 12B), but no lateral root-related differences were observed under control conditions. Interestingly, *cyp79b2-2cyp79b3-2* mutant seedlings grown on 125 mM NaCl supplemented medium, developed significantly fewer lateral roots per cm of main root at 10 days after germination (Figure 6A). This is consistent with the observed positive correlation between fold change in *CYP79B2* expression upon salt stress and lateral root density (Figure 5C). Double mutant seedlings also developed shorter lateral roots at 12 days after germination, consistent with the mapped traits in the GWAS (Figure 6B-C, Supplemental Figure 11B). Conversely, ectopic overexpression of *CYP79B2* lead to an increase in lateral root length and number of lateral roots both in control and salt stress (Supplemental Figure 13B-D). Interestingly, lateral root density in this line (Supplemental Figure 13C) was only increased when exposed to high salinity.

To investigate whether the observed changes in root system architecture were due to lateral root elongation or development, the developmental stages of lateral roots in *cyp79b2-2cyp79b3-2* and p35S:CYP79B2 seedlings were compared to those of the wild-type in both control and salt stress (Figure 7). In agreement with the number of laterals measured in the RSA assay (Supplemental figure 13), ectopic over-expression of *CYP79B2* leads to an increase in the total number of primordia and lateral roots combined while no difference is observed for the *cyp79b2-2cyp79b3-2* mutant compared to wildtype Col-0 (Figure 7A). However, we did observe a relatively higher proportion of lateral roots in primordial stage in *cyp79b2-2cyp79b3-2*, independent of treatment (Figure 7B). Consistent with earlier work (Mcloughlin et al. 2012), salt stress leads to an increased relative frequency of primordia stuck in developmental stage 5 (Figure 7B). Interestingly, ectopic over-expression of *CYP79B2* reduces the relative number of primordia in this stage independent of condition, possibly explaining the increased number of lateral roots observed. Our data indicates that lateral root development is affected by *CYP79B2* and *CYP79B3* expression, but it is unclear whether this process also plays a role in the observed changes in root system architecture caused by salt stress, as most effects are found in both control and salt stress. Although we might expect a decreased number of lateral roots in *cyp79b2-2cyp79b3-2* mutant in salt stress, it is important to note that lateral root density is dependent on the main root length as well. Furthermore, root system architecture assays only count visible lateral roots, so a lower number of lateral roots observed in these assays might also be due to decreased elongation of lateral roots.
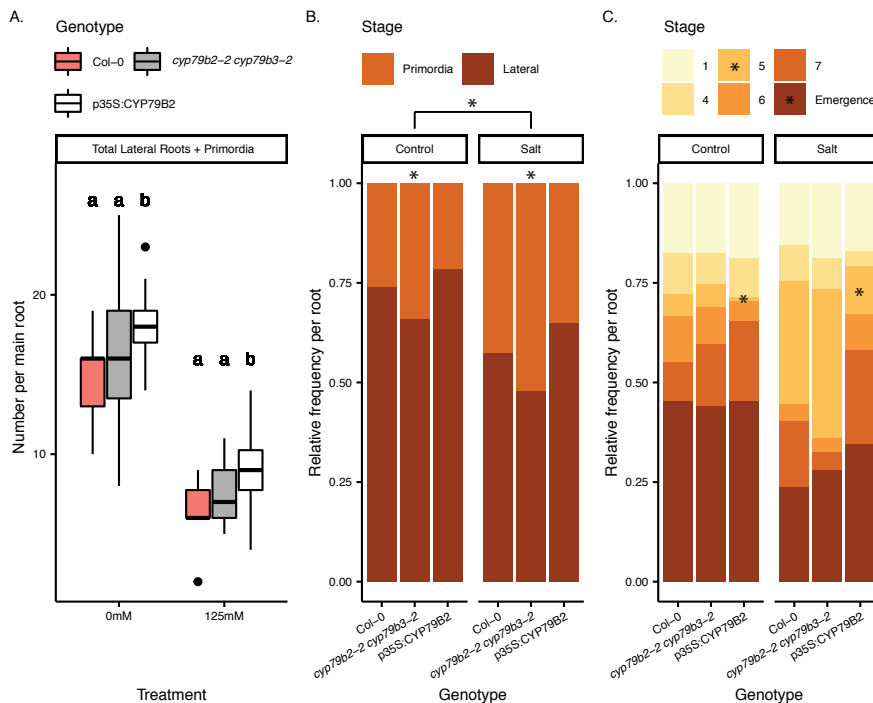
**Figure 7. Ectopic over-expression of *CYP79B2* leads to a reduced frequency of primordia stuck in developmental stage 5 during salt stress, thereby contributing to an increased total number of lateral roots.** (**A**) 10-day old seedlings of Col-0 (pink), *cyp79b2-2cyp79b3-2* (grey), p35S:CYP79B2 (white), transferred to ½ MS plates supplemented with 0 (control) or 125 mM of NaCl after 4 days, were fixed and the stage of each primordia and lateral root was determined under the microscope (stages defined as described in McLoughlin et al. 2012). The middle line inside the box represents the median of the combined number of lateral and primordia roots per main root (n=20). Lower and upper box boundaries represent 25th and 75th percentiles. Lower and upper error lines represent 10th and 90th percentiles. Dots represent data falling outside 10th and 90th percentiles. Significant differences were determined by a two-way ANOVA, followed by a manual contrast post-hoc test within treatments if significant differences were found. Different letters indicate significant differences within treatment ($p<0.05$). (**B**) The average relative frequency of lateral and primordia roots present in roots presented in (**A**). (**C**) The average relative frequency of each stage of primordia present in roots presented in (**A**). Significant differences for (**B**) and (**C**) were determined by a two-way ANOVA, followed by a Tukey post-hoc test. An asterisk indicated in the legend indicates significant differences ($p<0.05$) for treatment, an asterisk in the bar indicates significant differences ($p<0.05$) between genotypes.
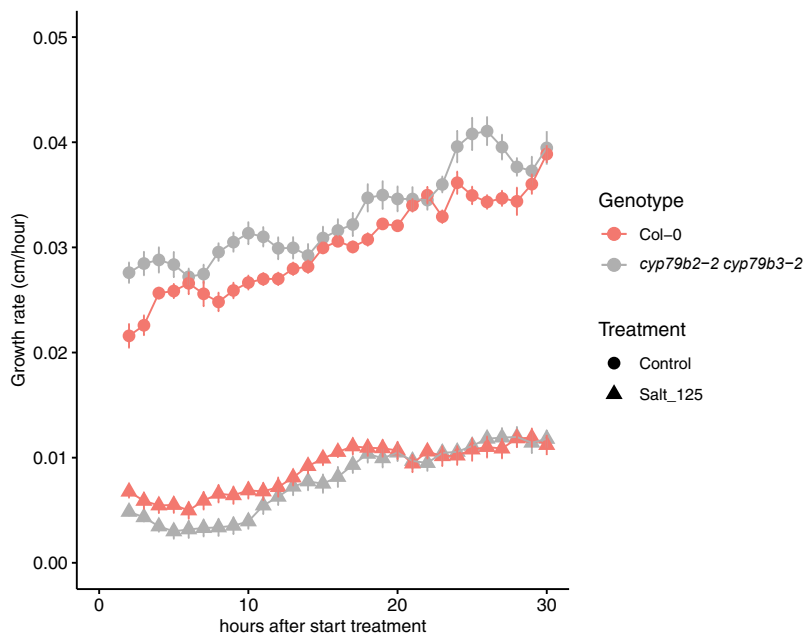
**Figure 8. Loss of function of *CYP79B2* and *CYP79B3* leads to a more pronounced quiescent phase in the main root during salt stress.** 7-day-old seedlings grown of Col-0 (pink) and *cyp79b2-2 cyp79b3-2* (grey) were transferred to ½MS plates supplemented with 0 (control, circles) or 125 (salt, triangles) mM of NaCl and pictures were taken every 20 minutes to quantify growth rate in the main root. Growth rate was calculated by taking the growth over 4 hours (2 before and 2 after the specific timepoint) and was then averaged over 1 hour for 12 replicates. Error bars represent the SE of the mean.

To investigate whether root elongation of *cyp79b2-2cyp79b3-2* plants was affected by salt stress, root growth of 7-day-old seedlings was followed with time-lapse imaging every 20 minutes (Figure 8). Unfortunately, quantification of lateral root growth rates proved more difficult than expected, because 7-day-old seedlings do not display many visible lateral roots yet and lateral roots grow at very different rates, leading to big variation. For the main root, we did observe a clear pattern of growth phases in response to salt stress (Figure 8). After exposure to salt stress, the growth rate first rapidly declines, and roots almost stop growing. This phase has been described as the quiescent phase (Geng et al. 2013), followed by recovery to a stable low growth rate. Wildtype roots reach a stable growth rate of approximately 0.01 cm/hour after 15 hours (Figure 8). In contrast, in *cyp79b2-2cyp79b3-2* seedlings a more pronounced quiescent phase with lower growth rates was observed, while a similar stable growth rate was found after 18 hours (Figure 8). In control conditions, *cyp79b2-2cyp79b3-2* actually grew faster, which is in agreement with their slightly longer main root independent of treatment (Supplemental Figure 11B). Apparently, this pronounced quiescent phase is too short to affect overall main root length in salt stress measured after 6 days of treatment. In lateral roots, however, the quiescent phase can take up to two days, thus a stronger quiescent phase or delay in

recovery could lead to bigger differences and explain the observed differences in lateral roots (Duan et al., 2013).

To examine whether the changes in root system architecture caused by altered *CYP79B2* expression affect salt tolerance, plant growth on soil was monitored. The *cyp79b2-2cyp79b3-2* mutant had a slightly lower dry weight compared to wildtype Col-0 plants independent of treatment (Figure 9A). In agreement, plants ectopically overexpressing *CYP79B2* were bigger in both control and salt treatment. Although dry weight was affected similarly in both treatments, loss-of-function of *CYP79B2* and *B3* led to a higher sodium/potassium ratio ($Na^+/K^+$ ratio) in the shoot specifically during salt stress (Figure 9B). The observed higher ratio in the double mutant is due to both a higher accumulation of sodium and a decrease in potassium content (Supplemental figure 14).
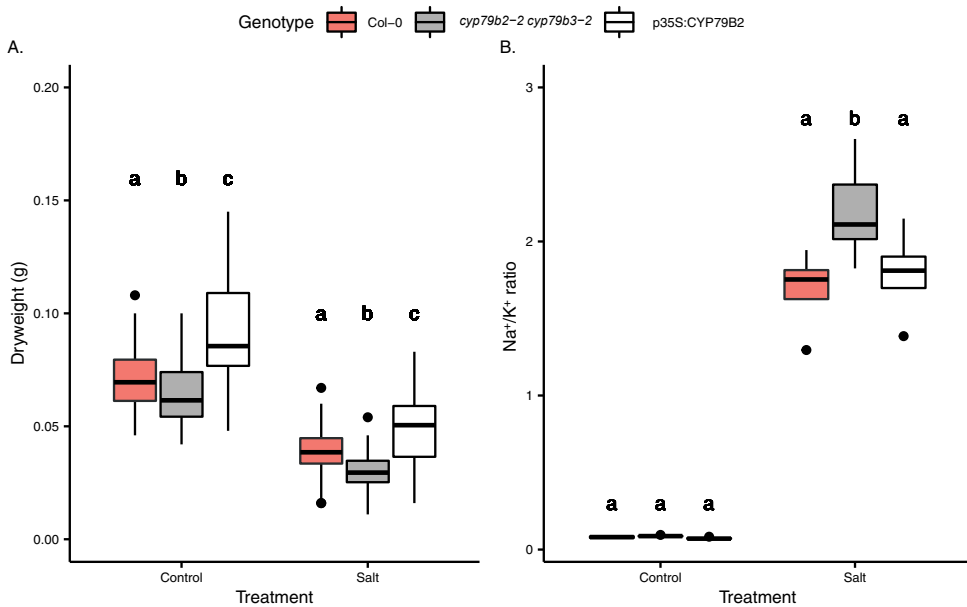


**Figure 9. Loss-of-function of *CYP79B2* and *CYP79B3* leads to reduced dry weight and increased $Na^+/K^+$ ratios when exposed to salt stress.** The rosette of 5-week-old Col-0 (pink), *cyp79b2-2 cyp79b3-2* (grey) and p35S:CYP79B2 (white) plants, transferred to control or salt treated soil after 1 week, were harvested and dryweight **(A)** and $Na^+/K^+$ ratios **(B)** were determined. The middle line inside the box represents the median (n=20). Lower and upper box boundaries represent 25th and 75th percentiles. Lower and upper error lines represent 10th and 90th percentiles. Dots represent data falling outside 10th and 90th percentiles. Significant differences were determined by a two-way ANOVA, followed by a manual contrast post-hoc test within treatments if significant differences were found. Different letters indicate significant differences within treatment.

## DISCUSSION

Salt stress not only reduces the development and growth of roots (West et al., 2004; Liu and Zhu, 1997; Kobayashi et al., 2016; Shelden et al., 2013; Tu et al., 2014), but also causes reprogramming and re-distribution of the root mass between main and lateral roots (Julkowska *et al.*, 2014). By studying natural variation for root architecture in Arabidopsis, we observed that the natural variation in RSA responses to salt stress is exhibited mainly through the emergence and elongation, rather than patterning, of lateral roots. The variance observed in traits related to root mass distribution between main and lateral root increased with salt stress exposure (Figure 1D), while the correlations between main root length and number of lateral roots remained unaltered by salt stress (Supplemental Dataset 3). Those trends are in agreement with the data on dynamic changes in RSA performed on a smaller number of Arabidopsis accessions (Julkowska *et al.*, 2014) and with the reduction of lateral root development under salt stress conditions observed in an earlier study (Kawa et al., 2016). In this study, we describe the traits with the most pronounced phenotypic plasticity in response to salt stress to be related to main root length, number of lateral roots, size of the apical zone and average lateral root length, as they make most significant contributions to Principal Components describing natural variation observed (Supplemental Dataset 4) and are subjected to G x E interactions (Supplemental Dataset 2). Collecting multi-trait phenotypes and performing multi-variate analysis, as presented in this work, will improve our understanding of how plant development affects performance under stress conditions. The data presented in this study are available through the Salt_NV_ Root App for the user to explore in more detail, compare individual accessions and also perform cluster analysis on the RSA traits of interest. This tool can thus provide additional insight for further exploration of natural variation in complex RSA traits and their relationship to plant performance.

While many GWAS studies published to date focus on single traits, such as ion accumulation, main root growth or compatible solute accumulation (Strauch et al., 2015; Baxter et al., 2010; Lachowiec et al., 2015; Slovak et al., 2014; Verslues et al., 2014), there is an increasing focus on multi-trait response phenotypes, including RSA response to stress (Rosas et al., 2013; Kawa et al., 2016). An advantage of performing GWAS on multi-trait phenotypes, also apparent in our study, is that additional confidence can be gained when the same candidate loci are mapped using different traits and / or different stress conditions, or when the multi-trait phenotypes are reduced to Principle Components that map to the overlapping loci (Figure 3A). Interestingly, 100 candidate loci identified by GWAS in this study contain genes involved in ethylene and ABA signaling, such as *EIN2* and S*nRK2.7* (Supplemental Dataset 11), indicating natural variation in hormonal control pathways that were earlier described to play a role in RSA responses to salt stress (Duan et al., 2013; Geng et al., 2013). The significant overlap between the identified candidate genes and salt stress-induced changes in gene expression (Dinneny et al., 2008, Supplemental Dataset 11) implies that the allelic variation might accumulate in the regions important for transcriptional regulation of genes involved in root remodeling in response to salt. Also, a meta-analysis on genetic architecture of abiotic and biotic stress responses, which included a selection of our

salt stress response data, implied genetic correlations with other abiotic stress responses (Thoen et al., 2017).

The association found in the promoter region of *HKT1* provides a link between ion sequestration and lateral root development. Our results suggest that some accessions with high *HKT1* expression develop shorter lateral roots under salt stress conditions (Figure 4B). Using transgenic lines with enhanced expression at the native root expression site (UAS-HKT1 lines), we confirmed that high *HKT1* expression indeed reduces lateral root formation under salt stress in Col-0 and C24 background (Figure 4C-D). Although sodium accumulation in the root stele is important for ion exclusion from shoot tissue (Moller et al., 2009; Kotula et al., 2015; Munns et al., 2012), in the young seedlings the high stelar sodium accumulation could potentially result in ABA-dependent lateral root quiescence (Duan et al., 2013) or even damage to the lateral root primordia. The exact mechanisms underlying the reduced lateral root development in lines overexpressing *HKT1* remain to be explored in future studies.

Our genetic and physiological data confirm our identified candidate gene *CYP79B2* to be involved in lateral root development under salinity stress, which suggests that genes identified in our GWAS are indeed involved in reshaping RSA under salt stress conditions. Significant correlations were found between salt-induced expression of *CYP79B2* and lateral root development under salinity stress (Figure 5). Further analysis of *CYP79B2* and *CYP79B3,* which are known to have partially overlapping functions, showed that these genes are required for the maintenance of lateral root growth under salt stress conditions, but not in control conditions (Figure 6). In the main root, lack of *CYP79B2* and *CYP79B3* expression causes a prolonged quiescent phase upon exposure to salt stress (Figure 8), indicating that CYP79B2 and CYP79B3 could be responsible for recovering root elongation rates in salinity. Lateral roots display a longer quiescent phase of up to 2 days (Duan et al. 2013), which could explain the more severe effect of *CYP79B2* and *CYP79B3* on lateral roots than on main roots. Although lateral root development also is affected by altered *CYP79B2* and *CYP79B3* expression, these changes were independent of treatment (Figure 7). It remains unclear whether alterations in development also contribute to maintenance of lateral root growth under salt stress. We do observe that ectopic overexpression of *CYP79B2* specifically decreases the number of primordia in stage 5 of development. Induction of expression of *CYP79B2* could thus alleviate the inhibitory effect of salt stress on this stage. As both *CYP79B2* and *CYP79B3* convert tryptophan to indole-3-acetaldoxime (IAOx), these data suggest the involvement of the IAOx pathway in shifting investments from main to lateral roots during salt stress. Both *CYP79B2* and *CYP79B3* were previously observed to be expressed at the site of newly developing lateral roots (Ljung et al., 2005). The IAOx pathway is *Brassica*-specific and can produce three types of active compounds: camalexin, indole glucosinolates and IAA (Hull et al., 2000; Zhao et al., 2002; Mikkelsen et al., 2000; Glawischnig et al., 2004; Sugawara et al., 2009). Both camalexin and indole glucosinolates act as defense compounds induced in both shoot and root upon pathogen attack (Glawischnig, 2007; Halkier and Gershenzon, 2006; Brown et al., 2003; Lemarié et al., 2015), but no clear link to root development has been found. The IAOx pathway has been shown to contribute to auxin production under heat stress conditions (Zhao et al., 2002).

NITRILASE 1 (NIT1), proposed to catalyze the last step of the IAOx pathway leading to auxin biosynthesis, was previously described to be involved in maintenance of lateral root development (Lehmann et al., 2017), and the expression of *NIT1* and *NIT2* was observed to be upregulated in response to salt stress (Bao and Li, 2002). We propose that the natural variation in promoter region of *CYP79B2* results in altered expression induction by salt stress, and that IAOx-pathway is necessary for maintenance of lateral root development under salt stress, most likely through production of auxin, although a role for other IAOx-pathway generated compounds cannot be excluded.

Previously, natural accessions that exhibited reduced lateral root emergence were associated with increased sensitivity to salt stress, while those with many, but shorter later roots showed better maintenance of $Na^+/K^+$ ratio under salt stress (Julkowska et al., 2014). As we found that enhanced *HKT1* expression reduced RSA development when 4-day-old seedlings were exposed to salt on agar plates (Figure 4), reduced salt tolerance might be expected. However, the salinity tolerance of the C24 UAS-HKT1 line was reported before to be enhanced when 3-week-old plants were exposed to salinity (Moller et al., 2009), and high *HKT1* expression was previously found to cause sodium exclusion from leaf tissue and therefore higher salt stress tolerance (Rus et al., 2006; Baxter et al., 2010; Munns et al., 2012). Conversely, *CYP79B2* or *CYP79B3* expression is necessary for maintenance of lateral root development (Figure 6), but salinity tolerance does not seem to be affected by altered expression (Figure 9). Plants lacking *CYP79B2* and *CYP79B3* are reduced in size, but this seems independent of salt treatment, which is in agreement with previous research (Crane et al., 2019). Plant ion homeostasis does seem to be affected by altered *CYP79B2* and *CYP79B3* expression (Figure 9, Supplemental Figure 14). Yet, as indole glucosinolate biosynthesis has been shown to affect phenylpropanoid biosynthesis, which leads to production of lignin among other compounds (Kim et al., 2015), it remains unclear whether the observed effects on ion homeostasis are related to alterations in root system architecture or are the effect of changes in accumulating phenylpropanoid products. Further investigation of the other candidate genes identified in this study and examining their contribution to RSA development and salt stress tolerance will provide more insight in how salt stress affects root morphology and how those changes would potentially increase salt stress tolerance of crops.

## MATERIALS & METHODS

*Plant material and growth conditions*

The Arabidopsis HapMap collection (Weigel and Mott, 2009) was obtained from the Arabidopsis Biological Resource Centre (www.abrc.osu.edu). The 360 accessions were propagated under long day conditions (21°C, 70% humidity, 16/8h light/dark cycle, 125 µmol/m²/s, Sylvania Britegrow F58W 1084 lamps), with 8 weeks vernalization (between 4 and 8°C, 70% humidity, 16/8h light/dark cycle) starting at the 3rd week after germination to ensure flowering of all the accessions. Accessions that failed to germinate or flower were excluded from the screen, resulting in 347 accessions in total (Supplemental Dataset 1). Seeds used for the experiments were between 2 months and 1 year old.

Seeds were surface sterilized in a desiccator of 1.6 L volume using 20 mL household bleach and 600 µL 40% HCl for 3 h and were put in the laminar flow for 1.5 h to remove toxic vapors. The seeds were stratified in 0.1% agar at 4°C in the dark for 72 h and sown on square petri dishes (12 x 12 cm) containing 50 mL of control growth medium consisting of ½ Murashige-Skoog, 0.5% sucrose, 0.1% M.E.S. monohydrate and 1% Daishin agar, pH 5.8 (KOH), dried for 1 h in a laminar flow. Plates were placed vertically at a 70° angle under long day conditions (21°C, 70% humidity, 16/8h light/dark cycle). Four-day-old seedlings were transferred to square petri dishes containing basic medium supplemented with 0, 75 or 125 mM NaCl. Each plate contained four seedlings of two genotypes (two seedlings per genotype). Plates were placed in the growth chamber following a random design. The plates were scanned with Epson perfection V700 scanner at 200 dpi every other day until 8th day post transfer. The 8-day-old seedlings grown in 0 mM NaCl were used for phenotyping of RSA in control conditions while for both salt stress conditions (75 and 125 mM NaCl) phenotypes of 12-day-old seedlings were scored. The pictures were analyzed with EZ-Rhizo software (Armengaud et al., 2009). The entire population of 347 accessions was screened over six individual experiments with Col-0 as internal reference (Supplemental Figure 1). The RSA phenotypes of individual accessions were calculated from four biological replicates, except for Nd-1, Tommegap and Tottarp, where the RSA phenotype in control conditions was measured only for 2 biological replicates.

*Analysis of natural variation in RSA phenotypes*

The collected data on RSA phenotypes was cleared of outliers by removing the accessions of which the standard deviation within the genotype was larger than the standard deviation within the HapMap population, and RSA phenotyping was repeated for these accessions in the next experimental batch. The natural variation in the studied population was further explored by using average values per accessions as an input for notched boxplots and calculating coefficient of variance per condition studied. The correlations among different RSA traits at different conditions are presented in Supplemental Dataset 3. 17 RSA parameters and three additional parameters consisting of the length of apical, branched, and basal zone represented as the portion of main root length (Apical / MRL, branched / MRL and basal / MRL respectively), were reduced to three PC by performing PCA (Supplemental Figures 2C, 3). The raw data was first

3

normalized per trait by applying Z-score normalization in individual phenotypes. The Principal Components were calculated using Mat Lab. The importance of individual RSA traits for each PC is presented in Supplemental Dataset 4. Individual PCs as well as the raw phenotypic data were used as input for Genome Wide Association Study (Supplemental Dataset 5).

The entire dataset and the Multi-Variate analysis was integrated into Shiny App based "Salt_NV_Root App", available at http://genseq-h0.science.uva.nl/shiny/App/Salt_NV_Root/. The user guide for the App is available at https://mmjulkowska.github.io/Salt_NV_RootApp/. The code for the App is available at https://github.com/mmjulkowska/Salt_NV_RootApp.

*GWAS on RSA phenotypes*
The RSA phenotypes were linked to published genomic data on accessions from a 250k SNP chip with average SNP density of one SNP in 500 bp (Horton et al., 2012). The narrow sense heritability of individual traits at different conditions was determined (Supplemental Dataset 6). Apart from one trait (excluded from further analysis), the estimated heritability for all traits was above 0.2. We performed GWAS using the entire SNP data set as well as excluding the SNPs with minor allele frequency of 0.01, 0.05 and 0.10 to avoid misleading associations. The associations between each SNP and individual RSA phenotypes were tested using a scan_GLS program (Kruijer et al., 2015), based on EMMA-X (Kang et al., 2008). The method implements Gao and Bonferroni corrections for multiple testing to minimize the false discovery rates. Both methods were applied on phenotypic values per accession with α of 0.01 and 0.05 and Minor Allele Frequency (MAF) of 0.00, 0.01, 0.05 and 0.10. We used 5.6 as the threshold value, as there were around 20000 SNPs with MAF > 0.01 and the threshold was therefore $-\log10(0.05/20000) = 5.6$. The overview of numbers of associated loci identified with individual traits with LOD > 5.6, including all rare alleles is presented in Supplemental Dataset 7.

The list of putative loci was selected using metrics considering the association when the individual values of each replica were mapped and when average values per genotype were used for GWAS. Furthermore, we selected for the associations mapped using only the SNP subset with MAF > 0.01, as the majority of the associations were identified with this SNP set, while excluding the rare alleles, represented by less than 3 accessions, that could skew the associations found. For the loci that were mapped with a SNP set including rare alleles, we used the more stringent Bonferroni threshold for further selection of associations, based on all SNPs used (including the rare SNPs), determined as $\log10(0.05/200\ 000) = 6.6$ (Supplemental Datasets 8 – 10). We selected the SNPs that were mapped with both average and individual replica trait values and –log10(p-value) above the Bonferroni threshold or mapped with the SNP subset of MAF > 0.01 (Supplemental Figure 4). Our selection yielded 49 associations with traits measured under control conditions and 154 associations specific to RSA traits measured under salt stress conditions (Supplemental Figure 4, Supplemental Datasets 8, 9 and 10). The candidates from all conditions studied were compared and the associations overlapping between individual traits and conditions were identified.

The enrichment analysis of the 100 candidate loci identified under salt stress conditions was performed with the hyper-geometrical test, using the phyper() function in R. We used 27,655 protein-coding genes as the "population size" parameter, with 1632 genes identified by Dinneny (et al., 2008) as responsive to salt stress. For testing the genes directly underlying the associated SNP, we used 10 genes that we identified to be altered in their expression, among 100 possible genes. For testing the genes in linkage disequilibrium with the identified SNP, we calculated the average number of genes per 10 kb upstream and downstream from identified SNP (27,655 genes per 119,146,348 bp resulting in 0.0002321095 gene per bp, and 4.64219 genes per 20 kbp – 10kb upstream and 10 kb downstream from the identified SNP). Subsequently, we used the average gene density to determine the number of possible candidate genes for 100 identified loci, ending up with 464,219 possible candidate genes. Therefore, the hyper-geometric test for the neighboring candidate genes was run with 70 genes that we identified to be altered in their expression among 464,219 possible genes.

The associations with average lateral root length and the ratio between average lateral root length were studied in greater detail (Supplemental Data set 12). To further fine-map the chosen loci, the RSA phenotypes were linked to the genotypic data based on whole-genome sequencing data of the different accessions (Alonso-Blanco et al., 2016) and covered 4,000,000 SNPs. For the accessions that were not sequenced, genome information was imputed based on the 250-k SNP chip data (Horton et al., 2012). Those imputations are known to have negligible effect on the GWAS outcomes (Cao et al., 2011). The GWAS was performed on the average trait value per genotype and the SNPs corresponding to the 6 loci that we identified (Supplemental Dataset 12) are presented in Supplemental Dataset 13.

For the selected associations (Supplemental Dataset 12) sequence information of 147 accessions belonging to the HapMap population was downloaded from the 1001 genomes project website (1001genomes.org) and aligned with ClustalO as described in Julkowska et al. (2016).

### Expression analysis of accessions

48 Arabidopsis accessions were selected based on different haplotypes of selected candidate loci as determined from SNP data and the pronounced differences between their RSA under all conditions studied (Supplemental Dataset 14). The accessions were used for studying the natural variation in the expression of candidate genes (Supplemental Dataset 14). The 4-day-old seedlings of 48 different accessions were transferred to plates supplemented with 0 or 75 mM NaCl. After 24 h, the seedlings were harvested, snap-frozen in liquid nitrogen and divided into root and shoot fraction. RNA extraction was performed with TRI-reagents (Sigma) with additional chloroform cleaning step, followed by TURBO DNase treatment (Ambion). The RNA was checked for the integrity on 2% agarose gel. The cDNA was synthesized from 1 μg total RNA using reverse transcriptase (Fermentas). The cDNA was diluted to approximately 10ng/μl. The diluted cDNA was used in a specific target amplification (STA) reaction and subjected to PCR on a Biomark genetic analysis system on a 96 x 96 Dynamic array, according to manufacturer's instructions (Fluidigm). The primer sequence for qPCR

was designed focusing on the 3' end and targeting the conserved sites with no / little natural variation in the sequence as found out in 1001 sequence browser. The sequences of the primers used are to be found in Supplemental Data set 18. For the loci 1, 2, 3, 4, and 6 the transcript levels of At1G07920, At1G13320, At3G04120, At5G12240, and At5G46630 were used for normalization of expression. Expression of the genes in the locus 5 was measured in a separate experiment, using At1G07920, At1G13320, At5G12240, and At5G46630 as reference transcripts for normalization, without At3G04120.

Samples of low quality were removed and Ct-values $\geq 30$ were set to 30 to reduce the background noise. The expression levels of target genes were calculated by $\Delta Ct = 2^{\text{-Ct-value target}} / 2^{\text{-Ct-value reference}}$. To normalize the expression for all five / four reference genes used; geometrical mean was calculated from delta-Ct normalized expression for each reference gene and the average expression per accession, tissue, and conditions were calculated for each putative candidate gene. For regression analysis between traits and expression, highly influential observations were not considered based on Cook's distance (if > 0.5).

### *T-DNA insertion and over-expression lines genotyping and phenotyping*
The T-DNA lines were ordered from the European Arabidopsis stock center (nasc. org.uk), except for the *cyp79b2-2 cyp79b3-2* line (Sugawara et al., 2009), which was kindly provided by Dr. Hiroyushi Kasahara (RIKEN Center for Sustainable Resource Science, Yokohama, Japan). The full list of T-DNA insertion lines used is to be found in Supplemental Dataset 16. The ectopic over-expression line p35S:CYP79B2 (Zhao et al., 2002) was kindly provided by Dr. John Celenza (Biochemistry and molecular biology, Boston University, USA).

The T-DNA insertion lines were genotyped by extracting DNA from leaf material ground in liquid nitrogen using 10% Chelex (Bio-rad) in MiliQ followed by 15 min incubation at 95°C and 15 min centrifugation at maximum speed in the standard tabletop centrifuge. The supernatant was used as an input for the PCR reaction. The primers used for T-DNA insertion lines identification are listed in Supplemental Dataset 16.

The RSA phenotypes of *HKT1* T-DNA insertion lines were studied as described above for the phenotyping of Arabidopsis accessions (n=16). A one-way ANOVA was used to analyze these data, as the control plants and salt treatment plants were not the same age. A Tukey post-hoc test was used to analyze differences between genotypes within treatments. The RSA phenotypes of *CYP79B2* and *CYP79B3* T-DNA insertion lines and the ectopic overexpression line p35S:CYP79B2 were studied as described above, but no sucrose was added in the medium (n=20) and RSA traits were quantified with SmartRoot (Lobet et al., 2011). For analyses of the single and double mutant lines on day 10 (Figure 6A, Supplemental Figure 12B), data of three experiments was pooled to increase statistical power. To correct for this, Experiment was included as random factor in a mixed linear model. For all other experiments data of one representative experiment is shown. Data was analyzed using a three-way ANOVA. For both, if a

significant interaction was found, a Bonferroni-corrected post-hoc within treatment (and day) analysis was used to analyze differences between genotypes.

The expression levels of gene of interest in T-DNA insertion lines and the p35S:CYP79B2 ectopic overexpression line were studied by qPCR analysis. RNA was extracted from whole seedlings grown on agar plates for 12 days in control conditions with TRI-reagents (Sigma Aldrich) with additional chloroform cleaning step, followed by TURBO DNase treatment (Ambion). The RNA was examined for the integrity on 2% agarose gel. The cDNA was synthesized from 1 µg total RNA using reverse transcriptase (Fermentas), diluted to approximately 10 ng/µl and used for qPCR using the Eva-Green kit (Solis Biodyne) and an Applied Biosystems sds7500 machine with three biological replicates and two technical replicates. The expression was normalized using AT1G13320 transcript levels. The expression levels of putative candidate genes were calculated by $\Delta Ct = 2^{- (Ct\text{-value target})} / 2^{- (Ct\text{-value reference})}$. The sequences of the primers used are listed in Supplemental Dataset 15.

*Scoring of lateral root stages*
Plants were germinated, grown and treated as described for root system architecture. Roots 10-day-old seedlings were fixed in 4% formaldehyde prepared in 0.025M phosphate buffer (pH 7.2) overnight at 4°C. The fixative was then replaced with 30% (aq. v/v) glycerol containing 2% (v/v) DMSO and left for at least 30 minutes at room temperature. Roots were then mounted in clearing solution and observed at least 1 hour after the sample preparation. The clearing solution was composed of 4.2 M NaCI and 8mM Na2S2O3 prepared in 65% (aq. v/v) glycerol supplemented with 2% (v/v) DMSO. Lateral root stages were scored under a light microscope as described in Mcloughlin et al. (2012). Stage 1 to 3 were combined into one stage.

*Timelapse imaging and analysis*
Plants were germinated as described for root system architecture. Six 7-day old seedlings were transferred to ½MS plates supplemented with either 0 or 125 mM of NaCl and placed in the timelapse set-up. The timelapse set-up consists of eight vertical plate holders (90°) placed next to each other in a row. A camera (CANON 1200D) on a rail moves to each frame to take a picture every 20 minutes. To enable imaging in the dark without change in image properties, the infra-red filter of the camera was removed and a lens which filters all light below 700nm was used. Behind the plate holders, a plate with infra-red LED lights of 940nm, moves simultaneously with the camera and switches on when the camera takes a picture.

Analysis of the image sequences was done by a script implemented in SmartRoot (Lobet et al., 2011). For each image sequence, the last image was traced by hand. For each root, the number of nodes was multiplied twice. Next, the tracing was copied to the previous image and for each node, based on the surrounding pixel intensity, it was checked whether the root below the tracing was still present. If not, that node was removed. If finished, this tracing was copied to the previous image and the process was repeated until all images were traced. After automated tracing, tracing was checked manually.

*Salinity tolerance assay*

To measure growth of plants in soil, seeds were stratified in water for 2 days at 4°C and then sown on soil. After 7 days seedlings were transferred to trays of 5x8 pots (Verspeentrays, Deens format, Desch-plantpak, The Netherlands), which were saturated with water containing 0 mM (control) or 75 mM (Salt) NaCl. To ensure equal and fast uptake of salt solution, the soil (Zaaigrond nr 1, SIR 27010-15, JongKind BV, The Netherlands) in these pots was left to dry for 4 days before applying the salt solution from below. After initial salt treatment, all trays were watered twice a week from below, to keep salt levels equal during the course of the experiment. To prevent effects of location and tray, plants were transferred following a randomized block design. A week after transfer, additional seedlings were removed, leaving one seedling in each pot.

Four weeks after the start of the treatment, rosettes were harvested for measurements of fresh weight, dry weight and ion measurements. Plants were cut at the base of their rosette and after weighing their fresh weight, stored in paper bags and left to dry in an oven on 60 degrees for approximately a week. Dry weight was measured, and plants were then pooled for measurement of sodium and potassium content.

*Sodium and potassium content*

After drying, 3-4 rosettes were pooled to have approximately 100 mg of material per sample. Dry material was grinded to a fine powder and weighed. Next, plant material was digested by adding 4 ml of $HNO_3$ (65%) and 2 ml of HCl (37%), leaving samples for 60 minutes, mixing in between. After addition of 1 ml of MQ water, tubes were closed and heated in a microwave. Samples were then diluted up to a total volume of 50ml and sodium and potassium content was measured by ICP. Ion content was corrected for the weight of the sample.

*Accession Numbers*

Sequence data from this article can be found in the Arabidopsis Genome Initiative or GenBank/EMBL databases under the accession numbers listed in Supplemental Dataset 1.

## SUPPLEMENTAL MATERIALS

Supplemental dataset 1-16 and Supplemental figure 1-12 can be found online at: http://www.plantcell.org/content/suppl/2017/11/07/tpc.16.00680.DC1
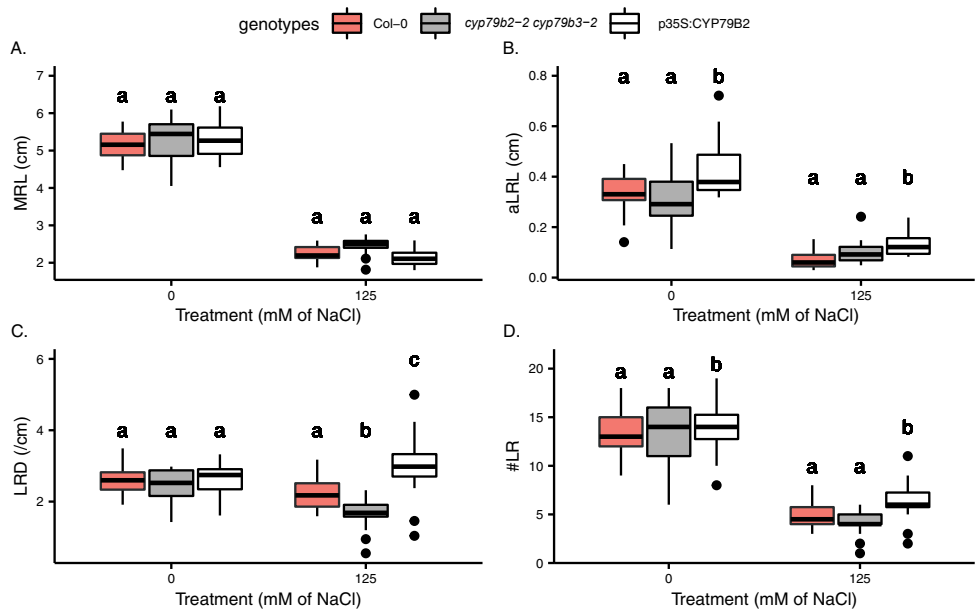


**Supplemental Figure 13. Ectopic overexpression of *CYP79B2* leads to an increased number and length of lateral roots.** (Supports figure 5) Main root length (**A**), average lateral root length (**B**), lateral root density (**C**) and number of lateral roots (**D**) of 10-day-old Col-0 (red), *cyp79b2-2cyp79b3-2* (grey), p35S:CYP79B2 (white) seedlings transferred to ½ MS plates supplemented with 0 or 125 mM of NaCl after 4 days. The middle line inside the box represents the median (n=20). Lower and upper box boundaries represent 25th and 75th percentiles. Lower and upper error lines represent 10th and 90th percentiles. Dots represent data falling outside 10th and 90th percentiles. Significant differences were determined by a two-way ANOVA, followed by a manual contrast post-hoc test within treatments if significant differences were found. Different letters indicate significant differences within treatment.
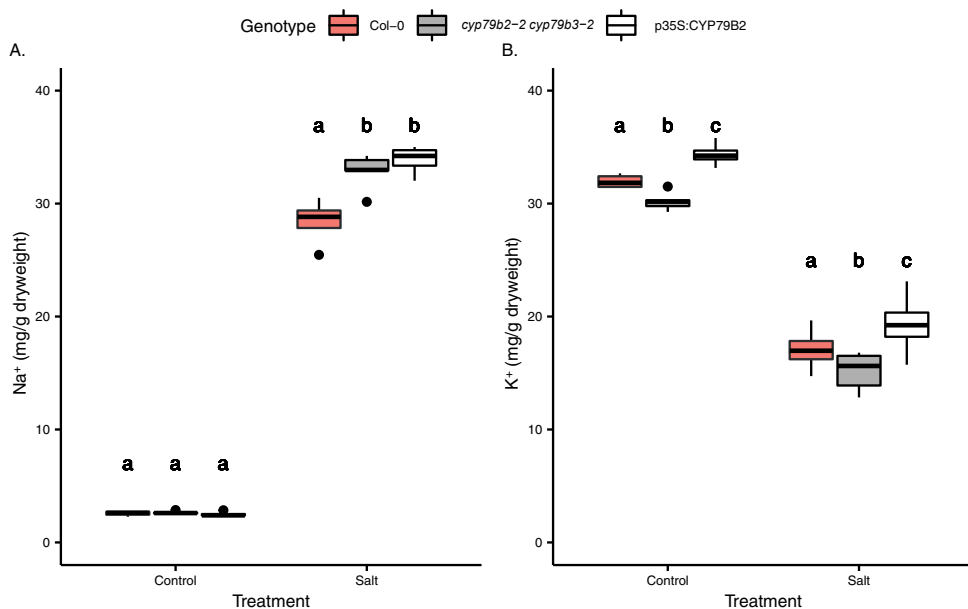
**Supplemental figure 14. Sodium and Potassium accumulation affected by altered epression of *CYP79B2* and *CYP79B3*.** (supports figure 7) The rosette of 5-week-old Col-0 (red), *cyp79b2-2cyp79b3-2* (grey) and p35S:CYP79B2 (white) plants, transferred to control or salt treated soil after 1 week, were harvested and **(A)** and the amount of sodium (Na$^+$) **(A)** and potassium (K$^+$) **(B)** were determined. The middle line inside the box represents the median (n=20). Lower and upper box boundaries represent 25th and 75th percentiles. Lower and upper error lines represent 10th and 90th percentiles. Dots represent data falling outside 10th and 90th percentiles. Significant differences were determined by a two-way ANOVA, followed by a manual contrast post-hoc test within treatments if significant differences were found. Different letters indicate significant differences within treatment.

## ACKNOWLEDGEMENTS

# REFERENCES

**Alonso-Blanco, C. et al.** (2016). 1,135 Genomes Reveal the Global Pattern of Polymorphism in Arabidopsis thaliana. Cell **166**: 481–491.

**Armengaud, P., Zambaux, K., Hills, A., Sulpice, R., Pattison, R.J., Blatt, M.R., and Amtmann, A.** (2009). EZ-Rhizo: integrated software for the fast and accurate measurement of root system architecture. The Plant Journal **57**: 945–956.

**Bao, F. and Li, J.Y.** (2002). Evidence that the auxin signaling pathway interacts with plant stress response. Acta Botanica Sinica **44**: 532–536.

**Baxter, I., Brazelton, J.N., Yu, D., Huang, Y.S., Lahner, B., Yakubova, E., Li, Y., Bergelson, J., Borevitz, J.O., Nordborg, M., Vitek, O., and Salt, D.E.** (2010). A Coastal Cline in Sodium Accumulation in Arabidopsis thaliana Is Driven by Natural Variation of the Sodium Transporter AtHKT1;1. PLoS Genet **6**: e1001193.

**Brown, P.D., Tokuhisa, J.G., and Reichelt, M.** (2003). Variation of glucosinolate accumulation among different organs and developmental stages of Arabidopsis thaliana. Phytochemistry **62**: 471–481.

**Cao, J. et al.** (2011). Whole-genome sequencing of multiple Arabidopsis thaliana populations. Nature Genetics **43**: 956–963.

**Choi, W.G., Toyota, M., Kim, S.H., Hilleary, R., and Gilroy, S.** (2014). Salt stress-induced Ca2+ waves are associated with rapid, long-distance root-to-shoot signaling in plants. Proceedings of the National Academy of Sciences **111**: 6497–6502.

**Crane, R.A., Cardénas Valdez, M., Castaneda, N., Jackson, C.L., Riley, C.J., Mostafa, I., Kong, W., Chhajed, S., Chen, S., and Brusslan, J.A.** (2019). Negative Regulation of Age-Related Developmental Leaf Senescence by the IAOx Pathway, PEN1, and PEN3. Front. Plant Sci. **10**: 1–14.

**Ding, L. and Zhu, J.K.** (1997). Reduced Na+ Uptake in the NaCl-Hypersensitive sos1 Mutant of Arabidopsis thaliana. Plant Physiology **113**: 795–799.

**Dinneny, J.R., Long, T.A., Wang, J.Y., Jung, J.W., Mace, D., Pointer, S., Barron, C., Brady, S.M., Schiefelbein, J., and Benfey, P.N.** (2008). Cell Identity Mediates the Response of Arabidopsis Roots to Abiotic Stress. Science **320**: 942–945.

**Duan, L., Dietrich, D., Ng, C.H., Chan, P.M.Y., Bhalerao, R., Bennett, M.J., and Dinneny, J.R.** (2013). Endodermal ABA Signaling Promotes Lateral Root Quiescence during Salt Stress in ArabidopsisSeedlings. The Plant Cell **25**: 324–341.

**Faiyue, B., Vijayalakshmi, C., Nawaz, S., Nagato, Y., Taketa, S., Ichii, M., Al-Azzawi, M.J., and Flowers, T.J.** (2010). Studies on sodium bypass flow in lateral rootless mutants lrt1and lrt2, and crown rootless mutant crl1of rice ( Oryza sativaL.). Plant Cell Environ.**33**:687-701.

**Galvan-Ampudia, C.S., Julkowska, M.M., Darwish, E., Gandullo, J., Korver, R.A., Brunoud, G., Haring, M.A., Munnik, T., Vernoux, T., and Testerink, C.** (2013). Halotropism Is a Response of Plant Roots to Avoid a Saline Environment. Current Biology **23**: 2044–2050.

**Geng, Y., Wu, R., Wee, C.W., Xie, F., Wei, X., Chan, P.M.Y., Tham, C., Duan, L., and Dinneny, J.R.** (2013). A Spatio-Temporal Understanding of Growth Regulation during the Salt Stress Response in Arabidopsis. The Plant Cell **25**: 2132–2154.

3

**Glawischnig, E., Hansen, B.G., Olsen, C.E., and Halkier, B.A.** (2004). Camalexin is synthesized from indole-3-acetaldoxime, a key branching point between primary and secondary metabolism in Arabidopsis. Proceedings of the National Academy of Sciences **101**: 8245–8250.

**Glawischnig, E.,** (2007). Camalexin. Phytochemistry **68**: 401–406.

**Halkier, B.A.** (2006). Biology and biochemistry of glucosinolates. Annu. Rev. Plant Biol. **57**: 303–333.

**Horton, M.W. et al.** (2012). Genome-wide patterns of genetic variation in worldwide Arabidopsis thaliana accessions from the RegMap panel. Nature Genetics **44**: 212–216.

**Hull, A.K., Vij, R., and Celenza, J.L.** (2000). Arabidopsis cytochrome P450s that catalyze the first step of tryptophan-dependent indole-3-acetic acid biosynthesis. Proceedings of the National Academy of Sciences **97**: 2379–2384.

**Jiang, C., Belfield, E.J., Mithani, A., Visscher, A., Ragoussis, J., Mott, R., C Smith, J.A., and Harberd, N.P.** (2013). ROS-mediated vascular homeostatic control of root-to-shoot soil Na delivery in Arabidopsis. EMBO J **32**: 914–914.

**Julkowska, M.M. and Testerink, C.** (2015). Tuning plant signaling and growth to survive salt. Trends in Plant Science **20**: 586–594.

**Julkowska, M.M., Hoefsloot, H.C.J., Mol, S., Feron, R., de Boer, G.J., Haring, M.A., and Testerink, C.** (2014). Capturing Arabidopsis Root Architecture Dynamics with ROOT-FIT Reveals Diversity in Responses to Salinity. Plant Physiology **166**: 1387–1402.

**Julkowska, M.M., Klei, K., Fokkens, L., Haring, M.A., Schranz, M.E., and Testerink, C.** (2016). Natural variation in rosette size under salt stress conditions corresponds to developmental differences between Arabidopsis accessions and allelic variation in the LRR-KISS gene. Journal of Experimental Botany **67**: 2127–2138.

**Kang, H.M., Zaitlen, N.A., Wade, C.M., Kirby, A., Heckerman, D., Daly, M.J., and Eskin, E.** (2008). Efficient Control of Population Structure in Model Organism Association Mapping. Genetics **178**: 1709–1723.

**Kawa, D., Julkowska, M.M., Sommerfeld, H.M., Horst, ter, A., Haring, M.A., and Testerink, C.** (2016). Phosphate-dependent root system architecture responses to salt stress. Plant Physiology **172**: 690–706.

**Kim, J.I., Dolan, W.L., Anderson, N.A., and Chapple, C.** (2015). Indole Glucosinolate Biosynthesis Limits Phenylpropanoid Accumulation in Arabidopsis thaliana . Plant Cell **27**: 1529–1546.

**Kobayashi, Y., Sadhukhan, A., Tazib, T., Nakano, Y., Kusunoki, K., Kamara, M., Chaffai, R., Iuchi, S., Sahoo, L., Kobayashi, M., Hoekenga, O.A., and Koyama, H.** (2016). Joint genetic and network analyses identify loci associated with root growth under NaCl stress in Arabidopsis thaliana. Plant Cell Environ **39**: 918–934.

**Kotula, L., Clode, P.L., Striker, G.G., Pedersen, O., Läuchli, A., Shabala, S., and Colmer, T.D.** (2015). Oxygen deficiency and salinity affect cell-specific ion concentrations in adventitious roots of barley ( Hordeum vulgare). New Phytologist **208**: 1114–1125.

**Kruijer, W., Boer, M.P., Malosetti, M., Flood, P.J., Engel, B., Kooke, R., Keurentjes, J.J.B., and van Eeuwijk, F.A.** (2015). Marker-Based Estimation of Heritability in Immortal Populations. Genetics **199**: 379–398.

**Lachowiec, J., Shen, X., Queitsch, C., and Carlborg, Ö.** (2015). A Genome-Wide Association Analysis Reveals Epistatic Cancellation of Additive Genetic Variance for Root Length in Arabidopsis thaliana. PLoS Genet **11**: e1005541.

**Lehmann, T., Janowitz, T., S nchez-Parra, B., Alonso, M.-M.P.R., Trompetter, I., Piotrowski, M., and Pollmann, S.** (2017). Arabidopsis NITRILASE 1 Contributes to the Regulation of Root Growth and Development through Modulation of Auxin Biosynthesis in Seedlings. Front Plant Sci **8**: 36.

**Lemarié, S., Robert-Seilaniantz, A., Lariagon, C., Lemoine, J., Marnet, N., Levrel, A., Jubault, M., Manzanares-Dauleux, M.J., and Gravot, A.** (2015). Camalexin contributes to the partial resistance of Arabidopsis thaliana to the biotrophic soilborne protist Plasmodiophora brassicae. Front Plant Sci **6**: 218.

**Li, Y., Huang, Y., Bergelson, J., Nordborg, M., and Borevitz, J.O.** (2010). Association mapping of local climate-sensitive quantitative trait loci in Arabidopsis thaliana. Proc. Natl. Acad. Sci. U.S.A. **107**: 21199–21204.

**Liu, J. and Zhu, J.K.** (1997). An Arabidopsis mutant that requires increased calcium for potassium nutrition and salt tolerance. Proceedings of the National Academy of Sciences **94**: 14960–14964.

**Liu, J.M., Zhao, J.Y., Lu, P.P., Chen, M., Guo, C.H., Xu, Z.S., Ma, Y.Z.** (2016). The E-Subgroup Pentatricopeptide Repeat Protein Family in Arabidopsis thaliana and Confirmation of the Responsiveness PPR96 to Abiotic Stresses. **7**: 14.

**Ljung, K., Hull, A.K., Celenza, J., Yamada, M., Estelle, M., Normanly, J., and Sandberg, G.** (2005). Sites and regulation of auxin biosynthesis in Arabidopsis roots. The Plant Cell **17**: 1090–1104.

**Lobet, G., Pagès, L., and Draye, X.** (2011). A novel image-analysis toolbox enabling quantitative analysis of root system architecture. Plant Physiology **157**: 29–39.

**Mäser, P. et al.** (2002). Altered shoot/root Na +distribution and bifurcating salt sensitivity in Arabidopsisby genetic disruption of the Na +transporter AtHKT1. Febs Letters **531**: 157–161.

**McLoughlin, F., Galvan-Ampudia, C.S., Julkowska, M.M., Caarls, L., Van Der Does, D., Laurière, C., Munnik, T., Haring, M.A., and Testerink, C.** (2012). The Snf1-related protein kinases SnRK2.4 and SnRK2.10 are involved in maintenance of root system architecture during salt stress. Plant J. **72**: 436–449.

**Mikkelsen, M.D., Hansen, C.H., Wittstock, U., and Halkier, B.A.** (2000). Cytochrome P450 CYP79B2 from Arabidopsis catalyzes the conversion of tryptophan to indole-3-acetaldoxime, a precursor of indole glucosinolates and indole-3-acetic acid. J. Biol. Chem. **275**: 33712–33717.

**Moller, I.S., Gilliham, M., Jha, D., Mayo, G.M., Roy, S.J., Coates, J.C., Haseloff, J., and Tester, M.** (2009). Shoot Na+ Exclusion and Increased Salinity Tolerance Engineered by Cell Type-Specific Alteration of Na+ Transport in Arabidopsis. The Plant Cell **21**: 2163–2178.

**Munns, R. and Gilliham, M.** (2015). Salinity tolerance of crops - what is the cost? New Phytologist **208**: 668–673.

**Munns, R. and Tester, M.** (2008). Mechanisms of Salinity Tolerance. Annu. Rev. Plant Biol. **59**: 651–681.

**3**

**Munns, R., James, R.A., Xu, B., Athman, A., Conn, S.J., Jordans, C., Byrt, C.S., Hare, R.A., Tyerman, S.D., Tester, M., Plett, D., and Gilliham, M.** (2012). Wheat grain yield on saline soils is improved by an ancestral Na+ transporter gene. Nat Biotechnol **30**: 360–364.

**OECD** (2012). Statistical Annex. In OECD-FAO Agricultural Outlook 2012 (Summary in Slovak), OECD-FAO Agricultural Outlook. (OECD Publishing), pp. 217–281.

**Rellán-Álvarez, R., Lobet, G., and Dinneny, J.R.** (2016). Environmental Control of Root System Biology. Annu. Rev. Plant Biol. **67**: 619–642.

**Ristova, D. and Busch, W.** (2014). Natural Variation of Root Traits: From Development to Nutrient Uptake. Plant Physiology **166**: 518–527.

**Robbins, N.E., Trontin, C., Duan, L., and Dinneny, J.R.** (2014). Beyond the Barrier: Communication in the Root through the Endodermis. Plant Physiology **166**: 551–559.

**Rosas, U., Cibrian-Jaramillo, A., Ristova, D., Banta, J.A., Gifford, M.L., Fan, A.H., Zhou, R.W., Kim, G.J., Krouk, G., Birnbaum, K.D., Purugganan, M.D., and Coruzzi, G.M.** (2013). Integration of responses within and across Arabidopsis natural accessions uncovers loci controlling root systems architecture. Proceedings of the National Academy of Sciences **110**: 15133–15138.

**Roy, S.J., Huang, W., Wang, X.J., Evrard, A., Schmockel, S.M., Zafar, Z.U., and Tester, M.** (2012). A novel protein kinase involved in Na +exclusion revealed from positional cloning. Plant Cell Environ **36**: 553–568.

**Rus, A., Baxter, I., Muthukumar, B., Gustin, J., Lahner, B., Yakubova, E., and Salt, D.E.** (2006). Natural Variants of AtHKT1 Enhance Na+ Accumulation in Two Wild Populations of Arabidopsis. PLoS Genet **2**: e210.

**Rus, A., Yokoi, S., Sharkhuu, A., Reddy, M., Lee, B.H., Matsumoto, T.K., Koiwa, H., Zhu, J.K., Bressan, R.A., and Hasegawa, P.M.** (2001). AtHKT1 is a salt tolerance determinant that controls Na+ entry into plant roots. Proceedings of the National Academy of Sciences **98**: 14150–14155.

**Shelden, M.C., Roessner, U., Sharp, R.E., Tester, M., and Bacic, A.** (2013). Genetic variation in the root growth response of barley genotypes to salinity stress. Functional Plant Biology **40**: 516.

**Slovak, R., Göschl, C., Su, X., Shimotani, K., Shiina, T., and Busch, W.** (2014). A Scalable Open-Source Pipeline for Large-Scale Root Phenotyping of Arabidopsis. The Plant Cell **26**: 2390–2403.

**Strauch, R.C., Svedin, E., Dilkes, B., Chapple, C., and Li, X.** (2015). Discovery of a novel amino acid racemase through exploration of natural variation in Arabidopsis thaliana. Proceedings of the National Academy of Sciences **112**: 11726–11731.

**Sugawara, S., Hishiyama, S., Jikumaru, Y., Hanada, A., Nishimura, T., Koshiba, T., Zhao, Y., Kamiya, Y., and Kasahara, H.** (2009). Biochemical analyses of indole-3-acetaldoxime-dependent auxin biosynthesis in Arabidopsis. Proc. Natl. Acad. Sci. U.S.A. **106**: 5430–5435.

**Tamura, K., Peterson, D., Peterson, N., Stecher, G., Nei, M., and Kumar, S.** (2011). MEGA5: Molecular Evolutionary Genetics Analysis Using Maximum Likelihood, Evolutionary Distance, and Maximum Parsimony Methods. Molecular Biology and Evolution **28**: 2731–2739.

**Thoen, M.P.M. et al.** (2017). Genetic architecture of plant stress resistance: multi-trait genome-wide association mapping. New Phytologist **213**: 1346–1362.

**Tu, Y., Jiang, A., Gan, L., Hossain, M., Zhang, J., Peng, B., Xiong, Y., Song, Z., Cai, D., Xu, W., Zhang, J., and He, Y.** (2014). Genome duplication improves rice root resistance to salt stress. Rice **7**: 135.

**Verslues, P.E., Lasky, J.R., Juenger, T.E., Liu, T.W., and Kumar, M.N.** (2014). Genome-Wide Association Mapping Combined with Reverse Genetics Identifies New Effectors of Low Water Potential-Induced Proline Accumulation in Arabidopsis. Plant Physiology **164**: 144–159.

**Weigel, D. and Mott, R.** (2009). The 1001 Genomes Project for Arabidopsis thaliana. Genome Biol **10**: 107.

**West, G., Inzé, D., and Beemster, G.T.S.** (2004). Cell cycle modulation in the response of the primary root of Arabidopsis to salt stress. Plant Physiology **135**: 1050–1058.

**Wu, S.J., Ding, L., and Zhu, J.K.** (1996). SOS1, a Genetic Locus Essential for Salt Tolerance and Potassium Acquisition. The Plant Cell **8**: 617–627.

**Zhao, Y., Hull, A.K., Gupta, N.R., Goss, K.A., Alonso, J., Ecker, J.R., Normanly, J., Chory, J., and Celenza, J.L.** (2002). Trp-dependent auxin biosynthesis in Arabidopsis: involvement of cytochrome P450s CYP79B2 and CYP79B3. Genes & Development **16**: 3100–3112.

**3**

**CHAPTER 4**

# A central role for IAN in maintaining lateral root development during salt stress

Iko T. Koevoets[1,3], Jacinto Gandullo[3], Noah De Croock[1], Wouter Kohlen[2], Kerstin Gühl[2], Francel Verstappen[1], Thijs de Zeeuw[1], Iris F. Kappers[1], Christa Testerink[1,3]

[1]Laboratory of Plant Physiology, [2]Laboratory of Molecular biology, Wageningen University & Research, 6708PB Wageningen, the Netherlands
[3]Plant Cell Biology, University of Amsterdam, Swammerdam Institute for Life Sciences, 1090GE Amsterdam, the Netherlands

**ABSTRACT**

Salinity of the soil is an increasing problem for agriculture. To develop crops that can withstand salt stress, its necessary to increase the knowledge on functional adaptations of the root system to cope with salt stress. Previously, the indole-3-acetaldoxime (IAOx) pathway has been shown to be involved in maintaining lateral root development during salt stress. In this study we further unravel which components of the IAOx pathway are involved in this process. First, a role for camalexin can be excluded, as camalexin is absent from salt stressed plants and camalexin deficient mutants are not affected in root system architecture in salt stress. Metabolomics profiling showed that indole glucosinolates (IGs) are increased upon salt stress, especially in the root. Levels of indole-3-acetonitrile (IAN), a breakdown product of IGs and precursor of indole-3-acetic acid (IAA), were also increased and IAN was able to rescue the salt specific lateral root density phenotype of *cyp79b2-2cyp79b3-2*. No differences between wildtype and *cyp79b2-2cyp79b3-2* on whole root IAA levels in control or salt stress were found. We did observe a decrease in DR5 signalling output in *cyp79b2-2cyp79b3-2* roots, although independent of treatment. Other studies have suggested IAN to directly influence the Transport Inhibitor Response 1 (TIR1) receptor. Alternatively, the effects on IAA could be more local and thus hard to measure on whole root level. Either way, IAN seems to play a central role in maintaining lateral root development during salt stress. IAN can be produced via IGs, but IAOx can also directly be converted to IAN by CYP71A family members. Based on expression and phenotyping data, we propose CYP71A19 converts IAOx to IAN in salt stress. Future studies need to confirm this role for CYP71A19. This study is the first study to suggest a central role for IAN in regulating plant developmental plasticity.

## INTRODUCTION

Plants are exposed to many abiotic and biotic stresses and to survive they rely on adapting both root and shoot development as well as growth to cope with stress. For most abiotic stresses, including drought, nutrient deprivation, flooding and salt stress, the root system is the first organ being exposed to stress and thus provides a key role in both sensing and acclimation (Lamers et al., 2020). Adaptation of root system architecture (RSA) has proven to be functional in many of these stresses (as reviewed in Koevoets et al., 2016). Since salt stress is an increasing problem threatening agriculture worldwide (Ivushkin et al., 2019), understanding how plants can functionally adapt their RSA to cope with salt stress will contribute to developing crops able to withstand salt stress.

Salt stress is known to not only inhibit root growth, but to remodel RSA by differentially influencing lateral and main roots (Julkowska et al., 2014). For example, the *Arabidopsis thaliana* accession Col-0 invests relatively more in lateral root growth than in main root growth when growing in saline conditions. Recently, Julkowska et al., (2017); Chapter 3) showed that, in Arabidopsis, natural variation in the expression of *CYTOCHROME P450 FAMILY 79 SUBFAMILY B2 (CYP79B2)* during salt stress was correlated with the relative investment in lateral roots during salt stress. In agreement, the double knock-out mutant of *cyp79b2-2cyp79b3-2* shows reduced lateral root density in salt stress (Julkowska et al., 2017; Chapter 3). CYP79B2 and its functional homologue CYP79B3 convert tryptophan (Trp) to indole-3-acetaldoxime (IAOx), the first step in the IAOx pathway (Hull et al., 2000; Mikkelsen et al., 2000). The Brassicaceae-specific IAOx pathway (Figure 1A) can produce three major products: camalexin, indole glucosinolates (IGs) and indole-3-acetic acid (IAA).

Camalexin is an indole alkaloid acting as a phytoalexin induced in Arabidopsis and other Brassicaceae by a wide range of plant pathogens to inhibit pathogen growth (as reviewed in Ahuja et al., 2012; Glawischnig, 2007). In addition to biotic stresses, abiotic elicitors inducing ROS production such as silver nitrate have been shown to induce camalexin production (Mert-Türk et al., 2003; Zhao et al., 1998). Although most studies have measured camalexin in leaves, camalexin has been detected in roots triggered by infection or the flagellar peptide Flg22 (Bednarek et al., 2005; Millet et al., 2010). However, no studies thus far have reported an effect of camalexin in root development.

IGs are the major glucosinolates produced in roots of Brassicaceae (Van Dam et al., 2009). Just as camalexin, IGs are well described to play a role in plant defense against biotic stress (as reviewed in Halkier, 2016; Halkier and Gershenzon, 2006). Although no role for IGs or other glucosinolates in abiotic stresses has been described, salt stress has been shown to induce IG accumulation (Chen et al., 2017). After biosynthesis, IGs are stored in the vacuole, where upon cell damage they come in contact with myrosinases that degrade them into several breakdown products. These breakdown products are described to be the active products influencing plant development and defense (as reviewed in Agerbirk et al., 2009). In the shoot, the myrosinases THIOGLUCOSIDE GLUCOHYDROLASE 1 (TGG1) and 2 (TGG2) break down IGs to several products

including indole-3-carbinol (I3C) (Barth and Jander, 2006; Pang et al., 2009). Although I3C is produced in the shoot, it has been reported to be transported to the root and inhibit root elongation (Katz et al., 2015; Katz and Chamovits, 2017). In the root, two other myrosinases are mainly active: TGG4 and TGG5 (Fu et al., 2016), which convert IGs to Indole-3-Acetonitrile (IAN). Both IAN and I3C have been shown to influence auxin signaling and thereby possibly root development (Katz et al., 2015).

Although $^{13}C_6$ labeled IAOx was shown to be incorporated into IAA (Sugawara et al., 2009), the contribution of the IAOx pathway in production of IAA, the most abundant auxin, has been under debate. The IAOx pathway is Brassicaceae specific and most IAOx is converted into IGs. The indole-3-pyruvic acid (IPyA) pathway, governed by the YUCCA and TRYPTOPHAN AMINOTRANSFERASE OF ARABIDOPSIS (TAA) enzymes, on the other hand has widely been accepted to be the major IAA production pathway for all plant families. However, some studies suggest that the IAOx pathway may play a role in finetuning local auxin production under stress. For example, under heat stress, loss of function of CYP79B2, CYP79B3 or both leads to reduced levels of free IAA (Zhao et al., 2002). Auxin is well known to influence lateral root development and creating auxin maxima is essential for primordia to develop and emerge (as reviewed in Du and Scheres, 2018; Lavenus et al., 2013). For long, modulation of auxin transport has been considered as the major regulator of auxin distribution patterns, but recently two studies showed the importance of local auxin biosynthesis for the formation of auxin maxima (Brumos et al., 2018; Matosevich et al., 2020). Auxin transport is disturbed by many stresses, including salt stress (Korver et al., 2018; Liu et al., 2015; Chapter 6). As *CYP79B2* and *CYP79B3* are specifically expressed at sites underlying lateral roots (Ljung et al., 2005), we hypothesize the IAOx pathway to be responsible for local auxin biosynthesis to maintain auxin maxima in lateral root primordia during salt stress.

In this study we investigate which downstream products of the IAOx pathway play a role in maintaining lateral root development during salt stress. With a combination of metabolomics and mutant studies we show that IAN, either directly produced from IAOx or via IGs, plays a central role in regulating root system architecture during salt stress. IAN can be produced via IGs, but more likely it is produced directly from IAOx by a novel characterized enzyme CYP71A19, which shows similar gene expression and effects on root system architecture as *CYP79B2* and *CYP79B3*. It is unclear whether IAN would directly influence auxin signaling or whether it would function via conversion to IAA. Regardless, our results show that during salt stress, not only auxin transport, but also auxin biosynthesis pathways play a major role in fine-tuning root development by sustaining root branching and outgrowth of lateral roots.

## RESULTS & DISCUSSION

*Roots accumulate more indole glucosinolates in response to salt stress*
Previously, Julkowska et al. (2017) have shown that the IAOx pathway is involved in maintaining lateral root development and growth during salt stress, via regulation of *CYP79B2* and *CYP79B3* (Chapter 3). The IAOx pathway (Figure 1A) can produce several compounds including IGs, IAA and camalexin. To investigate the role of these compounds in maintaining lateral root development during salt stress, we first investigated changes in camalexin and the IG metabolome upon salt stress in both the wildtype and *cyp79b2-2cyp79b3-2* mutant. 10-day-old seedlings were treated for 48 hours with 125mM of NaCl. Next, root and shoot tissue were separately harvested and analyzed with LC-MS.

No camalexin was detected in any of the samples (Figure 1B). In addition, camalexin deficient mutants *cyp71a12-a13* and *PAD3* (Müller et al., 2015; Schuhegger et al., 2006) were not affected in root system architecture in both control and salt stress (Supplemental figure 1). These findings together indicate camalexin is not involved in maintaining lateral root development during salt stress. In support, the pathway to produce camalexin is not active in the absence of pathogens or other known triggers (Schuhegger et al., 2007), which is in agreement with our metabolomic data (no camalexin measured in control or salt conditions).

As expected, the four most common IGs glucobrassicin (IMG), 1-methoxyglucobrassicin/ 4-methoxyglucobrassicin (mIMG) and 4-hydroxyglucobrassicin (hIMG) were absent in the *cyp79b2-2cyp79b3-2* double mutant (Figure 1B). In wildtype seedlings, all IGs showed an increased accumulation in roots exposed to salt stress. hIMG was specific to the root system, while IMG, mIMG were also present in the shoot. IMG was the only compound that showed an increased accumulation in salt stress in the shoot. Previous studies showed a similar increase in whole seedlings of Arabidopsis (Chen et al., 2017). The observed increase upon salt stress is not surprising as *CYP79B2* and *CYP79B3* are upregulated by salt stress (Julkowska et al., 2017; Kawa et al., 2016) and the IG pathway has a high basal activity (Mikkelsen et al., 2004). This high activity is well illustrated by the mutant in SUPERROOT1, an enzyme involved in the first steps of IG biosynthesis (Boerjan, 1995; Mikkelsen et al., 2004). In absence of SUPERROOT1 (SUR1), the accumulating IAOx is further metabolized to IAA, leading to overproduction of IAA and the proliferation of lateral roots. Unfortunately, this high basal activity makes analysis of mutants in the IG pathway hard to interpret and hence confirming a role of IGs in salt stress needs another approach.
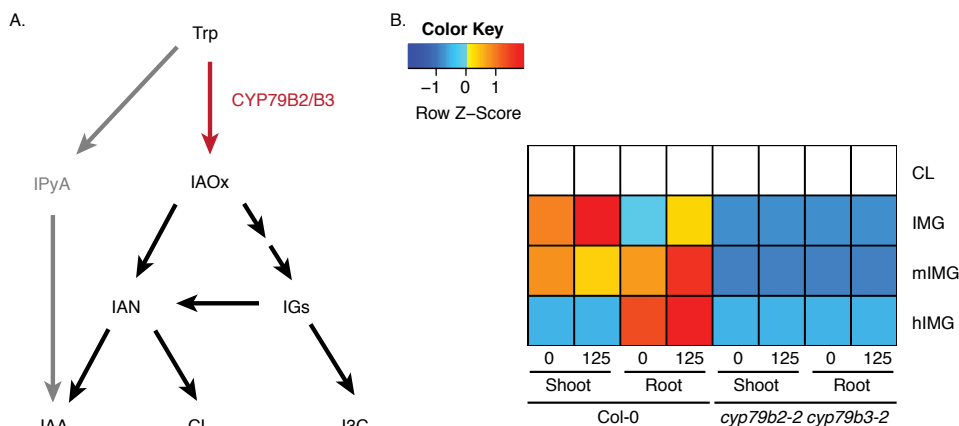
**Figure 1.** Indole glucosinolates are upregulated by salt stress (**A**) Overview of the IAOx pathway: tryptophan (Trp) is converted to indole-acetaldoxime (IAOx) by CYP79B2 and CYP79B3. IAOx can then be converted into indole-3-acetonitrike (IAN) directly or via Indole Glucosinolates (IGs). IGs can also be broken down into indole-3-carbinol (I3C). IAN can be converted into camalexin (CL) or indole-3-acetic acid (IAA). Although the IAOx pathway can produce IAA, the indole-3-pyruvic acid (IPyA) pathway (in grey) is considered the major IAA biosynthesis pathway. (**B**) 10-day-old seedlings of Col-0 and *cyp79b2-2cyp79b3-2* were treated for 48 hours with 0 (control) or 125 mM (salt) of salt treatment. Roots and shoots were harvested separately and levels of CL and the major Indole IGs, glucobrassicin (IMG), 1-methoxyglucobrassicin/4-methoxyglucosbrassicin (mIMG) and 4-hydroxyglucobrassicin (hIMG) were determined using LC-MS. Heatmap colors show normalized response within each representative feature of the compound (n=5). Supplemental table 1 shows feature mass and retention time. Camalexin was absent from all samples and thus is shown in white.

*IAN can rescue the cyp79b2-b3 lateral root density phenotype in salt stress*

Most known physiological effects of IGs are dependent on their two major breakdown products: IAN and I3C (Agerbirk et al., 2009). We thus investigated whether either IAN or I3C could rescue the reduced lateral root density in salt stress of *cyp79b2-2cyp79b3-2* (Julkowska et al., 2017; Chapter 3). Indeed, supplementation of either IAN or I3C diminished the difference in lateral root density between wildtype and the *cyp79b2-2cyp79b3-2* in salt stress (Figure 2). However, while IAN increases the lateral root density of *cyp79b2-2cyp79b3-2*, I3C rather reduced the lateral root density in wild-type. IAN and I3C thus seem to have opposite effects on lateral root density. While IAN rescues the mutant phenotype, I3C addition seems to mimic the mutant phenotype in wildtype.

The observed opposite effects on root phenotype might be due to their observed opposite effect on auxin signaling: I3C inhibits and IAN promotes auxin signaling (Katz et al., 2015), possibly by their predicted binding to the TIR1 receptor (Katz et al., 2015). In addition, IAN is a precursor of IAA (Figure 1A). It is thus probable that either auxin signaling, IAA biosynthesis or both are affected in the *cyp79b2-2cyp79b3-2* mutant.
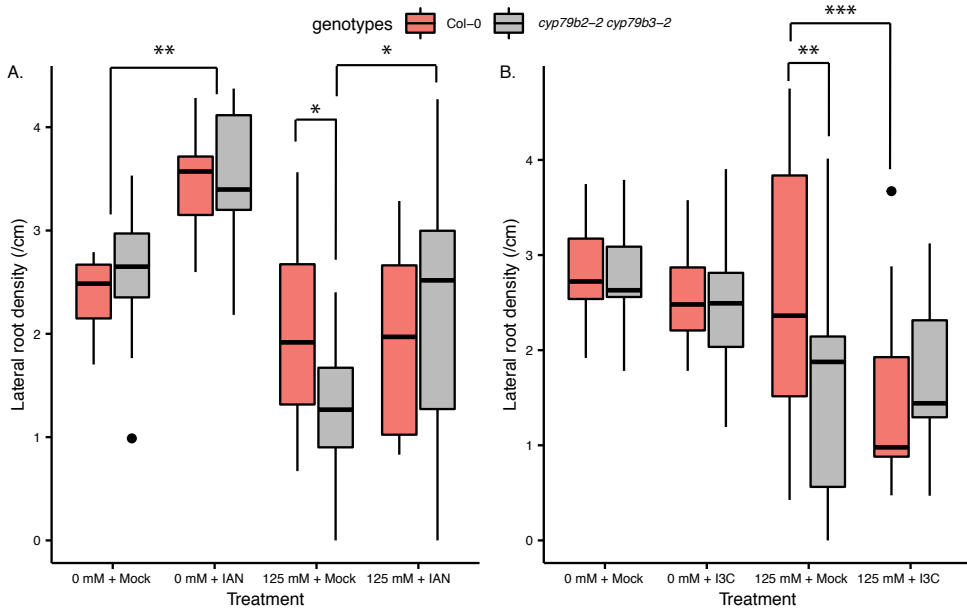
**Figure 2. IAN can rescue the lateral root density phenotype of *cyp79b2-2cyp79b3-2* during salt stress.** Lateral root density of 12-day old Col-0 (pink) and *cyp79b2-2cyp79b3-2* (grey) seedlings transferred to ½ MS plates supplemented with 0 (control) or 125 (salt) mM of NaCl and (A) 0 or 5 mM of IAN or (B) 0 or 100 mM of I3C after 4 days. The middle line inside the box represents the median (n=20). Lower and upper box boundaries represent 25th and 75th percentiles. Lower and upper error lines represent 10th and 90th percentiles. Dots represent data falling outside 10th and 90th percentiles. Significant differences were determined by a two-way ANOVA, followed by a manual contrast post-hoc test if significant differences were found. Asterisks indicate significant differences between genotypes, within salt treatment (*<0.05, **<0.01, ***<0.001).

*Auxin signaling, but not IAA biosynthesis is affected in cyp79b2-2cyp79b3-2 mutants*
To further investigate whether the observed effect of I3C and IAN is due to either auxin signaling or IAA biosynthesis, we measured the intensity of DR5 signal in the root tips of the auxin reporter pDR5:mVENUS crossed into Col-0 or *cyp79b2-2cyp79b3-2* background. No significant effect of salt treatment on DR5 signal was found for either of the genotypes after 1 or 3 hours of salt treatment (Figure 3). We did observe a decreased DR5 signal in *cyp79b2-2cyp79b3-2* roots independent of treatment compared to that in wildtype roots.

As a decreased DR5 signal in root tips of *cyp79b2-2cyp79b3-2* was observed, we expected an accompanying decreased level of IAA. However, free IAA levels in roots of *cyp79b2-2cyp79b3-2* were similar to those in Col-0 (Figure 4A). After 1 hour of salt stress an increase in IAA levels was observed in both genotypes, indicating that this increase is probably due to an increased production via other IAA biosynthesis pathways. Indeed, publicly available microarray data shows several *YUCCAs* functioning in the IPyA pathway are upregulated during salt stress in the epidermis and cortex of the root (as reviewed in Korver et al., 2018). We cannot exclude that *cyp79b2-2cyp79b3-2* does have local differences in IAA levels, as only entire roots were measured. In addition, in the

*cyp79b2-2cyp79b3-2* mutant, IAA biosynthesis might be compensated by upregulation of other pathways located in other root tissues. It is important to note that free IAA is only present in very low concentrations (for example 25-50 times less then IAN) as high turnover of IAA into conjugates and breakdown products occurs (Kowalczyk and Sandberg, 2001). A full profile of auxin related metabolites in the *cyp79b2-2cyp79b3-2* mutant, preferably in separate parts of the root, would give more insight.
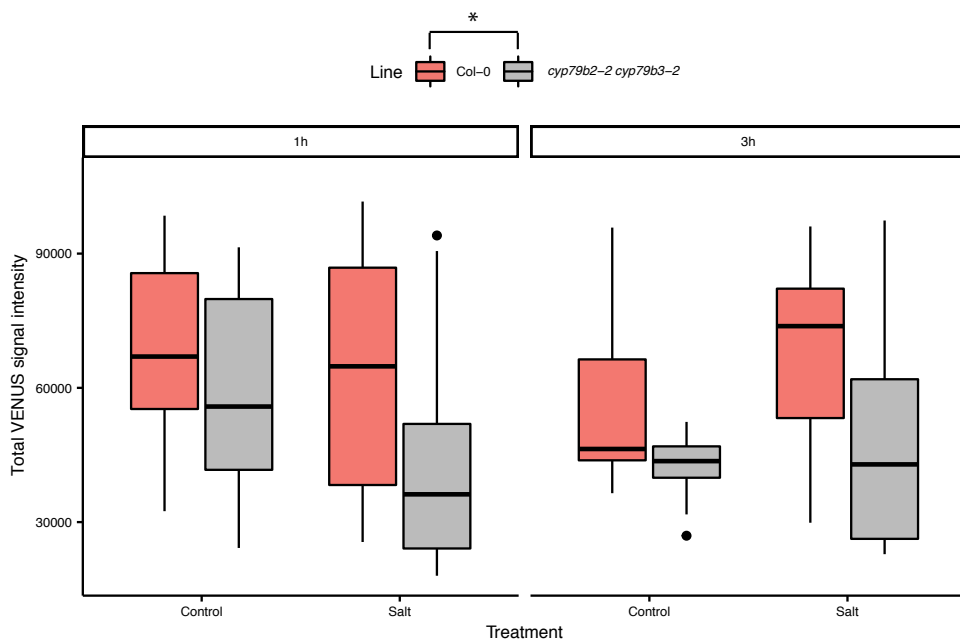


**Figure 3. Loss-of-function of CYP79B2 and CYP79B3 leads to reduced DR5 signalling in the tip of the main root in both control and salt stress.** Total intensity in nuclei of root tip cells of pDR5:;N7-VENUS crossed into Col-0 (pink) or *cyp79b2-2cyp79b3-2* (grey) background was measured with confocal microscopy after 1 hour and 3 hours of 0 (control) or 125 mM (salt) of salt treatment. The middle line inside the box represents the median (n=12). Lower and upper box boundaries represent 25th and 75th percentiles. Lower and upper error lines represent 10th and 90th percentiles. Dots represent data falling outside 10th and 90th percentiles. Significant differences were determined by a three-way ANOVA. No significant interactions between treatment, time and genotype were found. Only the overall effect of genotype was significant as indicated with an asterisk (*<0.05).

Alternatively, DR5 signaling could be affected by IAN or I3C directly, as both have been predicted to bind the TIR1 receptor (Katz et al., 2015) and both compounds are lacking in the *cyp79b2-2cyp79b3-2* mutant (Kim et al., 2008; Sugawara et al., 2009). I3C has been shown to decrease DR5 signaling (Katz et al., 2015), so lack of I3C in the mutant would not explain the observed lower DR5 levels. Therefore, we decided to further focus our studies on IAN. We confirmed absence of IAN in the *cyp79b2-2cyp79b3-2* double mutant (Figure 4B) and found that 1 hour of salt stress increased levels of IAN in wildtype roots. If IAN would directly promote DR5 signaling, the absence of IAN is

consistent with lower DR5 levels in the *cyp79b2-2cyp79b3-2* mutant. However, in that case we cannot explain a lack of increase in DR5 signal in salt stress in Col-0, as IAN itself does increase. Besides a possible compensation of IAA levels by the IPya pathway, I3C levels might also increase upon salt stress, in which case they would act oppositely and would thereby counteract an increase in DR5 levels. As such, it will be hard to predict the effect of increased IG production and/or myrosinase activity in response to salt on plant responses. Modeling might therefore be key to solve this complex puzzle, as is illustrated by Vik et al. (2018) for herbivory or other tissue disrupting attacks.
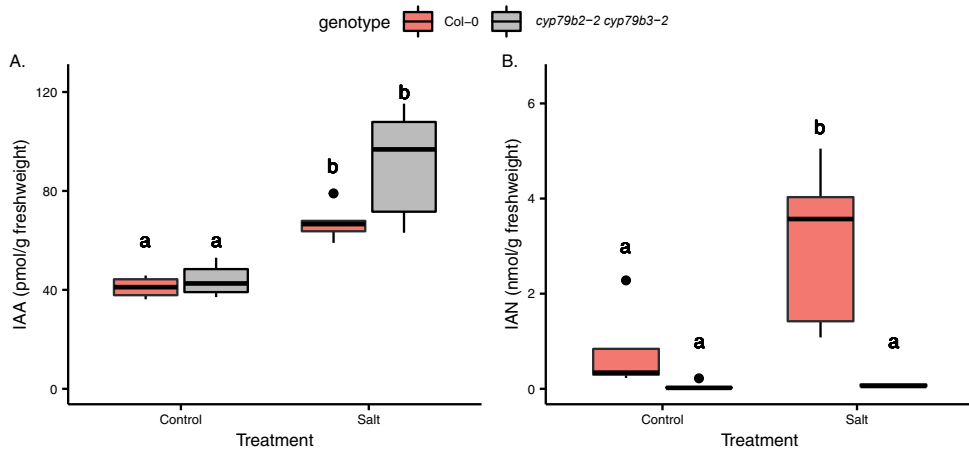


**Figure 4. Loss-of-function of CYP79B2 and CYP79B3 affects IAN, but not IAA levels in whole roots.** IAA (**A**) and IAN (**B**) levels in Col-0 (pink) and *cyp79b2-2cyp79b3-2* (grey) were measured with LC-MS in 10-day old seedlings after 1 hour of 0 (control) or 125 mM (salt) of salt treatment. The middle line inside the box represents the median (n=5). Lower and upper box boundaries represent 25th and 75th percentiles. Lower and upper error lines represent 10th and 90th percentiles. Dots represent data falling outside 10th and 90th percentiles. Different letters indicate significant differences determined by a two-way ANOVA, followed by a Tukey post-hoc test.

*CYP71A19 and A20 are likely candidates converting IAOx to IAN during salt stress*

Based on our data showing that the *cyp79b2-2cyp79b3-2* mutant lacks IAN, that IAN is able to rescue the lateral root density phenotype of *cyp79b2-2cyp79b3-2* and that IAN levels are increased by salt stress, we hypothesize that IAN plays a role in maintaining lateral root development during salt stress. IAN is a breakdown product of IGs, but Sugawara et al. (2009) showed that IAN levels were not significantly reduced in the *sur1–1* mutant in comparison to those in wild type, suggesting that IG metabolism is not a major pathway for IAN synthesis under normal growth conditions. IAOx can also be directly converted into IAN by the CYP71A12 and CYP71A13 enzymes leading to camalexin biosynthesis (Müller et al., 2015; Nafisi et al., 2007). Double KO mutants of *CYP71A12* and *CYP71A13* did not show a root phenotype in salt stress (Supplemental figure 1), but several isoforms (CYP71A12-28) of these enzymes exist and are all predicted to convert IAOx to IAN (Kumar and Mahadevan, 1963). We

studied expression levels of these genes to select likely candidates converting IAOx to IAN in salt stress.

Based on the Klepikova atlas (Klepikova et al., 2016; Figure 5A; Supplemental table 1), we have compared CYP71A family members in order to find root expressed members. CYP71A14, 15, 16, 19 and 20 are specifically root expressed in seedlings and CYP71A12, 27 and 28 are relatively highly expressed in both hypocotyl and root. The other CYP71A members are primarily expressed in other tissues and CYP71A13 and CYP71A18 are not expressed in seedlings at all. This division of root and non-root expressed CYP71A members is consistent with expression in mature plants (Supplemental table 2).

Next, we used micro-array data publicly available via the EfP browser to further select possible candidates (Dinneny et al., 2008; Voß et al., 2015; Winter et al., 2007). Of the root expressed members, especially *CYP71A19* and *CYP71A20* show high induction of expression upon salt treatment (Figure 5B; Supplemental table 3). Both members also show higher expression after root bending (Figure 5C; Supplemental table 4), which indicates expression at sites of lateral root development. Although *CYP71A12*, known to be involved in camalexin biosynthesis (Müller et al., 2015), also shows induction upon salt stress and high expression after root bending (Figure 5B-C), double KO mutants of *CYP71A12* and *CYP71A13* did not show a root phenotype in salt stress (Supplemental figure 1) and camalexin production was not affected by salt stress (Figure 1B).
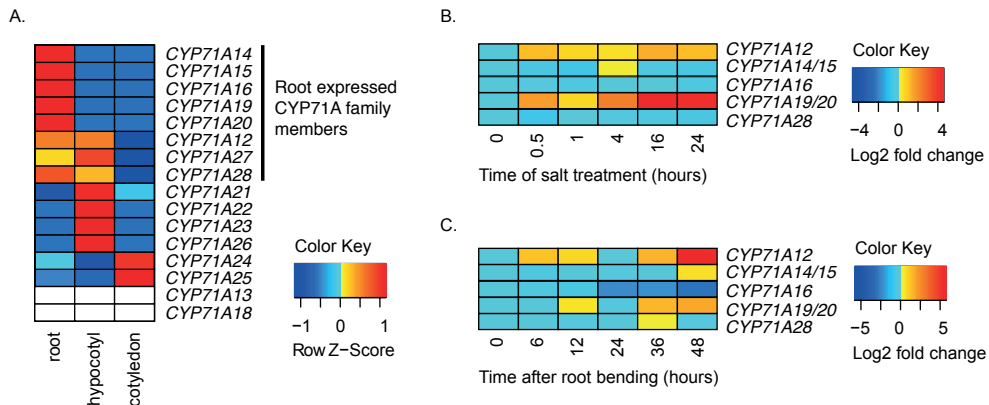


**Figure 5. *CYP71A19* and *CYP71A20* are root expressed members of the *CYP71A* family induced by auxin and in lateral root initiation** (**A**) Relative expression of *CYP71A* family members in seedling root, hypocotyl and cotyledon, based on the Klepikova atlas (Klepikova et al., 2016). Heatmap colors are relative within each gene. (**B**) Expression of root expressed *CYP71A* family members in response to salt stress based on the EfP browser (Dinneny et al., 2008; Winter et al., 2007). Colors represent log2 fold change in expression compared to 0 hours of salt treatment. The same probe has been used for *CYP71A14* and *CYP71A15* as well as for *CYP71A19* and *CYP71A20* expression. (**C**) Expression of root expressed *CYP71A* family members in response to root bending at the site of bending based on the EfP browser (Voß et al., 2015; Winter et al., 2007). Bending induces formation of a lateral root primordium. Heatmap colors represent log2 fold change in expression compared to 0 hours after root bending. Because of their similarity, the same probe has been used for *CYP71A14* and *CYP71A15*, as well as for *CYP71A19* and *CYP71A20* expression. Supplemental table 2-4 show the absolute values retrieved from the EfP browser and used as input for these heatmaps.

*Localization of CYP71A19 expression overlaps with expression of CYP79B3 and is upregulated by salt stress*

As CYP71A19 and CYP71A20 showed most promise as candidates converting IAOx to IAN in salt stress, we further studied expression of *CYP71A19* and *CYP71A20*. Unfortunately, expression levels of *CYP71A20* were too low to detect, thus we focused on expression of *CYP71A19*. RT-qPCR confirmed *CYP71A19* to be induced by salt stress (Figure 6A). *CYP79B2* and *B3* show distinct expression patterns localized in the tip of both main and lateral root and underlying developing lateral roots (Ljung et al., 2005). Confocal imaging of pCYP79B3:CFP confirmed this pattern and in the root tip pCYP79B3:CFP was clearly observed in the cortex and endodermal initial cells, extending to the cortex and endodermis cell layers (Figure 6B). pCYP71A19:mVENUS showed a similar pattern, although expression in the root tip was less pronounced (Figure 6A). These findings support a possible role of CYP71A19 in converting IAOx to IAN during salt stress in the root. However, conversion assays by for example expression of *CYP71A19* will have to confirm this role.
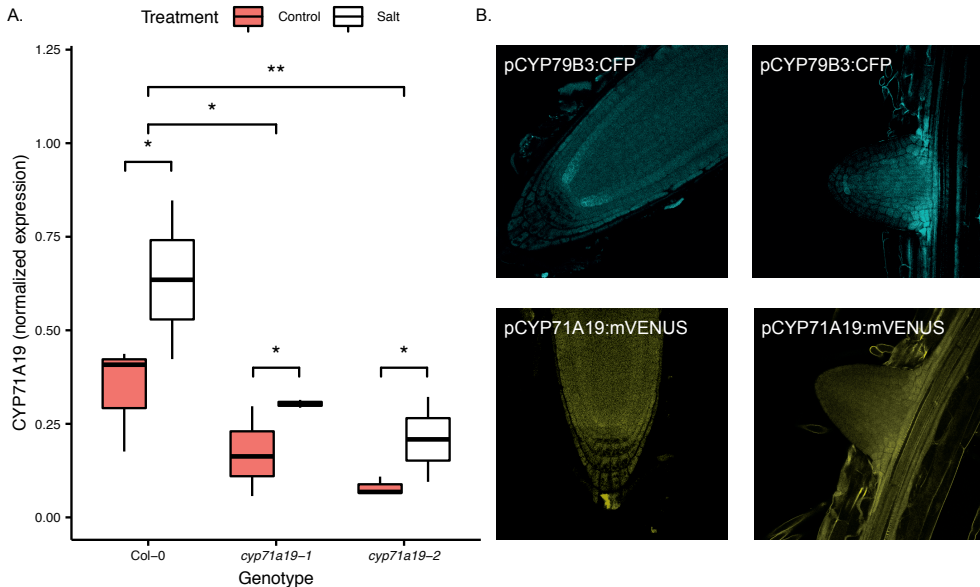


**Figure 6. CYP71A19 expression is upregulated by salt stress and overlaps in localisation with CYP79B3 expression.** (**A**) Roots of 8-day-old seedlings of Col-0, *cyp71a19-1*, *cyp71a19-2*, treated with 0 (control) or 75 (salt) mM of NaCl for 4 days, were harvested and analysed with RT-qPCR for expression of *CYP71A19* and reference gene at2g28390. Boxplots show *CYP71A19* expression, normalized for reference gene expression. The middle line inside the box represents the median (n=3). Lower and upper box boundaries represent 25th and 75th percentiles. Lower and upper error lines represent 10th and 90th percentiles. Dots represent data falling outside 10th and 90th percentiles. A two-way ANOVA was done to determine significant differences. Asterisks indicate significant difference following Dunnett post-hoc test (* $p < 0.05$, ** $p < 0.01$, *** $p < 0.001$ (**B**) Confocal images of the main root tip (left) and a just emerged lateral (right) of 8-day old seedlings of pCYP79B3:CFP (top) and pCYP71A19:mVENUS (below). No treatment has been applied. Brightness of images has been adapted to facilitate observation of the location of expression and should not be compared for intensity.

*Knock-down mutants of CYP71A19 show reduced lateral root development in salt stress*
As the *cyp79b2-2 cyp79b3-2* mutant displays reduced lateral root density in salt stress, we hypothesize that if CYP71A19 would convert IAN during salt stress, lack of *CYP71A19* expression would lead to a similar phenotype. Indeed *cyp71a19-1* and *cyp71a19-2*, both T-DNA insertion knock-down mutants (Figure 6A; Supplemental Figure 2), show a similar reduction in lateral root density in 125mM of salt stress (figure 7C) as the *cyp79b2-2cyp79b3-2* double mutant, with no consistent effect on other RSA parameters (Figure 7).
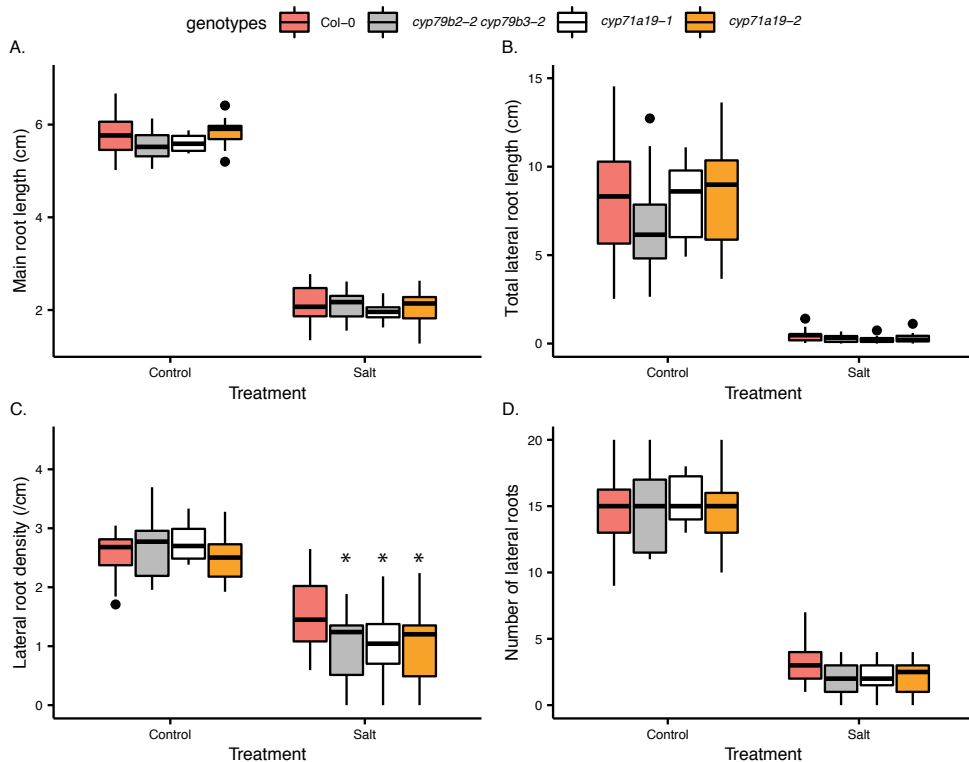


**Figure 7. Knock-down mutants of *CYP71A19* show reduced lateral root density in salt stress.** Main root length (**A**), average lateral root length (**B**), lateral root density (**C**) and number of lateral roots (**D**) of 12-day old Col-0 (pink), *cyp79b2-2cyp79b3-2* (grey), *cyp71a19-1* (white) and *cyp71a19-2* (orange) seedlings transferred to ½ MS plates supplemented with 0 (control) or 125 (salt) mM of NaCl after 4 days. The middle line inside the box represents the median (n=20). Lower and upper box boundaries represent 25th and 75th percentiles. Lower and upper error lines represent 10th and 90th percentiles. Dots represent data falling outside 10th and 90th percentiles. Significant differences were determined by a two-way ANOVA, followed by a manual contrast post-hoc test if significant differences were found. Asterisks indicate a significant difference with Col-0 within treatment (* $p<0.05$, ** $p<0.01$, *** $p<0.001$).

*Ectopic Overexpression of NIT1 specifically decreases lateral root density*
Nitrilases are enzymes that have been shown to be able to convert IAN to IAA (Vorwerk et al., 2001), making them interesting candidates to study for their possible role in salt-induced root developmental responses possibly downstream of CYP79 and CYP71 action. While nitrilase KO and silencing lines exhibit similar root development as Col-0 (Figure 8; Lehmann et al., 2017), NIT overexpression lines on the other hand, show an increased lateral root density in control conditions (Lehmann et al., 2017). If the observed phenotype of the mutant in the IAOx pathway (*cyp71a19-1, cyp71a19-2, cyp79b2-2cyp79b3-2*) would be explained by loss of IAA biosynthesis via this pathway, then indeed we would expect the overexpression lines to have the opposite phenotype and to display an increased lateral root density. In salt stress though, we found lateral root density of the overexpression lines to be reduced compared to wildtype (Figure 8C), while no effect on lateral root development of the knock-out or silencing lines was found. These results indicate IAA biosynthesis from IAN is not key to maintaining lateral root development during salt stress. However, the affinity of the nitrilases for IAN is very low in comparison to other (synthetic) chemicals (Vorwerk et al., 2001) and thus it is not clear whether these nitrilases might also have another role in planta.

Possibly, IAN itself could play a role in regulating root architecture and the *NIT1* overexpression lines would in that case reduce IAN availability due to high turnover. Although Lehmann et al (2017) show that two-week-old seedlings overexpressing *NIT1* contained increased levels of IAN and free IAA in comparison to wildtype, this effect could not be shown in older plants. These results show that interpreting effects of overexpressed genes acting in metabolic pathways can be challenging. We propose a direct role of IAN in maintaining lateral root development during salt stress. Thus far IAN has not been considered an active compound, although molecular modeling has predicted it to be able to bind the TIR1 receptor (Katz et al., 2015). A first step in confirming IAN to actively influence auxin signaling, could be to show interaction with TIR1 by using radioactively labeled IAN as previously shown for IAA, 2,4-D, 1-NAA and 2-NAA (Dharmasiri et al., 2005; Kepinski and Leyser, 2005).
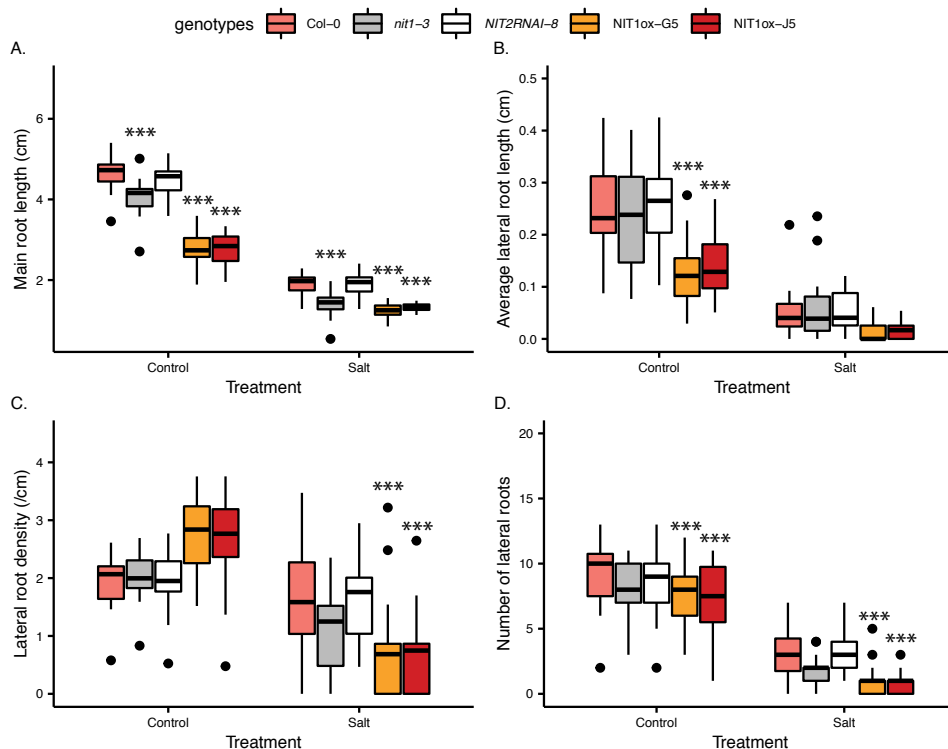
4

**Figure 8. Over-expression of *NITs* leads to reduced lateral root density in salt stress.** Main root length (**A**), total lateral root length (**B**), lateral root density (**C**) and number of lateral roots (**D**) of 12-day old Col-0 (pink), *nit1-3* (grey), NIT2RNAI-8 (white), NIT1ox-G5 (orange) and NIT1ox-J5 (red) seedlings transferred to ½ MS plates supplemented with 0 (control) or 125 (salt) mM of NaCl after 4 days. The middle line inside the box represents the median (n=20). Lower and upper box boundaries represent 25th and 75th percentiles. Lower and upper error lines represent 10th and 90th percentiles. Dots represent data falling outside 10th and 90th percentiles. Significant differences were determined by a two-way ANOVA, followed by a manual contrast post-hoc test if significant differences were found. Asterisks indicate a significant difference with Col-0 within treatment (* $p<0.05$, ** $p<0.01$, *** $p<0.001$).

## CONCLUSION

Salt stress leads to remodeling of root system architecture. In Arabidopsis, the IAOx pathway was shown to play a role in maintaining lateral root development and growth during salt stress (Julkowska et al., 2017; Chapter 3). In this study we used a combination of metabolomics and mutant analyses to investigate the contribution of downstream products in the IAOx pathway responsible for this developmental response. We show that the metabolite IAN plays a central role in maintaining lateral root growth during salt stress. IAN can either be produced via indole glucosinolates, which are induced by salt stress, or via direct conversion putatively facilitated by the novel enzyme CYP71A19. Our results do not directly support a role for IAA in the process, as IAA content of

*cyp79b2-2cyp79b3-2* mutants in both control conditions and salt stress was not affected. In addition, overexpression of NITs, converting IAN to IAA, causes a reduction of lateral root density in salt stress rather than an increase. We therefore propose a direct role of IAN in maintaining lateral root development during salt stress. Furthermore, we show that during salt stress, not only auxin transport, but also auxin biosynthesis pathways play a major role in maintaining lateral root development.

## MATERIALS AND METHODS

### Plant material and growth conditions

For all experiments, wild-type Columbia-0 (Col-0) was used as a reference. T-DNA insertion lines *cyp71a19-1* (SALK_067027.37.90) and *cyp71a19-2* (SAIL_500_G07) were obtained from Nottingham Arabidopsis Stock Center (NASC; nasc.org.uk). The *cyp79b2-2cyp79b3-2* knock-out mutant (Sugawara et al., 2009) was kindly provided by Hiroyushi Kasahara (RIKEN Center for Sustainable Resource Science, Yokohama, Japan). The *cyp71a12 cyp71a13* (Müller et al., 2015) and the *pad3* (Nafisi et al., 2007) knock-out mutants were kindly provided by Erich Glawischnig (Institute for Genetics, Technical University Munich, Germany). The DR5::N7-VENUS line ((Galvan-Ampudia et al., 2013; Heisler et al., 2005) was kindly provided by Jiri Friml (Institute of Science and Technology, Austria). The pCYP79B3:CFP line was kindly provided by Viola Willemsen (Laboratory of Plant developmental Biology, Wageningen University, The Netherlands). The *nit1-3, NIT2RNAI-8*, NIT1ox-G5 and NIT1ox-J5 (Lehmann et al., 2017) were kindly provided by Stephan Pollman (Center for Plant Biotechnology and Genomics, University of Madrid, Spain).

The pCYP71A19:mVENUS construct was made by amplifying the CYP71A19 promoter with forward primer (including an AttB4 site) 5'- GGGGACAACTTTG-TATAGAAAAGTTGGCCATCTTTTTTTTTTTGTAGGAG -3' and reverse primer (including AttB1r site) 5'-GGGGACTGCTTTTTTGTACAAACTTGTTCTAAT-TCAATCTCTCATGTAAAGTATTTAG-3'. Next, the promoter was cloned into a pGEM box1 P4P1R entry clone. Through multisite gateway, the full construct with the promoter in box1, N7-VENUS in box2 and tNOS in box3, was cloned. The construct was then transformed into *Arabidopsis thaliana* accession col-0 with agrobacterium transformation through floral dipping.

Seeds were surface sterilized in a desiccator of 1.6 L volume by exposing them to the vapour of 20 ml household bleach and 600 μL 40% HCl for 3 hours and subsequently placed in the laminar flow for 1.5 hours to remove toxic vapors. The seeds were stratified in 0.1% agar at 4°C in the dark for 2 to 4 days and sown on square petri dishes (12 x 12 cm) containing 40 ml of control growth medium consisting of ½ Murashige-Skoog (MS), 0.1% M.E.S. Monohydrate and 1% Daishin agar, the pH 5.8 (KOH), previously dried for 1 h in a laminar flow. Plates were placed vertically at a 70° angle. For all experiments, plants were grown under controlled conditions at long day (16/8 hours) in 21°C and 70% humidity. Experiments presented in Figure 1B, 2B, 6A, 8 and Supplemental figure 1 and 2 were grown under TL lighting (125 μmol/m2/s, Sylvania

4

Britegrow F58W 1084 lamps) at Amsterdam University. Experiments presented in Figure 2A, 3, 4, 6B and 7 were grown under LED lighting (125 μmol/m2/s, LuxaLight 4300K ledstrips) at Wageningen University.

*Confirmation of T-DNA insertion lines*
The T-DNA insertion lines were genotyped by extracting DNA from leaf material ground in liquid nitrogen using 10% Chelex (Bio-rad) in MiliQ followed by 15 min incubation at 95°C and 15 min centrifugation at maximum speed in a standard tabletop centrifuge. The supernatant was used as an input for the PCR reaction. The primers used for T-DNA insertion lines identification are listed in Supplemental table 5.

*Root system architecture assays*
Four-day-old seedlings germinated and grown in conditions as described above, were transferred to ½MS agar plates supplemented with 0 or 125 mM NaCl. Each plate contained four seedlings of two genotypes (two seedlings per genotype). Plates were placed following a random design. The plates were scanned with Epson perfection V700 scanner at 400 dpi at 10 and 12 days after germination (6 and 8 days after transfer). The root scans were traced with the ImageJ plugin Smartroot (Lobet et al., 2011). Each experiment was repeated at least two times with similar results, except for the IAN and I3C complementation (Figure 2) and the NIT lines (Figure 8).

*Extractions of indole glucosinolates and camalexin and LC-MS analysis*
For determination of indole glucosinolates via untargeted LC-MS analysis, wild type and *cyp79b2b3* knock-out mutants were germinated on mesh on top of ½MS agar plates as described above. Eight days after germination, plants were transferred to ½MS agar plates supplemented with 0 or 125mM of NaCl. After two days of treatment, plants were separated into roots and shoots and flash-frozen into liquid nitrogen. Several plants grown on the same plate were pooled to obtain samples of approximately 100mg fresh weight. Tissue was ground to a fine powder at -80°C using 3-mm stainless steel beads at 50 Hz for 1 min in a TissueLyser LT (Qiagen, Germantown, USA). Approximately 100mg per sample was used for metabolite extraction. Pooled samples were made by combining equal amounts of freeze-dried material from all root samples and all shoot samples and all root and shoot samples combined. Pooled samples were treated similarly and simultaneously as the experimental samples and used as a quality control.

Samples were extracted with 300μL 75% methanol ($0.125^w/_v$% formic acid), adjusted to the exact weight of the sample. Next, the samples were sonicated at room temperature at 40kHz for 15min and then centrifuged for 10min at 15000rpm (Vos et al., 2007). A 180 μl aliquot of each sample was transferred into a LC-MS vial and analysed within 24hrs after extraction. The sequence of analysis started and ended with an extract from the overall samples pool, whereas root- and shoot-pooled samples were placed in random sequence in between the respective samples type, i.e. the pooled sample of root material was analysed in between root samples.

LC-MS analyses were performed according to (Mokochinski et al., 2018). In short, separation of compounds in the crude extracts was performed using an HPLC system

(Waters Acquity, Milford, USA) generating a flow rate of 0.19mL.min$^{-1}$ and a 45min gradient of 5 to 75% acetonitrile in water (0.1% formic acid), on a C18 reversed phase column (Luna 150×2 mm i.d., 3 μm; Phenomenex, Torrance, USA) at 40°C. Detection of eluting compounds was by a PDA detector (Waters) at 210–600 nm and subsequently an LTQ-Orbitrap FTMS hybrid mass spectrometer (ThermoScientific, Bremen, Germany). Samples were analysed in negative ionization mode. A mass resolution of 60,000 FWHM was employed during data acquisition in a mass range of m/z 90–1350.

*LC-MS – Data Pre-processing, multi-variate analysis and metabolite annotation*
Baseline correction and peak-wise alignment was done using Metalign (Lommen 2009). The threshold for signal to noise ratio was set at 3. Data were filtered by removing peaks that were present in less than 4 samples over the entire dataset. The peak amplitudes were normalized to 10,000 total peak amplitude for each sample (relative abundance of peaks compared to the total peak amplitude) and this relative abundance of metabolites was expressed as Measured Ion Counts which were used as parameter for further multivariate analysis.

To investigate differences in metabolomic profiles, the mass signal dataset was subjected to multi-variate analyses and subsequent relevant metabolite selection (peak picking) using the web-based online tool MetaboAnalyst 3.0 (Xia and Wishart, 2016). Metabolites were annotated using an in-house database (Wageningen Plant Research Bioscience, the Netherlands) based on comparisons of retention time, accurate mass, and isotopic composition as well as on-line available metabolite databases such as KNApSAcK, KEGG and MassBank. For camalexin specially, a standard compound (Sigma Aldrich) was injected separately and in combination with a pooled sample for optimized annotation. Supplemental table 1 shows the selected features mass and retention time.

*Extraction of indole-3-acetic acid and indole-3-acetonitrile*
For the extraction of indole-3-acetic acid (IAA) and indole-3-acetonitrile (IAN) from *A. thaliana* seedlings, wildtype and *cyp79b2b3* knock-out mutants were germinated on mesh on top of ½MS agar plates as described above. After 8 days, plants were transferred to ½MS liquid medium supplemented with 0 or 125 mM of NaCl. After 1 hour, roots were separated and snap frozen in liquid nitrogen, several plants pooled into samples of ~20 mg. Tissue was ground to a fine powder at -80˚C using 3-mm stainless steel beads at 50 Hz for 1 min in a TissueLyser LT (Qiagen, Germantown, USA). Ground samples were extracted with 1 mL of 100% methanol (MeOH) containing stable isotope-labeled [13C6]IAA as internal standard (IS, Supplemental Table 6 at an end concentration of 100 nM per sample. Samples were vortexed, ultrasonicated for 30 seconds and extracted at 4˚C overnight on a shaker. Subsequently, samples were centrifuged at 12000 rpm for 10 min in a tabletop centrifuge set at 4˚C Supernatants were transferred to amber 4-mL glass vials. Pellets were re-extracted with 1 mL of 100% MeOH for 1 h at 4˚C. After centrifugation as above, both supernatants were pooled before evaporating to dryness in a speed vacuum system (SPD121P, ThermoSavant, Hastings, UK). Residue was dissolved in 1 mL of 1M formic acid (FA) and loaded on a 30 mg Oasis MCX Cartridge (Waters, Milford, USA). The cartridge was equilibrated with 1 mL of MeOH and Equilibrated with 1 mL 1M FA prior to sample loading. Subsequently, the cartridge

was washed with 1 mL of 1M FA and eluted with 1mL of 100% MeOH. The 100% MeOH was evaporated in a speed vacuum system (SPD121P, ThermoSavant, Hastings, UK) at RT and the residue stored at -20˚C until further analysis.

### Detection and Quantification of IAA and IAN by Liquid Chromatography-Tandem Mass Spectrometry

Samples were resuspended in 100 µL of acetonitrile/water (0.1% formic acid) (20:80, v/v) and filtered through a 0.45 mm Minisart SRP4 filter (Sartorius, Goettingen, Germany). Analyses of IAA and IAN was performed by comparing retention times and mass transitions with those of unlabeled standards (Supplemental Table 6) using a Waters XevoTQs mass spectrometer equipped with an electrospray ionization source coupled to an Acquity UPLC system (Waters, Milford, USA). Chromatographic separations were conducted on an Acquity UPLC BEH C18 column (100 mm, 2.1 mm, 1.7 mm; Waters, USA) by applying either a acetonitrile/water (0.1% formic acid) gradient. The column was operated at 40˚C with a flow rate of 0.25 mL•min$^{-1}$. The column was equilibrated for 30 min using acetonitrile/water (0.1% formic acid, 20/80, v/v) 0.25 mL•min$^{-1}$ at the start of a run. The acetonitrile/water (0.1% formic acid) gradient started from 20% (v/v) acetonitrile, increasing to 70% (v/v) acetonitrile in 17 min. To wash the column, the water/acetonitrile gradient was increased to 100% (v/v) acetonitrile in a 1.0 min gradient, which was maintained for 1.0 min before going back to 20% acetonitrile using a 1.0 min gradient, prior to the next run. The sample injection volume was 3 µL. The mass spectrometer was operated in positive electrospray ionization mode. Cone and desolvation gas flows were set to 150 and 1000 l•h$^{-1}$, respectively. The capillary voltage was set at 3.5, the source temperature at 150˚C, and the desolvation temperature at 550˚C. The cone voltage was optimized for each standard compound using the IntelliStart MS Console (Waters, Milford, USA). Argon was used for fragmentation by collision-induced dissociation. Multiple reaction monitoring (MRM) was used for quantification. Parent–daughter transitions for the different (stable isotope labeled) compounds were set using the IntelliStart MS Console. MRM transitions selected for compound identification and quantification are shown in Supplemental Table 6. The cone voltage was set to 40 eV. To determine sample concentrations, a 10-point calibration curve was constructed for both IAA and IAN ranging from 1 µM to 190 pM and each dilution also contained a known amount of the [13C6]IAA-labelled internal standard.

### DR5 imaging

pDR5:mVENUS was crossed into *cyp79b2-2 cyp79b3-2* background and plants homozygous for both mutations as well as the fluorescent marker were selected. For confocal imaging of pDR5:mVENUS in wildtype and *cyp79b2-2cyp79b3-2* knock-out background, seedlings were germinated on ½MS agar plates as described above. After 6 and 7 days, the plates were turned 90 degrees to induce lateral root formation in similar stage at the bend of the root. After 8 days, plants were transferred to ½MS liquid medium supplemented with 0 or 125 mM of NaCl. After 1 or 3 hours, root samples were fixed with 4% PFA (paraformaldehyde) in 1 x PBS for 1 hour. Next, plants were cleared in ClearSee solution (Kurihara et al., 2015) for at least 24 hours. Root samples were stained for 60 minutes in a 0.2% Calcofluor-white solution in ClearSee.

After discarding the staining solution roots were rinsed with ClearSee once, before a second rinse in ClearSee for 30 minutes. Subsequently, root samples were mounted in a ClearSee solution in between microscope slides and coverslip with 0.2 mm spacers. Samples were sealed using nail polish to ensure successful prolonged imaging of samples.

Images were acquired in 8-bit format using a Leica TCS SP8 confocal laser scanning microscope with a 40x NA=1.1 water-immersion objective. VENUS and Calcofluor-white emission were sequentially scanned with a Leica HyD-detector in photon counting mode. Excitation and detection of fluorophores were configured as follows: VENUS was excited by a 488 nm argon-ion laser, and emission was detected at 500-525 nm with the pinhole set to 1.3 Airy unit. Calcofluor-white was exited using a 405 nm diode laser, and emission was detected at 425-475 nm.

For quantitative analysis of DR5::N7-VENUS expression, Z-stacks with 0,2 um intervals including all nuclei with VENUS expression in the root tip, were generated. Generated Z-stacks (TIFF) were used to create SUM-slice projections for further signal quantification. From these projections, background signal was subtracted using Fiji process math subtract (value 5). The background subtraction value was based on average measured background signal of generated projections. Projections were gaussian blurred (sigma=1) and converted to 8-bit images. To select nuclei in the projections, a threshold (25-255) was created for the projections, and this threshold was converted to a mask. Integrated density was measured (Fiji analyze particles) on this mask to quantify total signal intensity of nuclei in the root tip. Roots containing only one mask were considered as outliers and removed.

*Localisation of expression*
For imaging pCYP71A19:mVENUS and pCYP79B3:CFP lines, plants were sterilized and grown on ½MS agar plates as described above. 8-day old seedlings were transferred to liquid ½MS medium for 3h, followed by fixation with 4% PFA (paraformaldehyde) in 1 x PBS for 1 hour. Next, plants were cleared in ClearSee solution (Kurihara et al., 2015) for at least 24 hours. Subsequently, root samples were mounted in a ClearSee solution in between microscope slides and coverslip with 0.2 mm spacers. Samples were sealed using nail polish to ensure successful prolonged imaging of samples.

Images were acquired in 8-bit format using a Leica TCS SP8 confocal laser scanning microscope with a 40x NA=1.1 water-immersion objective. VENUS or CFP emission were sequentially scanned with a Leica HyD-detector in photon counting mode. Excitation and detection of fluorophores were configured as follows: VENUS was excited by a 488 nm argon-ion laser, and emission was detected at 500-525 nm with the pinhole set to 1.3 Airy unit. CFP was exited using a 405 nm diode laser, and emission was detected at 425-475 nm. Brightness of images has been adapted to easily observe the localisation of expression. These images should not be used for quantification.

*Quantitative real-time PCR*
For gene expression, plants were germinated as described above and transferred to ½MS agar plates supplemented with 0 or 75mM of NaCl after 4 days. After 4 days

of treatment, roots were cut off, snap frozen in liquid nitrogen and grinded to a fine powder. RNA extraction was performed with TRI-reagents (Sigma) with additional chloroform cleaning step, followed by TURBO DNase treatment (Ambion). The cDNA was synthesized from 1 μg total RNA using reverse transcriptase (Fermentas), diluted to approximately 10 ng/μl and used for qPCR using the Eva-Green kit (Solis Biodyne) and an Applied Biosystems sds7500 machine. Per biological replicate 2 technical replicates were used The expression was normalized for transcript levels of the reference gene AT2G28390 (SAND; forward primer 5'-AACTCTATGCAGCATTTGATCCACT-3'; reverse primer 5'-TGATTGCATATCTTTAT

CGCCATC-3'). *CYP71A19* expression was measured using forward primer 5'- TGA-GAGGTGGCAGAGATGTG-3' and reverse primer 5'- AGACCGGACCATTTTGT-TGC-3'. *TPS12* expression was measured using forward primer 5'-CGCGAAGTGTCT-TTAAACTTATG-3' and reverse primer 5'-GATTTGCTCTCACGAGTGTATTG-3'. The expression levels of genes of interest were calculated by $\Delta Ct = 2-$ (Ct-value target)/ $2-$ (Ct-value reference).

*Statistics*
Statistical analysis was performed with R software. Data was visually checked for normal distribution by visual inspection of Q-Q plots before further analysis. Linear models (two-way ANOVA) were fitted using the lm function of the stats package. Linear Mixed-Effects Models were fitted with the lmer function of the lme4 package. If results were significant, post-hoc analysis with manual contrasts were done with the ghlt function of the multcomp package. Details on statistics can be found in the legend of each figure.

## SUPPLEMENTAL MATERIALS
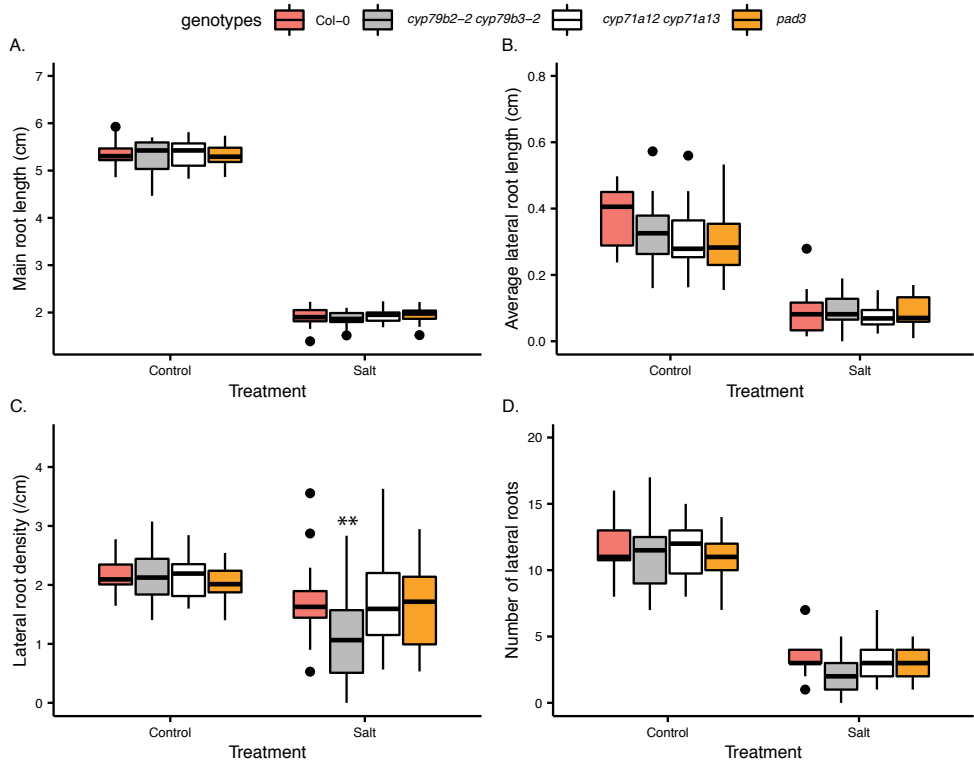


**Supplemental figure 1. Mutants downstream in camalexin biosynthesis do not show reduced lateral root density during salt stress.** Main root length (**A**), average lateral root length (**B**), lateral root density (**C**) and number of lateral roots (**D**) of 10-day old Col-0 (red), *cyp79b2-2cyp79b3-2* (grey), *cyp71a12cyp71a13* (white) and *pad3* (orange) seedlings transferred to ½ MS plates supplemented with 0 (control) or 125 (salt) mM of NaCl after 4 days. The middle line inside the box represents the median (n=20). Lower and upper box boundaries represent 25th and 75th percentiles. Lower and upper error lines represent 10th and 90th percentiles. Dots represent data falling outside 10th and 90th percentiles. Significant differences were determined by a two-way ANOVA, followed by a manual contrast post-hoc test if significant differences were found. Asterisks indicate a significant difference with Col-0 within treatment (* p<0.05, ** p<0.01, *** p<0.001).

A.



B.
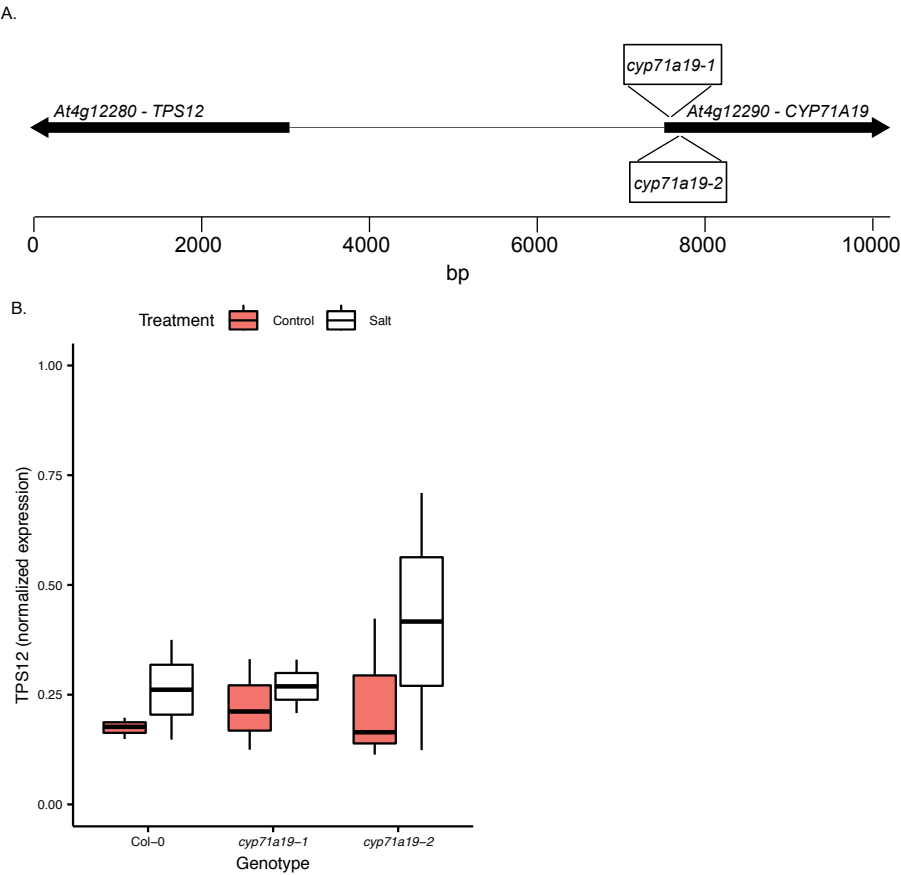


**Supplemental figure 2. T-DNA insertion mutants *cyp71a19-1* and *cyp71a19-2* are not affected in *TPS12* expression. (A)** Two T-DNA insertion mutants located in the 5'UTR (*cyp71a19-1*, SALK_067027) and exon (*cyp71a19-2*, SAIL_500_G07) of *CYP71A19* were selected for studying the role of *CYP71A19* in salt stress. *CYP71A19* shares a promoter with *TPS12.* **(B)** Root tissue of 10-day old Col-0, *cyp71a19-1* and *cyp71a19-2* seedlings, treated with 0 (control, pink) or 75 (salt, white) mM of NaCl, was harvested and analyzed with RT-qPCR for gene expression of *TPS12* and reference gene At2G28390. Boxplots show *TPS12* expression, normalized for reference gene expression. The middle line inside the box represents the median (n=3). Lower and upper box boundaries represent 25th and 75th percentiles. Lower and upper error lines represent 10th and 90th percentiles. Dots represent data falling outside 10th and 90th percentiles. Significant differences were determined by a two-way ANOVA. No significant differences were found.

**Supplemental Table 1.** Selected features for IMG, mIMG, hIMG and Camalexin.

| Peak | Rt, min | [M-H]- | Putative Identification | Common name | Abbreviation |
|------|---------|--------|-------------------------|-------------|--------------|
| 1336 | | 199.0329 | 3-(1,3-thiazol-2-yl)-1H-indole | Camelexin | CL |
| 4226 | 16.12 | 447.0533 | Indol-3-ylmethylglucosinolate | Glucobrassicin | IMG |
| 4603 | 18.65 | 463.0484 | 1-Hydroxy-3-indolylmethyl; 4-Hydroxy-3-indolylmethyl | 1-Hyroxyglucobrassicin; 4-Hydroxyglucobrassicin | hIMG |
| 4936 | 21.47 | 477.0641 | 4-Methoxy-3-indolylmethyl | 4-Methoxyglucobrassicin | mIMG |

**Supplemental Table 2.** Expression of *CYP71A* family members in different tissues based on the Klepikova Atlas (Klepikova et al., 2016).

| Gene | root (without apex) | root apex | Seedling root | Seedling hypocotyl | seedling cotyledon | Dry seeds | Mature leaf (whole) | Senescent leaf (petiole) | Mature flower (stage 3) |
|---|---|---|---|---|---|---|---|---|---|
| CYP71A12 | 8.78 | 0.96 | 0.09 | 0.09 | 0.05 | 0 | 0.27 | 12.23 | 0.09 |
| CYP71A13 | 0 | 0 | 0 | 0 | 0 | 0 | 0.1 | 6.88 | 1.22 |
| CYP71A14 | 3.59 | 4.25 | 5.59 | 0 | 0 | 0.7 | 0 | 0 | 0.11 |
| CYP71A15 | 0.08 | 0.18 | 0.19 | 0 | 0 | 3.7 | 0 | 0 | 0 |
| CYP71A16 | 8.21 | 39.95 | 6.54 | 0 | 0 | 0 | 0 | 0 | 0 |
| CYP71A18 | 0.23 | 0 | 0 | 0 | 0 | 0 | 0 | 0.19 | 1.1 |
| CYP71A19 | 13.07 | 0.99 | 1.34 | 0 | 0 | 7.75 | 0 | 0 | 0 |
| CYP71A20 | 6.01 | 5.23 | 3.41 | 0 | 0 | 0.75 | 0 | 0 | 0 |
| CYP71A21 | 0.19 | 0.1 | 0.07 | 3.87 | 1.52 | 0 | 8.65 | 7.48 | 0.18 |
| CYP71A22 | 0 | 0.07 | 0 | 2.69 | 0 | 0.6 | 16.46 | 7.56 | 1.07 |
| CYP71A23 | 0 | 0.05 | 0 | 0.06 | 0 | 0 | | | |
| CYP71A24 | 0 | 0 | 0.08 | 0 | 0.18 | 0 | 1.22 | | |
| CYP71A25 | 0.15 | 0.38 | 0.3 | 0.2 | 1.46 | 0 | 3.6 | 0.53 | 4.4 |
| CYP71A26 | 0 | 0 | 0 | 0.39 | 0 | 0.09 | 0.43 | | 0 |
| CYP71A27 | 28.3 | 9.13 | 16.29 | 25.87 | 0 | 0 | 0 | 0 | |
| CYP71A28 | 2.62 | 0.67 | 0.65 | 0.48 | 0 | 0 | 0 | | |
| CYP79B2 | 112.69 | 44.38 | 43.16 | 97.51 | 29.76 | 0.14 | 18.87 | 61.13 | 11.12 |
| CYP79B3 | 73.18 | 18.86 | 27.31 | 88.02 | 20.96 | 0.09 | 26.33 | 36.98 | 4.17 |

4

**Supplemental Table 3.** Expression of *CYP71A* family members and *CYP79B2* and *B3* in the root in response to salt stress based on Dinneny et al. 2008. Relative expression (_rel) is relative to 0h.

| Gene | 0hr_MS | 30min_NaCl | 1hr_NaCl | 4hr_NaCl | 16hr_NaCl | 32hr_NaCl | 0h_rel | 30min_rel | 1hr_rel | 4hr_rel | 16hr_rel | 32hr_rel |
|---|---|---|---|---|---|---|---|---|---|---|---|---|
| *CYP71A12* | 6.16 | 16.54 | 10.81 | 10.23 | 20.04 | 16.02 | 0 | 1.42 | 0.81 | 0.73 | 1.70 | 1.38 |
| *CYP71A14* | 71.72 | 50.08 | 45.44 | 78.11 | 52.94 | 50.49 | 0 | -0.52 | -0.66 | 0.12 | -0.44 | -0.51 |
| *CYP71A15* | 71.72 | 50.08 | 45.44 | 78.11 | 52.94 | 50.49 | 0 | -0.52 | -0.66 | 0.12 | -0.44 | -0.51 |
| *CYP71A16* | 128.27 | 111.35 | 97.61 | 124.92 | 122.76 | 96.44 | 0 | -0.20 | -0.39 | -0.04 | -0.06 | -0.41 |
| *CYP71A19* | 2.71 | 11.45 | 5.01 | 20.66 | 137.77 | 116.73 | 0 | 2.08 | 0.89 | 2.93 | 5.67 | 5.43 |
| *CYP71A20* | 2.71 | 11.45 | 5.01 | 20.66 | 137.77 | 116.73 | 0 | 2.08 | 0.89 | 2.93 | 5.67 | 5.43 |
| *CYP71A27* | NA | NA | NA | NA | NA | NA | NA | NA | NA | NA | NA | NA |
| *CYP71A28* | 7.02 | 4.25 | 7.03 | 5.87 | 5.32 | 4.83 | 0 | -0.72 | 0.00 | -0.26 | -0.40 | -0.54 |
| *CYP79B2* | 198.28 | 237.46 | 130.9 | 73.86 | 324.71 | 300.87 | 0 | 0.26 | -0.60 | -1.42 | 0.71 | 0.60 |
| *CYP79B3* | 109.94 | 110.17 | 54.97 | 20.07 | 90.01 | 56.24 | 0 | 0.00 | -1.00 | -2.45 | -0.29 | -0.97 |

**Supplemental Table 4.** Expression of *CYP71A* family members and *CYP79B2* and *B3* in the root in response to bending (hours after bending) based on Voß et al., 2015. Relative expression (_rel) is compared to 0h.

| Gene | 0h | 6h | 12h | 24h | 36h | 48h | 0h_rel | 6h_rel | 12h_rel | 24h_rel | 36h_rel | 48h_rel |
|---|---|---|---|---|---|---|---|---|---|---|---|---|
| *CYP79B2* | 79.76 | | 346.01 | 1072.82 | 876.49 | 918.55 | 0 | NA | 2.117 | 3.750 | 3.458 | 3.526 |
| *CYP79B3* | 61.65 | | 403.03 | 1004.41 | 857.45 | 750.36 | 0 | NA | 2.709 | 4.026 | 3.798 | 3.605 |
| *CYP71A12* | 1.2 | 3.98 | 2.7 | 1.26 | 5.24 | 225.65 | 0 | 1.730 | 1.170 | 0.070 | 2.127 | 7.555 |
| *CYP71A14* | 21.31 | 15.04 | 20.97 | 17.57 | 20.67 | 42.48 | 0 | -0.503 | -0.023 | -0.278 | -0.044 | 0.995 |
| *CYP71A15* | 21.31 | 15.04 | 20.97 | 17.57 | 20.67 | 42.48 | 0 | -0.503 | -0.023 | -0.278 | -0.044 | 0.995 |
| *CYP71A16* | 188.95 | 137.3 | 117.97 | 25.49 | 25.88 | 14.03 | 0 | -0.461 | -0.680 | -2.890 | -2.868 | -3.751 |
| *CYP71A19* | 6.89 | 6.86 | 12.85 | 5.58 | 29.48 | 40.56 | 0 | -0.006 | 0.899 | -0.304 | 2.097 | 2.557 |
| *CYP71A20* | 6.89 | 6.86 | 12.85 | 5.58 | 29.48 | 40.56 | 0 | -0.006 | 0.899 | -0.304 | 2.097 | 2.557 |
| *CYP71A27* | NA | NA | NA | NA | NA | NA | NA | NA | NA | NA | NA | NA |
| *CYP71A28* | 12.49 | 12.01 | 10.51 | 12.39 | 13.93 | 10.5 | 0 | -0.057 | -0.249 | -0.012 | 0.157 | -0.250 |

**Supplemental Table 5.** Overview of t-DNA insertion lines studied including the primers used for genotyping t-DNA insertion lines.

| t-DNA line | mutant name | target gene | FW (5' -> 3') | REV (5' -> 3') |
|---|---|---|---|---|
| SALK_113348 | *cyp79b2-2* | At4g39950 | CCCATATCGGCTAAGAAGGAC | AAGTTGTGATGACGGAACTCG |
| GABI_198F06 | *cyp79b3-2* | At2g22330 | TGGCAGAGAAAATGCCATAAC | TCTCAATTCTCCGACCAACAC |
| SALK_067027 | *cyp71a19-1* | At4g13290 | TTCAAGATGTCATGAGCAACG | GCCTCCACTTCCATTTCTACC |
| SAIL_500_G07 | *cyp71a19-2* | At4g13290 | AGATATCCAACCCGGATTTTG | TTCAAGATGTCATGAGCAACG |

**Supplemental Table 6.** Multiple reactions monitoring (MRM) transitions table for all plant growth regulators and corresponding internal standards used in this study.

| Number | Compound | Retention Time | Mass* | MRM transition | Cone V. | Coll. Energy |
|---|---|---|---|---|---|---|
| 1 | IAA | 3.34 | 176.25 | 103.2 | 30 | 25 |
| | | | | 130.2‡ | 30 | 15 |
| 2 | [13C6]IAA | 3.32 | 182.1 | 109.2 | 30 | 25 |
| | | | | 136.2‡ | 30 | 15 |
| 3 | IAN | 5.81 | 157.2 | 90 | 30 | 30 |
| | | | | 117 | 30 | 20 |
| | | | | 130.05 | 30 | 10 |

## ACKNOWLEDGEMENTS

4

# REFERENCES

Agerbirk, N., De Vos, M., Kim, J. H., and Jander, G. (2009). Indole glucosinolate breakdown and its biological effects. *Phytochem. Rev.* 8, 101–120. doi:10.1007/s11101-008-9098-0.

Ahuja, I., Kissen, R., and Bones, A. M. (2012). Phytoalexins in defense against pathogens. *Trends Plant Sci.* 17, 73–90. doi:10.1016/j.tplants.2011.11.002.

Barth, C., and Jander, G. (2006). Arabidopsis myrosinases TGG1 and TGG2 have redundant function in glucosinolate breakdown and insect defense. *Plant J.* 46, 549–562. doi:10.1111/j.1365-313X.2006.02716.x.

Bednarek, P., Schneider, B., Svatoš, A., Oldham, N. J., and Hahlbrock, K. (2005). Structural complexity, differential response to infection, and tissue specificity of indolic and phenylpropanoid secondary metabolism in Arabidopsis roots. *Plant Physiol.* 138, 1058–1070. doi:10.1104/pp.104.057794.

Boerjan, W. (1995). superroot, a Recessive Mutation in Arabidopsis, Confers Auxin Overproduction. *Plant Cell Online* 7, 1405–1419. doi:10.1105/tpc.7.9.1405.

Brumos, J., Robles, L. M., Yun, J., Vu, T. C., Jackson, S., Alonso, J. M., et al. (2018). Local Auxin Biosynthesis Is a Key Regulator of Plant Development. *Dev. Cell* 47, 306-318.e5. doi:10.1016/j.devcel.2018.09.022.

Chen, Y., Wang, Y., Huang, J., Zheng, C., Cai, C., Wang, Q., et al. (2017). Salt and methyl jasmonate aggravate growth inhibition and senescence in Arabidopsis seedlings via the JA signaling pathway. *Plant Sci.* 261, 1–9. doi:10.1016/j.plantsci.2017.05.005.

Van Dam, N. M., Tytgat, T. O. G., and Kirkegaard, J. A. (2009). Root and shoot glucosinolates: A comparison of their diversity, function and interactions in natural and managed ecosystems. *Phytochem. Rev.* 8, 171–186. doi:10.1007/s11101-008-9101-9.

Dharmasiri, N., Dharmasiri, S., and Estelle, M. (2005). The F-box protein TIR1 is an auxin receptor. *Nature* 435, 441–445. doi:10.1038/nature03543.

Dinneny, J. R., Long, T. a, Wang, J. Y., Jung, J. W., Mace, D., Pointer, S., et al. (2008). Cell identity mediates the response of Arabidopsis roots to abiotic stress. *Science (80-. ).* 320, 942–945. doi:10.1126/science.1153795.

Du, Y., and Scheres, B. (2018). Lateral root formation and the multiple roles of auxin. *J. Exp. Bot.* 69, 155–167. doi:10.1093/jxb/erx223.

Fu, L., Wang, M., Han, B., Tan, D., Sun, X., and Zhang, J. (2016). Arabidopsis myrosinase genes AtTGG4 and AtTGG5 are root-tip specific and contribute to auxin biosynthesis and root-growth regulation. *Int. J. Mol. Sci.* 17, 1–16. doi:10.3390/ijms17060892.

Galvan-Ampudia, C. S., Julkowska, M. M., Darwish, E., Gandullo, J., Korver, R. A., Brunoud, G., et al. (2013). Halotropism is a response of plant roots to avoid a saline environment. *Curr. Biol.* 23, 2044–2050. doi:10.1016/j.cub.2013.08.042.

Glawischnig, E. (2007). Camalexin. *Phytochemistry* 68, 401–406. doi:10.1016/j.phytochem.2006.12.005.

Halkier, B. A. (2016). *General Introduction to Glucosinolates*. Elsevier Ltd doi:10.1016/bs.abr.2016.07.001.

Halkier, B. A., and Gershenzon, J. (2006). Biology and Biochemistry of Glucosinolates. *Annu. Rev. Plant Biol.* 57, 303–333. doi:10.1146/annurev.arplant.57.032905.105228.

Heisler, M. G., Ohno, C., Das, P., Sieber, P., Reddy, G. V., Long, J. A., et al. (2005). Patterns of auxin transport and gene expression during primordium development revealed by live imaging of the Arabidopsis inflorescence meristem. *Curr. Biol.* 15, 1899–1911. doi:10.1016/j.cub.2005.09.052.

Hull, A. K., Vij, R., and Celenza, J. L. (2000). Arabidopsis cytochrome P450s that catalyze the first step of tryptophan-dependent indole-3-acetic acid biosynthesis. *Proc. Natl. Acad. Sci.* 97, 2379–2384. doi:10.1073/pnas.040569997.

Ivushkin, K., Bartholomeus, H., Bregt, A. K., Pulatov, A., Kempen, B., and de Sousa, L. (2019). Global mapping of soil salinity change. *Remote Sens. Environ.* 231, 111260. doi:10.1016/j.rse.2019.111260.

Julkowska, M. M., Hoefsloot, H. C. J., Mol, S., Feron, R., de Boer, G.-J., Haring, M. a, et al. (2014). Capturing Arabidopsis root architecture dynamics with ROOT-FIT reveals diversity in responses to salinity. *Plant Physiol.* 166, 1387–1402. doi:10.1104/pp.114.248963.

Julkowska, M. M., Koevoets, I. T., Mol, S., Hoefsloot, H. C. J., Feron, R., Tester, M., et al. (2017). Genetic Components of Root Architecture Remodeling in Response to Salt Stress. *Plant Cell*, tpc.00680.2016. doi:10.1105/tpc.16.00680.

Katz, E., and Chamovits, D. A. (2017). Wounding of Arabidopsis leaves induces indole-3-carbinol-dependent autophagy in roots of Arabidopsis thaliana. *Plant J.*, 1–9. doi:10.1111/ijlh.12426.

Katz, E., Nisani, S., Yadav, B. S., Woldemariam, M. G., Shai, B., Obolski, U., et al. (2015). The glucosinolate breakdown product indole-3-carbinol acts as an auxin antagonist in roots of Arabidopsis thaliana. *Plant J.* 82, 547–555. doi:10.1111/tpj.12824.

Kawa, D., Julkowska, M., Montero Sommerfeld, H., Horst, A. ter, Haring, M. A., and Testerink, C. (2016). Phosphate-dependent root system architecture responses to salt stress. *Plant Physiol.*, pp.00712.2016. doi:10.1104/pp.16.00712.

Kepinski, S., and Leyser, O. (2005). The Arabidopsis F-box protein TIR1 is an auxin receptor. *Nature* 435, 446–451. doi:10.1038/nature03542.

Kim, J. H., Lee, B. W., Schroeder, F. C., and Jander, G. (2008). Identification of indole glucosinolate breakdown products with antifeedant effects on Myzus persicae (green peach aphid). *Plant J.* 54, 1015–1026. doi:10.1111/j.1365-313X.2008.03476.x.

Klepikova, A. V., Kasianov, A. S., Gerasimov, E. S., Logacheva, M. D., and Penin, A. A. (2016). A high resolution map of the Arabidopsis thaliana developmental transcriptome based on RNA-seq profiling. *Plant J.* 88, 1058–1070. doi:10.1111/tpj.13312.

Koevoets, I. T., Venema, J. H., Elzenga, J. T. M., and Testerink, C. (2016). Roots Withstanding their Environment: Exploiting Root System Architecture Responses to Abiotic Stress to Improve Crop Tolerance. *Front. Plant Sci.* 07, 1335. doi:10.3389/fpls.2016.01335.

Korver, R. A., Koevoets, I. T., and Testerink, C. (2018). Out of Shape During Stress: A Key Role for Auxin. *Trends Plant Sci.* 23, 783–793. doi:10.1016/j.tplants.2018.05.011.

Kowalczyk, M., and Sandberg, G. (2001). Quantitative Analysis of Indole-3-Acetic Acid Metabolites in Arabidopsis1. *Plant Physiol.* 127, 1845–1853. doi:10.1104/pp.010525.1.

Kumar, S., and Mahadevan, S. (1963). 3-INDOLEACETALDOXIME HYDRO-LYASE: A PYRIDOXAL-5'-PHOSPHATE ACTIVATED ENZYME. *Arch Biochem Biophys* 103. doi:10.1016/0003-9861(63)90446-6.

**4**

Kurihara, D., Mizuta, Y., Sato, Y., and Higashiyama, T. (2015). ClearSee: A rapid optical clearing reagent for whole-plant fluorescence imaging. *Dev.* 142, 4168–4179. doi:10.1242/dev.127613.

Lamers, J., Der Meer, T. Van, and Testerink, C. (2020). How plants sense and respond to stressful environments. *Plant Physiol.* 182, 1624–1635. doi:10.1104/PP.19.01464.

Lavenus, J., Goh, T., Roberts, I., Guyomarc'h, S., Lucas, M., De Smet, I., et al. (2013). Lateral root development in Arabidopsis: Fifty shades of auxin. *Trends Plant Sci.* 18, 1360–1385. doi:10.1016/j.tplants.2013.04.006.

Lehmann, T., Janowitz, T., Sánchez-Parra, B., Alonso, M.-M. P., Trompetter, I., Piotrowski, M., et al. (2017). Arabidopsis NITRILASE 1 Contributes to the Regulation of Root Growth and Development through Modulation of Auxin Biosynthesis in Seedlings. *Front. Plant Sci.* 8. doi:10.3389/fpls.2017.00036.

Liu, W., Li, R.-J., Han, T.-T., Cai, W., Fu, Z.-W., and Lu, Y.-T. (2015). Salt Stress Reduces Root Meristem Size by Nitric Oxide-Mediated Modulation of Auxin Accumulation and Signaling in Arabidopsis. *Plant Physiol.* 168, 343–356. doi:10.1104/pp.15.00030.

Ljung, K., Hull, A. K., Celenza, J., Yamada, M., Estelle, M., Normanly, J., et al. (2005). Sites and regulation of auxin biosynthesis in Arabidopsis roots. *Plant Cell* 17, 1090–104. doi:10.1105/tpc.104.029272.

Lobet, G., Pagès, L., and Draye, X. (2011). A Novel Image Analysis Toolbox Enabling Quantitative Analysis of Root System Architecture. *Plant Physiol.* 157, 29–39. doi:10.1104/pp.111.179895.

Matosevich, R., Cohen, I., Gil-Yarom, N., Modrego, A., Friedlander-Shani, L., Verna, C., et al. (2020). Local auxin biosynthesis is required for root regeneration after wounding. *Nat. Plants* 6, 1020–1030. doi:10.1038/s41477-020-0737-9.

Mert-Türk, F., Bennett, M. H., Mansfield, J. W., and Holub, E. B. (2003). Camalexin accumulation in Arabidopsis thaliana following abiotic elicitation or inoculation with virulent or avirulent Hyaloperonospora parasitica. *Physiol. Mol. Plant Pathol.* 62, 137–145. doi:10.1016/S0885-5765(03)00047-X.

Mikkelsen, M. D., Hansen, C. H., Wittstock, U., and Halkier, B. A. (2000). Cytochrome P450 CYP79B2 from Arabidopsis catalyzes the conversion of tryptophan to indole-3-acetaldoxime, a precursor of indole glucosinolates and indole-3-acetic acid. *J. Biol. Chem.* 275, 33712–33717. doi:10.1074/jbc.M001667200.

Mikkelsen, M. D., Naur, P., and Halkier, B. A. (2004). Arabidopsis mutants in the C-S lyase of glucosinolate biosynthesis establish a critical role for indole-3-acetaldoxime in auxin homeostasis. *Plant J.* 37, 770–777. doi:10.1111/j.1365-313X.2004.02002.x.

Millet, Y. A., Danna, C. H., Clay, N. K., Songnuan, W., Simon, M. D., Werck-Reichhart, D., et al. (2010). Innate immune responses activated in Arabidopsis roots by microbe-associated molecular patterns. *Plant Cell* 22, 973–990. doi:10.1105/tpc.109.069658.

Mokochinski, J. B., Mazzafera, P., Sawaya, A. C. H. F., Mumm, R., de Vos, R. C. H., and Hall, R. D. (2018). Metabolic responses of Eucalyptus species to different temperature regimes. *J. Integr. Plant Biol.* 60, 397–411. doi:10.1111/jipb.12626.

Müller, T. M., Böttcher, C., Morbitzer, R., Götz, C. C., Lehmann, J., Lahaye, T., et al. (2015). TRANSCRIPTION ACTIVATOR-LIKE EFFECTOR NUCLEASE-Mediated Generation and Metabolic Analysis of Camalexin-Deficient cyp71a12 cyp71a13 Double Knockout Lines. *Plant Physiol.* 168, 849–58. doi:10.1104/pp.15.00481.

Nafisi, M., Goregaoker, S., Botanga, C. J., Glawischnig, E., Olsen, C. E., Halkier, B. A., et al. (2007). Arabidopsis cytochrome P450 monooxygenase 71A13 catalyzes the conversion of indole-3-acetaldoxime in camalexin synthesis. *Plant Cell* 19, 2039–2052. doi:10.1105/tpc.107.051383.

Pang, Q., Chen, S., Li, L., and Yan, X. (2009). Characterization of glucosinolate - Myrosinase system in developing salt cress Thellungiella halophila. *Physiol. Plant.* 136, 1–9. doi:10.1111/j.1399-3054.2009.01211.x.

Schuhegger, R., Nafisi, M., Mansourova, M., Petersen, B. L., Olsen, C. E., Svatoš, A., et al. (2006). CYP71B15 (PAD3) catalyzes the final step in camalexin biosynthesis. *Plant Physiol.* 141, 1248–1254. doi:10.1104/pp.106.082024.

Schuhegger, R., Rauhut, T., and Glawischnig, E. (2007). Regulatory variability of camalexin biosynthesis. *J. Plant Physiol.* 164, 636–644. doi:10.1016/j.jplph.2006.04.012.

Sugawara, S., Hishiyama, S., Jikumaru, Y., Hanada, A., Nishimura, T., Koshiba, T., et al. (2009). Biochemical analyses of indole-3-acetaldoxime-dependent auxin biosynthesis in Arabidopsis. *Proc. Natl. Acad. Sci. U. S. A.* 106, 5430–5435. doi:10.1073/pnas.0811226106.

Vik, D., Mitarai, N., Wulff, N., Halkier, B. A., and Burow, M. (2018). Dynamic Modeling of Indole Glucosinolate Hydrolysis and Its Impact on Auxin Signaling. *Front. Plant Sci.* 9, 1–16. doi:10.3389/fpls.2018.00550.

Vorwerk, S., Biernacki, S., Hillebrand, H., Janzik, I., Müller, A., Weiler, E. W., et al. (2001). Enzymatic characterization of the recombinant Arabidopsis thaliana nitrilase subfamily encoded by the NIT2/NIT1/NIT3-gene cluster. *Planta* 212, 508–516. doi:10.1007/s004250000420.

Vos, R. C. De, Moco, S., Lommen, A., Keurentjes, J. J., Bino, R. J., and Hall, R. D. (2007). Untargeted large-scale plant metabolomics using liqui chromatography coupled to mass spectrometry. *Nat. Protoc.* 2, 778–791.

Voß, U., Wilson, M. H., Kenobi, K., Gould, P. D., Robertson, F. C., Peer, W. A., et al. (2015). The circadian clock rephases during lateral root organ initiation in Arabidopsis thaliana. *Nat. Commun.* 6. doi:10.1038/ncomms8641.

Winter, D., Vinegar, B., Nahal, H., Ammar, R., Wilson, G. V., and Provart, N. J. (2007). An "electronic fluorescent pictograph" Browser for exploring and analyzing large-scale biological data sets. *PLoS One* 2, 1–12. doi:10.1371/journal.pone.0000718.

Xia, J., and Wishart, D. S. (2016). Using MetaboAnalyst 3.0 for Comprehensive Metabolomics Data Analysis. *Curr. Protoc. Bioinforma.* 55, 14.10.1-14.10.91.

Zhao, J., Williams, C. C., and Last, R. L. (1998). Induction of arabidopsis tryptophan pathway enzymes and camalexin by amino acid starvation, oxidative stress, and an abiotic elicitor. *Plant Cell* 10, 359–370. doi:10.1105/tpc.10.3.359.

Zhao, Y., Hull, A. K., Gupta, N. R., Goss, K. A., Alonso, J., Ecker, J. R., et al. (2002). Trp-dependent auxin biosynthesis in Arabidopsis: involvement of cytochrome P450s CYP79B2 and CYP79B3. *Genes Dev.* 16, 3100–3112. doi:10.1101/gad.1035402.5.

4

**CHAPTER 5**

# Natural variation in the promoter of *UGT74E2* affects bolting time of Arabidopsis in response to salt stress

Iko T. Koevoets[1,2], Jessica A. Meyer[1], Suzanne Holleman[2], Christa Testerink[1,2]

[1]Laboratory of Plant Physiology, Wageningen University & Research, 6708PB Wageningen, the Netherlands
[2]Plant Cell Biology, University of Amsterdam, Swammerdam Institute for Life Sciences, 1090GE Amsterdam, the Netherlands

**ABSTRACT**

In their life cycle, plants go through the floral transition, changing from a vegetative to reproductive stage. Periods of drought or salinity of the soil greatly influence this transition, but the mechanisms underlying the impact of abiotic stress on timing of flowering remain largely elusive this far. In this study we investigated natural variation in bolting and flowering time in response to salt stress in 95 accessions of *Arabidopsis thaliana*. Most accessions showed a delay in bolting and flowering time in response to salt, while early bolting was hardly observed. Genome wide association study (GWAS) revealed several loci associated with relative bolting and flowering time upon salt stress. One significant SNP was located in the intergenic region between *UDP-glycosyltransferase 74E2 (UGT74E2)* and *BTB AND TAZ DOMAIN PROTEIN* 3 (*BT3*). This region showed major variation in comparison to Col-0 in accessions in which bolting was delayed, whereas non-delayed accessions showed similar sequences as Col-0. Gene expression of *UGT74E2* was found to be induced by salt stress in Col-0, whereas accessions delayed in bolting by salt stress showed a reduction in *UGT74E2* expression by salt stress. Ectopic overexpression of *UGT74E2* delayed bolting in both control and salt conditions. *UGT74E2* encodes an Indole-3-butyric acid (IBA) glucosyltransferase, conjugating IBA to IBA-glc. Thus, induction of *UGT74E2* might lead to a reduction of IBA as UGT74E2 conjugates it to IBA-glc. In contrast, a reduction of expression in *UGT74E2*, as observed in the delayed accessions, might lead to less conversion of IBA to IBA-glc and thus increased IBA content, probably causing the delay in bolting time. We further investigated the promoter region of *UGT74E2* to identify transcription factors putatively binding the region with sequence variation in delayed accessions. Co-expression analysis, followed by biclustering on hormone and stress treatment, revealed seven transcription factors putatively binding the promoter of *UGT74E2*. All of these transcription factors were described before to be involved in the timing of flowering, water-deficit stress or both. These transcription factors provide a good starting point for further research on *UGT74E2* and its regulatory network, providing more insight in fine-tuning of the floral network under stress.

## INTRODUCTION

During their lives, plants go through different developmental phases. The three main phases are the juvenile vegetative phase, the mature vegetative phase and the reproductive phase (as reviewed in Poethig 1990, Chuck and Hake 2005). In the second transition, called the floral transition, plants start producing reproductive organs. In both nature and agriculture, controlling the moment of transition from one phase to the other can be crucial for yield, reproduction and survival. For example, the length of the growth season restricts the optimal time for a plant to go into floral transition and start reproducing. In plant breeding, focus has long been on developing crops with maximum yield in optimal conditions. However, abiotic stress is increasingly causing problems for food production. For example, over 1 billion ha of land is affected by salinity (Ivushkin et al., 2019), leading to strongly reduced production. Thus, plant breeders need to take into account abiotic stress resilience, when developing new varieties. More knowledge on regulation of phase change and its effects on plant growth will provide opportunities to improve yields (Colasanti and Coneva, 2009; Jung and Müller, 2009).

The timing of flowering under optimal conditions has been extensively studied in the past decades (as reviewed in Kinoshita & Richter, 2020). The endogenous pathway in Arabidopsis is mainly controlled by the shift between two microRNAs: miR156 and miR172 (as reviewed in Huijser & Schmid, 2011; Wang, 2014). In juvenile plants miR156 is present in very high concentrations. miR156 represses different *SQUAMOSA PROMOTER BINDING-LIKE* (*SPL*) transcription factors, which in their turn induce miR172 (Wu et al., 2009). During aging, miR156 decreases in concentration, allowing the concentration of miR172 to increase. miR172 and the SPLs activate both the vegetative and the floral transition.

Although the endogenous pathway is key in regulating developmental transitions, plants need to adapt to the environmental circumstances to ensure reproduction in a changing environment. For most plant species, including Arabidopsis, the photoperiodic pathway is a key regulator of the timing of flowering. This pathway is regulated by daylength and ensures the plant flowers during the right time of year. The key players of this pathway are CONSTANS (CO), GIGANTEA (GI) and FLOWERING LOCUS T (FT). GI is part of the circadian clock regulatory network and together with other clock genes it regulates *CO* transcription (Sawa et al., 2007). CO binds the promoter of *FT*, leading to increased expression (Adrian et al., 2010; Samach et al., 2000). FT then travels from the leaf to the meristem, where it interacts with other proteins to initiate floral transition (Jaeger and Wigge, 2007).

Increasingly, studies show that other external cues, including abiotic stress, play a major role in regulating timing of floral transition (as reviewed in Cho, Yoon, & An, 2017; Kazan & Lyons, 2016). When exposed to abiotic stress plants follow one of two strategies: (1) flowering early to ensure reproduction, with the disadvantage of not reaching maximum yield or (2) flowering late to ensure maximum yield but with the risk of not surviving the stress. GI plays a major role in integrating most stress effects into the pathway regulating the timing of flowering (as reviewed in Kazan and

Lyons, 2016b). Under water deficit conditions, plants are known to exhibit a so-called "drought escape response" (DE response), by accelerating the floral transition before drought endangers survival. The DE response is enabled by a GI-facilitated increase in expression of *FT* (Riboni et al., 2013, 2016).

Interestingly, salt stress generally has the opposite effect, delaying bolting and flowering time in several plant species including Arabidopsis (Li et al., 2007). Although only a limited number of studies has focused on the effect of salt stress on the floral transition, previous studies have shown that salt stress affects several components in the flowering pathway. High salinity affects the key regulating GI-CO-FT module by degrading GI, leading to reduced CO activity and thus lower *FT* activation (Kim et al., 2013). In addition, the transcription factor NAC WITH TRANSMEMBRANE MOTIF 1-LIKE 8 (NTL8) dissociates from the membrane during salt stress, moves to the nucleus and inhibits expression of *FT* (Kim et al., 2007; Kim and Park, 2007). More downstream, *BROTHER OF FT AND TFL1* (*BFT*) is strongly induced by salt stress (Ryu et al., 2011). BFT binds to FD, preventing FT-FD interaction, which is crucial for activation of the floral transition in the meristem (Ryu et al., 2014). Yet, our understanding of the molecular mechanism underlying the effect of salinity on timing of flowering is far from complete.

Genomic screens using available genetic variation in natural populations has shown to deliver many loci with the potential of breeding more resilient crops (Huang and Han, 2014). Genome Wide Association Study (GWAS) is a method exploiting natural variation in a population by correlating the phenotypic differences to the genotypic differences (as reviewed in Korte & Ashley, 2013). Due to its high heritability, flowering time is a particularly well suited trait for genotype-phenotype correlations and many flowering genes have been mapped through either QTL or GWAS (as reviewed in Ehrenreich et al., 2009).

Here, natural variation in accessions of *Arabidopsis* has been exploited to find new candidate genes involved in regulation of flowering time in response to salt stress. First, bolting and flowering time with and without salt stress was measured for 95 Arabidopsis that are part of the HapMap collection (Weigel and Mott, 2009) and for which the sequence of 250k SNPs are available. Next, through GWAS mapping we set out to find loci that explain part of the variation between these accessions. These loci can provide more knowledge on the molecular mechanisms behind timing of flowering during salt stress and are possible targets for further plant breeding. One identified locus, associated with the effect of salt stress on bolting time, contains large natural variation in the promoter region of *UDP-glycosyltransferase 74E2* (*UGT74E2).* This variation correlates with induction of expression of *UGT74E2* by salt stress in a set of accessions and provides a promising starting point to identify upstream transcription factors involved in timing of flowering under salinity stress.

## RESULTS

*Natural Variation in flowering time in response to salt stress*

To investigate natural variation in the timing of flowering in response to salt stress, 120 Arabidopsis accessions were grown in salt or control treatment and flowering traits were recorded. From these accessions, 95 accessions flowered within the time frame of the experiment in both control and salt stress (see Supplemental table 1). Further analysis was based on these accessions only. Natural variation in the following flowering traits were recorded: bolting time (day inflorescence reaches 1cm), flowering time (day of first open flower) and the number of rosette leaves when flowering (Figure 1). Accessions bolted between 19 to 33 days after germination. For most accessions, bolting time was either not affected or delayed by salt stress, with a variation of the average response to salt between 0.95 and 1.2. Flowering was observed between day 22 and day 35 after germination. The variation in flowering time response to salt stress was smaller and ranged from 0.9 to 1.1. Both bolting and flowering time displayed a normal distribution in terms of response to salt stress. Accessions varied widely in the number of rosette leaves when flowering, ranging from 5 to 21 leaves on average. Across accessions, both decreases and increases in number of leaves were found as a response to salt, showing a wide variation in response between 0.8 and 1.2, while the variation within accessions was also larger for this trait. For all three traits, Col-0, the reference accession, did not display a significant effect of salt stress in our growth conditions.

To confirm our results, six early-bolting accessions, six relatively delayed accessions and four accessions that were not affected by salt were selected for repetition with an increased number of replicates (Supplemental figure 1). All six delayed accessions in the GWAS screen were confirmed to be significantly delayed in bolting time by salt stress in our repetition. For three of these, salt stress also significantly delayed flowering time and increased the number of rosette leaves at flowering time. None of the early-bolting accessions in the GWAS screen were significantly earlier in bolting time or showed a decrease in the number of leaves by salt stress in our repetition, though No-0 did show significantly early flowering in salt stress. Surprisingly, Rak-2 showed a significant delay in flowering time in response to salt stress, while it was recorded to be early flowering in response to salt stress in our GWAS screen. This could be due to an effect of different light conditions, as the GWAS screening (Sep-Oct) and the repetition (Apr-May) experiments were done at different times of the year in the greenhouse.

Although for all traits correlations between control and salt are very strong (r=0.91-0.93), the relative response to salt stress in bolting or flowering time does not correlate with control bolting or flowering time (r=0.14 and r=0.048, respectively), indicating that the effect of salt stress on flowering time in a particular accession is independent of its flowering time under control condition. A weak, but significant, negative correlation (r=-0.44) between the number of leaves under control and the relative response to salt stress was observed. All three traits are strongly correlated with each other, except for the number of leaves in relative response to salt, which shows no correlations to the ratio of bolting or flowering time. All correlations are displayed in Supplemental table 2.
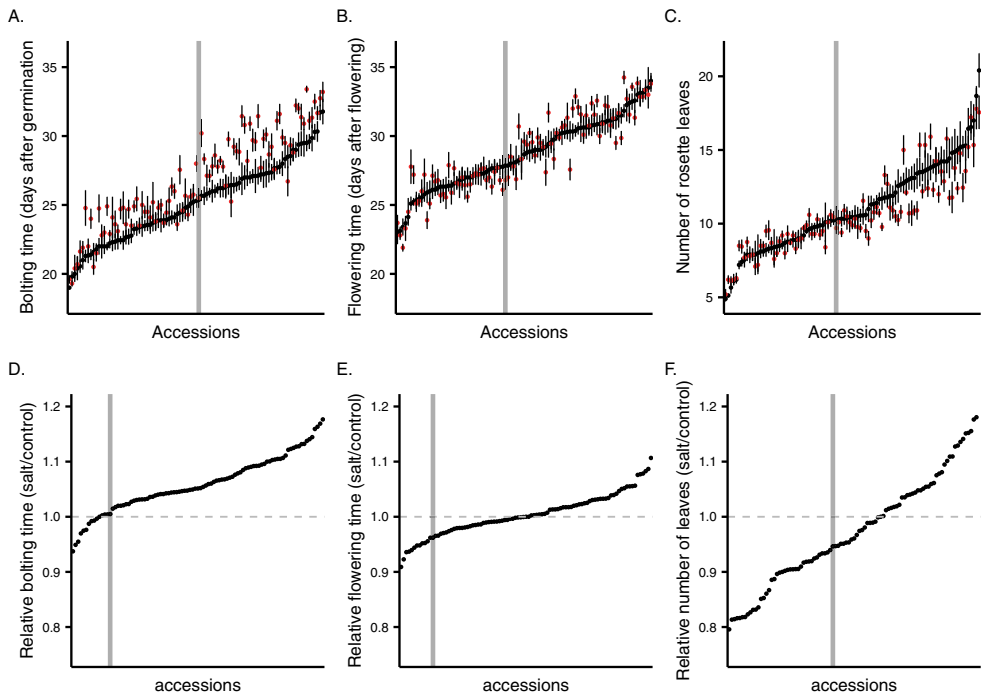
**Figure 1. Natural variation in flowering traits in 95 accessions of Arabidopsis thaliana.** The average day of bolting (**A**), flowering (**B**) and number of rosette leaves (**C**) for both control (black) and salt (red). Accessions are ordered based on their control value. Error bars display SE of the mean (n=5-10). The response to salt for each trait (**D-F**) is shown as the ratio between salt and control (salt/control). The values are ordered from low to high response. The dotted line displays a response of 1, which equals no change in response to salt stress. Col-0 is annotated with a shaded bar.

## GWAS reveals several loci explaining natural variation in bolting and flowering time in response to salt stress

To identify candidate loci explaining natural variation in bolting and flowering time in response to salt stress, the average of each trait for control, salt and response (ratio) was used for GWAS analysis. Pseudoheritability for both bolting and flowering time traits was very high, with all three bolting traits displaying a pseudoheritability of 1 (Supplemental table 3). As the number of rosette leaves displayed a very low pseudoheritability between 0 and 0.06, we decided to focus our GWAS analysis on bolting and flowering time.
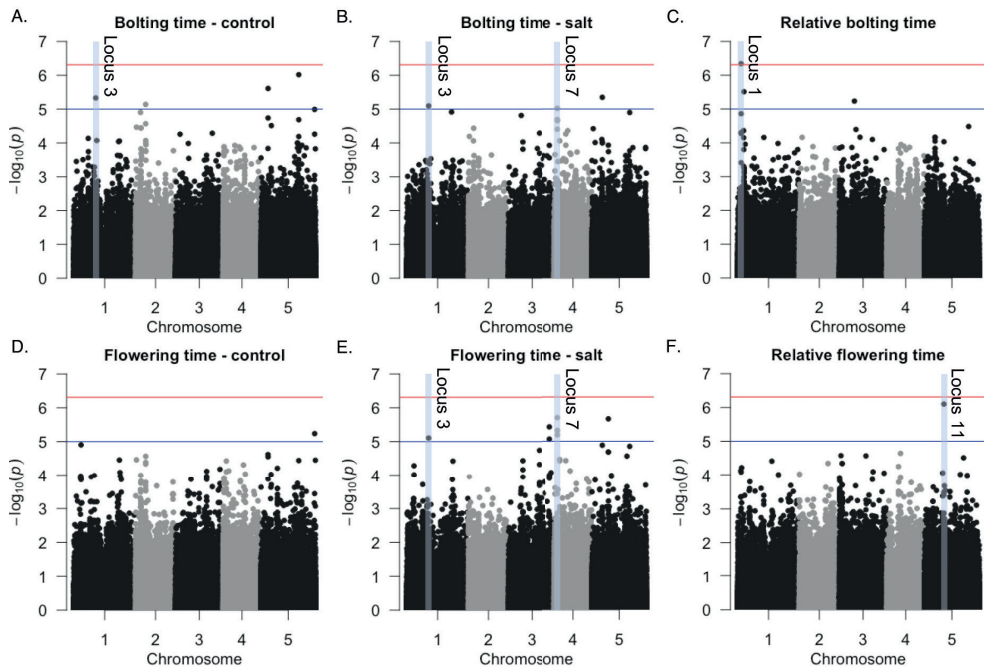
**Figure 2. Manhattan plots of bolting time (A-C) and flowering time (D-F) in control and salt and the relative response.** Each plot shows the LOD score of each SNP in the 250k database on the 5 chromosomes of Arabidopsis thaliana. All loci above the arbitrary threshold of LOD=5.0 (blue line) have been annotated in supplemental table 4. Locus 1, 3, 7 and 11 have been highlighted in blue. Locus 1 is the only SNP above the Bonferroni-corrected threshold p<0.1 indicated by the red line.

In total, 16 SNPs, located in 13 genomic loci, with a LOD score above 5.0, were identified (Figure 2). Loci 3 and 7 are the only SNPs mapped for multiple traits. The significant SNPs in both loci 3 and 7 are in linkage disequilibrium (LD) with a number of other SNPs in a larger area. Locus 3 was mapped on day of bolting in both control and salt conditions as well as on day of flowering in salt. Locus 3 contains a significant SNP in the *SIT4* gene coding for a phosphatase-associated family protein (chromosome 1, position 10784793). This SNP is in LD with 6 other SNPs in a region of approximately 30kb. Locus 7 was mapped to be associated with both day of bolting and flowering in salt conditions Locus 7 contains three significant SNPs, of which one is located in an exon and the other two in an intron of *CASP-LIKE PROTEIN 1C1* (*CASPL1C1*; AT4G03540). These three SNPs are in LD with up to 16 additional SNPs in a region of approximately 40kb.

Only two loci were mapped for the relative response to salt stress: locus 1 and locus 11. Locus 11, associated with relative flowering time, contains a significant SNP located in the intergenic region between *Na$^+$/H$^+$ EXCHANGER 1* (*NHX1*; AT5G27150) and AT5G27170. This SNP is in LD with two other SNPs, of which one is also located in this intergenic region and the other is located in the exon of AT5G27280, 40kb downstream of the significant SNP. NHX1 is part of the protein family of vacuolar Na$^+$/

H$^+$ antiporters (NHX1-4) that are important for maintaining cellular pH and Na$^+$ and K$^+$ homeostasis (Bassil et al., 2011).

Although above loci are potentially interesting, applying a strict Bonferroni threshold (p<0.1), only one significant SNP, in Locus 1 (Chromosome 1, position 1706467), remained. This SNP was mapped for relative bolting time (Figure 2C) and is located in the intergenic region between *UDP-glycosyltransferase 74E2* (*UGT74E2;* AT1G05680) and *BTB AND TAZ DOMAIN PROTEIN 3* (*BT3*; AT1G05690). Six other SNPS are in LD with this SNP, one of which is located in an exon of *UGT74E2*, two are located in the 5'UTR of *BT3* and three are located in the intergenic region. *UGT74E2* encodes an Indole-3-butyric acid (IBA) glucosyltransferase, which conjugates IBA to IBA-glc (Tognetti et al., 2010). BT3 is a scaffold protein acting functionally redundant with BT1 and BT2 in male and female gamete development (Robert et al., 2009). As locus 1 showed the highest LOD score (6.34), above the Bonferroni-corrected threshold, and was mapped with the trait relative bolting time in response to salt stress, this locus was selected for further characterization.
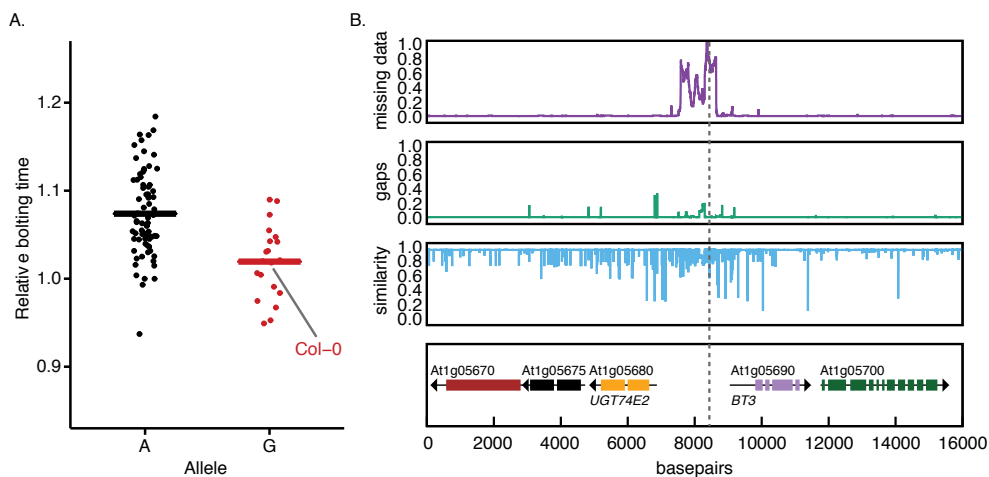


**Figure 3. The intergenic region between UGT74E2 and BT3 contains major missing data and a prominent gap in 20 percent of sequenced accessions.** (**A**) The relative bolting time (ratio salt/control) of accessions with either an A (black) or a G (red) at the position of the significant SNP in locus 1 (Chromosome 1, position 1706467) as observed in the GWAS screen. The horizontal line represents the average of all accessions containing an A (black) or a G (red) on this position. (**B**) Genetic variation in locus 1 containing *UGT74E2* and *BT3* was studied in all sequenced accessions in the 1001 genome database. From top to bottom the graphs represent the portion of accessions containing missing data, gaps and similarity to Col-0 respectively. The data is aligned with the genes as shown in the lowest panel. The location of the significantly associated SNP is indicated with a dashed line.
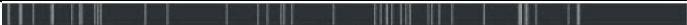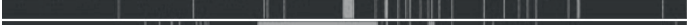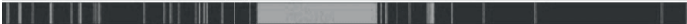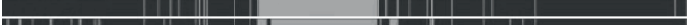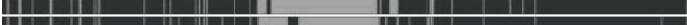
*Accessions showing a large delay in bolting time under salt stress show a 1000 bp region of high variation in the intergenic region between UGT74E2 and BT3*

Twenty accessions, including Col-0, contain a G in the position of the significant SNP on locus 1 and 75 accessions contain an A. The average relative bolting time of accessions containing the A allele is 1.07 (delayed in salt), whereas the average for the G allele accessions is 1.01 (no change; Figure 3A). Only two accessions containing the A allele showed a relative bolting time below 1 (MIB-28 and Kelsterbach-2), while all others (97,5%) showed a relative bolting time above 1. In contrast, 30 percent of the G allele accessions were observed to have a relative bolting time below 1 and none had a relative bolting time above 1.1.

To further determine genetic variation in Locus 1, the 1001 genome database (Weigel and Mott, 2009) was utilized to compare the available sequences of *Arabidopsis* accessions approximately 8000bp up and down of the associated SNP (Figure 3B). While most regions contain little variation, both the *UGT74E2* genetic region and the intergenic region between *UGT74E2* and *BT3*, show low similarity. In the intergenic region, a large amount of missing data was observed in an area of approximately 1000 base pairs (Figure 3B, top panel), which can be due to high variation, high number of repeats or the presence of gaps. In addition, in this same region, roughly 20 percent of accessions contained a gap of approximately 200 base pairs (Figure 3B, second panel). The associated SNP is located on the edge of this gap and in the middle of the region of missing data.

Next, among the 15 accessions with the lowest and highest relative bolting time, those that were sequenced were checked for presence of high variation, a gap or missing data in this area (Table 1). As shown before, all strongly delayed accessions have the A allele and all but one of these (Ler-1) showed missing data or major variation in this region. In contrast, only one accession that was not delayed by salt stress (Ct-1) showed a gap or major variation in this region. Interestingly, Ct-1 also has the A allele, which might indicate that the associated SNP is strongly linked to the region of high variation. As this region is located in the promoter region of both *UGT74E2* and *BT3*, this region would likely affect gene expression of one or both genes.

5

**Table 1. Most accessions delayed in bolting time show a large region of variation in the intergenic region between *UGT74E2* and *BT3*.** The sequence of the intergenic region between *UGT74E2* and *BT3* of 15 accessions either delayed or non-delayed by salt stress in bolting time are displayed, in combination with their relative bolting time and the allele for the significant SNP (S) in locus 1. The variation is shown in comparison to Col-0, black areas are similar and grey areas are dissimilar. Grey areas can be caused by SNPs, deletion, insertions or missing data. Sequences are retrieved from the 1001 genome browser project (Weigel and Mott, 2009).

| Accession | Relative bolting time | SNP | Sequence |
|---|---|---|---|
| *Reference accession Col-0* | | | |
| Col-0 | 1.02 | G | |
| *Accessions not delayed by salt stress* | | | |
| No-0 | 0.95 | G | |
| Rak-2 | 0.95 | G | |
| Or-0 | 0.97 | G | |
| Ca-0 | 0.98 | G | |
| Mz-0 | 0.99 | G | |
| Li-7 | 1.00 | A | |
| Nd-1 | 1.00 | G | |
| Ct-1 | 1.02 | A | |
| *Accessions most delayed by salt stress* | | | |
| Kro-0 | 1.12 | A | |
| Oy-0 | 1.12 | A | |
| Lip-0 | 1.13 | A | |
| Boot-1 | 1.13 | A | |
| Hn-0 | 1.14 | A | |
| HR-5 | 1.14 | A | |
| Gie-0 | 1.16 | A | |
| Hs-0 | 1.16 | A | |
| Hovdala-2 | 1.16 | A | |
| Mnz-0 | 1.17 | A | |
| Ler-1 | 1.18 | A | |

*Presence of a 1000bp region of variation in the intergenic region between UGT74E2 and BT3 is related to induction of UGT74E2 expression upon salt stress*

As major variation in the intergenic region between *UGT74E2* and *BT3* is found, we further investigated the effect of salt stress on gene expression of *UGT74E2* and *BT3*. In the publicly available microarray AtGenExpress global stress dataset (Kilian et al., 2007), *UGT74E2* is induced by salt in both roots and shoots of Col-0, although in shoots this induction is observed only after 12 hours of treatment (Supplemental figure 2A). In our conditions, *UGT74E2* was upregulated in 2-week-old seedlings after 7 days of salt treatment (Figure 4), but not earlier or later (11 or 17 days; 4- or 10-days salt treatment, respectively). In contrast, *BT3* is not affected in expression by salt stress based on public data (Supplemental figure 2B), which was confirmed in our conditions (figure 4). No difference between *UGT74E2* expression in control or salt stressed plants was observed after transition to flowering (supplemental figure 3) in either leaf or meristem.
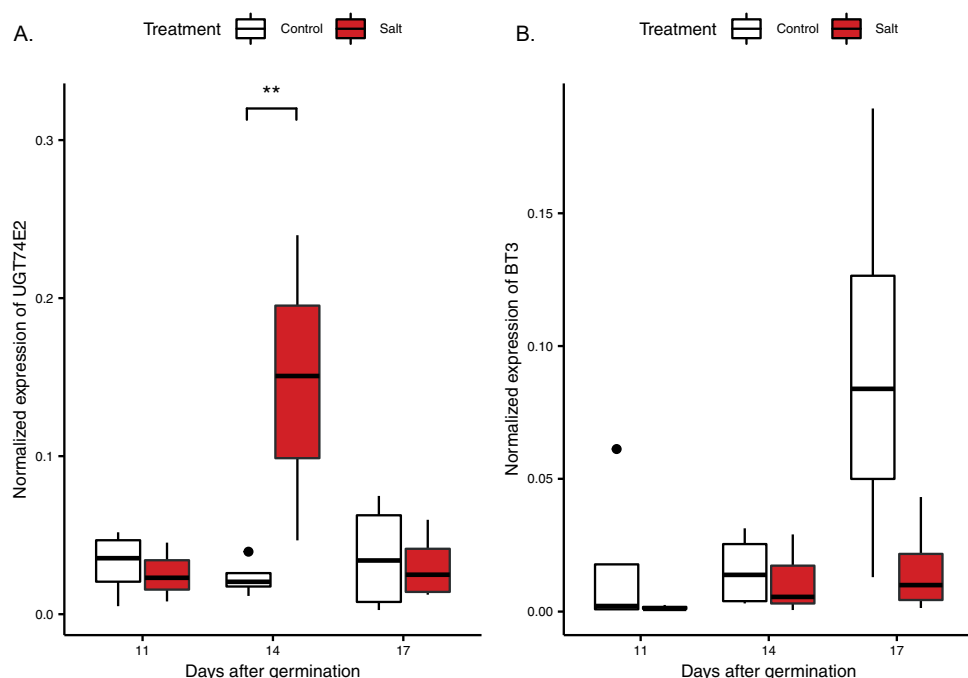
**Figure 4. *UGT74E2* expression is upregulated in salt stress 14 days after germination.** 11- and 14-day old Col-0 seedlings grown in soil, treated with control (white) or salt (red) from day 7, were harvested and analyzed with qPCR for *UGT74E2*, *BT3* and reference gene *at2G28390* expression. Boxplots show gene expression of *UGT74E2* (**A**) and *BT3* (**B**) normalized for expression of the reference gene. The middle line inside the box represents the median (n=4). Lower and upper box boundaries represent 25th and 75th percentiles. Lower and upper error lines represent 10th and 90th percentiles. Dots represent data falling outside 10th and 90th percentiles. Significant differences were determined by a two-way ANOVA. A significant effect of the interaction between the day and the treatment was found for *UGT74E2*, no significant differences were found for *BT3*. Asterisks indicate a significant difference following a manual contrast post-hoc comparison within days (* $p<0.05$, ** $p<0.01$, *** $p<0.001$).

Next, *UGT74E2* expression was measured in the previously selected accessions based on bolting time and the presence of variation in the intergenic region (Table 1). Interestingly, a significant difference was found in the relative expression in response to salt stress in delayed accessions in comparison to non-delayed accessions (Figure 5). Most accessions that are delayed in bolting time upon salt stress showed a relative decrease in expression of *UGT74E2*. Conversely, for most accessions showing no delay in bolting time upon salt stress, no change or an induction of *UGT74E2* expression was found. The presence of variation in the intergenic region of *UGT74E2* and *BT3* also clearly correlates to delay in bolting time and thus might explain this difference in induction of expression by salt stress.

5
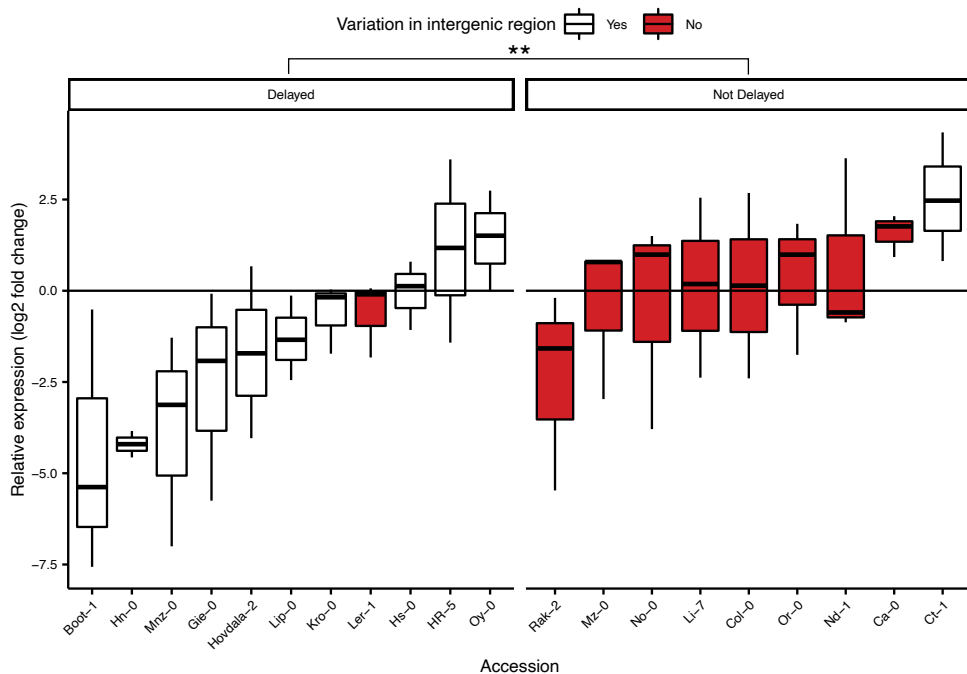
**Figure 5. Relative expression of *UGT74E2* in response to salt stress is reduced in most accessions observed to be delayed in bolting time.** 14-day old Arabidopsis seedlings of selected accessions (figure 3), treated with control or salt stress from day 7, were harvested and analyzed with qPCR for *UGT74E2* and reference gene *at2G28390* expression. *UGT74E2* expression was normalized for reference gene expression. Boxplots show relative expression of *UGT74E2* in response to salt stress (log2 fold change). Presence of variation in the intergenic region between *UGT74E2* and *BT3* is indicated in white (present) or red (not present). The middle line inside the box represents the median (n=3). Lower and upper box boundaries represent 25th and 75th percentiles. Lower and upper error lines represent 10th and 90th percentiles. Dots represent data falling outside 10th and 90th percentiles. Asterisks indicate a significant difference following a two-way ANOVA (* $p<0.05$, ** $p<0.01$, *** $p<0.001$).

## *Overexpression of UGT74E2 leads to delayed flowering*

To further determine the effect of *UGT74E2* expression on bolting and flowering time, we phenotyped two knock-out mutants and two over-expression lines (Supplemental figure 4). The knock-out lines did not show an effect on bolting or flowering time in either control or salt stress conditions, which could be due to low levels of expression of *UGT74E2* in wildtype Col-0 (Supplemental figure 5). On the other hand, constitutive ectopic overexpression of *UGT74E2* led to a consistent delay in bolting and flowering time in both control and salt stress (figure 6A). This effect was consistent over several experiments, also when first growing the plants in 12/12-hour light conditions to synchronize growth to prevent effects of germination speed or possible early floral transition before salt treatment (figure 6B).
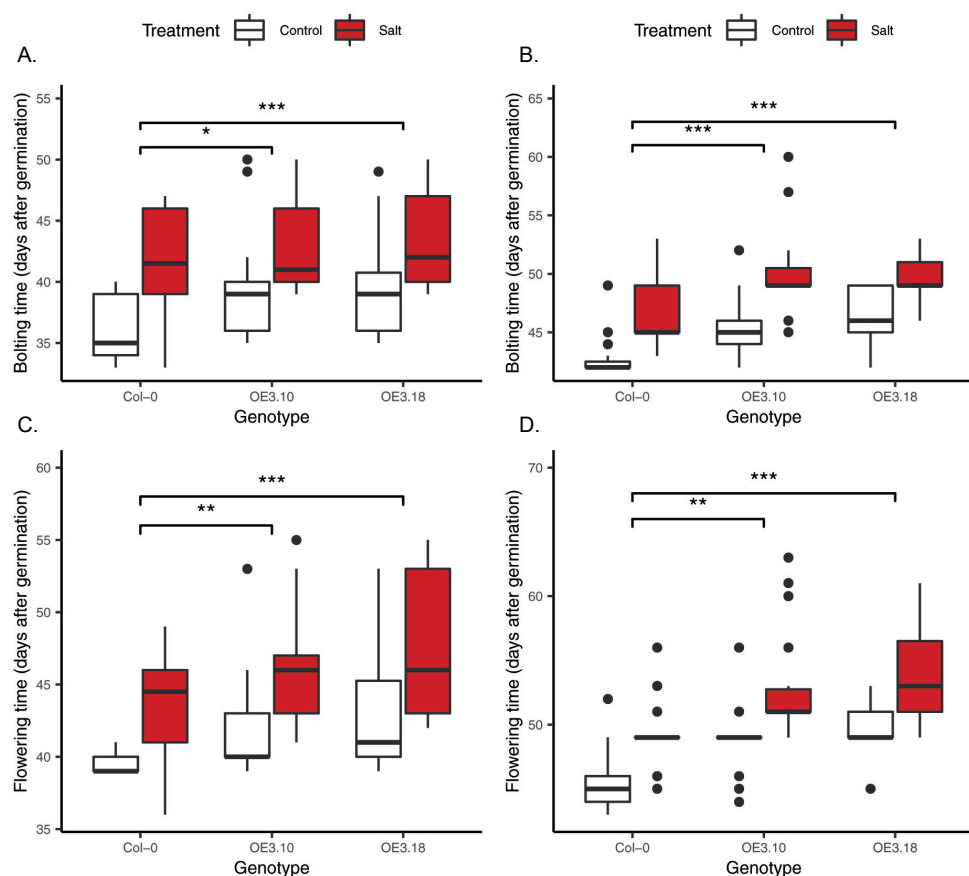
**Figure 6. *UGT74E2* ectopic over-expression lines are delayed in both bolting and flowering time independent of treatment.** Bolting and flowering time during control (white) and salt treatment (red) in Col-0 and *UGT74E2* over-expression lines OE3.10 and OE13.8 were measured in long day (**A**) or pre-treatment of 12/12 hours for 3 weeks followed by transfer to long day conditions (**B**). The middle line inside the box represents the median (n=23). Lower and upper box boundaries represent 25th and 75th percentiles. Lower and upper error lines represent 10th and 90th percentiles. Dots represent data falling outside 10th and 90th percentiles. A significant effect of both treatment and genotype was determined by a linear mixed model, with random factor of tray, genotypes did not respond differently to the treatment. Genotypes were compared using pairwise post-hoc Tukey tests, significant differences are indicated with asterisks (* < 0.05, ** <0.01, ***<0.001).

### Promoter analysis predicts a number of candidate transcription factors in regulation of *UGT74E2* expression during salt stress

As variation in the intergenic region between *UGT74E2* and *BT3* seems to be linked to altered gene expression upon salt stress, we further investigated this region for transcription factor binding sites using PlantPAN (PlantPAN.itps.ncku.edu.tw). In this specific region putative binding sites for 1025 transcription factors were found. Next, relevant candidate transcription factors were selected based on co-expression with *UGT74E2* (Supplemental table 5). Only few (6) transcription factors putatively binding the selected region showed coexpression with *UGT74E2* during environmental stress

(including salt, drought, wounding, heat and oxidative stress) or developmental stages (including seeds, shoots before and after floral transition and different stages of flowers). The correlation in expression, although significant, was also relatively weak (PCC values below 0.7). On the other hand, many transcription factors putatively binding the region of variation in the promoter of *UGT74E2* were coexpressed in samples exposed to hormone treatment (including abscisic acid, gibberelin, auxin, brassinosteroids and jasmonic acid). In total, 106 transcription factors putatively binding the selected region were coexpressed under these treatments and 45 of these showed a strong correlation coefficient of 0.9 or higher.
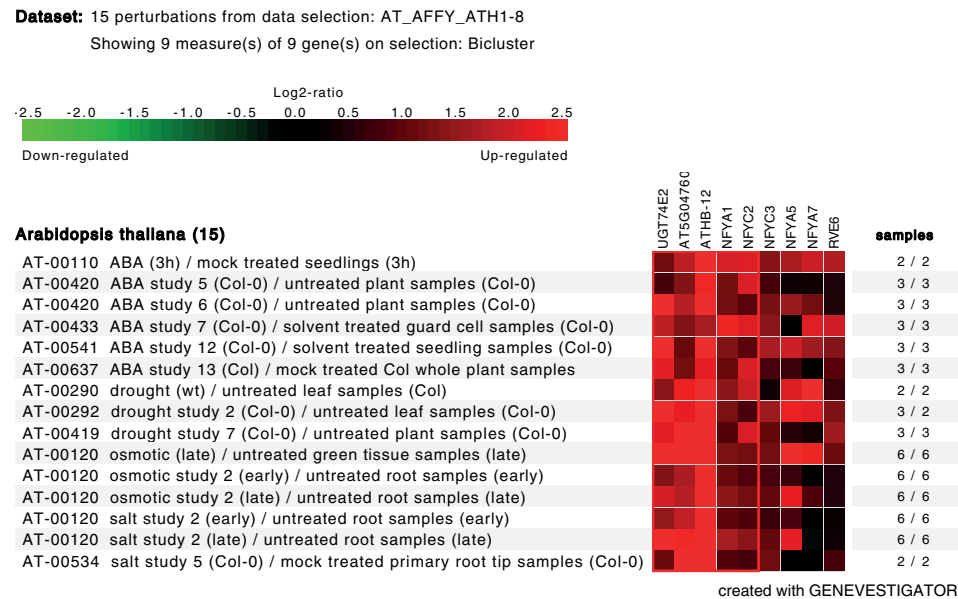


**Figure 7. *UGT74E2* forms a cluster with 8 transcription factors putatively binding the region of variation in its promoter, based on expression in stress conditions.** All transcription factors with a putative binding site in the region of variation in the promoter of *UGT74E2*, coexpressed with *UGT74E2* in one of the datasets on plantPAN were compared for stress induced expression in GENEVESTIGATOR (Zimmermann et al., 2004).

As these transcription factors were found coexpressed either in different stresses, hormonal treatments or developmental stages, we performed a further selection based on bicluster analysis in GENEVESTIGATOR (Zimmermann et al., 2004). All 112 transcription factors found in the coexpression analysis (Supplemental table 5) were compared for induction of expression under hormonal and stress treatment. A bicluster is a set of genes with an almost identical expression for a group of treatments. Biclusters do not have to be similar in other conditions, thereby distinguishing from more regular coexpression analysis. Eight biclusters that contained *UGT74E2* and a minimum of 4 additional genes for at least 10 treatments were identified. In total, eight transcription factors clustered with UGT74E2 in one of these biclusters: AT5G04760 (*EPCR2*),

*ARABIDOPSIS THALIANA HOMEOBOX 12* (*ATHB-12*), *NUCLEAR FACTOR Y SUBUNIT A1* (*NFYA1 / HAP2A*), *C2* (*NFYC2*), *C3* (*NFYC3*), *A5* (*NFYA5*), *A7* (*NFYA*) and *REVEILLE 6* (*RVE6*). Interestingly, all of these genes showed upregulation in response to ABA, drought, osmotic and salt treatment in both root and shoot (figure 7). Four of these transcription factors showed biclustering on all 15 treatments (AT5G05760, *ATHB-12*, *NFYA1*, *NFYC3*; figure 7), whereas the other four showed clustering for a selection of these 15 treatments.

## DISCUSSION

GWAS presents a powerful approach for identification of new starting points for research and breeding targets (Examples discussed in Challa and Neelapu, 2018). In this study, we used GWAS for finding new candidate loci influencing the effect of salt stress on the timing of bolting and flowering in Arabidopsis. We have used a limited set of 95 accessions, selected specifically for flowering without vernalization. This selection does limit the statistical power compared to the full HapMap set and the genetic variation is probably skewed as vernalization requirements likely reflect adaptation to climatic variables including latitude (Bloomer and Dean, 2017; Stinchcombe et al., 2004). Even so, a number of interesting loci were identified and one clear candidate gene, *UGT74E2*, identified as being involved in regulating the effect of salt stress on the floral transition.

Our natural variation data shows large variation between accessions in the timing of bolting and flowering time in both control and salt stress. Interestingly, almost all accessions show either no effect or a delay in bolting time upon salt stress (figure 1D) and repetition of some of the early flowering accessions only showed one accession (No-0) to flower significantly early under salt stress compared to control conditions. This indicates that in Arabidopsis early flowering upon exposure to salt stress is a rare response, at least in the collection used. Both bolting and flowering time display very high pseudoheritability. Although a calculated pseudoheritability of 1.0 seems unlikely, it is known that flowering traits are highly heritable, and the heritability is probably close to 1. Previous studies have indeed shown similar heritability values for flowering time (Li et al., 2010; Sasaki et al., 2015; Seren et al., 2012). Unfortunately, the number of rosette leaves at time of flowering showed very low or even no pseudoheritability, likely caused by high variation within accessions. As several accessions display a different rosette structure or start branching quite early, scoring the number of leaves can be complex and technical errors might explain the variation within accessions observed in this study.

SNPs mapped for the response of bolting or flowering time to salt stress were not mapped for other traits. This is in agreement with the low or absent correlation between the response to salt stress and other traits. Two loci did map to several traits: locus 3, mapped on day of bolting in both control and salt conditions and on day of flowering in salt, and locus 7, mapped on day of bolting and flowering in salt conditions. Both loci contain a number of SNPs in LD in a large region of 30 to 40kb. In addition, also locus 11 contains SNPs in LD in a large region of 40kb. Often, defining one gene

responsible for the phenotypic variation explained by such a large area is not possible. Interestingly, locus 3 was mapped before in a GWAS on proline accumulation during drought stress (Verslues et al., 2014). Proline is not only involved in drought and salt tolerance, but accumulation of proline also affects floral transition and embryo development (as reviewed in Trovato, Forlani, Signorelli, & Funck, 2019). The locus 3 SNP was only present in 11 of our 95 accessions and screening a higher number of accessions might increase the strength of the observed correlation. Verslues et al. (2014) however, did not find an effect of individual knock-out mutants of genes in the locus on proline accumulation. This result illustrates an interesting problem presented by the most common strategy of narrowing the selection of candidate genes following GWAS: screening knock-out mutants. GWAS identifies regions of genetic variation correlating with, and possibly explaining phenotypic variation. This genetic variation does not have to lead to a non-functional gene. Alternatively, differences in gene expression, for example localization or induction by stress, could explain the found phenotypic variation. In addition, Col-0 is used as the reference accession and most knock-out mutants are in Col-0 background. However, if Col-0 has low expression of the genes involved in the phenotypic response, knock-out mutants are not expected to show severe phenotypes. Last, several genes in a locus could together influence phenotypic variation, or genetic redundancy might occur with homologs at other genomic locations and as a consequence knock-out mutants in a single gene might not affect a phenotype severely enough to be observed. Nonetheless, this locus being mapped both in Verslues et al. (2014) and in our study shows that natural variation in this region might influence plant responses to salt and drought stress.

To find genes involved in regulating changes in the floral transition caused by salt stress, we next investigated the loci identified for relative bolting and flowering time: locus 1 and 11. Locus 11 was mapped for the trait relative flowering time and was especially of interest as it contained the gene coding for the ion transporter NHX1. NHX1 plays a role in many plant processes including cell expansion, flower development and seedling establishment, especially under stresses influencing the ion homeostasis under salt stress (Apse et al., 2003; Bassil et al., 2011). Previously, *nhx1nhx2* mutants were shown to be affected in growth and flower development and addition of sodium positively influenced their growth (Bassil et al., 2011). For future research, it would be interesting to further investigate how ion homeostasis, facilitated by NHX1 and possibly other NHX proteins, could influence the floral transition.

In this study, we further focused on locus 1, as it was mapped on relative bolting time, a better indicator for the timing of floral transition then flowering time, and also contained the only SNP with a LOD score above the Bonferroni threshold (LOD score = 6.34). Locus 1 contains a number of SNPs in LD with this significant SNP, which are located in the intergenic region of *UGT74E2* and *BT3*, or in the genetic region of these genes. Further investigation of natural variation in this locus (figure 3) showed a region of about 1000bp containing high variation and this variation was linked to the significant SNP. Accessions delayed for flowering in salt stress generally showed high variation in this region (Table 1). The affected region is located in the predicted promoters of both

*UGT74E2* and *BT3*, strongly indicating that expression of one or both of the genes would influence bolting time in response to salt stress.

*UGT74E2* expression was upregulated by salt stress (figure 4), confirming publicly available microarray data (supplemental figure 2). As *BT3* did not show upregulation in either root or shoot (figure 4; supplemental figure 2), we further focused on *UGT74E2*. Interestingly, our data indicates that the timing of upregulation of *UGT74E2* in Col-0 is quite specific, as this change in expression is not visible in younger (11 days after germination, 4 days of treatment) or older plants (flowering plants, 7- weeks old). We suggest that this timing is coinciding with the moment plants approach floral transition, thereby possibly influencing the transition, but a more detailed timeseries would be required to address this.

UGT74E2 is an IBA glucosyltransferase and overexpression of the gene has shown to increase IBA, IBA-glc and several IAA conjugation and degradation products. External application of IBA or IBA-glc was shown to severely delay bolting time in control conditions with approximately 50 days (Tognetti et al., 2010). In agreement, overexpression of *UGT74E2* delayed bolting time with approximately 7 days. This is consistent with our results (figure 6), showing a similar delay in bolting time of the OE line in comparison to wildtype, independent of stress. Based on these results, we hypothesize that upon exposure to salt stress an increase in *UGT74E2* expression would lead to increased levels of IBA, delaying the floral transition. Accessions displaying a strong delay in bolting time by salt stress in the GWAS screen, containing large variation in the promoter, would therefore be expected to show stronger upregulation of *UGT74E2*, leading to a delay in flowering time. However, these delayed accessions showed the opposite; a decrease in expression upon exposure to salt stress (Figure 5). Predicting the effect of changes in gene expression on the metabolome is quite challenging. Although constitutive ectopic overexpression increases both IBA and IBA-glc levels in seedlings, short-term induction of *UGT74E2* could actually lead to a reduction in IBA, influencing a delay in flowering time (figure 8). Induction of *UGT74E2* expression as observed in for example Col-0 might actually lead to a reduction in IBA, preventing a delay in bolting, as was observed for Col-0 in our GWAS screen. So, accessions showing a reduction of *UGT74E2* expression, would have less conversion of IBA to IBA-glc and might actually have temporarily higher levels of IBA, delaying bolting. Thus, our results suggest that in contrast to the ectopic overexpression studies, natural repression of *UGT74E2,* probably leading to an increase in IBA, is important for a salt induced delay in bolting time in the "late" accessions.

In future research, measurements of IBA and derived metabolites will be useful to further address the role of UGT and its substrates and products in timing of flowering, although the timing of these measurements can be of much influence. As these accessions are not all bolting around the same time in control conditions, the timing of changes in *UGT74E2* expression might also be different. On the other hand, no correlation was found between control bolting time and relative bolting time (Supplemental table 2), so accessions delayed in bolting time by salt stress show the same variation in control

5

bolting time as accessions that are not delayed. The observed reduction in expression in delayed accessions seems to be independent of their flowering time in control.
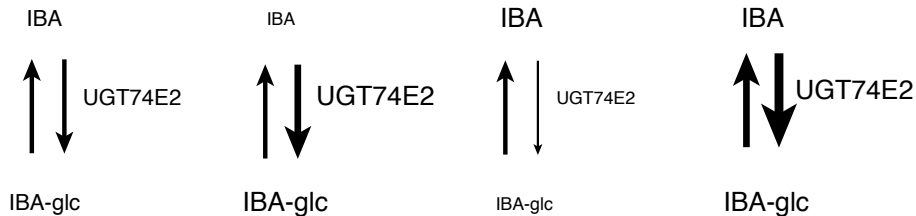


**Figure 8.** Hypothetical model of the influence of (**A**) standard, (**B**) induced, (**C**) reduced or (**D**) constitutive ectopic overexpression of UGT74E2 on IBA and IBA-glc content. The size of UGT74E2, IBA and IBA-glc indicate their relative presence to standard. The size of the arrow indicates the relative conversion rate to standard.

As a correlation between bolting time and the induction of *UGT74E2* expression was observed, natural variation in its promoter region was further investigated. Accessions delayed in bolting time by salt stress showed large variation or missing data in a 1000bp region in the promoter, possibly caused by the presence of a gap. The downregulation of *UGT74E2* in these accessions could be explained by the absence of a binding site for a positively regulating transcription factor in this region. Out of the many transcription factors putatively binding this region, we selected eight transcription factors based on bicluster analysis (figure 7). These transcription factors showed high correlation with *UGT74E2* expression in salt, drought, osmotic and ABA treatment. For all these transcription factors, Except for AT5G04670, previous studies have confirmed roles in regulation of the timing of flowering, development under salt or other water-deficit stress conditions, or both. *RVE6*, together with its partially redundant homologs *RVE8* and *RVE4*, is part of the circadian clock mechanism, controlling the clock's pace (Hsu et al., 2013). Mutants in these genes show a delay in flowering and an increase in growth rate (Gray et al., 2017).

ATHB-12 is a homeobox transcription factor which is involved in growth and development in both normal conditions and water-stressed plants. Its expression is induced during water-deficit conditions and this induction is dependent on ABA (Olsson et al., 2004). In addition to reduced shoot and root size, loss-of-function of *ATHB-12* leads to a delay in bolting time and in water-deficit conditions seed set is strongly affected (Hur et al., 2015; Ré et al., 2014). Other reports indicate a role for ATHB-12 in regulating stem growth rates of the inflorescence through regulation of GA levels (Son et al., 2010). Taken together, all studies indicate a role for ATHB-12 in regulating development in both vegetative and flowering stages, especially during drought stress.

The Nuclear factor Y (NF-Y) protein family is conserved throughout eukaryotes and forms a heterotrimeric complex of three subunits A, B and C, although increasing

evidence also shows interaction with other proteins (as reviewed in Zhao et al., 2017). In plants, each subunit is encoded by multiple genes with expression in different tissues, developmental stages and environmental conditions. Thereby, their potential role is complex, and combinations of several subunits play essential roles in plant growth, development and stress. Interestingly, we identified 5 different subunits (A1, A5, A7, C2 and C3) in our bicluster analysis and in our co-expression analysis we also found subunit B1. Out of these subunits, A1, A5, B1 and C2 have been annotated to be involved in regulating flowering time (Mu et al., 2013; Wenkel et al., 2006). In addition, A1, A5 and B1 have been annotated to be involved in ABA sensitivity, drought or salt stress (Li et al., 2008, 2013; Mu et al., 2013; Warpeha et al., 2007). Wenkel et al., (2006) have shown that subunit B1 (atHAP3a) and C2 (atHAP5a) can interact with CO, together stimulating the floral transition. Interestingly, over-expression of subunit A1 (atHAP2a) delays flowering, probably because of competition with CO for binding of subunit B1 and C2. High expression of A1 in salt stress could thus lead to a delay in flowering. Together, these subunits might form the heteromeric complex that regulates *UGT74E2*.

Based on their described roles, these transcription factors are qualified candidates for further research into the regulation of timing of flowering during salt stress. Binding assays to confirm binding of these transcription factors to the promoter of *UGT74E2* could confirm their role in IBA regulation of flowering time and expand the knowledge of the transcriptional network regulating timing of flowering in salt stress conditions. Interestingly, both *UGT74E2* and the transcription factors described above are highly upregulated by drought and salt stress. While in many physiological processes drought and salt stress have similar effects, flowering time is described to be early in drought and delayed in salt. It would be very interesting to further investigate how these transcription factors play a role in either or both processes.

Although auxin has been studied for many developmental processes, the role of auxin in regulation of the floral transition is still under debate (as reviewed in Wu et al., 2020). Here, we show a possible role for IBA in regulation of bolting time under stress. Although some studies question a role for IBA *in planta* (Novák et al., 2012), its role in root development is strongly supported by several studies (as reviewed Frick & Strader, 2017). As IBA indirectly can also influence IAA homeostasis, both compounds might be involved in integrating stress signals into the regulation of floral transition.

In our study we identified a role for UGT74E2 in regulation of bolting time during salt stress. Interestingly, ectopic constitutive overexpression of *UGT74E2* not only influences bolting time, but also leads to altered architecture in both vegetative and reproductive organs and an increased tolerance to osmotic stress (Tognetti et al., 2010). Kim et al. (2013) have previously shown that in absence of salt stress GI interacts with SALT OVERLY SENSITIVE2 (SOS2), preventing SOS2 to activate SALT OVERLY SENSITIVE1 (SOS1). The degradation of GI during salt stress, resulting in a delay in flowering time, is crucial to activate SOS1 leading to increased salinity tolerance. Thus, both studies show a direct link between a delay in flowering time and increased salt tolerance, although the effect of salt on flowering time is not addressed in these studies. Discovering pathways regulating flowering time during salt stress is not only important

5

for increasing knowledge on optimal timing of flowering, but also for improving salt tolerance. Further research on flowering time under suboptimal conditions such as salt stress, will help provide agriculture with resilient plants, optimizing both flowering time and tolerance to stresses.

## MATERIALS AND METHODS

*Plant materials and growth conditions*
Out of the 360 accessions of the Arabidopsis HapMap collection (Weigel and Mott, 2009), 120 accessions were selected based on the property to flower without vernalization during propagation. Out of these 120 accessions, 95 accessions flowered (at least 5 plants in both control and salt conditions) during the course of our phenotyping experiment and were used for further analysis (see supplemental table 1). The UGT74E2 overexpression and knock-out lines (Tognetti et al., 2010) are in Col-0 background and were kindly provided by Frank van Breusegem (Plant Systems Biology, VIB).

For GWAS, the accessions were grown in the greenhouse of the University of Amsterdam in September and October 2016. Natural daylength was 13 hours at the start and 11 hours at the end of the experiment. A selection of accessions was repeated in the same conditions in April and May 2017, with a natural daylength of 14 hours at the start and 15 hours and the end of the experiment. In both cases, a long day was established by additional artificial light (16h light / 8h dark). The temperature was controlled between 18 and 20°C and the average humidity was between 60 and 80%. For all other assays, plants were grown in a controlled growth chamber in long day (16h light / 8h dark) at 20°C/18°C (day/night) and 70% humidity, unless stated otherwise.

After 7 days seedlings were transferred to trays of 5x8 pots (Verspeentrays, Deens format, Desch-plantpak, The Netherlands), which were saturated with water containing 0 mM (control) or 75 mM (Salt) NaCl. To ensure equal and fast uptake of salt solution, the soil (Zaaigrond nr 1, SIR 27010-15, JongKind BV, The Netherlands) in these pots was left to dry for 4 days before applying the salt solution from below. After initial salt treatment, all trays were watered twice a week from below with water of the same composition as the initial administration, to keep salt levels equal during the course of the experiment. To prevent effects of location and tray, plants were transferred following a randomized block design. A week after transfer, additional seedlings were removed, leaving one seedling in each pot.

*Flowering time assay*
Flowering phenotypes were scored from 14 days after germination (7 days of treatment) till the end of the experiment. The GWAS study was ended 37 days after germination and only accessions of which at least 5 replicates flowered at the end of the experiment in both control and salt stress conditions were taken into consideration during the analysis. Two flowering phenotypes were scored daily: bolting time, the day the inflorescence stem reaches 1 cm, and flowering time, the day the first flower opens. As soon as plants opened their first flower, the number of rosette leaves was counted. The mutant lines

were phenotyped in the same way, except weekend days were not scored during these experiments. The mutant assays were ended after all surviving plants reached flowering. However, for each experiment, a cut-off bolting time was chosen based on the median bolting time, above which plants were not taken along for further analysis.

*Quantitative real-time PCR*
Expression levels of genes of interest in shoots and roots were confirmed by RT-qPCR. Plants were grown and treated as described before. Shoots of approximately 10-20 seedlings were pooled for one biological replicate. For mature plants, 2-3 leaves or the shoot meristem of one plant were used per sample. RNA was extracted using TRI-reagent (Sigma Aldrich) followed by the synthesis of cDNA with the iScript cDNA Synthesis kit (Bio-Rad) from 1μg total RNA. 10-15 ng of RNA was used for each reaction with Sygreen blue mix Lo-ROX (Sopachem) together with 10 μM of target primer. Per biological replicate 2 technical replicates were used. The expression was normalized using the reference gene AT2G28390 (SAND; forward primer 5'-AACTCTATGCAGCATTTGATCCACT-3'; reverse primer 5'-TGATTGCATATCTTTATCGCCATC-3'). *UGT74E2* expression was measured using forward primer 5'- GAATCGTCCTCATACCCGAAT-3' and reverse primer 5'- GCTTTGGACCCATTTCAACA-3'. *BT3* expression was measured using forward primer 5'- CATTGCTACTCGGTCCCATCTC-3' and reverse primer 5'-TCATCACTTTCCATCCCTCTGTTG-3'.

*Genome Wide Association Studies*
The data collected in the GWAS experiment was first checked for outliers. Two trays were discarded because of watering problems leading to an uneven watering of these plants and unreliable data. No other outliers were removed. GWAS data was analyzed using the GWAPP online tool (Seren et al., 2012). Traits with a heritability <0.2 were not further analyzed. Each trait was checked for normal distribution via visual inspection of a histogram. As the data of all traits followed a normal distribution, the AMM model, taken population structure in consideration, was used for GWAS. Only SNPs with a minimum allele count (mac) of more than 10 were taken into account. The threshold for significant SNPs of p<4.88e-07 (LOD score of more than 6.31) was determined by correcting p<0.10 with Bonferroni correction taking into account the number of SNPs compared (204741 SNPs). In addition, SNPs above the arbitrary threshold of LOD>5.0 were also further investigated.

*Sequence comparisons*
To assess sequence similarity of locus 1, sequence information of all sequenced accessions available in the 1001 Genomes Project (Weigel and Mott, 2009) was retrieved from the 1001 Genomes Project Website (1001genomes.org) and aligned with ClustalO. A comparison of the sequences based on sequence similarity, gaps and missing data was performed and plotted using the Gnu-plot software package (as described in Julkowska et al., 2016). For comparison of early and delayed accessions, the 1001 genome browser sequences were aligned and visualized in benchling (benchling.com).

*Promoter analysis*

PlantPAN 3.0 (PlantPAN.itps.ncku.edu.tw) was used to identify putative transcription factor binding sites in the selected variable region in the promoter of *UGT74E2*, ranging from 1650bp to 550bp upstream of the 5'UTR of *UGT74E2*. The algorithm annotated all putative binding sites in this 1100 bp region of highest variation. PlantPAN 3.0 provided a coexpression analysis under environmental stresses, hormone treatment and developmental stages using Pearson correlation coefficient (PCC) or spearman's rho, with a threshold of 0.6 and an SVM score of 1.00. Bicluster analysis on these transcription factors was done with GENEVESTIGATOR (Zimmermann et al., 2004). From the Affymetrix Arabidopsis ATH1 Genome Array, all stress and hormone treated samples were compared for Log2 fold expression values (532 treatments, 1351 samples). Biclustering was done for upregulated genes with a threshold of 0.8 and a minimum number of 10 treatments and 5 genes.

*Statistics*

Statistical analysis was performed with R software. Data was visually checked for normal distribution by visual inspection of Q-Q plots before further analysis. Linear models (two-way ANOVA) were fitted using the lm function of the stats package. Linear Mixed-Effects Models were fitted with the lmer function of the lme4 package. If results were significant, post-hoc analysis with manual contrasts were done with the ghlt function of the multcomp package. Details on statistics can be found in the legend of each figure.

## SUPPLEMENTAL MATERIALS
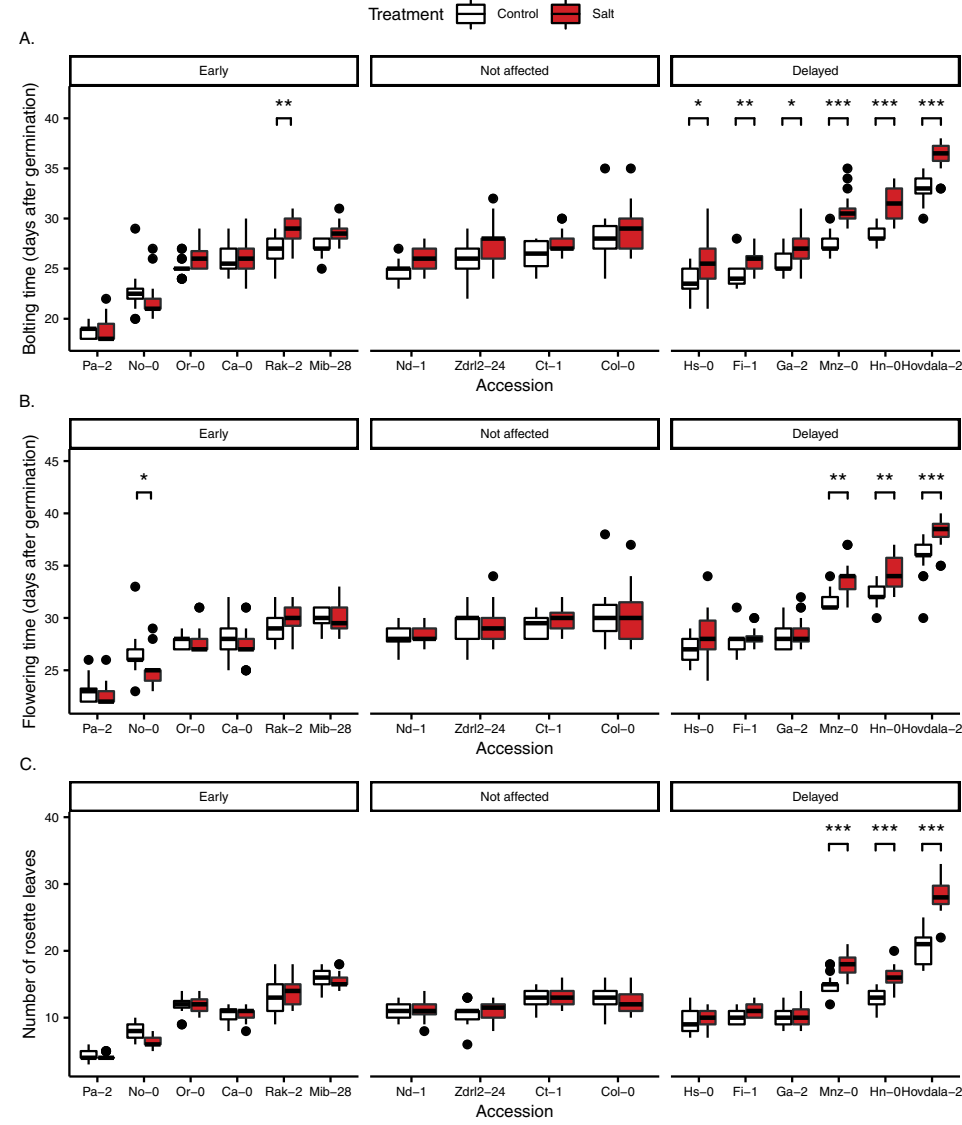


**Supplemental figure 1. Repetition of bolting and flowering time in a selection of accessions.** A selection of accessions observed in the GWAS screen to have relatively early, not affected or delayed bolting time in salt stress (figure 1) were grown in the greenhouse in long day conditions to measure bolting time **(A)**, flowering time **(B)** and the number of rosette leaves **(C)** during control (white) and salt treatment (red). The middle line inside the box represents the median (n=20). Lower and upper box boundaries represent 25th and 75th percentiles. Lower and upper error lines represent 10th and 90th percentiles. Dots represent data falling outside 10th and 90th percentiles. Significant differences were determined by a linear mixed model with random factor tray, where a significant difference in the response to salt stress between accessions was observed. Asterisks indicate significant differences following a manual contrast post-hoc comparison within accessions (* p<0.05, ** p<0.01,*** p<0.001).
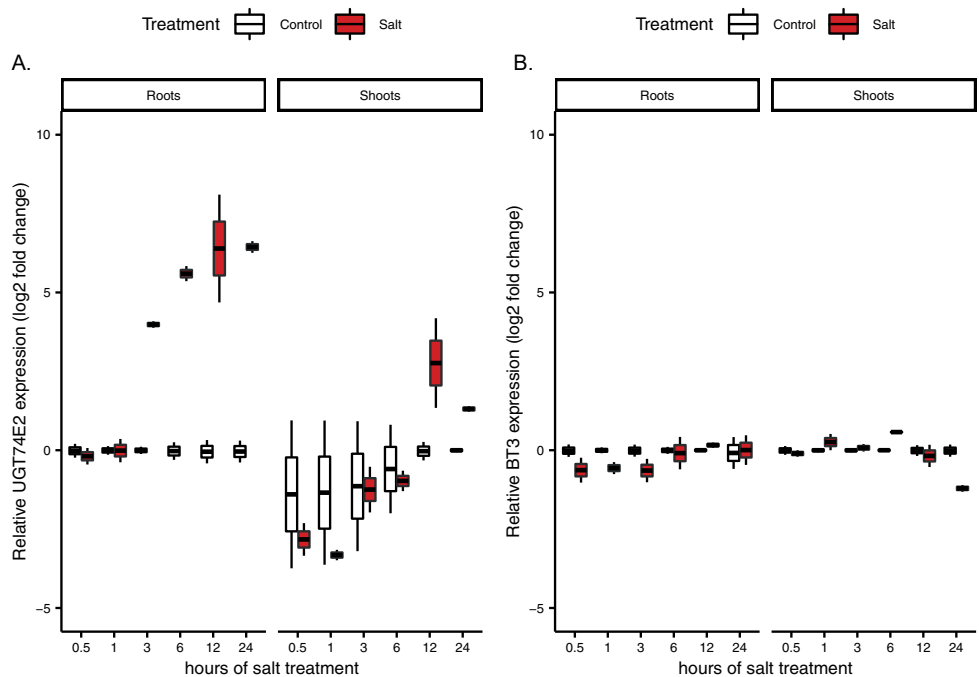
**Supplemental Figure 2. Expression of *UGT74E2* is induced by salt stress in both roots and shoots, whereas BT3 expression is unaffected.** Publicly available micro-array dataset (AtGenExpress global stress dataset (Kilian et al., 2007)) was used to retrieve expression data of *UGT74E2* (A) and *BT3* (B) in both root and shoot of x-day old seedlings, treated for several hours with control (white) or salt (red) treatment. Boxplots show log2 fold change of *UGT74E2* and *BT3* expression in comparison to control. The middle line inside the box represents the median (n=2). Lower and upper box boundaries represent 25th and 75th percentiles. Lower and upper error lines represent 10th and 90th percentiles. Dots represent data falling outside 10th and 90th percentiles.
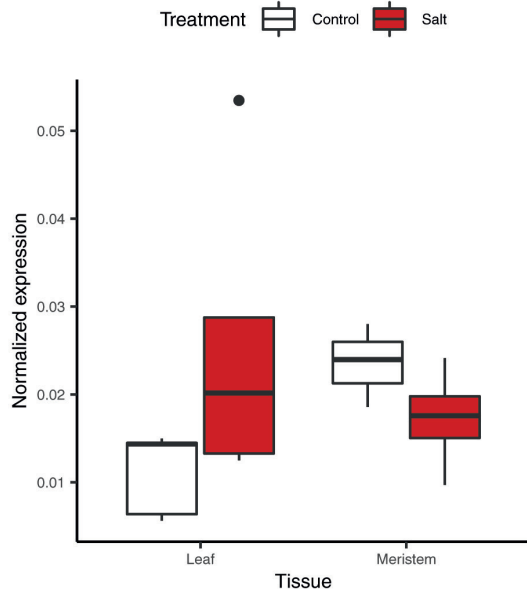
**Supplemental figure 3. Normalized expression of *UGT74E2* in flowering plants is not affected by long term salt treatment in either leaf or meristem.** Leaf (8-12th leaf) and meristem tissue of 7-week old Col-0 plants treated with control (white) or salt (red) for 6 weeks were separated and harvested and analyzed for gene expression of *UGT74E2* and reference gene *At2G28390* by qPCR. Boxplots show gene expression of *UGT74E2* normalized for expression of the reference gene. The middle line inside the box represents the median (n=5). Lower and upper box boundaries represent 25th and 75th percentiles. Lower and upper error lines represent 10th and 90th percentiles. Dots represent data falling outside 10th and 90th percentiles. Significant differences were determined by a two-way ANOVA, but none were found.
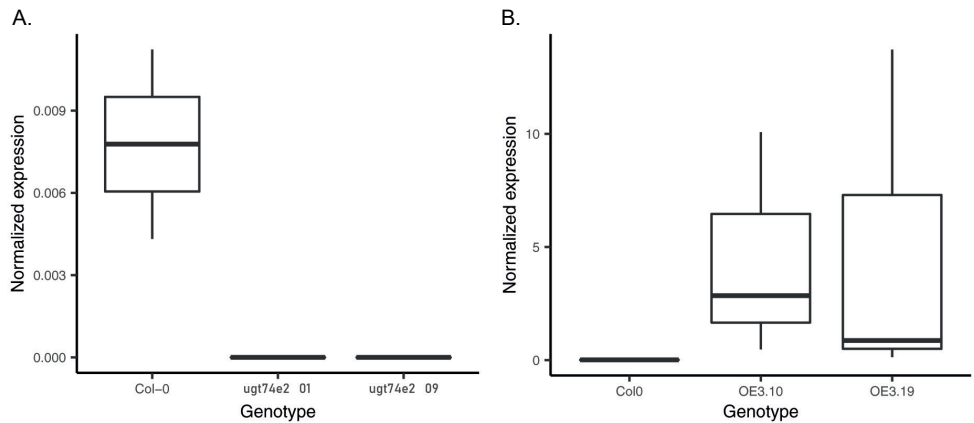


**Supplemental figure 4. Confirmation of *UGT74E2* knock-out and over-expression lines.** Shoot tissue of 7-day old seedlings was harvested and analyzed for gene expression of *UGT74E2* and reference gene *At2G28390* by qPCR. (A) Normalized expression of both knock-out lines *ugt74e2-01* and *ugt74e2-09* was undetectable by qPCR. (B) Both over-expression lines OE3.10 and OE3.19 showed highly increased expression in comparison to Col-0. The middle line inside the box represents the median (n=3). Lower and upper box boundaries represent 25th and 75th percentiles. Lower and upper error lines represent 10th and 90th percentiles. Dots represent data falling outside 10th and 90th percentiles.
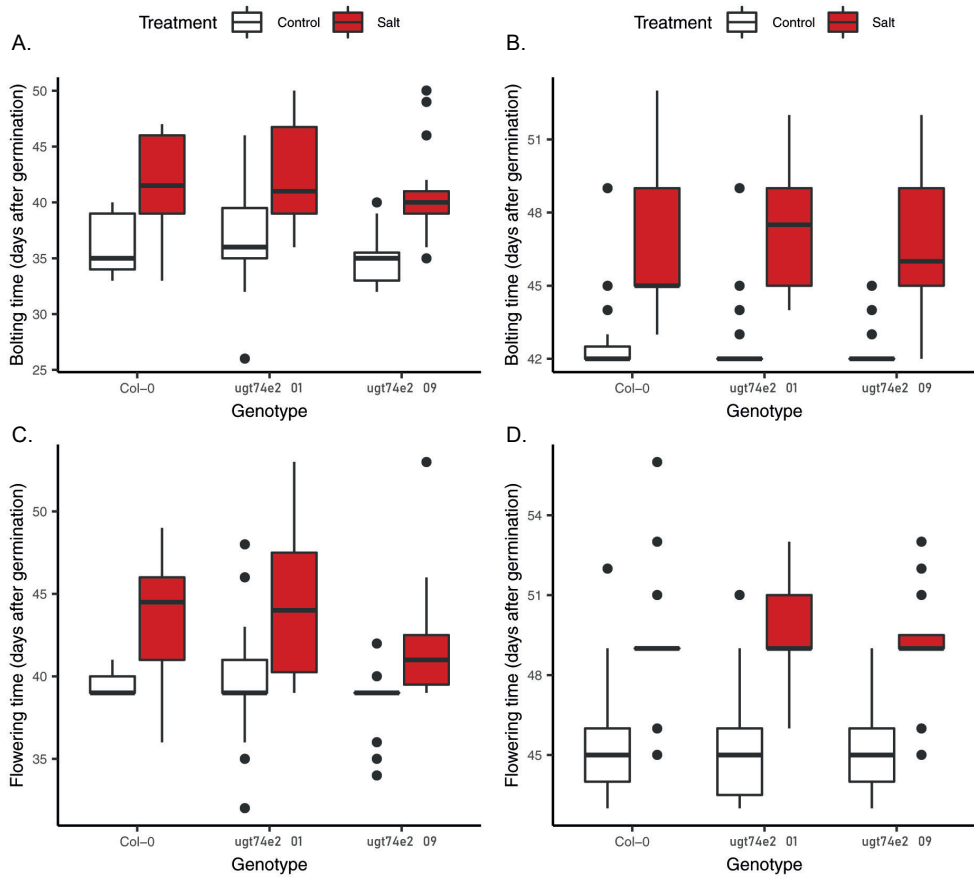
**Supplemental figure 5. *Ugt74e2* knock-out mutants are not affected in bolting or flowering time in control or salt treatment.** Bolting and flowering time during control (white) and salt treatment (red) in Col-0 and knock-out mutants *ugt74e2-01* and *ugt74e2-09* were measured in long day (**A**) or pre-treatment of 12/12 hours for 3 weeks and then transferred to long day (**B**). The middle line inside the box represents the median (n=23). Lower and upper box boundaries represent 25th and 75th percentiles. Lower and upper error lines represent 10th and 90th percentiles. Dots represent data falling outside 10th and 90th percentiles. Significant differences were determined by a linear mixed model with random factor tray, but only the effect of the treatment was significant. Genotypes did not differ in both overall phenotype and response to the treatment.

**Supplemental Table 1.** The selected Arabidopsis Accessions including ABRC and Nordborg coding. Only Accessions that flowered with at least 5 plants in both control and salt conditions were taken into account for GWAS analysis and are listed here.

| Accession | ABRC-code | Nordborg-code | Accession | ABRC-code | Nordborg-code |
|---|---|---|---|---|---|
| LAC-5 | CS76158 | 96 | Gu-1 | CS28332 | 7150 |
| MIB-28 | CS76183 | 178 | Go-0 | CS28282 | 7151 |
| MOG-37 | CS76189 | 242 | Ha-0 | CS28336 | 7163 |
| TOU-A1-62 | CS76256 | 328 | Hn-0 | CS28350 | 7165 |
| UKNW06-059 | CS76275 | 5380 | Kelsterbach-2 | CS28382 | 7188 |
| UKNW06-060 | CS76276 | 5381 | Kr-0 | CS28419 | 7201 |
| UKID48 | CS76273 | 5753 | Kro-0 | CS28420 | 7206 |
| DraIV1-14 | CS76119 | 5896 | Li-3 | CS28454 | 7224 |
| DraIV6-35 | CS76123 | 6005 | Li-7 | CS28461 | 7231 |
| Hovdala-2 | CS76143 | 6039 | Mnz-0 | CS28495 | 7244 |
| ZdrI2-24 | CS76307 | 6448 | Nw-0 | CS28573 | 7258 |
| CSHL-5 | CS28181 | 6744 | No-0 | CS28564 | 7275 |
| An-1 | CS76091 | 6898 | Ob-1 | CS28580 | 7277 |
| Col-0 | CS76113 | 6909 | Old-1 | CS28583 | 7280 |
| Ct-1 | CS76114 | 6910 | Or-0 | CS28587 | 7282 |
| Cvi-0 | CS76116 | 6911 | Pa-2 | CS28595 | 7291 |
| Est-1 | CS76127 | 6916 | Pr-0 | CS28651 | 7310 |
| HR-5 | CS76144 | 6924 | Sei-0 | CS28729 | 7333 |
| Kin-0 | CS76153 | 6926 | Si-0 | CS28739 | 7337 |
| Ler-1 | CS76164 | 6932 | Tsu-0 | CS28780 | 7373 |
| Mrk-0 | CS76191 | 6937 | Uk-2 | CS28788 | 7379 |
| Mt-0 | CS76192 | 6939 | Wa-1 | CS28804 | 7394 |
| Mz-0 | CS76193 | 6940 | Ws | CS28823 | 7397 |
| Nd-1 | CS76197 | 6942 | Wt-3 | CS28833 | 7408 |
| NFA-8 | CS76199 | 6944 | Wl-0 | CS28822 | 7411 |
| Oy-0 | CS76203 | 6946 | Zu-1 | CS28847 | 7418 |
| Ra-0 | CS76216 | 6958 | Jl-3 | CS28369 | 7424 |
| Ull2-3 | CS76293 | 6973 | Nc-1 | CS28527 | 7430 |
| Van-0 | CS76297 | 6977 | PHW-20 | CS28620 | 7490 |
| Wt-5 | CS76304 | 6982 | Lp2-2 | CS76176 | 7520 |
| Ang-0 | CS28018 | 6992 | Gy-0 | CS76139 | 8214 |
| An-2 | CS28017 | 6996 | Fei-0 | CS76129 | 8215 |
| Bs-2 | CS28097 | 7004 | Bu-0 | CS76103 | 8271 |
| Be-1 | CS28063 | 7011 | Gd-1 | CS76134 | 8296 |
| Boot-1 | CS28091 | 7026 | Hi-0 | CS76140 | 8304 |
| Bsch-0 | CS28099 | 7031 | Hs-0 | CS76145 | 8310 |
| Blh-1 | CS76098 | 7034 | Ka-0 | CS76149 | 8314 |

5

| Accession | ABRC-code | Nordborg-code | | Accession | ABRC-code | Nordborg-code |
|---|---|---|---|---|---|---|
| Ca-0 | CS28128 | 7062 | | Lc-0 | CS76159 | 8323 |
| Da-0 | CS28200 | 7094 | | Lip-0 | CS76168 | 8325 |
| Di-1 | CS28208 | 7098 | | Lm-2 | CS76173 | 8329 |
| Db-0 | CS28202 | 7100 | | Na-1 | CS76195 | 8343 |
| Dra-2 | CS28214 | 7105 | | Per-1 | CS76210 | 8354 |
| Ede-1 | CS28217 | 7110 | | Rak-2 | CS76217 | 8365 |
| Ep-0 | CS28236 | 7123 | | Rsch-4 | CS76222 | 8374 |
| Est-0 | CS28243 | 7128 | | St-0 | CS76231 | 8387 |
| Fi-1 | CS28252 | 7139 | | Sav-0 | CS76225 | 8412 |
| Ga-2 | CS28274 | 7141 | | Kelsterbach-4 | CS76152 | 8420 |
| Gie-0 | CS28280 | 7147 | | | | |

**Supplemental table 3.** Pseudoheritability of traits as calculated by GWAPP (without transformation).

| trait | pseudoheritability |
|---|---|
| DayOfBolting_control | 1 |
| DayOfBolting_salt | 1 |
| DayOfBolting_ratio | 1 |
| DayOfFlowering_control | 0.24 |
| DayOfFlowering_salt | 1 |
| DayOfFlowering_ratio | 0.88 |
| nLeaves_control | 0 |
| nLeaves_salt | 0.06 |
| nLeaves_ratio | 0 |

**Supplemental table 5.** Transcription factors putatively binding the region of variation in the promoter of *UGT74E2* (1650 to 550bp upstream) and coexpressed with *UGT74E2* in either environmental stress, developmental stages or hormonal treatment. The pearson correlation coefficient (PCC) value shows the strength of correlation in terms of expression.

| Coexpression dataset | Correlation coefficient | Locus Name | Symbol | PCC value |
|---|---|---|---|---|
| Environmental stress | Spearman's rho | AT5G04760 | AT5G04760 | 0.64 |
| Environmental stress | Spearman's rho | AT4G35580 | NTL9 | 0.6 |
| | | | | |
| Developmental Stages | PCC | AT1G07640 | OBP2 | 0.72 |
| Developmental Stages | PCC | AT1G51700 | ADOF1 | 0.64 |
| Developmental Stages | PCC | AT3G61890 | ATHB-12 | 0.62 |
| Developmental Stages | PCC | AT1G01060 | LHY | 0.61 |
| | | | | |
| Hormonal treatment | PCC | AT3G11440 | ATMYB65 | 0.98 |
| Hormonal treatment | PCC | AT1G32240 | KAN2 | 0.98 |
| Hormonal treatment | PCC | AT5G06100 | MYB33 | 0.98 |
| Hormonal treatment | PCC | AT4G34680 | GATA3 | 0.97 |
| Hormonal treatment | PCC | AT1G75240 | AtHB33 | 0.97 |
| Hormonal treatment | PCC | AT3G05690 | UNE8 | 0.97 |
| Hormonal treatment | PCC | AT4G17950 | AT4G17950 | 0.97 |
| Hormonal treatment | PCC | AT5G06839 | bZIP65 | 0.97 |
| Hormonal treatment | PCC | AT3G26744 | ICE1 | 0.96 |
| Hormonal treatment | PCC | AT4G26150 | GATA22 | 0.96 |
| Hormonal treatment | PCC | AT1G14900 | HMGA | 0.96 |
| Hormonal treatment | PCC | AT5G06960 | OBF5 | 0.95 |
| Hormonal treatment | PCC | AT3G24050 | GATA1 | 0.95 |
| Hormonal treatment | PCC | AT1G77850 | ARF17 | 0.95 |
| Hormonal treatment | PCC | AT5G66320 | GATA5 | 0.95 |
| Hormonal treatment | PCC | AT2G20110 | AT2G20110 | 0.95 |
| Hormonal treatment | PCC | AT4G04890 | PDF2 | 0.95 |
| Hormonal treatment | PCC | AT3G16870 | GATA17 | 0.95 |
| Hormonal treatment | PCC | AT4G21750 | ATML1 | 0.95 |
| Hormonal treatment | PCC | AT5G16560 | KAN | 0.94 |
| Hormonal treatment | PCC | AT1G51600 | TIFY2A | 0.94 |
| Hormonal treatment | PCC | AT3G22780 | TSO1 | 0.94 |
| Hormonal treatment | PCC | AT4G24470 | TIFY1 | 0.94 |
| Hormonal treatment | PCC | AT2G46530 | ARF11 | 0.94 |
| Hormonal treatment | PCC | AT1G23380 | KNAT6 | 0.94 |
| Hormonal treatment | PCC | AT5G10030 | TGA4 | 0.94 |
| Hormonal treatment | PCC | AT2G01060 | AT2G01060 | 0.94 |
| Hormonal treatment | PCC | AT1G19485 | AT1G19485 | 0.93 |
| Hormonal treatment | PCC | AT5G03790 | ATHB51 | 0.93 |

5

**153**

| Coexpression dataset | Correlation coefficient | Locus Name | Symbol | PCC value |
|---|---|---|---|---|
| Hormonal treatment | PCC | AT3G61830 | ARF18 | 0.93 |
| Hormonal treatment | PCC | AT2G21060 | ATGRP2B | 0.93 |
| Hormonal treatment | PCC | AT4G18020 | APRR2 | 0.93 |
| Hormonal treatment | PCC | AT4G36620 | GATA19 | 0.92 |
| Hormonal treatment | PCC | AT1G17590 | NF-YA8 | 0.92 |
| Hormonal treatment | PCC | AT5G06950 | TGA2 | 0.91 |
| Hormonal treatment | PCC | AT1G08320 | TGA9 | 0.91 |
| Hormonal treatment | PCC | AT1G59750 | ARF1 | 0.91 |
| Hormonal treatment | PCC | AT3G24120 | AT3G24120 | 0.91 |
| Hormonal treatment | PCC | AT3G20910 | NF-YA9 | 0.91 |
| Hormonal treatment | PCC | AT4G29000 | AT4G29000 | 0.91 |
| Hormonal treatment | PCC | AT3G13445 | TFIID-1 | 0.91 |
| Hormonal treatment | PCC | AT1G55110 | AtIDD7 | 0.91 |
| Hormonal treatment | PCC | AT5G62260 | AT5G62260 | 0.9 |
| Hormonal treatment | PCC | AT1G72830 | HAP2C | 0.9 |
| Hormonal treatment | PCC | AT3G12250 | TGA6 | 0.9 |
| Hormonal treatment | PCC | AT4G00180 | YAB3 | 0.89 |
| Hormonal treatment | PCC | AT3G57390 | AGL18 | 0.89 |
| Hormonal treatment | PCC | AT2G38880 | NF-YB1 | 0.89 |
| Hormonal treatment | PCC | AT3G16857 | ARR1 | 0.89 |
| Hormonal treatment | PCC | AT4G00730 | ANL2 | 0.88 |
| Hormonal treatment | PCC | AT3G14230 | RAP2.2 | 0.88 |
| Hormonal treatment | PCC | AT5G37020 | ARF8 | 0.87 |
| Hormonal treatment | PCC | AT5G04760 | AT5G04760 | 0.87 |
| Hormonal treatment | PCC | AT1G55520 | TBP2 | 0.87 |
| Hormonal treatment | PCC | AT1G17920 | HDG12 | 0.87 |
| Hormonal treatment | PCC | AT5G66730 | AT5G66730 | 0.86 |
| Hormonal treatment | PCC | AT1G18330 | EPR1 | 0.85 |
| Hormonal treatment | PCC | AT1G30490 | ATHB9 | 0.85 |
| Hormonal treatment | PCC | AT3G27010 | TCP20 | 0.85 |
| Hormonal treatment | PCC | AT1G33060 | ANAC014 | 0.84 |
| Hormonal treatment | PCC | AT3G61150 | HD-GL2-1 | 0.83 |
| Hormonal treatment | PCC | AT1G43700 | VIP1 | 0.83 |
| Hormonal treatment | PCC | AT1G54830 | NF-YC3 | 0.82 |
| Hormonal treatment | PCC | AT5G08520 | AT5G08520 | 0.82 |
| Hormonal treatment | PCC | AT3G14020 | NF-YA6 | 0.82 |
| Hormonal treatment | PCC | AT2G33860 | ETT | 0.82 |
| Hormonal treatment | PCC | AT5G52660 | AT5G52660 | 0.82 |
| Hormonal treatment | PCC | AT5G12840 | HAP2A | 0.81 |

| Coexpression dataset | Correlation coefficient | Locus Name | Symbol | PCC value |
|---|---|---|---|---|
| Hormonal treatment | PCC | AT5G60450 | ARF4 | 0.81 |
| Hormonal treatment | PCC | AT1G19850 | MP | 0.8 |
| Hormonal treatment | PCC | AT4G35580 | NTL9 | 0.8 |
| Hormonal treatment | PCC | AT4G01280 | AT4G01280 | 0.8 |
| Hormonal treatment | PCC | AT4G30080 | ARF16 | 0.79 |
| Hormonal treatment | PCC | AT3G55370 | OBP3 | 0.79 |
| Hormonal treatment | PCC | AT1G30330 | ARF6 | 0.78 |
| Hormonal treatment | PCC | AT5G38140 | NF-YC12 | 0.78 |
| Hormonal treatment | PCC | AT3G16940 | AT3G16940 | 0.78 |
| Hormonal treatment | PCC | AT4G35550 | ATWOX13 | 0.78 |
| Hormonal treatment | PCC | AT2G02080 | AtIDD4 | 0.77 |
| Hormonal treatment | PCC | AT1G14580 | AT1G14580 | 0.77 |
| Hormonal treatment | PCC | AT5G65590 | AT5G65590 | 0.76 |
| Hormonal treatment | PCC | AT5G08130 | BIM1 | 0.76 |
| Hormonal treatment | PCC | AT4G17570 | GATA26 | 0.75 |
| Hormonal treatment | PCC | AT3G21175 | TIFY2B | 0.75 |
| Hormonal treatment | PCC | AT2G03500 | AT2G03500 | 0.73 |
| Hormonal treatment | PCC | AT1G54160 | NFYA5 | 0.72 |
| Hormonal treatment | PCC | AT3G61120 | AGL13 | 0.72 |
| Hormonal treatment | PCC | AT5G39660 | CDF2 | 0.72 |
| Hormonal treatment | PCC | AT1G70510 | KNAT2 | 0.69 |
| Hormonal treatment | PCC | AT2G45650 | AGL6 | 0.69 |
| Hormonal treatment | PCC | AT1G22070 | TGA3 | 0.69 |
| Hormonal treatment | PCC | AT5G09410 | EICBP.B | 0.68 |
| Hormonal treatment | PCC | AT5G66940 | AT5G66940 | 0.68 |
| Hormonal treatment | PCC | AT1G69170 | AT1G69170 | 0.68 |
| Hormonal treatment | PCC | AT1G30500 | NF-YA7 | 0.67 |
| Hormonal treatment | PCC | AT5G50480 | NF-YC6 | 0.66 |
| Hormonal treatment | PCC | AT4G18770 | MYB98 | 0.65 |
| Hormonal treatment | PCC | AT1G56170 | HAP5B | 0.63 |
| Hormonal treatment | PCC | AT5G28300 | GT2L | 0.63 |
| Hormonal treatment | PCC | AT2G28350 | ARF10 | 0.63 |
| Hormonal treatment | PCC | AT3G60030 | SPL12 | 0.63 |
| Hormonal treatment | PCC | AT1G26790 | AT1G26790 | 0.62 |
| Hormonal treatment | PCC | AT4G00940 | AT4G00940 | 0.62 |
| Hormonal treatment | PCC | AT4G16110 | ARR2 | 0.61 |
| Hormonal treatment | PCC | AT3G45610 | AT3G45610 | 0.61 |
| Hormonal treatment | PCC | AT1G13450 | GT-1 | 0.61 |

5

| Coexpression dataset | Correlation coefficient | Locus Name | Symbol | PCC value |
|---|---|---|---|---|
| Hormonal treatment | Spearman's rho | AT5G16560 | KAN | 0.68 |
| Hormonal treatment | Spearman's rho | AT2G45650 | AGL6 | 0.62 |
| Hormonal treatment | Spearman's rho | AT5G06839 | bZIP65 | 0.62 |
| Hormonal treatment | Spearman's rho | AT5G62940 | DOF5.6 | 0.62 |
| Hormonal treatment | Spearman's rho | AT3G14020 | NF-YA6 | 0.61 |

**ACKNOWLEDGEMENTS**

# REFERENCES

Adrian, J., Farrona, S., Reimer, J. J., Albani, M. C., Coupland, G., and Turck, F. (2010). Cis-regulatory elements and chromatin state coordinately control temporal and spatial expression of FLOWERING LOCUS T in arabidopsis. *Plant Cell* 22, 1425–1440. doi:10.1105/tpc.110.074682.

Apse, M. P., Sottosanto, J. B., and Blumwald, E. (2003). Vacuolar cation/H+ exchange, ion homeostasis, and leaf development are altered in a T-DNA insertional mutant of AtNHX1, the Arabidopsis vacuolar Na+/H+ antiporter. *Plant J.* 36, 229–239. doi:10.1046/j.1365-313X.2003.01871.x.

Bassil, E., Tajima, H., Liang, Y. C., Ohto, M. aki, Ushijima, K., Nakano, R., et al. (2011). The arabidopsis Na+/H+ antiporters NHX1 and NHX2 control vacuolar ph and K+ homeostasis to regulate growth, flower development, and reproduction. *Plant Cell* 23, 3482–3497. doi:10.1105/tpc.111.089581.

Bloomer, R. H., and Dean, C. (2017). Fine-tuning timing: Natural variation informs the mechanistic basis of the switch to flowering in Arabidopsis thaliana. *J. Exp. Bot.* 68, 5439–5452. doi:10.1093/jxb/erx270.

Challa, S., and Neelapu, N. R. R. (2018). *Genome-Wide Association Studies (GWAS) for Abiotic Stress Tolerance in Plants.* Elsevier Inc. doi:10.1016/B978-0-12-813066-7.00009-7.

Cho, L. H., Yoon, J., and An, G. (2017). The control of flowering time by environmental factors. *Plant J.* 90, 708–719. doi:10.1111/tpj.13461.

Chuck, G., and Hake, S. (2005). Regulation of developmental transitions. *Curr. Opin. Plant Biol.* 8, 67–70. doi:10.1016/j.pbi.2004.11.002.

Colasanti, J., and Coneva, V. (2009). Mechanisms of floral induction in grasses: something borrowed, something new. *Plant Physiol.* 149, 56–62. doi:10.1104/pp.108.130500.

Ehrenreich, I. M., Hanzawa, Y., Chou, L., Roe, J. L., Kover, P. X., and Purugganan, M. D. (2009). Candidate gene association mapping of Arabidopsis flowering time. *Genetics* 183, 325–335. doi:10.1534/genetics.109.105189.

Frick, E. M., and Strader, L. C. (2017). Roles for IBA-derived auxin in plant development. *J. Exp. Bot.*, 1–9. doi:10.1093/jxb/erx298.

Gray, J. A., Shalit-Kaneh, A., Chu, D. N., Hsu, P. Y., and Harmer, S. L. (2017). The REVEILLE clock genes inhibit growth of juvenile and adult plants by control of cell size. *Plant Physiol.* 173, 2308–2322. doi:10.1104/pp.17.00109.

Hsu, P. Y., Devisetty, U. K., and Harmer, S. L. (2013). Accurate timekeeping is controlled by a cycling activator in Arabidopsis. *Elife* 2013, 1–20. doi:10.7554/eLife.00473.

Huang, X., and Han, B. (2014). Natural Variations and Genome-Wide Association Studies in Crop Plants. *Annu. Rev. Plant Biol.* 65, 531–551. doi:10.1146/annurev-arplant-050213-035715.

Huijser, P., and Schmid, M. (2011). The control of developmental phase transitions in plants. *Development* 138, 4117–4129. doi:10.1242/dev.063511.

Hur, Y. S., Um, J. H., Kim, S., Kim, K., Park, H. J., Lim, J. S., et al. (2015). Arabidopsis thaliana homeobox 12 (ATHB12), a homeodomain-leucine zipper protein, regulates leaf growth by promoting cell expansion and endoreduplication. *New Phytol.* 205, 316–328. doi:10.1111/nph.12998.

5

Ivushkin, K., Bartholomeus, H., Bregt, A. K., Pulatov, A., Kempen, B., and de Sousa, L. (2019). Global mapping of soil salinity change. *Remote Sens. Environ.* 231, 111260. doi:10.1016/j.rse.2019.111260.

Jaeger, K. E., and Wigge, P. A. (2007). FT Protein Acts as a Long-Range Signal in Arabidopsis. *Curr. Biol.* 17, 1050–1054. doi:10.1016/j.cub.2007.05.008.

Julkowska, M. M., Klei, K., Fokkens, L., Haring, M. A., Schranz, M. E., and Testerink, C. (2016). Natural variation in rosette size under salt stress conditions corresponds to developmental differences between Arabidopsis accessions and allelic variation in the LRR-KISS gene. *J. Exp. Bot.* 67, 2127–2138. doi:10.1093/jxb/erw015.

Jung, C., and Müller, A. E. (2009). Flowering time control and applications in plant breeding. *Trends Plant Sci.* 14, 563–573. doi:10.1016/j.tplants.2009.07.005.

Kazan, K., and Lyons, R. (2016a). The link between flowering time and stress tolerance. *J. Exp. Bot.* 67, 47–60. doi:10.1093/jxb/erv441.

Kazan, K., and Lyons, R. (2016b). The link between flowering time and stress tolerance. 67, 47–60. doi:10.1093/jxb/erv441.

Kilian, J., Whitehead, D., Horak, J., Wanke, D., Weinl, S., Batistic, O., et al. (2007). The AtGenExpress global stress expression data set: Protocols, evaluation and model data analysis of UV-B light, drought and cold stress responses. *Plant J.* 50, 347–363. doi:10.1111/j.1365-313X.2007.03052.x.

Kim, S. G., Kim, S. Y., and Park, C. M. (2007). A membrane-associated NAC transcription factor regulates salt-responsive flowering via FLOWERING LOCUS T in Arabidopsis. *Planta* 226, 647–654. doi:10.1007/s00425-007-0513-3.

Kim, S. G., and Park, C. M. (2007). Membrane-mediated salt stress signaling in flowering time control. *Plant Signal. Behav.* 2, 517–518. doi:10.4161/psb.2.6.4645.

Kim, W. Y., Ali, Z., Park, H. J., Park, S. J., Cha, J. Y., Perez-Hormaeche, J., et al. (2013). Release of SOS2 kinase from sequestration with GIGANTEA determines salt tolerance in Arabidopsis. *Nat. Commun.* 4, 1312–1357. doi:10.1038/ncomms2357.

Kinoshita, A., and Richter, R. (2020). Genetic and molecular basis of floral induction in Arabidopsis thaliana. *J. Exp. Bot.* 71, 2490–2504. doi:10.1093/jxb/eraa057.

Korte, A., and Ashley, F. (2013). The advantages and limitations of trait analysis with GWAS : a review Self-fertilisation makes Arabidopsis particularly well suited to GWAS. *Plant Methods* 9, 29.

Li, K., Wang, Y., Han, C., Zhang, W., Jia, H., and Li, X. (2007). GA signaling and CO/FT regulatory module mediate salt-induced late flowering in Arabidopsis thaliana. *Plant Growth Regul.* 53, 195–206. doi:10.1007/s10725-007-9218-7.

Li, W. X., Oono, Y., Zhu, J., He, X. J., Wu, J. M., Iida, K., et al. (2008). The Arabidopsis NFYA5 transcription factor is regulated transcriptionally and posttranscriptionally to promote drought resistance. *Plant Cell* 20, 2238–2251. doi:10.1105/tpc.108.059444.

Li, Y., Huang, Y., Bergelson, J., Nordborg, M., and Borevitz, J. O. (2010). Association mapping of local climate-sensitive quantitative trait loci in Arabidopsis thaliana. *Proc. Natl. Acad. Sci. U. S. A.* 107, 21199–21204. doi:10.1073/pnas.1007431107.

Li, Y. J., Fang, Y., Fu, Y. R., Huang, J. G., Wu, C. A., and Zheng, C. C. (2013). NFYA1 Is Involved in Regulation of Postgermination Growth Arrest Under Salt Stress in Arabidopsis. *PLoS One* 8, 1–11. doi:10.1371/journal.pone.0061289.

Mu, J., Tan, H., Hong, S., Liang, Y., and Zuo, J. (2013). Arabidopsis transcription factor genes NF-YA1, 5, 6, and 9 play redundant roles in male gametogenesis, embryogenesis, and seed development. *Mol. Plant* 6, 188–201. doi:10.1093/mp/sss061.

Novák, O., Hényková, E., Sairanen, I., Kowalczyk, M., Pospíšil, T., and Ljung, K. (2012). Tissue-specific profiling of the Arabidopsis thaliana auxin metabolome. *Plant J.* 72, 523–536. doi:10.1111/j.1365-313X.2012.05085.x.

Olsson, A. S. B., Engström, P., and Söderman, E. (2004). The homeobox genes ATHB12 and ATHB7 encode potential regulators of growth in response to water deficit in Arabidopsis. *Plant Mol. Biol.* 55, 663–677. doi:10.1007/s11103-004-1581-4.

Poethig, R. S. (1990). Phase Change and the Regulation of Shoot Morphogenesis in Plants Articles Phase Change and the Regulation of Shoot Morphogenesis in Plants. *Science (80-. ).* 250, 923–930. doi:10.1126/science.250.4983.923.

Ré, D. A., Capella, M., Bonaventure, G., and Chan, R. L. (2014). Arabidopsis AtHB7 and AtHB12 evolved divergently to fine tune processes associated with growth and responses to water stress. *BMC Plant Biol.* 14, 1–14. doi:10.1186/1471-2229-14-150.

Riboni, M., Galbiati, M., Tonelli, C., and Conti, L. (2013). GIGANTEA enables drought escape response via abscisic acid-dependent activation of the florigens and SUPPRESSOR of OVEREXPRESSION of CONSTANS11[c][w]. *Plant Physiol.* 162, 1706–1719. doi:10.1104/pp.113.217729.

Riboni, M., Test, A. R., Galbiati, M., Tonelli, C., and Conti, L. (2016). ABA-dependent control of GIGANTEA signalling enables drought escape via up-regulation of FLOWERING LOCUS T in Arabidopsis thaliana. *J. Exp. Bot.* 67, 6309–6322. doi:10.1093/jxb/erw384.

Robert, H. S., Quint, A., Brand, D., Vivian-Smith, A., and Offringa, R. (2009). BTB and TAZ domain scaffold proteins perform a crucial function in Arabidopsis development. *Plant J.* 58, 109–121. doi:10.1111/j.1365-313X.2008.03764.x.

Ryu, J. Y., Lee, H. J., Seo, P. J., Jung, J. H., Ahn, J. H., and Park, C. M. (2014). The arabidopsis floral repressor BFT delays flowering by competing with FT for FD binding under high salinity. *Mol. Plant* 7, 377–387. doi:10.1093/mp/sst114.

Ryu, J. Y., Park, C., and Seo, P. J. (2011). The Floral Repressor BROTHER OF FT AND TFL1 ( BFT ) Modulates Flowering Initiation under High Salinity in Arabidopsis. 295–303. doi:10.1007/s10059-011-0112-9.

Samach, A., Onouchi, H., Gold, S. E., Ditta, G. S., Schwarz-Sommer, Z., Yanofsky, M. F., et al. (2000). Distinct roles of constans target genes in reproductive development of Arabidopsis. *Science (80-. ).* 288, 1613–1616. doi:10.1126/science.288.5471.1613.

Sasaki, E., Zhang, P., Atwell, S., Meng, D., and Nordborg, M. (2015). "Missing" G x E Variation Controls Flowering Time in Arabidopsis thaliana. *PLoS Genet.* 11, 1–18. doi:10.1371/journal.pgen.1005597.

Sawa, M., Nusinow, D. A., Kay, S. A., and Imaizumi, T. (2007). FKF1 and GIGANTEA complex formation is required for day-length measurement in Arabidopsis. *Science (80-. ).* 318, 261–265. doi:10.1126/science.1146994.

Seren, U., Vilhjalmsson, B. J., Horton, M. W., Meng, D., Forai, P., Huang, Y. S., et al. (2012). GWAPP: A Web Application for Genome-Wide Association Mapping in Arabidopsis. *Plant Cell* 24, 4793–4805. doi:10.1105/tpc.112.108068.

5

Son, O., Hur, Y. S., Kim, Y. K., Lee, H. J., Kim, S., Kim, M. R., et al. (2010). ATHB12, an ABA-inducible homeodomain-leucine zipper (HD-Zip) protein of arabidopsis, negatively regulates the growth of the inflorescence stem by decreasing the expression of a gibberellin 20-oxidase gene. *Plant Cell Physiol.* 51, 1537–1547. doi:10.1093/pcp/pcq108.

Stinchcombe, J. R., Weinig, C., Ungerer, M., Olsen, K. M., Mays, C., Halldorsdottir, S. S., et al. (2004). A latitudinal cline in flowering time in Arabidopsis thaliana modulated by the flowering time gene FRIGIDA. *Proc. Natl. Acad. Sci. U. S. A.* 101, 4712–4717. doi:10.1073/pnas.0306401101.

Tognetti, V. B., Van Aken, O., Morreel, K., Vandenbroucke, K., van de Cotte, B., De Clercq, I., et al. (2010). Perturbation of indole-3-butyric acid homeostasis by the UDP-glucosyltransferase UGT74E2 modulates Arabidopsis architecture and water stress tolerance. *Plant Cell* 22, 2660–2679. doi:10.1105/tpc.109.071316.

Trovato, M., Forlani, G., Signorelli, S., and Funck, D. (2019). "Proline Metabolism and Its Functions in Development and Stress Tolerance," in *Osmoprotectant-Mediated Abiotic Stress Tolerance in Plants: Recent Advances and Future Perspectives*, eds. M. A. Hossain, V. Kumar, D. J. Burritt, M. Fujita, and P. S. A. Mäkelä (Cham: Springer International Publishing), 41–72. doi:10.1007/978-3-030-27423-8_2.

Verslues, P. E., Lasky, J. R., Juenger, T. E., Liu, T. W., and Nagaraj Kumar, M. (2014). Genome-wide association mapping combined with reverse genetics identifies new effectors of low water potential-induced proline accumulation in Arabidopsis. *Plant Physiol.* 164, 144–159. doi:10.1104/pp.113.224014.

Wang, J. W. (2014). Regulation of flowering time by the miR156-mediated age pathway. *J. Exp. Bot.* 65, 4723–4730. doi:10.1093/jxb/eru246.

Warpeha, K. M., Upadhyay, S., Yeh, J., Adamiak, J., Hawkins, S. I., Lapik, Y. R., et al. (2007). The GCR1, GPA1, PRN1, NF-Y signal chain mediates both blue light and abscisic acid responses in arabidopsis. *Plant Physiol.* 143, 1590–1600. doi:10.1104/pp.106.089904.

Weigel, D., and Mott, R. (2009). The 1001 genomes project for Arabidopsis thaliana. *Genome Biol.* 10, 107. doi:10.1186/gb-2009-10-5-107.

Wenkel, S., Turck, F., Singer, K., Gissot, L., Le Gourrierec, J., Samach, A., et al. (2006). CONSTANS and the CCAAT box binding complex share a functionally important domain and interact to regulate flowering of Arabidopsis. *Plant Cell* 18, 2971–2984. doi:10.1105/tpc.106.043299.

Wu, G., Park, M. Y., Conway, S. R., Wang, J. W., Weigel, D., and Poethig, R. S. (2009). The Sequential Action of miR156 and miR172 Regulates Developmental Timing in Arabidopsis. *Cell* 138, 750–759. doi:10.1016/j.cell.2009.06.031.

Wu, M., Wu, J., and Gan, Y. (2020). The new insight of auxin functions: transition from seed dormancy to germination and floral opening in plants. *Plant Growth Regul.* 91, 169–174. doi:10.1007/s10725-020-00608-1.

Zhao, H., Wu, D., Kong, F., Lin, K., Zhang, H., and Li, G. (2017). The Arabidopsis thaliana nuclear factor Y transcription factors. *Front. Plant Sci.* 7, 1–11. doi:10.3389/fpls.2016.02045.

Zimmermann, P., Hirsch-Hoffmann, M., Hennig, L., and Gruissem, W. (2004). GENEVESTIGATOR. Arabidopsis microarray database and analysis toolbox. *Plant Physiol.* 136, 2621–2632. doi:10.1104/pp.104.046367.

**CHAPTER 6**
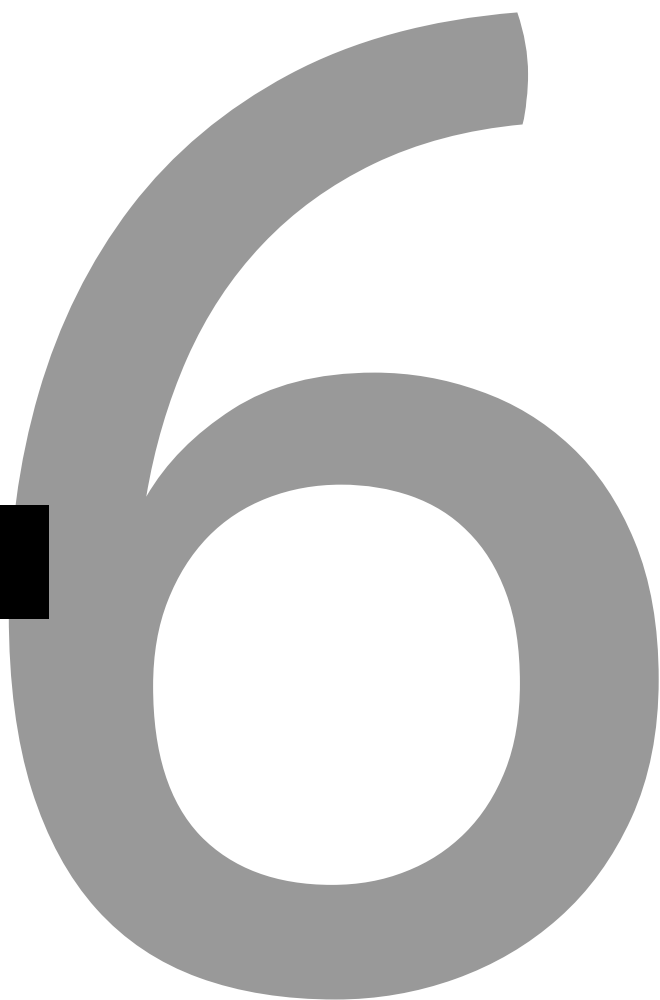
# Out of shape during stress: a key role for auxin

Ruud A. Korver[1,2], Iko T. Koevoets[2] and Christa Testerink[2]

[1]University of Amsterdam, Plant Cell Biology, Swammerdam Institute for Life Sciences, 1090GE Amsterdam, the Netherlands
[2]Laboratory of Plant Physiology, 6708PB Wageningen University & Research, Wageningen, the Netherlands

## GLOSSARY

**Acropetal transport:** Transport from the base to the apex.

**Auxins:** Plants contain multiple types of auxins, of which Indole-3-acetic acid (IAA; also referred to as auxin) is the most abundant endogenous form regulating the majority of auxin-mediated effects in plants. Four other forms of endogenously produced auxins are indole-3-butyric acid (IBA), indole-3-propionic acid (IPA), 4-Chloroindole-3-acetic acid (4-CI-IAA) and 2-phenylacetic acid (PAA).

**Basipetal transport:** Transport from apex to the base.

**Halotropism:** Directional growth of the main root away from a higher salt concentration when exposed to a salt gradient.

**IAA conjugation:** As part of IAA homeostasis, IAA can be conjugated, leading to inactive compounds of which some can be converted back to auxin and act as storage forms. The two main types of IAA conjugation are: Ester conjugation (IAA-sugar conjugate, reversible) and amide conjugation (IAA-amino acid conjugate, some are reversible).

**IAA oxidation:** In addition to conjugation, IAA can also be oxidized. Oxidation always leads to degradation of auxin and is the major pathway responsible for fast IAA turnover.

**IAA metabolism:** All enzymatic pathways leading to biosynthesis, conjugation or degradation (oxidation) of IAA.

### ABSTRACT

In most abiotic stress conditions, including salinity and water deficit, developmental plasticity of the plant root is regulated by the phytohormone auxin. Often, changes in auxin concentration are attributed to changes in shoot-derived long distance auxin flow. However, recent evidence suggests important contributions by short distance auxin transport from local storage and local auxin biosynthesis, conjugation and oxidation during abiotic stress. Here, we discuss current knowledge on long distance auxin transport in stress responses and subsequently debate how short distance auxin transport and IAA metabolism play a role in influencing eventual auxin accumulation and signalling patterns. Our analysis stresses the importance of considering all these components together and highlights the use of mathematical modelling for predictions of plant physiological responses.

**Auxin on the move during stress**

Drought and increasing salinity are abiotic stresses that cause major decreases in crop yield worldwide. Drought causes loss of crops through water deficit, whereas increasing soil salinity induces osmotic and ionic stress in the plants. Both abiotic stresses are a threat to the amount of arable land fit for our food production. Although the development of crops tolerant to these conditions has received attention [1], more research focus has been on generating biotic stress resistance and increasing yield of edible parts of the plant. Now that we face a rapid deterioration of arable land, research on the tolerance to abiotic stresses has substantially increased. Phenotypic plasticity, including developmental modifications to root system architecture (RSA), are vital for tolerance to water deficiency and high soil salinity.

RSA and root growth rates during plant development under optimal conditions have been well studied and it has long been established that these require the phytohormone **auxin**. Recently our fundamental understanding of root developmental plasticity during abiotic stress has markedly improved [2]. Unsurprisingly, auxin plays an important role during abiotic stress-induced changes in the root. Through the creation of local auxin maxima, cell elongation is locally inhibited and the emergence of lateral roots can be arrested. On the other hand, local auxin minima were found to be a signal that triggers the transition from cell division to cell differentiation in Arabidopsis roots [3]. Different processes that together determine auxin-mediated regulation of growth and development during abiotic stress are auxin transport, biosynthesis, **conjugation**, perception and signalling. Auxin transport has received much attention and the role of Polar Auxin Transport (PAT) by auxin carrier proteins during unstressed conditions and gravitropism has been well established [4-6]. By contrast, the changes in PAT during abiotic stresses remain largely unknown. How changes in local auxin biosynthesis and conjugation of auxin during abiotic stress affect root responses is another relatively young field of research. The integration of all these different aspects of auxin homeostasis is complicated, because of the many involved factors all influencing each other and the crosstalk between auxin and other hormones. One promising solution to this problem is the quickly emerging field of computational modelling of the auxin processes in the plant root.

6
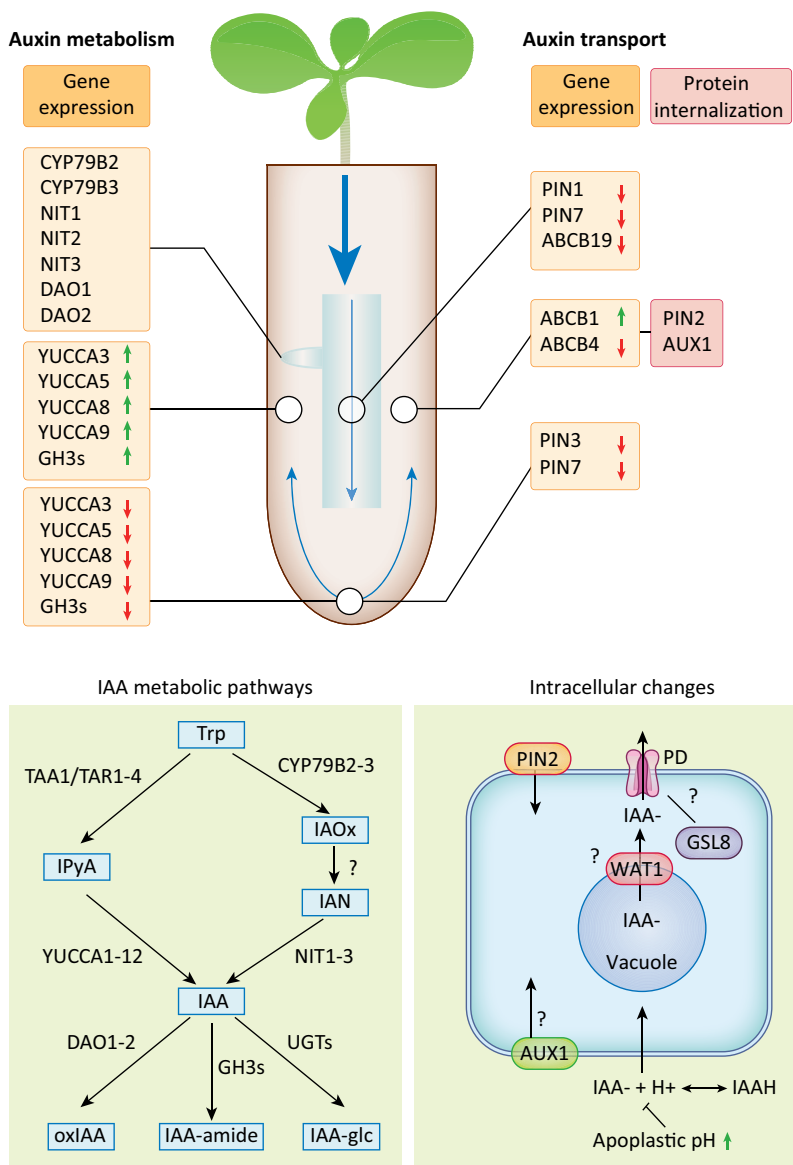
**Figure 1. Schematic overview of salt-stress induced changes in auxin bio-synthesis, conjugation and transport related processes in the root of Arabidopsis.**

**IAA metabolism (A):** The level of IAA is tightly regulated by IAA biosynthesis, IAA conjugation and degradation, together determining the IAA status of a cell. The lower panel shows part of the known IAA biosynthesis (for a complete overview see [21, 22]) and conjugation pathways and the known involved genes or gene families. Based on micro-array data of two different studies (see supplemental table 1), we have identified gene expression patterns with promising possibilities for influencing eventual IAA accumulation patterns and signalling. For genes in the IAOx pathway, we observe strong expression in zone 4 (see figure 2C), which is the zone containing primordia and lateral roots. All genes are also influenced by salt stress in a time depended matter (see supplemental table 1). We see a similar pattern for DAO1 and DAO2. Both DAO1 and CYP79B2-3 have been linked to lateral root development and show expression specifically underlying newly formed lateral roots. YUCCA 3, 5, 8 and 9 together with the GH3 family genes show up regulation in the epidermis and cortex during salt stress whereas they are down regulated in the columnella (see figure

2B). **Auxin transport (B):** During salt stress, expression of the auxin efflux carriers PIN1, PIN7 and ABCB19 in the stele is down regulated. In the columnella, PIN3 and PIN7 are downregulated. In epidermal and cortical cells, PIN2 and ABCB4 auxin efflux carriers are down-regulated where ABCB1 is slightly up-regulated. In epidermal cells, on a cellular level, PIN2 is internalized and changes in AUX1 abundance at the plasma membrane during halotropism were observed, providing evidence that AUX1 is also being internalized [9]. Putatively, the activity of the tonoplast located WAT1 undergoes changes to alter intracellular auxin levels following a change in cytosolic pH. In order to create local auxin maxima, the passive flow of IAA- molecules through the plasmodesmata (PD) might need to be blocked. This is putatively achieved through GSL8-mediated callose deposition. The apoplastic pH increase following salt exposure of the root potentially inhibits the passive influx of IAAH into the cell. Blue arrows depict auxin flow, grey boxes show up (green arrow) or down (red arrow) regulation of genes during salt stress. Black boxes show plasma membrane proteins that are internalized upon salt stress. Question marks show processes that influence local auxin concentrations but have not yet been proven to be involved in local auxin changes during abiotic stress.

## Auxin Transport from shoot to root

The main mechanism to maintain the "upside-down fountain" auxin flow in the root is PAT. Emphasizing the role of long distance shoot derived auxin transport in abiotic stress are recent advancements in the understanding of the changes in auxin carrier proteins and other proteins influencing auxin flow in the root (Figure 1). Internalisation of the auxin efflux carrier PIN-formed 2 (PIN2) either during **halotropism** on the side of the root facing a higher salt concentration [7] , or during osmotic stress treatments [8] has been shown. Subsequently, combining *in planta* salt stress experiments with computational modelling, it was concluded that internalisation of PIN2 is not sufficient to explain the alteration of auxin flow during halotropism [9], and changes in PIN-formed 1 (PIN1) and Auxin transporter protein 1 (AUX1) were shown to co-facilitate the fast change of auxin flow. Besides root growth, auxin efflux carriers are suggested to regulate meristem size during salt stress [10]. Lower PIN1, PIN3 and PIN7 expression and Auxin Resistant 3 (AXR3)/Indole-3-Acetic Acid 17 (IAA17) stabilization during salt stress are proposed to influence the root meristem size through increasing NO levels.

Another large family of auxin carriers influencing auxin flow in the root is the ABCB transporter family [11]. Recently, several studies have shown a role for ABCB transporters during salt stress. Out of 22 different ABCB transporters in rice (*Oryza sativum*), expression of 21 was found to change in response to salinity and drought [12, 13]. Of the root-expressed ABCB auxin transporters, expression of ABCB1 and 19 was slightly up-regulated, whereas ABCB 4 showed down-regulation after one hour of salt stress. Reduced **acropetal** auxin transport was observed in an *abcb19* null mutant while **basipetal** transport was unaltered [14].

Other genes, whose loss of function mutants were recently observed to exhibit altered auxin flow in the root, are putatively involved in abiotic stress tolerance. Mutants of InteractoR Of SYnaptotagmin 1 (ROSY1-1) showed a decrease in basipetal auxin transport and exhibited increased salt tolerance, which was ascribed to the interaction between ROSY1-1 and Synaptotagin-1 (SYT1) [15]. Furthermore, Zinc-Induced Facilitator-Like 1 (ZIFL1), a Major Facilitator Superfamily (MFS) transporter regulates shootward auxin efflux in the root [16]. *zifl1* loss of function mutants were observed to

have lower PIN2 protein abundance in epidermal root cells after external application of IAA and had gravitropic bending defects.

**Auxin transport from close by**

Changes in auxin transport between different intracellular compartments also influences the auxin available for the formation of local auxin maxima. Auxin located in the acidic vacuole, with a pH of 5.0 to 5.5, will tend to move towards the cytosol which has a pH of approximately 7. During salt stress the cytosolic pH drops [17], thus theoretically reducing the passive auxin efflux from the vacuole. Apoplastic pH is also suggested to be involved in passive auxin influx into the cells (see Box 1).

Isolated vacuoles from protoplasts lacking the tonoplast located auxin carrier Walls Are Thin 1 (WAT1) were found to accumulate significantly more radiolabelled auxin than wildtype vacuoles, indicating active transport of auxin from the vacuole to the cytoplasm by WAT1 [18]. Recently, an auxin transport facilitator family, located on the endoplasmic reticulum (ER) was identified. PIN-likes (PILS) are believed to be involved in auxin homeostasis through auxin accumulation at the ER, in this way limiting the IAA available for nuclear auxin signalling. The change in available IAA alters the cells sensitivity to auxin. Also, a higher auxin export from *pils2/pils5* protoplast cells was observed [19]. In addition, a *pils2* Arabidopsis mutant, and even more so in a *pils2/pils5* double mutant, showed significantly longer roots than wildtype and a higher lateral root density, suggesting involvement in auxin dependent root growth.

Other forms of passive auxin transport include movement without the interference of membranes. IAA is a small molecule and is therefore able to move freely through the plasmodesmata (PD) in its ionized form (IAA-). To restrict free cell-to-cell movement of IAA during auxin gradient formation, GLUCAN SYNTHASE LIKE 8 (GSL8) induces an increase of plasmodesmal-localized callose. This reduces the symplasmic permeability to maintain local auxin maxima [20]. GSL8 expression was found to be up-regulated by adding exogenous IAA. Although these results show the importance of local auxin movement, the relation to abiotic stress remains to be elucidated.

*Controlling the levels of auxin*
Besides transport, the levels of auxin (IAA) are determined by biosynthesis and conjugation. Both processes have recently shown to be affected by abiotic stress in the root.

Although a number of IAA biosynthesis pathways has been described [21, 22], the indole-3-pyruvic acid (IPyA) pathway is considered to be responsible for most IAA biosynthesis in higher plants [23, 24]. In addition, for the Brassicaceae family, the indole-3-acetaldoxime (IAOx) pathway has been increasingly identified to play a role during several stress responses [25-27], whereas the significance of the other pathways is still under debate and needs further research [21, 22]. Here, we will focus on the IPyA and IAOx pathways and how these pathways are modulated during abiotic stress.

*Box 1. Apoplastic pH and auxin movement*

Auxin transport is, next to active processes, dependent on passive movement of IAA into or between cells and movement through the apoplast. Auxin concentration influences apoplastic pH, which in turn influences passive auxin transport into cells. In roots, high cellular auxin concentrations inhibit cell elongation. While in the shoot, in accordance with the acid growth theory, auxin causes cell elongation [66, 67].

The effect of auxin on apoplastic pH has been shown by the addition of exogenous auxin to arabidopsis roots, which induced a fast alkanization of the apoplast [68]. However, after prolonged exposure (8 hours) the root apoplast becomes acidified. Similarly, an initial alkanization of the apoplast followed by acidification after 19 hours was found when endogenous auxin levels were elevated by induced expression of YUCCA6 [68]. Barbez and colleagues continue to show that the cell wall acidification triggers cell elongation in A. thaliana seedlings. Their data implies that endogenous auxin concentrations regulate apoplast acidification which in turn regulates cell elongation. During exposure of roots to a salt gradient, auxin redistributes in the root [7, 69], suggesting local alterations in apoplastic pH levels during salt stress might influence cell elongation. In addition, following one hour of NaCl exposure of the root, a transient increase in apoplastic pH was observed [17]. One hour after the transient increase in apoplastic pH upon a 100mM NaCl pulse, the apoplastic pH was back to control levels. The cytoplasmic pH slightly decreased upon NaCl exposure but did not recover. The changes in passive auxin transport as a result of this alteration in apoplast pH have never been studied in vivo. Nonetheless, a mathematical/computational model linking auxin and pH dynamics has been created [61]. The main conclusions from this model are that long-term auxin-induced apoplast acidification leads to an increase of all auxin transport over the plasma membrane and significantly higher auxin concentrations in the cytoplasm. However, it has also been reported that the passive auxin influx would be negligible at low apoplastic pH (<5,7) in protoplasts [70]. This would mean that all changes in intracellular auxin levels would be through active auxin transport and there is no role for passive auxin transport in pH induced alteration of cell elongation during abiotic stress. In vivo measurements of cellular auxin in- and efflux during apoplast acidification are required to elucidate the role of passive auxin transport over the plasma membrane.

**6**

The IPyA pathway (see figure 1) generates IAA via a two-step conversion from tryptophan with IPyA as intermediate [27-29]. The family of YUCCA proteins governs the second step of the pathway [27]. Eleven YUCCA isoforms have been described in Arabidopsis and specific roles for several YUCCAs are slowly being elucidated. The YUCCAs can be divided in mainly root or shoot active proteins [30, 31]. YUC3, 5, 7, 8 and 9 display distinct expression patterns in the root, whereas other YUCCAs show minor or no expression in the root [30]. This illustrates the specificity of different genes in this pathway for specific developmental processes. Although little research on the specificity of YUCCAs for different stresses has been done, several gene expression studies do indicate this specificity. For example, YUC2, 5, 8 and 9 show upregulation in plants experiencing shade [32] and the knock-out mutant of those 4 YUCCAs lacks

shade induced hypocotyl elongation [33]. Several papers show that overexpression of the IPyA pathway leads to increased salt tolerance in several species [34-36]. For example, it was shown that in cucumber specific YUCCAs are expressed in high and low temperature and in response to salinity [36]. In salinity, CsYUC10b is strongly upregulated and CsYUC10a and CsYUC11 are strongly downregulated, whereas overexpression of CsYUC11 leads to higher salinity tolerance [36]. For Arabidopsis, the role of specific YUCCAs during salt stress is so far unknown. Analysis of previously published micro-array data [37, 38] confirms the root specificity of YUC3, 5, 8 and 9 (supplemental table 1). Furthermore, tissue-specific micro-array data indicates a shift from strong expression of YUCCAs in columnella during control to strong expression in the epidermis and cortex during salt stress (figure 1 & 2A, supplemental table 1). As expression of YUCCAs is low in the epidermis and cortex in control conditions and thus auxin levels in these cells would mainly depend on transport, this is an interesting shift. As salt stress also has major effects on auxin transport, epidermal biosynthesis likely affects auxin distribution during stress and is expected to have consequences for growth responses in the root.

The IAOx pathway (see figure 1) is brassica specific and has mostly been described for its role in secondary metabolism, producing both indole glucosinolates and camalexin [27, 39-41]. However, more recently, several papers have pointed out a possible involvement of this pathway in local IAA production, specifically in stress conditions [25-27, 42]. Sugawara et al. showed that when plants were fed $^{13}C_6$-labeled IAOx, 40% of the $^{13}C_6$ atoms was incorporated into IAA, confirming that IAA can be formed from IAOx [42]. ln 2002, Zhao et al. showed that a *cyp79b2cyp79b3* double knock-out mutant showed reduced growth and reduced IAA production specifically under higher temperatures [27]. Recently, the same mutant was observed to have decreased lateral root growth during salt stress [25]. Whereas the IPyA pathway is mainly active in the differentiation and elongation zone of the main (and lateral) root, genes in the IAOx pathway are, next to expression in the QC, strongly expressed in cells underlying newly developing lateral roots and lateral root primordia [43]. In accordance, all genes described in this pathway show strong expression in the differentiation zone (figure 2A-B, supplemental table 1) and their expression during salt stress is strongly time dependent (supplemental table 1), suggesting a major role for this pathway in salt regulated lateral root development in Arabidopsis.

Levels of free IAA are tightly regulated by several conjugation and degradation processes (Figure 1) [44]. Although IAA itself is both the active and transported compound in plants, it has a very high turn-over. *In planta*, the level of IAA conjugates and catabolites is strongly correlated with the level of free IAA in both root and shoot, showing high levels of conjugates and catabolites when high levels of free IAA occur [45, 46]. Levels of IAA catabolites are in general higher than free IAA [45]. The strict regulation of free IAA levels is nicely illustrated by analysis of mutants in specific conjugation pathways, as lower conjugation via one pathway often leads to higher conjugation in other pathways and only minor changes in free IAA levels [47].
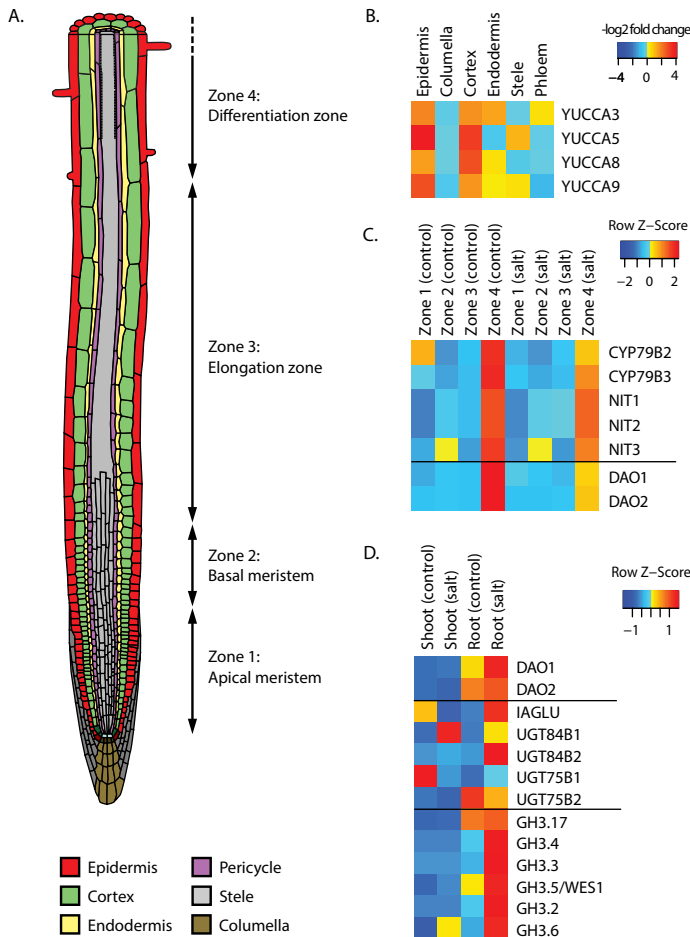
**Figure 2. Illustration of gene expression of auxin homeostasis related genes showing patterns that could be relevant for IAA accumulation patterns in abiotic stress.** (**A**) Heatmaps are based on micro-array data of two different studies (see supplemental table 1, [37, 38]). For tissue-specific and zone specific expression patterns, the root has been divided in different tissues and in 4 different root zones, as illustrated. Figure has been adapted from [73] (**B**) Heatmap of the relative expression (log2 fold change) upon salt stress of YUC3, 5, 8 and 9 in different root tissues. (**C**) Heatmap of expression of genes in the IAOx pathway and oxidation in different root zones during control and salt stress. The heatmap is normalized per gene. (**D**) Heatmap of expression of IAA conjugation involved genes in shoot and root during control and salt stress. The heatmap is normalized per gene.

Ester conjugation is mainly governed by several UDP-glucosyltransferase (UGTs). In supplemental table 1 we have summarized the UGTs currently known to conjugate IAA, but this list is probably not complete. These enzymes respond differently to salt stress (Figure 2C, supplemental table 1), which might point at specific roles for specific UGTs.

A group of Gretchen Hagen 3 (GH3) family member enzymes form amide conjugates of IAA [48]. All involved GH3s appear to be strongly expressed in roots and are upregulated upon salt stress (Figure 1C, supplemental table 1). In addition, GH3.5/ WES1 is induced by many abiotic and biotic stresses and by ABA treatment [49]. Interestingly, upregulation of GH3s upon salt seems to be specific to epidermis, comparable to upregulation of YUCCAs.

Oxidation is responsible for most IAA turn-over and leads to degradation of the compound [50]. Plants contain 10-100 times more oxIAA than IAA conjugates, showing that the oxidation pathway is very active [45]. Two DIOXYGENASE FOR AUXIN OXIDATION (DAO1 and DAO2) enzymes have been described to be responsible for the first step of oxidation [51, 52]. DAO1 and 2 show strong expression in zone 4, similar to genes in the IAOx pathway (see figure 2B, supplemental table 1). Zhang et al. (2016) has shown that DAO1 is expressed in cells underlying newly developing lateral roots and that the knock-out has increased lateral root density [52], indicating a possible role for IAA oxidation in root responses to salt stress.

Next to the main auxin IAA, 3 other auxins have been described [53]. Among those, only IBA has clearly shown to be of importance in (root) development [54]. For example, oscillations in IBA production determine pre-branch sites, cells that possibly can form lateral roots in later developmental stages [55, 56]. IBA can, just like IAA, be conjugated. In addition, it can be converted to IAA and possibly back [57]. IBA and its conjugates are thereby also a possible storage form of IAA and can influence IAA homeostasis. Conjugation of IBA has been shown to affect salt tolerance, as overexpression of UGT74E2, an IBA conjugating enzyme, leads to increased salt tolerance [58]. Whether IBA directly or indirectly – as a storage form of IAA – plays a role remains to be elucidated.

These examples show the importance of including IAA biosynthesis, conjugation and degradation in the bigger picture of auxin homeostasis and accumulation, as these processes might play major roles in specific regulation of local auxin-mediated responses. However, the wide range of IAA metabolic pathways and involved enzymes and their response to salt stress, shows the complexity of interpreting and predicting changes in auxin homeostasis. If we combine this complexity with the observed changes in auxin transport and auxin signalling, predicting the effect of changes in any of these steps can be daunting. More knowledge on specific regulation of biosynthesis and conjugation enzymes, together with a more comprehensive view of all processed affecting auxin levels and response, will greatly improve our eventual power in predicting the effects of changes in these different components. Incorporation of IAA metabolic pathways into models will also be a great leap forward for predicting auxin accumulation patterns inside the plant, as both processes, in addition to auxin transport, might interfere with auxin levels.

*Box 2. Important advances in root modelling*

In order to create a realistic root model for reliable predictions about changes in auxin flow and local auxin concentrations, several model characteristics need improvement. Two things that help towards perfecting static 2D models of the root are a realistic root shape and known auxin feedback loops. Van den Berg et al., (2016) have shown that both root shape and auxin feedback are important to show experimentally observed changes in auxin flow during halotropism [9].

Another characteristic of the models that needs advancement is movement. While informative in short term changes, predictions by static models become less realistic over time because they lack the changes in local auxin maxima needed for or caused by growth and bending. Interestingly, recently growing and bending root models have been realised. For example, a model describing a growing and bending root in which local changes in auxin concentrations can be predicted by changing the dynamics of PIN polarization under influence of changing elastic fields due to root bending was made [71]. Similar to existing experimental data, the auxin concentration was highest at the maximum curvature in the root.

Comparable to growing versus static models, the 2D models that are being used now to make predictions of auxin levels are valuable, however ideally we would want to use a 3D model. Due to the high complexity, not many 3D root models have been attempted. And the ones that are available have yet to incorporate many factors. One such 3D model which aims to simulate lateral root emergence through LAX3 and PIN3 modelling has been published [72]. The three-dimensional mathematical model incorporates LAX3 expression and auxin transport. It was found that for the experimentally observed LAX3 spatial expression to be robust, auxin inducible activity of the PIN3 efflux carrier is required. Consecutive induction of LAX3 and PIN3 ensures stable LAX3 expression.

### Understanding auxin's share in stress responses through computational modelling

6

Predicting the overall role and impact of auxin biosynthesis and short distance transport compared to long-distance transport in the plant root during development and stress response is a complex process, despite improvements in the sensitivity of *in vivo* auxin reporters [59]. To integrate all components of the different processes affecting local auxin levels, the computational strength of mathematical modelling has been proven to be helpful. Many different models concerning auxin or related processes have been created [60].

While highly instrumental, the current root models have not yet incorporated all relevant parameters and are generally too static to accurately predict the magnitude of the influence of local auxin biosynthesis, conjugation, short- and long distance transport on the roots stress response over longer time periods. Interestingly, recent advantages in root modelling show promising results to help overcome these issues (see Box 2).

Nonetheless, many valuable insights concerning short distance auxin transport have come from computational modelling. Up until today, most computer models are either analytic one-cell models or describe overall changes in the whole root. Both have shown to be informative in their own way. For the interplay between auxin and pH, Steinacher *et al.* (2012) predict the effect of auxin on intra- and extracellular pH and how this in turn affects auxin concentrations [61]. Their main findings point towards a role for auxin activated proton pumps, which alter proton fluxes affecting auxin transport. By combining the chemiosmotic hypothesis of auxin transport with auxin-induced apoplastic acidification (AAA) they predict increased influx and efflux of auxin resulting in higher cytosolic auxin concentrations. Another recent single cell computational model involving lateral root emergence shows the value of computational modelling in local processes involving lateral roots. Mellor *et al.* (2015) show that an experimentally observed 'all-or-nothing' Auxin transporter-like protein 3 (LAX3) expression pattern may be explained by bi-stability to create a genetic 'switch' [62]. The model was found to agree with the experimental data only when the exogenously added auxin was decreased over time, suggesting auxin conjugation and subsequent degradation. This observation nicely shows the added value of modelling.

An example of the relevance of incorporation of auxin conjugation and degradation into auxin computational modelling is a mathematical model describing GH3-mediated auxin conjugation [63]. The model includes the up-regulation of GH3 by auxin, thus regulating its own degradation, and positive feedback of auxin on the LAX3 influx carrier. The model predicts oscillation of GH3 and LAX3 mRNA levels after an extracellular auxin increase. Also, the initial predicted increase of GH3 suggests a possible cellular mechanism to protect cell auxin homeostasis during extracellular auxin changes.

To increase our understanding of long distance auxin transport, Mitchison *et al.* showed in a single cell model that combinations of changes in auxin carriers are necessary to mimic experimentally observed auxin flows [64]. Similarly, van den Berg *et al.* and Moore *et al.* show in a whole root model the importance of changes in auxin influx carriers next to efflux carriers for altered auxin flow [9, 65].

Up to date, a model incorporating the changes in auxin biosynthesis and interplay between the different synthesis pathways has yet to be made. This follows logically from the fact that much about auxin biosynthesis is still unknown. However, for the full understanding of changes of auxin in the root during stress the incorporation of realistic changes in auxin synthesis are necessary.

Nonetheless, multiple studies have now shown model predictions supporting experimental data and have given suggestions for follow-up experiments. Where *in planta* experiments take up a lot of time in creating the tools to change single parameters, multiple parameters are easily changed in the models and putative regulators of auxin flow can be found. These regulators can then be verified by *in planta* experiments. Ideally, a growing and bending model incorporating as many factors as possible - different auxin carriers, hormonal feedback, mechanical feedback, pH changes and the ability to simulate different stresses - would be used to make predictions about growth

rate and direction during abiotic stress. Next to that, what modern models are still missing is the ability to show changes in RSA during stress. To elucidate the mechanisms behind different RSA strategies during different abiotic stresses, a model incorporating LR emergence and growth through the prediction of the local auxin concentrations is required. Again, such a complex model would have to take into account a lot of factors dealing with local auxin maxima around LRP's. Looking at the future of research on complex biological processes, such as the auxin machinery in the plant root, it becomes clear that the field of mathematical modelling will be playing a key role.

6

## REFERENCES

1    Mickelbart, M.V.*, et al.* (2015) Genetic mechanisms of abiotic stress tolerance that translate to crop yield stability. *Nat Rev Genet* 16, 237-251

2    Koevoets, I.T.*, et al.* (2016) Roots Withstanding their Environment: Exploiting Root System Architecture Responses to Abiotic Stress to Improve Crop Tolerance. *Frontiers in plant science* 7, 1335

3    Di Mambro, R.*, et al.* (2017) Auxin minimum triggers the developmental switch from cell division to cell differentiation in the Arabidopsis root. *Proceedings of the National Academy of Sciences of the United States of America* 114, E7641-E7649

4    Adamowski, M. and Friml, J. (2015) PIN-dependent auxin transport: action, regulation, and evolution. *The Plant cell* 27, 20-32

5    Naramoto, S. (2017) Polar transport in plants mediated by membrane transporters: focus on mechanisms of polar auxin transport. *Curr Opin Plant Biol* 40, 8-14

6    Armengot, L.*, et al.* (2016) Regulation of polar auxin transport by protein and lipid kinases. *Journal of experimental botany* 67, 4015-4037

7    Galvan-Ampudia, C.S.*, et al.* (2013) Halotropism is a response of plant roots to avoid a saline environment. *Current biology : CB* 23, 2044-2050

8    Zwiewka, M.*, et al.* (2015) Osmotic Stress Modulates the Balance between Exocytosis and Clathrin-Mediated Endocytosis in Arabidopsis thaliana. *Molecular plant* 8, 1175-1187

9    van den Berg, T.*, et al.* (2016) Modeling halotropism: a key role for root tip architecture and reflux loop remodeling in redistributing auxin. *Development* 143, 3350-3362

10   Liu, W.*, et al.* (2015) Salt stress reduces root meristem size by nitric oxide-mediated modulation of auxin accumulation and signaling in Arabidopsis. *Plant physiology* 168, 343-356

11   Geisler, M.*, et al.* (2017) A Critical View on ABC Transporters and Their Interacting Partners in Auxin Transport. *Plant Cell Physiol* 58, 1601-1614

12   Chai, C. and Subudhi, P.K. (2016) Comprehensive Analysis and Expression Profiling of the OsLAX and OsABCB Auxin Transporter Gene Families in Rice (Oryza sativa) under Phytohormone Stimuli and Abiotic Stresses. *Frontiers in plant science* 7, 593

13   Han, E.H.*, et al.* (2017) 'Bending' models of halotropism: incorporating protein phosphatase 2A, ABCB transporters, and auxin metabolism. *Journal of experimental botany* 68, 3071-3089

14   Cho, M.*, et al.* (2014) Block of ATP-binding cassette B19 ion channel activity by 5-nitro-2-(3-phenylpropylamino)-benzoic acid impairs polar auxin transport and root gravitropism. *Plant physiology* 166, 2091-2099

15   Dalal, J.*, et al.* (2016) ROSY1, a novel regulator of gravitropic response is a stigmasterol binding protein. *Journal of plant physiology* 196-197, 28-40

16   Remy, E.*, et al.* (2013) A major facilitator superfamily transporter plays a dual role in polar auxin transport and drought stress tolerance in Arabidopsis. *The Plant cell* 25, 901-926

17    Gao, D., *et al.* (2004) Self-reporting Arabidopsis expressing pH and [Ca2+] indicators unveil ion dynamics in the cytoplasm and in the apoplast under abiotic stress. *Plant physiology* 134, 898-908

18    Ranocha, P., *et al.* (2013) Arabidopsis WAT1 is a vacuolar auxin transport facilitator required for auxin homoeostasis. *Nat Commun* 4, 2625

19    Barbez, E., *et al.* (2012) A novel putative auxin carrier family regulates intracellular auxin homeostasis in plants. *Nature* 485, 119-122

20    Han, X., *et al.* (2014) Auxin-callose-mediated plasmodesmal gating is essential for tropic auxin gradient formation and signaling. *Developmental cell* 28, 132-146

21    Di, D.-W., *et al.* (2015) The biosynthesis of auxin: how many paths truly lead to IAA? *Plant Growth Regulation* 78, 275-285

22    Tivendale, N.D., *et al.* (2014) The shifting paradigms of auxin biosynthesis. *Trends in plant science* 19, 44-51

23    Mashiguchi, K., Tanaka, K., Sakai, T., Sugawara, S., Kawaide, H., Natsume, M., ... & McSteen, P. (2011) The main auxin biosynthesis pathway in Arabidopsis. *Proceedings of the National Academy of Sciences of the United States of America* 108, 18512-18517

24    Won, C., Shen, X., Mashiguchi, K., Zheng, Z., Dai, X., Cheng, Y., ... & Zhao, Y. (2011) Conversion of tryptophan to indole-3-acetic acid by TRYPTOPHAN AMINOTRANSFERASES OF ARABIDOPSIS and YUCCAs in Arabidopsis. *Proceedings of the National Academy of Sciences of the United States of America* 108, 18518-18523

25    Julkowska, M.M., *et al.* (2017) Genetic Components of Root Architecture Remodeling in Response to Salt Stress. *The Plant cell* 29, 3198-3213

26    Lehmann, T., *et al.* (2017) Arabidopsis NITRILASE 1 Contributes to the Regulation of Root Growth and Development through Modulation of Auxin Biosynthesis in Seedlings. *Frontiers in plant science* 8, 36

27    Zhao, Y., Hull, A. K., Gupta, N. R., Goss, K. A., Alonso, J., Ecker, J. R., ... & Celenza, J. L. (2002) Trp-dependent auxin biosynthesis in Arabidopsis: involvement of cytochrome P450s CYP79B2 and CYP79B3. *Genome research* 16, 3100-3112

28    Stepanova, A.N., *et al.* (2008) TAA1-mediated auxin biosynthesis is essential for hormone crosstalk and plant development. *Cell* 133, 177-191

29    Tao, Y., *et al.* (2008) Rapid synthesis of auxin via a new tryptophan-dependent pathway is required for shade avoidance in plants. *Cell* 133, 164-176

30    Chen, Q., *et al.* (2014) Auxin overproduction in shoots cannot rescue auxin deficiencies in Arabidopsis roots. *Plant Cell Physiol* 55, 1072-1079

31    Cheng, Y., *et al.* (2006) Auxin biosynthesis by the YUCCA flavin monooxygenases controls the formation of floral organs and vascular tissues in Arabidopsis. *Genes & development* 20, 1790-1799

32    Li, L., *et al.* (2012) Linking photoreceptor excitation to changes in plant architecture. *Genes & development* 26, 785-790

33    Nozue, K., *et al.* (2015) Shade avoidance components and pathways in adult plants revealed by phenotypic profiling. *PLoS Genet* 11, e1004953

6

34      Ke, Q*., et al.* (2015) Transgenic poplar expressing Arabidopsis YUCCA6 exhibits auxin-overproduction phenotypes and increased tolerance to abiotic stress. *Plant Physiol Biochem* 94, 19-27

35      Kim, J.I*., et al.* (2013) Overexpression of Arabidopsis YUCCA6 in potato results in high-auxin developmental phenotypes and enhanced resistance to water deficit. *Molecular plant* 6, 337-349

36      Yan, S*., et al.* (2016) Different cucumber CsYUC genes regulate response to abiotic stresses and flower development. *Sci Rep* 6, 20760

37      Dinneny, J.R*., et al.* (2008) Cell Identity Mediates the Response of Arabidopsis Roots to Abiotic Stress. *Science* 320, 942-945

38      Kilian, J*., et al.* (2007) The AtGenExpress global stress expression data set: protocols, evaluation and model data analysis of UV-B light, drought and cold stress responses. *The Plant journal : for cell and molecular biology* 50, 347-363

39      Glawischnig, E., Hansen, B. G., Olsen, C. E., & Halkier, B. A. (2004) Camalexin is synthesized from indole-3-acetaldoxime, a key branching point between primary and secondary metabolism in Arabidopsis. *Proceedings of the National Academy of Sciences of the United States of America* 101, 8245-8250

40      Hull, A.K*., et al.* (1999) Arabidopsis cytochrome P450s that catalyze the first step of tryptophan-dependent indole-3-acetic acid biosynthesis. *Proceedings of the National Academy of Sciences of the United States of America* 97, 2379–2384

41      Mikkelsen, M.D*., et al.* (2000) Cytochrome P450 CYP79B2 from Arabidopsis catalyzes the conversion of tryptophan to indole-3-acetaldoxime, a precursor of indole glucosinolates and indole-3-acetic acid. *The Journal of biological chemistry* 275, 33712-33717

42      Sugawara, S*., et al.* (2009) Biochemical analyses of indole-3-acetaldoximedependent auxin biosynthesis in Arabidopsis. *Proceedings of the National Academy of Sciences of the United States of America* 106, 5430-5435

43      Ljung, K*., et al.* (2005) Sites and regulation of auxin biosynthesis in Arabidopsis roots. *The Plant cell* 17, 1090-1104

44      Ludwig-Muller, J. (2011) Auxin conjugates: their role for plant development and in the evolution of land plants. *Journal of experimental botany* 62, 1757-1773

45      Kowalczyk, M. and Sandberg, G. (2001) Quantitative Analysis of Indole-3-Acetic Acid Metabolites in Arabidopsis. *Plant physiology* 127, 1845-1853

46      Östin, A., Kowalyczk, M., Bhalerao, R.P., and Sandberg, G. (1998) Metabolism of Indole-3-Acetic Acid in Arabidopsis. *Plant physiology* 118, 285-296

47      Mellor, N*., et al.* (2016) Dynamic regulation of auxin oxidase and conjugating enzymes AtDAO1 and GH3 modulates auxin homeostasis. *Proceedings of the National Academy of Sciences of the United States of America* 113, 11022-11027

48      Staswick, P.E*., et al.* (2005) Characterization of an Arabidopsis enzyme family that conjugates amino acids to indole-3-acetic acid. *The Plant cell* 17, 616-627

49      Park, J.E*., et al.* (2007) GH3-mediated auxin homeostasis links growth regulation with stress adaptation response in Arabidopsis. *The Journal of biological chemistry* 282, 10036-10046

50    Zhang, J. and Peer, W.A. (2017) Auxin homeostasis: the DAO of catabolism. *Journal of experimental botany* 68, 3145-3154

51    Porco, S*., et al.* (2016) Dioxygenase-encoding AtDAO1 gene controls IAA oxidation and homeostasis in Arabidopsis. *Proceedings of the National Academy of Sciences of the United States of America* 113, 11016-11021

52    Zhang, J*., et al.* (2016) DAO1 catalyzes temporal and tissue-specific oxidative inactivation of auxin in Arabidopsis thaliana. *Proceedings of the National Academy of Sciences of the United States of America* 113, 11010-11015

53    Simon, S. and Petrasek, J. (2011) Why plants need more than one type of auxin. *Plant Sci* 180, 454-460

54    Frick, E.M. and Strader, L.C. (2018) Roles for IBA-derived auxin in plant development. *Journal of experimental botany* 69, 169-177

55    De Rybel, B*., et al.* (2012) A role for the root cap in root branching revealed by the non-auxin probe naxillin. *Nat Chem Biol* 8, 798-805

56    Xuan, W*., et al.* (2015) Root Cap-Derived Auxin Pre-patterns the Longitudinal Axis of the Arabidopsis Root. *Current biology : CB* 25, 1381-1388

57    Liu, X*., et al.* (2012) Transport of indole-3-butyric acid and indole-3-acetic acid in Arabidopsis hypocotyls using stable isotope labeling. *Plant physiology* 158, 1988-2000

58    Tognetti, V.B*., et al.* (2010) Perturbation of indole-3-butyric acid homeostasis by the UDP-glucosyltransferase UGT74E2 modulates Arabidopsis architecture and water stress tolerance. *The Plant cell* 22, 2660-2679

59    Liao, C.Y*., et al.* (2015) Reporters for sensitive and quantitative measurement of auxin response. *Nat Methods* 12, 207-210, 202 p following 210

60    Morales-Tapia, A. and Cruz-Ramirez, A. (2016) Computational Modeling of Auxin: A Foundation for Plant Engineering. *Frontiers in plant science* 7, 1881

61    Steinacher, A*., et al.* (2012) A computational model of auxin and pH dynamics in a single plant cell. *J Theor Biol* 296, 84-94

62    Mellor, N*., et al.* (2015) Modelling of Arabidopsis LAX3 expression suggests auxin homeostasis. *J Theor Biol* 366, 57-70

63    Mellor, N*., et al.* (2016) GH3-Mediated Auxin Conjugation Can Result in Either Transient or Oscillatory Transcriptional Auxin Responses. *Bull Math Biol* 78, 210-234

64    Mitchison, G. (2015) The Shape of an Auxin Pulse, and What It Tells Us about the Transport Mechanism. *PLoS Comput Biol* 11, e1004487

65    Moore, S*., et al.* (2017) A recovery principle provides insight into auxin pattern control in the Arabidopsis root. *Sci Rep* 7, 43004

66    Rayle, D.L.a.C., R. (1970) Enhancement of Wall Loosening and Elongation by Acid Solutions. *Plant physiology* 46, 250-253

67    Rayle, D.L.a.C., R. E. (1992) The Acid Growth Theory of Auxin-Induced Cell Elongation Is Alive and Well. *Plant physiology* 99, 1271-1274

68    Barbez, E*., et al.* (2017) Auxin steers root cell expansion via apoplastic pH regulation in Arabidopsis thaliana. *Proceedings of the National Academy of Sciences of the United States of America* 114, E4884-E4893

6

69    Wang, Y., *et al.* (2009) Auxin redistribution modulates plastic development of root system architecture under salt stress in Arabidopsis thaliana. *Journal of plant physiology* 166, 1637-1645

70    Rutschow, H.L., *et al.* (2014) The carrier AUXIN RESISTANT (AUX1) dominates auxin flux into Arabidopsis protoplasts. *The New phytologist* 204, 536-544

71    Romero-Arias, J.R., *et al.* (2017) Model of polar auxin transport coupled to mechanical forces retrieves robust morphogenesis along the Arabidopsis root. *Phys Rev E* 95, 032410

72    Peret, B., *et al.* (2013) Sequential induction of auxin efflux and influx carriers regulates lateral root emergence. *Mol Syst Biol* 9, 699

73    Peret, B. (2017) Primary and lateral root.ai. figshare

**CHAPTER 7**

# General Discussion

Salt stress is a major problem in agriculture. Although aboveground processes, such as flowering, are essential for high yield, the root system contains big potential to increase plants' ability to cope with salt stress. In **Chapter 2** we reviewed the current known functional responses to different abiotic stresses. Next, we exploited natural variation in Arabidopsis to find candidate genes involved in responses to salt stress in the root. Genome Wide Association Studies **(Chapter 3)** and the subsequent follow up experiments stressed the importance of the IAOx pathway **(Chapter 4)**, for maintaining lateral root development during salt stress. In **Chapter 5** we showed that also in the shoot auxin metabolism plays a role, in regulating timing of flowering in response to salt stress. In **chapter 6** we discussed how both auxin metabolism and transport are affected by salt stress and how mathematical modelling is key to further unravel these complex interactions. Here, I discuss two additional steps in future research expanding on this thesis: taking one step back (upstream regulation) and one step forward (salt tolerance).

### One step back: the power of knowing what is upstream

In **Chapter 3** and **Chapter 5** new candidate genes involved in the salt induced cellular regulatory networks have been identified. Both *CYP79B2*, involved in lateral root development, and *UGT74E2*, involved in the timing of flowering, encode enzymes that are part of auxin metabolic pathways. Interestingly, natural variation was found in the promoter of both genes, indicating differences in transcriptional regulation between accessions. Indeed, induction of both genes under salt stress correlated with either root architecture (*CYP79B2*) or bolting time (*UGT74E2).* Thus, natural variation in these promoters can provide nice molecular entries to further expand the regulatory networks known to be involved in salt stress.

In addition, *CYP79B2* was recently found as a target of Subclass 1 SnRK2 protein kinases, which function as regulators of the mRNA decay pathways (Kawa et al., 2020; Soma et al., 2017). Earlier, McLoughlin et al., (2012) showed that SnRK2.10 is expressed in the vasculature tissue underlying newly forming lateral roots, a pattern very similar to that of *CYP79B2* and *CYP79B3* (Ljung et al., 2005; Chapter 4). The knock-out phenotype of snrk2.4/2.10 (McLoughlin et al., 2012) is also highly similar to that of the double knock-out mutant *cyp79b2-2 cyp79b3-2* (Julkowska et al., 2017; Chapter 3). Last, the kinetics of SnRK2 protein kinase activity over time during salt stress is very similar to the expression levels of *CYP79B2* and *CYP79B3* (McLoughlin et al., 2012; Dinneny et al., 2008). It thus seems very probable that both genes are targets of the SnRK2-mRNA decay pathway. However, further research needs to investigate whether *CYP79B2* transcripts are direct targets of the SNRKs or whether other transcripts in turn affecting *CYP79B2* expression are targets of the decay machinery (Kawa et al., 2020). Regardless, the subclass 1 SnRK2 protein kinases offer a valuable new starting point for unraveling the upstream regulatory pathways of *CYP79B2* and the IAOx pathway. For *UGT74E2* we show in **Chapter 5** that a specific part of the promoter contains large variation between accessions and that this variation is linked to its expression. This region offers interesting starting points for further research by elucidating the action of

7

several predicted candidate transcription factors binding to this region, for finding the mechanisms involved in finetuning flowering time under salt stress.

**One step forward: the contribution of changes in the root system to salt tolerance**

With the research presented in this thesis we have expanded the current knowledge on adaptations of the root system architecture in Arabidopsis in response to salt stress. As discussed in **Chapter 2**, we expect these changes to be functional to cope with salt stress. A first indication of such a functional response is presented by Julkowska et al. (2014), who showed that the development of a high number of shorter lateral roots correlated with a lower $Na^+/K^+$ balance in the shoot. In **Chapter 3** we further study two candidate genes involved in regulating lateral root development during salt stress. Our data showed that the link between lateral root development and salt tolerance is not straightforward. Although enhanced *HKT1* expression in the root pericycle leads to both a reduction in lateral root length and number (Julkowska et al. (2017); Chapter 3), Møller et al., (2009) showed these same plants coped better with salt stress. Enhanced *HKT1* expression leads to exclusion of $Na^+$ from leaf tissue (Rus et al., 2006; Munns et al., 2012; Møller et al., 2009). Similarly, altered *CYP79B2* or *CYP79B3* expression, although affecting lateral roots, does not show a specific effect on growth in salt stress, but does affect the $Na^+/K^+$ balance in the shoot (Julkowska et al. 2017; Chapter 3). However, Kim et al., (2015) show that loss of function of *CYP79B2* and *CYP79B3* leads to increased phenylpropanoid accumulation. One of the major endproducts of the phenylpropanoid pathway is lignin, the main compound of the Casparian strip (Naseer et al., 2012). The Casparian strip not only limits uptake of sodium, but also limits loss of potassium (Pfister et al., 2014; Geldner, 2013). A change in lignification could have major effects on this balance. Separating the effect of the root system architecture changes and other changes in the plant thus proofs to be challenging, and further research is necessary to elucidate the link between root system architecture and salt tolerance.

A possible explanation for the observed correlation between shorter lateral roots and higher salt tolerance might be linked to alterations in the growth dynamics of plants in salt stress. Upon exposure to salt, lateral roots enter a quiescence phase, in which growth is arrested for one to two days (Duan et al., 2013). In addition, lateral root primordia are inhibited at stage 5 and 6 of their development (McLoughlin et al., 2012; Chapter 3). Quiescence is induced by abscisic acid (ABA), which is rapidly upregulated under salt stress due to the decrease in osmotic potential (Jia et al., 2002). ABA in turn induces DELLAs, which inhibit both gibberellin (GA) and brassinosteroid (BR) signalling (Gallego-Bartolome et al., 2012; Achard et al., 2006). Stress-induced reduction of growth has been shown to benefit the plant (Achard et al., 2006). It is thus proposed that the quiescence phase is essential to induce changes to cope with salt stress. The quiescence phase is followed by a partial growth recovery that is mainly guided by an increase in GA and BR levels (Geng et al., 2013). Research has shown that endodermal specific constitutive expression of ABA INSENSITIVE1 (abi1-1), a repressor of ABA signalling, can shorten the quiescence phase in both main and lateral roots (Geng et al., 2013; Duan et al., 2013). Accordingly, constitutive expression of BRASSINAZOLE

RESISTANT1 (bzr1-D), leading to enhanced BR signaling, shortens the quiescence phase and induces recovery of main root growth (Geng et al., 2013). Inhibition of GA biosynthesis with paclobutrazol strongly inhibits recovery of main root growth (Geng et al., 2013). This shows that the balance between hormones determines the growth dynamics under salt stress and the right balance is hypothesized to be essential for salt tolerance. In future research, it would be worth manipulating the growth dynamics by affecting hormone signaling pathways specifically in the root and the effect this has on salt tolerance.

Alternatively, the observed advantage of shorter lateral roots, might be related to a reduction in uptake area. The root system plays an essential role in preventing $Na^+$ from entering the vascular system and reaching the shoot. Lateral roots are optimally developed for water and nutrient uptake, but this capacity might make them the weakest part of the root system when preventing salt uptake. Inhibiting lateral root elongation might be favorable to decrease the area available for uptake, explaining why accessions with short lateral roots might take up less $Na^+$ and maintain a low $Na^+/K^+$ balance. Salt enters the root system either through the apoplast or through the symplast. In the apoplast, the Casparian strip serves as a barrier for ion and nutrient leakage and in rice it has been shown to block $Na^+$ uptake (Geldner, 2013; Krishnamurthy et al., 2011, 2009; Barberon et al., 2016). In response to salt, the Casparian strip in the main root of maize thickens (Karahara et al., 2004), while in cotton it develops closer to the root tip (Reinhardt and Rost, 1995) and in Arabidopsis it occurs earlier in developing lateral roots (Duan et al., 2013). In addition, Wang et al. (2020) showed that salinity increases suberization of the Casparian strip in Arabidopis roots. Mutants affected in biosynthesis of suberin take up more $Na^+$, indicating the importance of suberization in salt tolerance (Wang et al., 2020).

The symplast route is controlled by ion transporters on the cell membrane. Both abundance and localisation of $Na^+$ transporters can strongly affect salt tolerance. Salt Overly Sensitive1 (SOS1) transports $Na^+$ out of the cell and is induced upon salt stress (Shi et al., 2000; Quintero et al., 2002; Qiu et al., 2004). Mutants of SOS1 are extremely sensitive to salt (Shi et al., 2000). In contrast, the High affinity $K^+$ Transporter (HKT1) imports $Na^+$ into the cell and therefore facilitates $Na^+$ uptake (Rus et al., 2001). In many Arabidopsis accessions, *HKT1* expression is inhibited during salt stress (Julkowska et al., 2017; Chapter 3). However, HKT1 also seems to retrieve $Na^+$ from the xylem and thereby prevents $Na^+$ from reaching the shoot (Davenport et al., 2007) and specific overexpression of HKT1 in the stele enhances salt tolerance (Møller et al., 2009). These examples illustrate that modulations of both apoplastic and symplastic salt uptake can affect salt tolerance. To fully understand how both routes contribute to salt uptake, future research should find ways to efficiently monitor flow rates of $Na^+$ through different parts of the plant. Previously, some studies have used the radio-active isotope $^{22}Na^+$ (Essah et al., 2003), but investing in developing alternative methods such as the use of fluorescent dyes (Park et al., 2009) could also pay off. With an efficient method one could then also study mutants or drugs affecting the apoplastic or symplastic pathway for salt flow to address how this would affect salt tolerance.

7

Above directions will give new insights into how modulation of the plant root system can lead to more salt tolerant plants. However, defining salt tolerance itself can be challenging, especially in terms of breeding. Although many studies indicate a higher plant biomass as the main readout for higher salt tolerance, this might not be accurate. Smaller plants might be better in surviving salt stress. Seed set might be a better proxy for salt tolerance, as it determines fitness, although seed quality might also be affected, and number of seeds would not per definition represent a higher fitness. In terms of breeding, salt tolerance might be defined depending on the crop, as crops grown for their vegetative parts need a different strategy than crops grown for their fruits. Thus, increasing knowledge on the effect of the timing of flowering by salt stress and other stresses will provide opportunities to improve yields (Colasanti & Coneva, 2009; Jung & Müller, 2009). In **Chapter 5**, we exploited natural variation in Arabidopsis to expand the current flowering network with players involved in fine-tuning flowering during salt stress. We found that induction of expression of *UGT74E2* during salt stress was linked to a delay in flowering. As previous studies showed that ectopic overexpression of *UGT74E2* leads to increased salt tolerance (Tognetti et al., 2010) and those plants were delayed in flowering, this indicates that a delay in flowering might be favorable. As the natural variation in the promoter of *UGT74E2* is correlated to the delay in timing of flowering, this provides an interesting new starting point for further research on the transcription factor network involved in regulating this phase transition during salt stress.

This thesis has provided new insights in above and belowground regulation of plant developmental plasticity in response to salt stress and has especially revealed a role for auxin homeostasis in this process. These new insights can on the one hand provide new starting points for expanding the knowledge on the regulatory networks in Arabidopsis during salt stress, and on the other hand increase our understanding of how plants can optimize their root systems to better cope with salt stress.

# REFERENCES

**Achard, P., Cheng, H., De Grauwe, L., Decat, J., Schoutteten, H., Moritz, T., Van Der Straeten, D., Peng, J., and Harberd, N.P.** (2006). Integration of plant responses to environmentally activated phytohormonal signals. Science **311**: 91–94.

**Barberon, M., Vermeer, J.E.M., De Bellis, D., Wang, P., Naseer, S., Andersen, T.G., Humbel, B.M., Nawrath, C., Takano, J., Salt, D.E., and Geldner, N.** (2016). Adaptation of Root Function by Nutrient-Induced Plasticity of Endodermal Differentiation. Cell **164**: 447–459.

**Davenport, R.J., Muñoz-Mayor, A., Jha, D., Essah, P.A., Rus, A., and Tester, M.** (2007). The Na+ transporter AtHKT1;1 controls retrieval of Na + from the xylem in Arabidopsis. Plant, Cell Environ. **30**: 497–507.

**Dinneny, J.R., Long, T. a, Wang, J.Y., Jung, J.W., Mace, D., Pointer, S., Barron, C., Brady, S.M., Schiefelbein, J., and Benfey, P.N.** (2008). Cell identity mediates the response of Arabidopsis roots to abiotic stress. Science (80-. ). **320**: 942–945.

**Duan, L., Dietrich, D., Ng, C.H., Chan, P.M.Y., Bhalerao, R., Bennett, M.J., and Dinneny, J.R.** (2013). Endodermal ABA signaling promotes lateral root quiescence during salt stress in Arabidopsis seedlings. Plant Cell **25**: 324–41.

**Essah, P.A., Davenport, R., and Tester, M.** (2003). Sodium Influx and Accumulation in Arabidopsis. Plant Physiol. **133**: 307–318.

**Gallego-Bartolome, J., Minguet, E.G., Grau-Enguix, F., Abbas, M., Locascio, a., Thomas, S.G., Alabadi, D., and Blazquez, M. a.** (2012). Molecular mechanism for the interaction between gibberellin and brassinosteroid signaling pathways in Arabidopsis. Proc. Natl. Acad. Sci. **109**: 13446–13451.

**Geldner, N.** (2013). The endodermis. Annu. Rev. Plant Biol. **64**: 531–558.

**Geng, Y., Wu, R., Wee, C.C.W., Xie, F., Wei, X., Chan, P.M.Y., Tham, C., Duan, L., and Dinneny, J.R.** (2013). A spatio-temporal understanding of growth regulation during the salt stress response in Arabidopsis. Plant Cell **25**: 2132–54.

**Jia, W., Wang, Y., Zhang, S., and Zhang, J.** (2002). Salt-stress-induced ABA accumulation is more sensitively triggered in roots than in shoots. J. Exp. Bot. **53**: 2201–2206.

**Julkowska, M.M., Hoefsloot, H.C.J., Mol, S., Feron, R., de Boer, G.-J., Haring, M. a, and Testerink, C.** (2014). Capturing Arabidopsis root architecture dynamics with ROOT-FIT reveals diversity in responses to salinity. Plant Physiol. **166**: 1387–1402.

**Julkowska, M.M., Koevoets, I.T., Mol, S., Hoefsloot, H.C.J., Feron, R., Tester, M., Keurentjes, J.J.B.B., Korte, A., Haring, M.A., de Boer, G.-J., and Testerink, C.** (2017). Genetic Components of Root Architecture Remodeling in Response to Salt Stress. Plant Cell: tpc.00680.2016.

**Karahara, I., Ikeda, A., Kondo, T., and Uetake, Y.** (2004). Development of the Casparian strip in primary roots of maize under salt stress. Planta **219**: 41–47.

**Kawa, D. et al.** (2020). SnRK2 Protein Kinases and mRNA Decapping Machinery Control Root Development and Response to Salt. Plant Physiol. **182**: 361–377.

**Kim, J.I., Dolan, W.L., Anderson, N.A., and Chapple, C.** (2015). Indole Glucosinolate Biosynthesis Limits Phenylpropanoid Accumulation in Arabidopsis thaliana . Plant Cell **27**: 1529–1546.

7

**Krishnamurthy, P., Ranathunge, K., Franke, R., Prakash, H.S., Schreiber, L., and Mathew, M.K.** (2009). The role of root apoplastic transport barriers in salt tolerance of rice (Oryza sativa L.). Planta **230**: 119–134.

**Krishnamurthy, P., Ranathunge, K., Nayak, S., Schreiber, L., and Mathew, M.K.** (2011). Root apoplastic barriers block Na + transport to shoots in rice (Oryza sativa L.). J. Exp. Bot. **62**: 4215–4228.

**Ljung, K., Hull, A.K., Celenza, J., Yamada, M., Estelle, M., Normanly, J., and Sandberg, G.** (2005). Sites and regulation of auxin biosynthesis in Arabidopsis roots. Plant Cell **17**: 1090–104.

**McLoughlin, F., Galvan-Ampudia, C.S., Julkowska, M.M., Caarls, L., Van Der Does, D., Laurière, C., Munnik, T., Haring, M.A., and Testerink, C.** (2012). The Snf1-related protein kinases SnRK2.4 and SnRK2.10 are involved in maintenance of root system architecture during salt stress. Plant J. **72**: 436–449.

**Møller, I.S., Gilliham, M., Jha, D., Mayo, G.M., Roy, S.J., Coates, J.C., Haseloff, J., and Tester, M.** (2009). Shoot Na+ exclusion and increased salinity tolerance engineered by cell type-specific alteration of Na+ transport in Arabidopsis. Plant Cell **21**: 2163–2178.

**Munns, R., James, R.A., Xu, B., Athman, A., Conn, S.J., Jordans, C., Byrt, C.S., Hare, R.A., Tyerman, S.D., Tester, M., Plett, D., and Gilliham, M.** (2012). Wheat grain yield on saline soils is improved by an ancestral Na + transporter gene. Nat. Biotechnol. **30**: 360–364.

**Naseer, S., Lee, Y., Lapierre, C., Franke, R., Nawrath, C., and Geldner, N.** (2012). Casparian strip diffusion barrier in Arabidopsis is made of a lignin polymer without suberin. Proc. Natl. Acad. Sci. **109**: 10101–10106.

**Park, M., Lee, H., Lee, J.S., Byun, M.O., and Kim, B.G.** (2009). In planta measurements of Na+ using fluorescent dye CoroNa Green. J. Plant Biol. **52**: 298–302.

**Pfister, A. et al.** (2014). A receptor-like kinase mutant with absent endodermal diffusion barrier displays selective nutrient homeostasis defects. Elife **3**: e03115.

**Qiu, Q.S., Guo, Y., Quintero, F.J., Pardo, J.M., Schumaker, K.S., and Zhu, J.K.** (2004). Regulation of Vacuolar Na+/H+ Exchange in Arabidopsis thaliana by the Salt-Overly-Sensitive (SOS) Pathway. J. Biol. Chem. **279**: 207–215.

**Quintero, F.J., Ohta, M., Shi, H., Zhu, J.-K., and Pardo, J.M.** (2002). Reconstitution in yeast of the Arabidopsis SOS signaling pathway for Na+ homeostasis. Proc. Natl. Acad. Sci. **99**: 9061–9066.

**Reinhardt, D.H. and Rost, T.L.** (1995). Salinity accelerates endodermal development and induces an exodermis in cotton seedling roots. Environ. Exp. Bot. **35**: 563–574.

**Rus, A., Baxter, I., Muthukumar, B., Gustin, J., Lahner, B., Yakubova, E., and Salt, D.E.** (2006). Natural variants of AtHKT1 enhance Na+ accumulation in two wild populations of Arabidopsis. PLoS Genet. **2**: 1964–1973.

**Rus, A., Yokoi, S., Sharkhuu, A., Reddy, M., Lee, B., Matsumoto, T.K., Koiwa, H., Zhu, J.-K., Bressan, R.A., and Hasegawa, P.M.** (2001). AtHKT1 is a salt tolerance determinant that controls Na+ entry into plant roots. Proc. Natl. Acad. Sci. U. S. A. **98**: 14150–14155.

**Shi, H., Ishitani, M., Kim, C., and Zhu, J.K.** (2000). The Arabidopsis thaliana salt tolerance gene SOS1 encodes a putative Na+/H+ antiporter. Proc. Natl. Acad. Sci. U. S. A. **97**: 6896–6901.

**Soma, F., Mogami, J., Yoshida, T., Abekura, M., Takahashi, F., Kidokoro, S., Mizoi, J., Shinozaki, K., and Yamaguchi-Shinozaki, K.** (2017). ABA-unresponsive SnRK2 protein kinases regulate mRNA decay under osmotic stress in plants. Nat. Plants **3**: 16204.

**Tognetti, V.B. et al.** (2010). Perturbation of indole-3-butyric acid homeostasis by the UDP-glucosyltransferase UGT74E2 modulates Arabidopsis architecture and water stress tolerance. Plant Cell **22**: 2660–2679.

**Wang, P., Wang, C.M., Gao, L., Cui, Y.N., Yang, H.L., de Silva, N.D.G., Ma, Q., Bao, A.K., Flowers, T.J., Rowland, O., and Wang, S.M.** (2020). Aliphatic suberin confers salt tolerance to Arabidopsis by limiting Na+ influx, K+ efflux and water backflow. Plant Soil **448**: 603–620.

7

# SUMMARY

Salinity of the soil is a major problem for agriculture. The number of salinized soils is rapidly increasing worldwide, and most crops are highly sensitive to salt (NaCl). To cope with salt stress, plants can adapt their growth and development. In Arabidopsis and in some crop species favorable adaptations of the root system to cope with abiotic stress have been described. Plants respond by a redistribution of root mass between main and lateral roots, yet the genetic machinery underlying this process is still largely unknown. In **Chapter 2** we review the currently known root system architecture (RSA) responses in Arabidopsis and a number of crop species to a range of abiotic stresses, including nutrient limitation, drought, salinity, flooding and extreme temperatures. Although the root system is the first part of the plant to encounter salt stress, aboveground plant development and especially timing of flowering are also important factors in determining yield. The research presented in this thesis aims at further unraveling how plants adapt and acclimate to cope with salt stress both belowground (root system architecture in **Chapter 2, 3, 4**) and aboveground (timing of flowering, **Chapter 5**).

Genomic screens using available genetic variation in natural populations have shown to be instrumental to identify loci with the potential of breeding more resilient crops. In this thesis we utilized natural variation in accessions of Arabidopsis to find new candidate genes involved in root development (**Chapter 3**) and timing of flowering (**Chapter 5**). In both chapters we identify candidate genes involved in auxin metabolism.

CYTOCHROME P450 FAMILY 79 SUBFAMILY B2 (CYP79B2), identified in **Chapter 3** to play a role in maintaining lateral root development**,** converts tryptophan to indole-3-acetaldoxime (IAOx). Changes in *CYP79B2* expression in salt stress are positively correlated with lateral root development in Arabidopsis accessions. The IAOx pathway can produce camalexin, indole glucosinolates and indole-3-acetic acid (IAA). In **Chapter 4** further investigation of this pathway puts the metabolic compound indole-3-acetonitrile (IAN) central in maintaining lateral root development during salt stress. IAN can either be synthesized as a breakdown product of indole glucosinolates, which we show to accumulate during salt stress or directly from IAOx by a novel candidate enzyme CYP71A19, which we characterize in this chapter.

Salinity of the soil greatly influences the timing of flowering, but the mechanisms underlying remain largely elusive this far. In **Chapter 5** we again exploit GWAS, this time to find candidate genes involved in the timing of flowering in response to salt stress. We show that a delay in flowering in response to salt stress is the common response in almost all studied accessions. Again, auxin metabolism seems to play a major role, as natural variation in the promoter of *UDP-glycosyltransferase 74E2 (UGT74E2)*, an IBA conjugase, is linked to the extent of delay in bolting in salt stress. Further investigation of the promoter region of *UGT74E2* revealed seven candidate transcription factors putatively binding the promoter and influencing its expression during salt stress. These transcription factors will provide a good starting point for further research on *UGT74E2* and its upstream regulators, to obtain more insight in fine-tuning of the network of timing of flowering under salt stress.

This thesis illustrates that salt induced changes in both above and belowground development are guided by changes in auxin metabolism. **Chapter 6** integrates the current knowledge on auxin transport and auxin metabolism during salt stress. Our analysis stresses the importance of considering all these components together and highlights the use of mathematical modelling for predictions of plant physiological responses. In **Chapter 7** we expand the **discussion** by taking one step back, looking at the upstream regulation of auxin metabolism under salt stress, and one step forward, discussing how altered root development might lead to salt tolerance.

## SAMENVATTING

Zoutstress is een groot probleem voor de landbouw. Het aantal verzilte bodems neemt snel toe en de meeste gewassen kunnen slecht overweg met een hoog zoutgehalte. Om met zoutstress om te gaan, kunnen planten hun groei en ontwikkeling aanpassen. Het wortelsysteem is het eerste deel van de plant dat met zoutstress wordt geconfronteerd. In *Arabidopsis thaliana* en in sommige gewassoorten zijn gunstige aanpassingen van het wortelstelsel om abiotische stress het hoofd te bieden beschreven. Planten reageren door een herverdeling van wortelmassa tussen hoofd- en zijwortels, maar de genetische machinerie die aan dit proces ten grondslag ligt, is nog grotendeels onbekend. In **Hoofdstuk 2** beschrijven we hoe Arabidopsis en een aantal gewassen hun wortelarchitectuur aanpassen in reactie op een reeks van abiotische stressfactoren, waaronder nutriëntenbeperking, droogte, zoutgehalte, overstromingen en extreme temperaturen. Alhoewel het wortelstelsel als eerste in aanraking komt met zout stress, bepaalt bovengrondse ontwikkeling en groei grotendeels de opbrengst van gewassen. Met name de timing van bloei speelt hierin een belangrijke rol. Het onderzoek dat in dit proefschrift wordt gepresenteerd richt zich op hoe planten omgaan met zout stress, zowel ondergronds (wortelarchitectuur in **Hoofdstuk 2, 3, 4**) als bovengronds (timing van bloei, **Hoofdstuk 5**).

Screening van beschikbare genetische variatie in natuurlijke populaties heeft veel genen opgeleverd met het potentieel om veerkrachtigere gewassen te kweken. In dit proefschrift hebben we natuurlijke variatie in accessies van *Arabidopsis thaliana* gebruikt om nieuwe kandidaatgenen te vinden die betrokken zijn bij wortelontwikkeling (**Hoofdstuk 3**) en timing van bloei (**Hoofdstuk 5**). In beide hoofdstukken identificeren we een kandidaatgen dat betrokken is bij het auxinemetabolisme.

CYTOCHROOM P450 FAMILIE 79 SUBFAMILIE B2 (CYP79B2), in **Hoofdstuk 3** aangetoond belangrijk te zijn voor laterale wortelontwikkeling in zout stress, zet tryptofaan om in indol-3-acetaldoxime (IAOx). Veranderingen in *CYP79B2*-expressie in zoutstress zijn positief gecorreleerd met laterale wortelontwikkeling bij Arabidopsis-accessies. De IAOx-route leidt naar camalexine, indoolglucosinolaten en indool-3-azijnzuur (IAA). In **Hoofdstuk 4** zet verder onderzoek het tussenproduct indol-3-acetonitril (IAN) centraal in het handhaven van laterale wortelontwikkeling tijdens zoutstress. We laten twee mogelijke biosynthetische routes van IAN zien: als een afbraakproduct van indoolglucosinolaten, die toenemen tijdens zoutstress, of via directe biosynthese vanuit IAOx door een nieuw kandidaat-enzym CYP71A19, verder beschreven in dit hoofdstuk.

Het zoutgehalte van de grond heeft grote invloed op de timing van de bloei, maar de onderliggende mechanismen zijn tot nu toe slechts beperkt beschreven. In **Hoofdstuk 5** gebruiken we opnieuw GWAS, dit keer om kandidaatgenen te vinden die betrokken zijn bij de timing van bloei als reactie op zoutstress. We laten zien dat vroege bloei als reactie op zoutstress zelden wordt waargenomen en dat bijna alle bestudeerde accessies vertraagd zijn in bloei. Opnieuw lijkt het auxinemetabolisme een belangrijke rol te spelen, aangezien natuurlijke variatie in de promotor van *UDP-glycosyltransferase 74E2*

*(UGT74E2),* een IBA-conjugase, correleert met de mate van vertraging van bloei in zoutstress. Verder onderzoek van het promotorgebied van *UGT74E2* onthulde zeven transcriptiefactoren die vermoedelijk de promotor binden en de expressie ervan beïnvloeden tijdens zoutstress. Deze transcriptiefactoren bieden een goed startpunt voor verder onderzoek naar *UGT74E2* en zijn regulatoir netwerk, waardoor meer inzicht wordt verkregen in de regulatie van inductie van bloei onder zout stress.

Dit proefschrift illustreert dat door zout veroorzaakte veranderingen in zowel boven- als ondergrondse ontwikkeling worden geleid door veranderingen in het auxinemetabolisme. **Hoofdstuk 6** integreert de huidige kennis over auxinetransport en auxinemetabolisme tijdens zoutstress. Onze analyse benadrukt het belang om al deze componenten samen te beschouwen en benadrukt het gebruik van wiskundige modellen voor voorspellingen van fysiologische reacties van planten. In **Hoofdstuk 7** breiden we de discussie uit door een stap terug te doen en te kijken naar de regulatie van auxine metabolisme onder zoutstress, en een stap voorwaarts in de discussie over hoe veranderde wortelontwikkeling zou kunnen leiden tot zouttolerantie.

## ACKNOWLEDGEMENTS

First of all, **Christa**, my supervisor, mentor, friend. Five years ago, I had to make a choice with whom I would start this journey and I am happy I chose you. Although our group grew enormously since I joined, we have been able to continue our regular meetings and I always felt like a priority when I came by your office with questions and fascinating results. Of course, your research experience has been of outmost importance during the project, but I especially valued your ability to keep viewing your team members as human beings with a personal life. You responded with excitement to my pregnancies and supported me in my quest of combining work and family. And although you were hesitant at first, you even supported my crazy idea of combining two jobs at the end of my PhD. I know you are probably a bit sad of seeing me leaving research, but I hope I can still provide you with many skilled new students inspired by my teaching!

I would like to thank **Enza zaden** for their willingness to support my project with an in-kind contribution and **Gert-Jan de Boer** as their representative, for your useful advice during our progress meetings. My external supervisor, **Eric Visser**, thank you for your input and support. Especially during the start-up phase, you have given me the chance to ventilate my thoughts and helped me to further explore my career possibilities. **Magdalena Julkowska**, I regularly mentioned you during my presentations as a "former colleague" and although we never officially were colleagues, it did feel like you were one of my closest colleagues. You were always open for feedback and I enjoyed following up on your work.

**Selene Kolman**, you were the driving force behind the development of the time-lapse. Although our goals were not always compatible, your ideas were enlightening. I had much fun guiding you through the scientific world. **Gerrit Hardeman and Johan Mozes**, thank you for all support during the development of the time-lapse. **Guillaume Lobet**, thank you for your willingness to help me with developing a method for analyzing the time-lapse data in Smartroot. Through your knowledge I became the Smartroot hero of the lab.

In some areas, I am glad that others took the lead and shared their expertise. **Iris Kappers**, thank you for guiding me through the world of metabolomics. **Wouter Kohlen**, although you were always busy, you also always found the time for both doing IAA measurements for me and critically reviewing my data, thanks. **Richard Immink,** our lab is not specialized in flowering and I was very happy I had you to back me up when further exploring the effects of salt on the floral transition.

My project would never have been a success without other people helping me around in and outside the lab. I am not a lab tiger, so I am glad that other people motivated to be so or helped me out when I struggled. **Jessica**, we worked together for quite a while and there is nobody I trust as much with my samples as you. Above that, you are great fun to work with. **Ringo,** I was very sad to leave you behind in the lab in Amsterdam. You helped me around when learning quite some new techniques, while also providing some nice music to guide the process. I am glad that you represent Amsterdam as my

paranymph during my thesis defense! **Thijs**, **Leo**, **Francel**, **Marielle** thanks for your willingness to help me at any time. **Ludek** and the rest of the greenhouse staff, I am thankful for your support and nice talks during my project. Thanks to the labmanagers at the **IBED** for helping me prepping my samples for analysis of sodium and potassium content. Of course, also a handful of MSc and BSc students have helped collecting results and came with many inspiring ideas enriching my project, thanks to **Daan, Suzanne, Güniz, Alice and Noah**, I wish you all the best in your future careers.

During my PhD project I worked together with a lot of inspiring team members in both Amsterdam and Wageningen. I got a warm welcome in Amsterdam when I started writing my research proposal. The plant science groups formed a very inspiring and active community providing me with many ideas and feedback during my work there. I would like to thank **all staff members** of those groups for their input. **Teun Munnik,** you're one of the most critical researchers I know and during the first two years you really helped my project take form. **Michel Haring**, your enthusiasm for plant science is contagious and I'm glad we kept in contact after me leaving. You helped me figure out the next steps in my career and I hope that when leaving Amsterdam for the second time, we will keep in touch again. **Dorota**, already during the writing process of my PhD proposal you welcomed me into the group and help me to find my way. **Ruud**, your critical view on research has always served me well and I enjoyed writing our opinion paper together. **Steven**, next to all your research ideas, I appreciated your genuine interest in me as a person and enjoyed our conversations on opposite desks. **Deji**, you have been there from the start of my project and together we moved to Wageningen. I am happy to see that you found your place in your current job. **Yanxia**, I was happy to welcome you in Amsterdam and to take along your experience, warmth and fun to Wageningen. **Yutao**, the steps you made during your project are enormous, I liked seeing you grow.

Together with **Hongfei, Jasper** and **Eva** I started my adventure at Wageningen University. It must have been exciting and challenging at the same time to start your PhD trajectory at a place where even the experienced team members were still struggling to find their way. I wish you all the best in finishing your PhD, especially in these strange times. **Jasper** and **Eva**, thanks for helping with my thesis cover design, it turned out perfect. **Eva**, as the two ladies from Amsterdam, I enjoyed travelling together to Wageningen and our meet-ups in Amsterdam as well. I am very happy to hand over the most precious part of my project to such a talented researcher and I am grateful having you next to me during my thesis defense.

In Wageningen our group grew quickly and got enriched with **Nora**, **Tom**, **Rumyana**, **Lot**, **Damian, Scott,** ready with their critical feedback at any time. Special thanks to staff members **Sander, Leónie, Henk** and **Wilco**, providing me with many ideas during the second half of my project. **Rina,** you are the backbone of PPH, thank you for the support in all areas. Last, I would also like to thank **all other lab members of PPH** for all input and fun during my years in Wageningen. Changing from labs was quite a challenge, but we got an enormous warm welcome.

Already during my thesis, I started working at the University of Amsterdam as teacher. I'd like to thank **Hanneke, Lotje** and **Dorian** for their flexibility to schedule meetings around my responsibilities for mijn PhD project. I enjoyed combining both jobs and your support to do so!

Tot slot, lieve familie, **Varda, Rik, Mit, Tosh**, dit proefschrift had hier niet gelegen zonder jullie. In de afgelopen jaren hebben jullie altijd paraat gestaan om de zorg voor de kinderen over te nemen. **Tosh,** bedankt voor het aanschaffen van een WIFI-versterker. Zonder jouw gastvrijheid in gekke corona tijden weet ik niet hoe ik mijn proefschrift te midden van een rondrennende peuter en huilende baby had moeten afronden. **Varda**, Aster is dol op je en ik geniet ervan om je met haar te zien. Naast alle uren zorg voor Aster (en Quin) die je op je hebt genomen, wil ik je ook bedanken voor het voorbeeld wat je voor me bent als moeder en mens. Jij hebt me altijd laten zien dat ik op elk moment in mijn leven mijn eigen keuzes kan maken en nieuwe uitdagingen aan kan gaan.

Lieve **Eelco,** ik leerde je kennen aan het begin van deze uitdaging en inmiddels zijn we 6 jaar verder. Van het begin af aan heb je me doen inzien dat een promotietraject ook gewoon een baan is en dat er meer is in het leven. Je hebt me doen groeien tot de zelfverzekerde persoon die ik nu ben en me daarmee het vertrouwen gegeven dat ik nodig had om mijn PhD traject tot een succes te maken. En natuurlijk hebben we samen het mooiste in ons leven op de wereld gezet: **Aster** en **Quin**. Lieve **Aster**, je bent één van de vrolijkste, slimste, mooiste mensen die ik ken. Ik wil je bedanken voor al het geduld wat je hebt gehad, elke keer weer als je me vroeg "ben je nu klaar met werken?" en ik helaas nee moest zeggen. Lieve kleine **Quin**, van jouw kant kon ik nog weinig geduld verwachten. Ik wil je echter bedanken voor al het geduld wat je mij hebt geleerd, de nachten en dagen dat ik met jou slapend of voedend in mijn armen heb gezeten. Want **Aster** en **Quin**, sinds jullie geboorte was het vele malen makkelijker om tegenslagen tijdens mijn onderzoek te verwerken, jullie waren zoveel belangrijker. En nu kan ik dan eindelijk zeggen: "ja, ik ben klaar".